STUDIES ON POLYMER NANOCOMPOSITE ADSORBENTS FOR DYE REMOVAL

A Thesis submitted

in fulfillment of the requirements

for the award of degree of

DOCTOR OF PHILOSOPHY

By

Shivani Kalotra
(Registration Number: 901401010)

Under the supervision of:

Dr. Rajeev Mehta
Professor and Head
Department of Chemical Engineering
Thapar Institute of Engineering and Technology, Patiala

Chemical Engineering Department
Thapar Institute of Engineering and Technology
Patiala-147004 (Punjab)
December 2021

CERTIFICATE

This is to certify that the thesis entitled, **"STUDIES ON POLYMER NANOCOMPOSITE ADSORBENTS FOR DYE REMOVAL"** submitted by **Ms. Shivani Kalotra,** Ph.D. student (Registration Number: 901401010) for the fulfillment of the requirements for the award of degree of Doctor of Philosophy in Chemical Engineering Department, Thapar Institute of Engineering and Technology, Patiala, is a record of the candidate's own work carried out by her from July 2014 to June 2021 in this institute under my supervision. The matter presented in this thesis has not been submitted in part or full for the award of any degree in any university or institute.

Rajeev Mehta

Dr. Rajeev Mehta
Professor and Head
Department of Chemical Engineering
Thapar Institute of Engineering and Technology, Patiala

ACKNOWLEDGEMENT

I wholeheartedly would like to offer my gratitude to almighty and supreme for guiding me throughout my journey.

Encapsulating my journey begins with acknowledging everyone who has been the pillar for strength throughout these times. Their mere presence has been encouraging me to achieve the feat of completing my Ph.D. I would use this platform to show my appreciation and indebtedness to all of them.

First and foremost, I would like to thank my Supervisor, **Dr. Rajeev Mehta**, for his fantastic and patient guidance through all the process. He has been a great mentor who has assisted, gave in-depth insight, and has been a torchbearer throughout these times. He has given unconditional support along with constructive criticism that helped me to be a better researcher and evolve as a person. I am really thankful to the Thapar Institute of Engineering and Technology and Chemical Engineering Department for providing me with all infrastructure, assistance, and guidance throughout the duration of my Ph.D.

Also, I thank **Dr. H. Bhunia,** Professor, Department of Chemical Engineering. With their constant support, the journey was more smooth.

I want to acknowledge my Doctoral Committee, **Dr. J.P. Kushwaha**, Professor and **Dr. S. K. Singh**, Professor, Department of Chemical Engineering, **Dr. O. P. Pandey**, Senior Professor, Department of Physics, Thapar Institute of Engineering and Technology, for their valuable suggestions.

I would like to thank my fellow researchers **Ms. Mansi Singh, Mr. Daksh Shelly, and Ms. Anushka Garg,** for continuous encouragement that helped me a lot in this journey.

I would also like to thank all the faculty members of the Chemical Engineering Department for their continuous support.

Most importantly, I would like to take the chance to thank my family for being a constant motivation factor that helped; getting through the long and difficult process of writing and completing my thesis would not have been possible without them.

Date: 17/12/21

Place: **Patiala**

Shivani Kalotra

Shivani Kalotra

TABLE OF CONTENTS

ABSTRACT

In the current century, wastewater treatment is a worldwide challenge. Every year, a large amount of wastewater is generated from cosmetics, plastics, paper, leather, rubber, printing, food, and pharmaceutical and textile industries. The textile dye pollutant water is highly toxic and is one of the major reasons for the environmental problems. The harmful chemicals present in the dyes create an adverse effect on human lives. India's textile sector alone generates about 60,000 metric tonnes of dyes.

Many different methods have been used to treat such contaminated wastewater. These methods are adsorption, reverse osmosis, membrane filtration, electrodialysis, ion exchange, coagulation, chemical precipitation, flocculation, biodegradation, etc. but adsorption is one of the most cost-effective and efficient methods for removing dyes from wastewater.

Many researchers have studied different types of adsorbents to remove dye effluent successfully, and activated carbon is the most popular one, but the operational cost of activated carbon is very high. Thus, there is a need to develop a low-cost and economical adsorbent with a higher surface area and higher adsorption rate. Nanotechnology provides the opportunity for researchers to treat wastewater effectively. Polymer nanocomposites material with improved physical properties plays an important role in higher textile wastewater treatment.

In the present work, we have synthesized high surface area nanocomposites through an in-situ polymerization process of aniline, using HCl as a catalyst and ammonium persulfate as an oxidizing agent. A probe sonicator has been used for nanodispersion of clays and CA powder. Micron-sized colloidal particle aggregates are broken down to the nanoscale level using a probe sonicator. Prior to sonication, a homogenizer was used to make a homogeneous suspension. The different synthesis processing routes were studied.

Further, the pure CA and prepared PANI, PANI/MMT, and PANI/CA nanocomposites were utilized as adsorbents for adsorption of Acid green 25 and Methylene blue dye in a batch process. Acid green 25 (anionic) and Methylene blue (cationic) dyes are highly soluble in water and at the same time, highly poisonous in nature. Thus, elimination of textile dyes is essential

before being discarded in the environment. The present work focuses on the treatment of these two harmful dyes by using nanocomposite adsorbents.

Although PANI/MMT nanocomposites have already been utilized as adsorbent to treat wastewater, no research has been done on adsorption of Acid green 25 using PANI/MMT nanocomposites adsorbent. For MB adsorption, only a single study has been reported.

Carbon aerogels have not been researched much in the past but lately because of their highly porous nature, it is attracting a lot of interest. Only a few studies are there on the synthesis of carbon aerogel/polyaniline nanocomposites material. There is a lack of study on the adsorption process through carbon aerogel-based adsorbents. Moreover, no research on AG25 dye adsorption with PANI/CA nanocomposites has been reported so far.

Adsorption study of Acid green and Methylene blue has been performed in a batch mode. The entire adsorption study was done by involving different parameters i.e. pH, initial dye concentration, time, adsorbent loading, and temperature.

In the adsorption study results of Acid green 25 dye onto PANI and PANI/MMT adsorbents, adsorbent dosage = 0.4 g, pH = 6, and contact period 30 minutes were determined to be optimal adsorption conditions. Complete removal of Acid Green 25 dye (AG25) was achieved with PANI/MMT nanocomposite adsorbent and 99.16% with pure PANI sample. The adsorption results onto PANI/MMT were superior to pure PANI. The pseudo-second order model performed well for adsorption kinetics. Langmuir model best describes adsorption thermodynamic properties.

An adsorption study was also performed with CA and PANI/CA adsorbent. The optimum parameters of this study were found to be pH = 7, adsorbent dose = 0.1 g for CA and 0.4 g for PANI/CA, time 0-30 min for CA, and 0-60 min for PANI/CA. Furthermore, the results of CA show better dye removal as compared to PANI/CA adsorbent. The effect of the initial AG25 dye concentration showed that the lower dye concentration is more favorable to remove more dye. The kinetics of AG25 onto CA and PANI/CA have been well described using the pseudo-second-order model. The highest correlation coefficient (R2= 1) values were achieved with the CA adsorbent. Two models, Langmuir and Freundlich, provided the best data fit of AG25 onto

CA. The Langmuir model best suited the data for PANI/CA, implying monolayer adsorption. On pure CA adsorbent, the maximum adsorption rate of 518 mg/g was achieved.

Methylene blue dye adsorption has been done on PANI and PANI/MMT adsorbent. PANI/MMT adsorbent shows better results as compared to pure PANI adsorbent. With a rise in the pH of the MB dye solution, the percentage adsorption of dye onto PANI was increasing. For PANI/MMT adsorbent, the maximum removal was attained at neutral pH. The kinetic study was performed with pseudo-first and second-order models. The pseudo-second-order model best represented it. MB adsorption isotherm best fits the Temkin model for PANI adsorbent and the Langmuir model for PANI/MMT adsorbent.

In this study, the prepared adsorbent material gave excellent adsorption results, and this is because of the different processing routes that have been used to prepare nanocomposites. Essentially, the key is in nano-dispersion of clay and CA. Acid green 25 and Methylene blue adsorbed at a very fast rate, at least by a factor of 20, as compared to earlier studies onto PANI and its nanocomposite adsorbents. Therefore it will be a great material for textile wastewater treatment. The synthesized materials have the potential to treat textile wastewater efficiently.

LIST OF PUBLICATIONS

Publications in SCI international journals

1. **Shivani Kalotra,** Rajeev Mehta (2020). Synthesis of polyaniline/clay nanocomposites by *in situ* polymerization and its application for the removal of Acid Green 25 dye from wastewater, Polymer Bulletin, 78(5), 2439-2463. DOI: https://doi.org/10.1007/s00289-020-03222-3. **Impact factor: 2.014**.
2. **Shivani Kalotra,** Rajeev Mehta (2021). Carbon aerogel and polyaniline/carbon aerogel adsorbents for Acid Green 25 dye: synthesis, characterization and an adsorption study, Chemical Engineering Communications. DOI: https://doi.org/10.1080/00986445.2021.1919650. **Impact factor: 2.32**.

Patent filled (In process)

1. **Shivani Kalotra** and Rajeev Mehta, "Removal of methylene blue dye through adsorption by polyaniline clay nanocomposites".

International/National Conferences

1. **Shivani Kalotra** and Rajeev Mehta**,** "*In-situ* polymerization of Polyaniline/Clay nanocomposite in the presences of ammonium persulfate as oxidising agent", 70th Annual Session of Indian Institute of Chemical Engineers (CHEMCON – 2017), Haldia Institute of Technology, Haldia, December 27 – 30, 2017.
2. **Shivani Kalotra** and Rajeev Mehta, "Synthesis of Polymer Nanocomposites with Halloysite clay and Montmorillonite clay: Synthesis and Characterization", 71th Annual Session of Indian Institute of Chemical Engineers (CHEMCON–2018), Dr. B. R. Ambedkar National Institute of Technology, Jalandhar, Punjab, December 27 – 30, 2018.
3. **Shivani Kalotra** and Rajeev Mehta, "Adsorption of a textile dye from wastewater using nanoclay as an adsorbent", National Conference on Pollution Control Technologies and Sustainable Development, Malaviya National Institute of Technology, Jaipur, October 03-04, 2019.

LIST OF FIGURES

LIST OF TABLES

ABBREVIATIONS

AG25	Acid green 25
MB	Methylene blue
PANI	Polyaniline
MMT	Montmorillonite clay
HNT	Halloysite clay
FTIR	Fourier-transform infrared spectroscopy
FESEM	Field Emission Scanning Electron Microscope
SEM	Scanning electron microscope
XRD	X-ray diffraction analysis
HRTEM	High-resolution transmission electron microscopy
BET	Brunauer–Emmett–Teller
UV-Vis spectroscopy	Ultraviolet–visible spectroscopy
ES	Emeraldine salt
EB	Doped state and emeraldine base
PB	Undoped state, pernigraniline base
LB	Leucoemeraldine base
PCN	Polymer nanocomposite
CA	Carbon aerogels
HCl	Hydrochloric acid
HNO_3	Nitric acid
H_2SO_4	Sulphuric acid
DBSA	Dodecylbenzene-sulfonic acid
H_3PO_4	Phosphoric acid
SLS	Sodium lauryl sulphate
TGA	Thermogravimetric analysis
DSC	Differential scanning calorimetry
XPS	X-ray photoelectron spectroscopy
AFM	Atomic force microscopy
AA-MMT	Amino acid modified-montmorillonite
CTAB	Cetyltrimethylammonium bromide
CNT	Carbon nanotubes
APS	Ammonium persulfate
NMP	N-methyl 2- pyrrolidone
DRS	Differential reflectance spectroscopy
DMA	Dynamic mechanical analyzer
DTA	Differential thermal analysis
XRF	X-ray fluorescence
TEM	Transmission electron microscopy
EDX	Energy Dispersive X-Ray Analysis

CHAPTER 1

INTRODUCTION

1.1 Background

Contamination in water produced from several industries such as paper, textiles, cosmetics, pharmaceuticals, leather, plastics, printing, and rubber is highly toxic and harmful to human beings **[1, 2]**. The textile industry, in particular, discharges a considerable amount of dye-bearing wastewater. Over 100000 dyes are available commercially with a gross annual production of over 7×10^5 tons **[3, 4].** There are three categories of dyes: anionic dyes, cationic dyes, non – ionic dyes; most of these are toxic, and some are carcinogenic.

Several methods are utilized to treat textile dyes i.e. membrane separation, adsorption, biodegradation, electrochemical processes, and ozonation, etc. **[5, 6, 7]**. This work focuses only upon an adsorption method for dye removal. Many scientists have investigated the removal of textile dye waste via various types of adsorbents, and the selection of an adsorbent depends upon its various characteristics like cost-effectiveness, easy recovery, non-toxic, easily available, and renewability**.** Nowadays, polymer/clay nanocomposites have gained interest in the research field and attained much attention in the industrial and academic space. The present study focuses on the *in-situ* polymerization and characterization of polyaniline, polyaniline/montmorillonite, carbon aerogel, and polyaniline/carbon aerogel nanocomposites for their use as an adsorbent. Adsorption behavior has been investigated using Acid green 25 dye (AG25) and Methylene blue dye (MB) as the adsorbates. The study also includes the synthesis and characterization of PANI/HNT nanocomposites. **Figure 1.1** presents the schematic flowchart of the present work. Characterization of nanocomposites was done using Fourier transform infrared spectroscopy, X-

ray powder diffraction, Scanning electron microscopy, Field emission scanning electron microscope, Transmission electron microscopy, BET (Brunauer Emmett Teller) analysis, and UV-Vis spectroscopy.

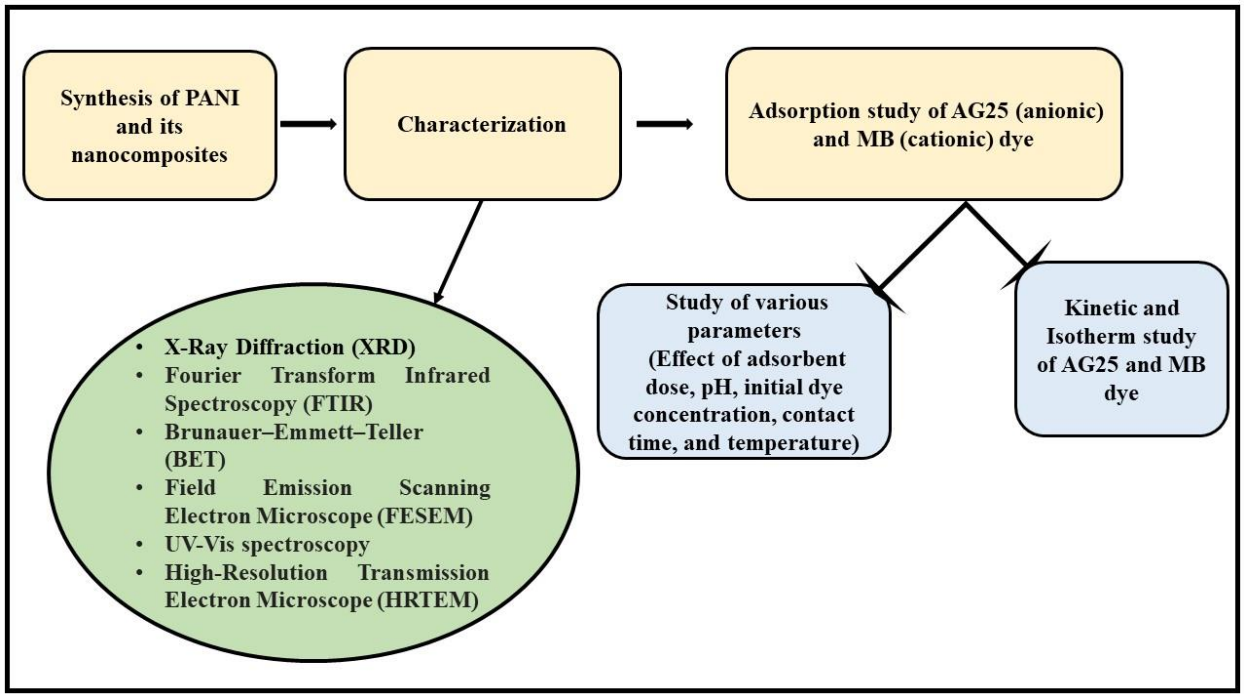

Figure 1.1 Schematic flowchart

1.2 Adsorbate used for wastewater treatment

1.2.1 Acid green 25 (Anionic Dye)

Acid dyes are anionic dyes, and they are highly soluble in water. Acid dyes are generally used in nylon, silk, and wool industries [**8].** Acid green 25 (AG25) is an anionic dye used in several applications, including textile, cosmetic, wood, leather, and paints industry **[9, 10]**. Acid green 25 dye effluent is very harmful to aquatic creatures. It also can cause many problems for human beings like skin and eye irritation. Therefore, it is important to eliminate AG25 dye from textile

wastewater through different treatment methods to protect our environment. The structure and characteristics of AG25 dye are presented in **Table 1.1 [11]**.

Table 1.1 Structure and characteristics of AG25 dye **[11]**.

AG25 dye Structure	Empirical Formula	Molecular Weight (g/mol)	Maximum Wavelength (nm)
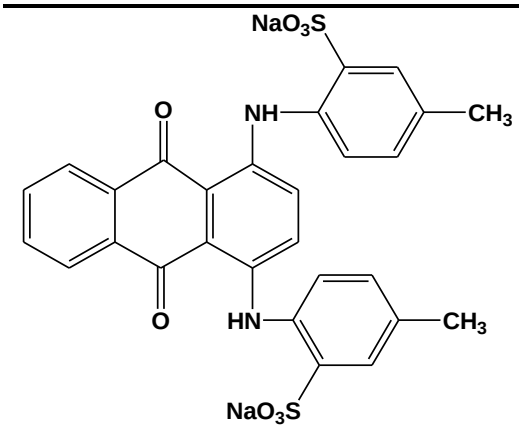	$C_{28}H_{20}N_2Na_2O_8S_2$	622.58	642

Table 1.2 Characteristics and structure of MB dye.

MB dye Structure	Empirical Formula	Molecular Weight (g/mol)	Maximum Wavelength (nm)
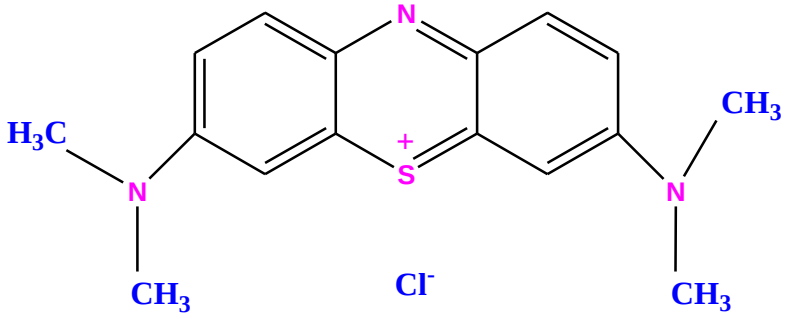	$C_{16}H_{18}ClN_3S$	319.85	665

1.2.2 Methylene blue (Cationic dye)

Methylene blue (MB) is a cationic dye known for its color visibility in the water. Cationic dyes, such as MB, are much more carcinogenic compared to anionic dyes. Even a small concentration of the dye creates toxic effects in humans as well as aquatic life. The presence of MB dye in wastewater leads to other harmful effects such as eyes burn, tissue necrosis, sweating, diarrhea, nausea, mental disorders, gastritis, and vomiting **[12-15].** MB dye structure and characteristics are depicted in **Table 1.2**.

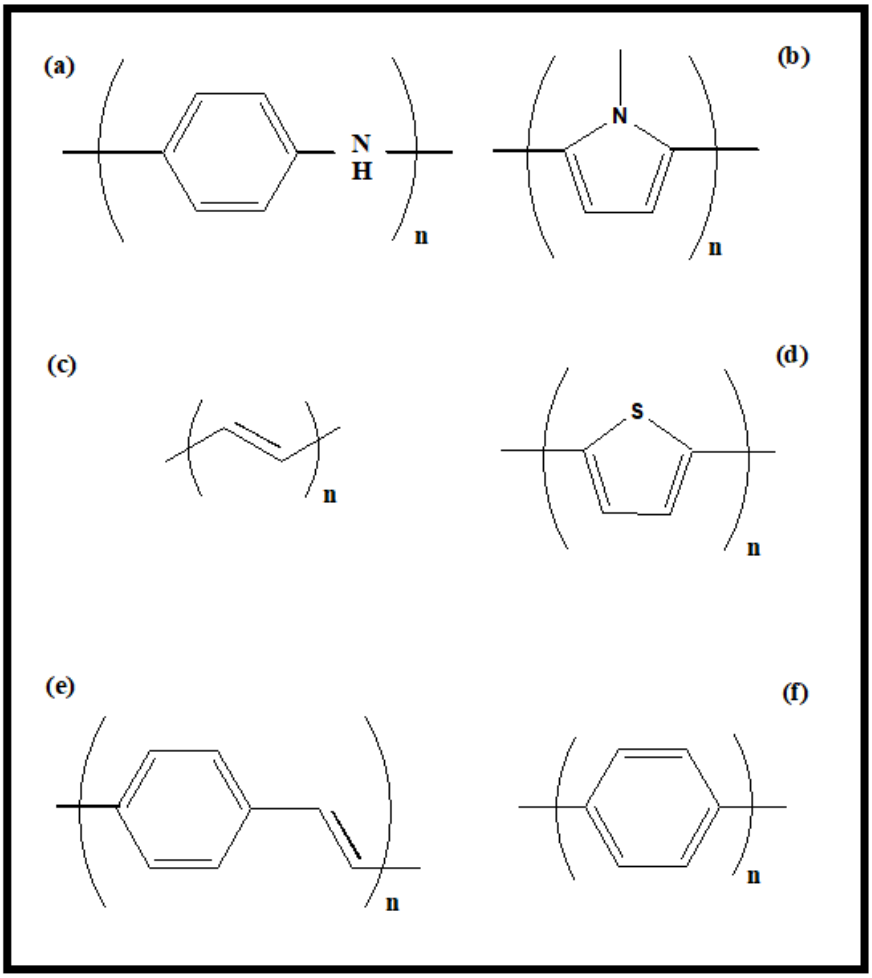

Figure 1.2 Structures of (a) Polyaniline, (b) Polypyrrole, (c) Polyacetylene, (d) Polythiophene, (e) Poly(p-phenylene vinylene) and (f) Poly(p-phenylene).

1.3 Adsorbents used for dye removal

1.3.1 Polyaniline

Polyaniline (PANI) has been extensively studied mainly because of its unique conductivity properties. The structure of PANI and several other conducting polymers are given in **Figure 1.2.** It has a great potential for industrial applications on a large scale. The broad applications of PANI are shown in **Figure 1.3 [16-22]**. The advantages of PANI are its easy synthesis, high electrical conductivity, low cost of raw materials, high stability, redox properties, lightweight, good processability, and outstanding magnetic and optical properties. PANI also exhibits relatively high porosity and surface and would be a good candidate for dye removal by adsorption.

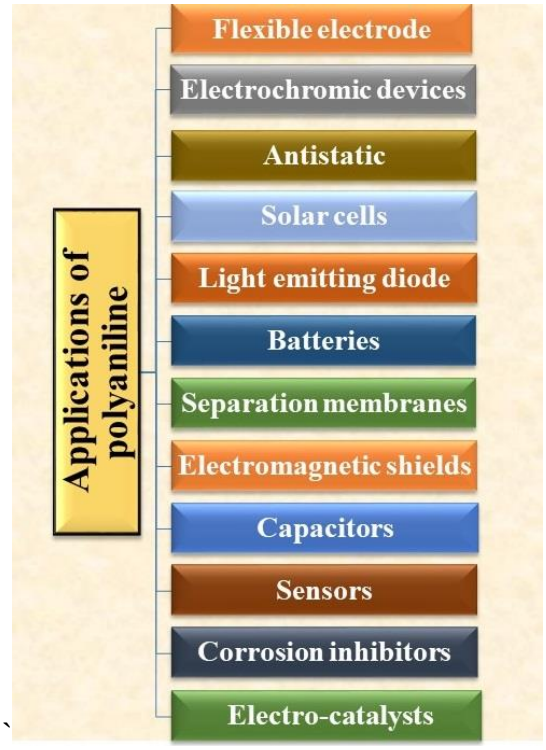

Figure 1.3 Applications of polyaniline

Polyaniline is synthesized from the aniline monomer either by electrochemical or chemical polymerization process **[23, 24]**. However, on a larger scale, chemical polymerization is the most suitable technique for the synthesis of polyaniline. Polyaniline is present in three oxidation states: emeraldine salt (ES) doped state and emeraldine base (EB) undoped state, pernigraniline base (PB), and leucoemeraldine base (LB) **[25, 26]**. The structure of polyaniline is presented in **Figure 1.4 [27].**

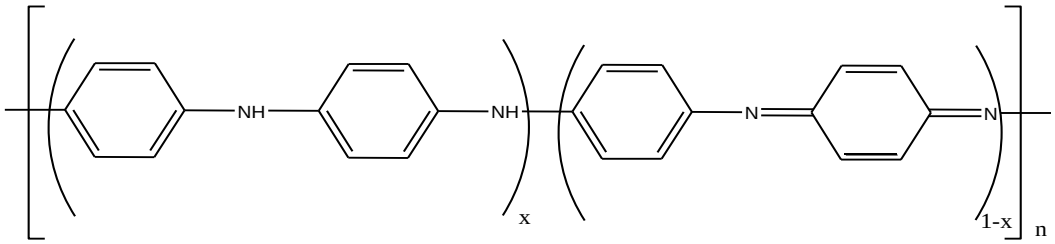

Figure 1.4 Structure of polyaniline **[27]**

In the general structural form of polyaniline, the oxidation state is described by (1-*x*) value, and the degree of polymerization is described by *n*. Leucoemeraldine base is fully reduced state and *x* = 1 for this state. Emeraldine is half oxidized state and *x* = 0.5. Pernigraniline base is a fully oxidized state, and *x* = 0 for this state **[27]**. The polyaniline emeraldine salt is a dark green powder (characteristic particle size: 3-100μm) of average density 1.36 g/mL and is soluble in various common organic solvents.

PANI synthesis has been researched a lot in the literature, but the optimization of the polymerization conditions has been related to PANI applications as a conductive polymer. Thus, there is an encryption scope for optimizing the polymerization condition of PANI for adsorption

applications. In addition, using PANI nanocomposite can be expected to significantly increase adsorption rate and quantity.

1.3.2 Polymer/clay nanocomposites

Polymer nanocomposites are such types of materials wherein at least one dimension of filler is less than 100 nm. Polymer nanocomposites are a better alternative to conventional filled polymers. A polymer nanocomposite (PCN) is a material with vastly improved properties compared to the individual constituent polymers. The PCN has been synthesized for most polymers of importance. The fillers used in the present study are nanoclays. The clay particles have several advantages: low cost, large surface area, high chemical stability, ultrafine particle size, high cation exchange capacity, high adsorption capacity, and ion exchange properties.

1.3.2.1 Nanofillers classification

Nanofillers are generally categorized as per their dimensions, i.e., one dimension, two dimensions, and three dimensions **[28-31]** as presented in **Figure 1.5**.

One dimension nanofillers: Nanofillers with one dimension are such types of fillers where only one dimension length is less than 100 nm (nanoplatelets). Some examples of one dimension nanofillers are montmorillonite (MMT) clays (layered silicate), carbon nanowalls, graphite nanoplatelets, etc**.** These one dimension nanofillers are frequently used in applications including biosensors, coatings, and biomedicine **[31].** Generally, these nanofillers are present in the shape of laminas, sheets, and shells.

Two-dimension nanofillers: Two dimensions nanofillers are such fillers wherein the length of two dimensions is usually less than 100 nm. Typically, these nanofillers are often in the form of

filaments, nanofibers, and nanotubes **[30,31]**. Examples of two dimensions nanofillers are gold nanotubes, silver nanotubes, carbon nanotubes, graphene, and cellulose whiskers, etc. **[31, 32].**

Three dimension nanofillers: Nanofillers with three dimensions are those where all three dimensions are in the nanometer scale (1-100 nm). The shapes of these nanofillers are cubical or spherical. Carbon black, nanoalumina, semiconductor nanoclusters, nano-silica, etc., are examples of three-dimensional nanofillers **[31, 32]**.

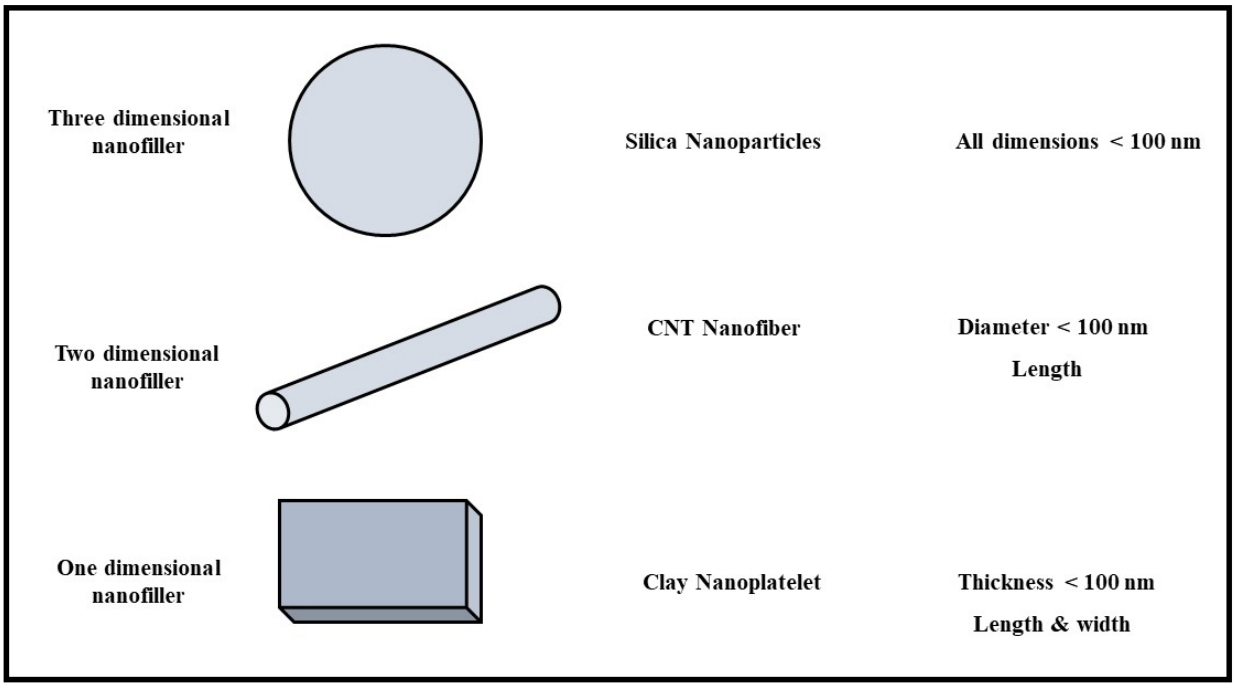

Figure 1.5 Typical dimensions of different nanofillers [**28]**.

1.3.2.2 Clays as nanofillers

Montmorillonite clay (MMT)

Montmorillonite (MMT) clay having the general formula $M_x(Al_{4-x}Mg_x)Si_8O_{20}(OH)_4$ belong to the family of 2:1 phyllosilicates (comprising of two tetrahedral and one octahedral sheet of average thickness 1 nm) **[33-35].** The structure of MMT clay is shown in **Figure 1.6 [36]**.

MMT is hydrophilic and should be compatible with PANI for the synthesis of polyaniline/clay nanocomposites. Because of its great cation exchange capacity, large surface area, and swelling ability, MMT clay is commonly used as a nanofiller to synthesize polymers nanocomposites. Moreover, combining polymer with clay can further improve their properties like optical, mechanical, electrical, and thermal properties **[21, 37]**.

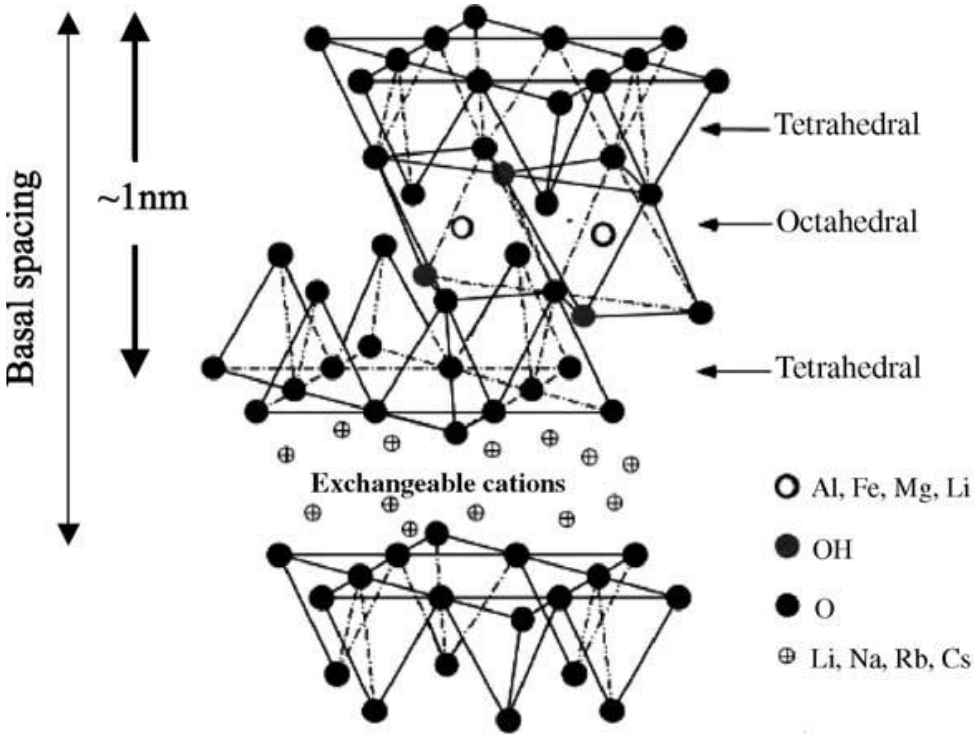

Figure 1.6 Montmorillonite (2:1 Phyllosilicates) clay structure **[36]**

Halloysite clay (HNT)

Halloysite (HNT) is a nano clay and is a 1:1 aluminosilicate, as shown in **Figure 1.7**. Halloysite has a hollow tubular structure with a chemical formula $Al_2Si_2O_5(OH)_4 2H_2O$. The external diameter of halloysite is 50 to 70 nm, and the length is 0.5 to 1 micrometer. A comparison of MMT and HNT clay is summarized in **Table 1.3 [38-40]**. Halloysite has numerous advantages like high cation exchange capacity, non-toxic, biocompatible, easier dispersion, high surface area, high aspect ratio, high porosity, high adsorption capacity, etc. **[40]**. Therefore, halloysite can be used as a nanofiller in nanocomposites synthesis to improve thermal and mechanical properties.

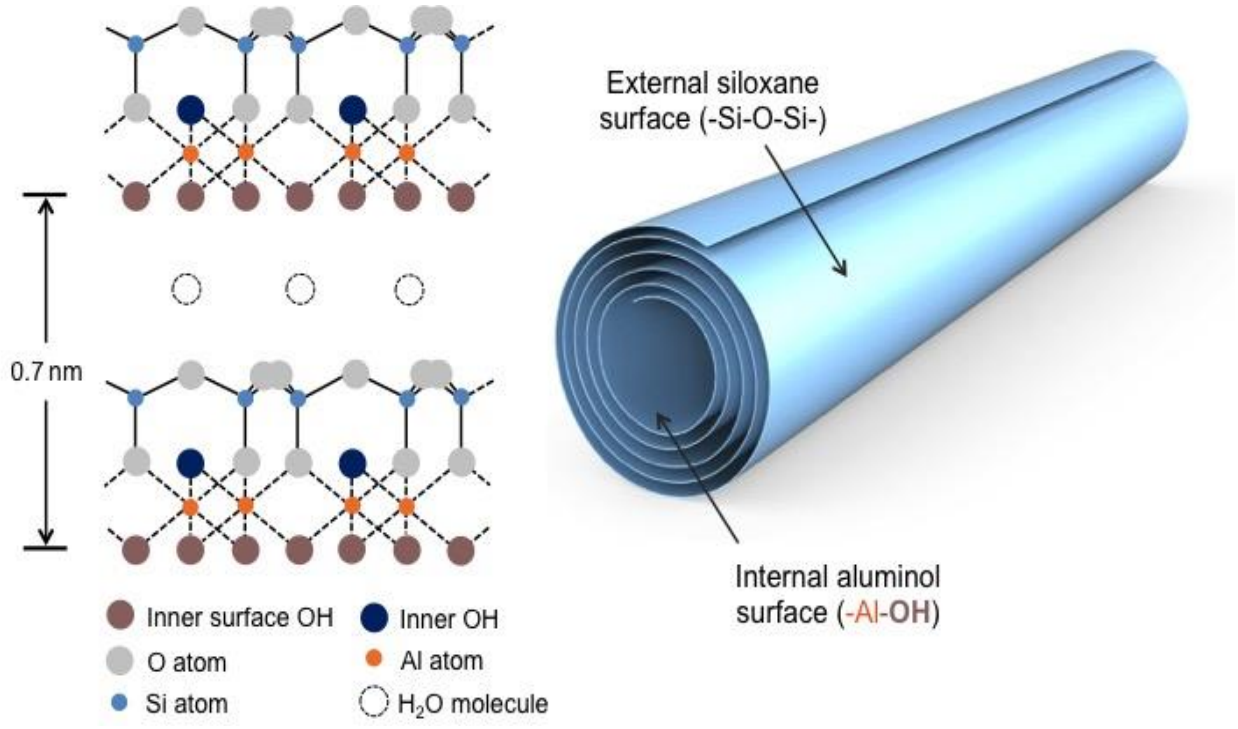

Figure 1.7 Structure of Halloysite clay **[41]**

Table 1.3 Characteristics of MMT and HNT clay **[38, 40]**

Clay	General Formula	Family	Structure
Montmorillonite (MMT)	$M_x(Al_{4-x}Mg_x)Si_8O_{20}(OH)_4$	2:1 Phyllosilicates (Two tetrahedral and one octahedral sheet)	Layered silicate
Halloysite (HNT)	$Al_2Si_2O_5(OH)_42H_2O$	1:1 Aluminosilicate (one tetrahedral and one octahedral sheet)	Tubular

1.3.2.3 Synthesis methods and different morphologies of polymer/clay nanocomposites

In-situ polymerization, melt intercalation, and solution polymerization is three methods by which polymer/clay nanocomposites can be synthesized. Out of these, *in-situ* polymerization is the most appropriate method due to its ease of achieving nanoscale interactions among the clay and polymer chains. From the synthesis of nanocomposites, three different types of structures can be attained depending upon the level of interaction between the hydrophobic polymer and layered silicate hydrophilic clay galleries (conventional, intercalated, and exfoliated nanocomposites) as depicted in **Figure 1.8**. Interaction and exfoliation chemistry can also depend on polymer and clay basic nature, synthesis methodology, and properties **[28].**

Conventional composite: In conventional composite, the d-spacing of layer silicate stays intact, which means polymer is unable to enter into the silicate layers, and the material is the same as the traditional composite.

Intercalated nanocomposite: The polymer is intercalated between inorganic clay layers, indicating a nanocomposite consisting of polymeric chains and intersperse inorganic layers. In this nanocomposite, the polymer insertion increases the basal spacing; however, the silicate sheets still exist in a stacked position.

Exfoliated nanocomposite: In this nanocomposite, the stacked clay layers are separated from one another and fully dispersed into the polymer matrix. The clay separation distance depends upon the clay filling. In an exfoliated structure, the interlayer spacing increases in the range of more than 80 -100°A **[28].** The properties enhancement in exfoliated nanocomposite is much more as compared to intercalated nanocomposite.

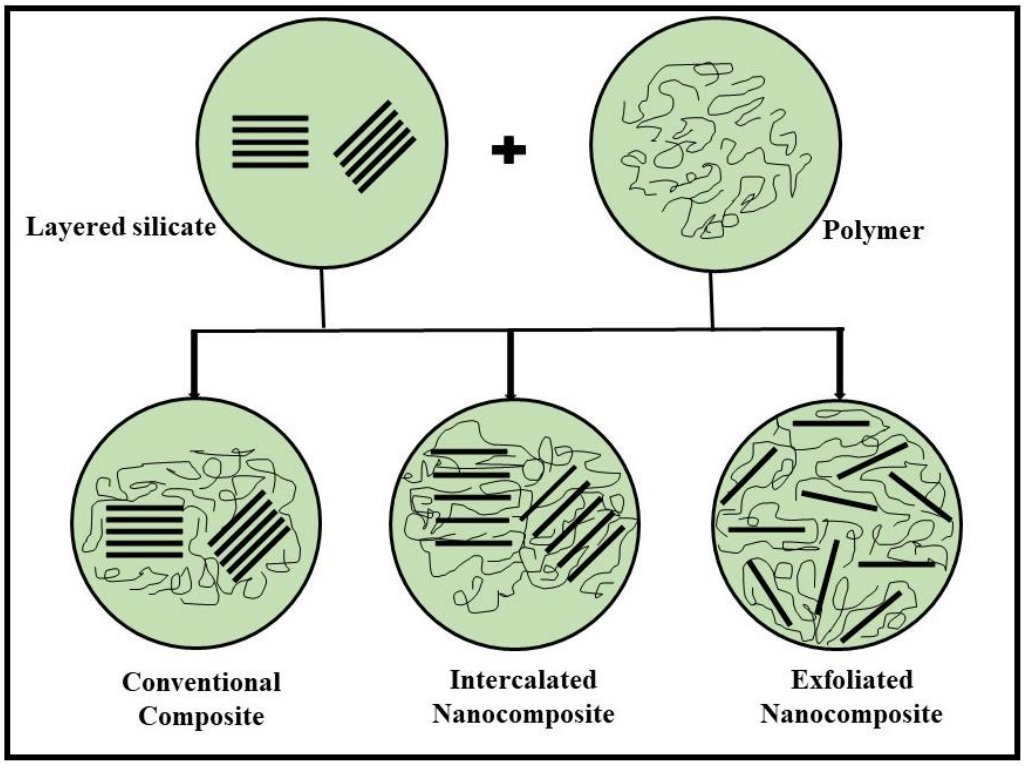

Figure 1.8 Different morphologies of polymer/clay nanocomposites **[42]**

1.3.3 Carbon aerogel

Carbon aerogel is a relatively new material in the nanotechnology industry, such as the aerospace and electronics industry. Porous carbon aerogels (CA) are mainly produced by sol-gel polymerization in the presence of resorcinol and formaldehyde **[43, 44]**. CA is available in three categories: organic, inorganic, and organic-inorganic.

Figure 1.9 Carbon aerogels: world's lightest material **[45]**

CA consist of a nanoporous structure with excellent physical properties such as high porosity, well-defined pore structure, large specific surface area, low density, high purity, high mechanical strength, conductivity, and high thermal & environmental stability. It has the distinction of being the lightest material in the world **[45]**. As can be seen in **Figure 1.9**, the carbon aerogel material is so light that it can perch on fragile flower petals without destroying them. The wide applications of CA are in the area of environmental protection, catalyst support, electromagnetic metamaterial, heavy metal or organic solvents absorption**,** biomedicine, hydrogen storage, biotechnology, thermal insulation, supercapacitors, adsorbents, membrane, energy storages and sensors **[44, 46-**

49]. Carbon aerogels have a three-dimensional structure with interconnected well-defined nano-sized particles. Carbon aerogels are available in four different forms, i.e., powder, monoliths, thin-film, and beads. The characteristics of carbon aerogels porous material are shown in **Figure 1.10**. The structure of CA is like a carbon sponge **[45]**. It has a high absorption capacity. It can absorb more than its weight.

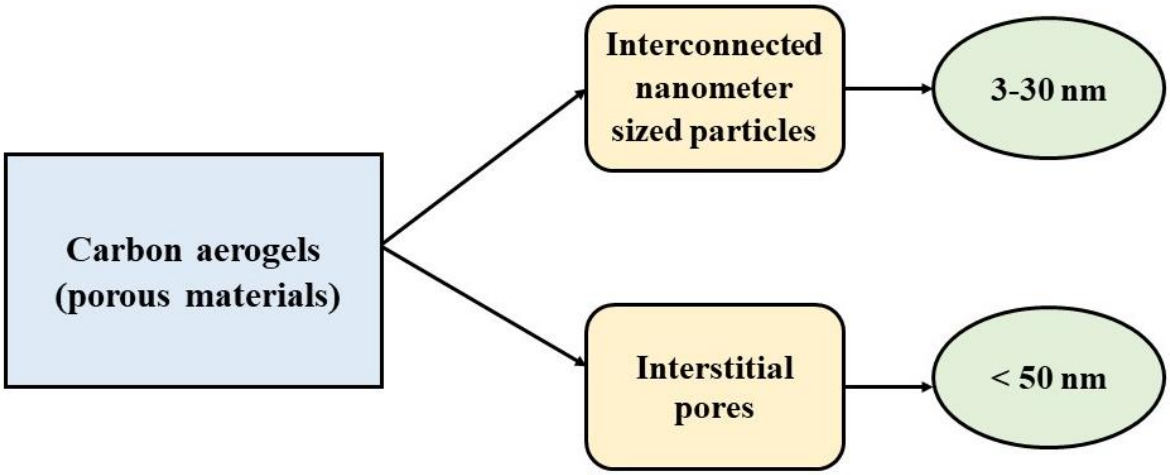

Figure 1.10 Characteristics of carbon aerogels

In this chapter, the basic information about polyaniline, clays, and carbon aerogels has been discussed. The next chapter will discuss the past, present, and future developments in the field of polyaniline, clay, carbon aerogels, and its nanocomposites.

References

[1] Koswojo R, Utomo RP, Ju YH, Ayucitra A, Soetaredjo FE, Sunarso J, Ismadji S (2010) Acid Green 25 removal from wastewater by organo-bentonite from Pacitan. Appl Clay Sci 48: 81-86. https://doi.org/10.1016/j.clay.2009.11.023.

[2] Salahuddin NA, Ayad MM, Essa ME (2015) Modified chitosan for efficient dye adsorption in low acid media. Int J Mater Chem 5:54-63. DOI: 10.5923/j.ijmc.20150503.02.

[3] Wang L, Zhang J, Wang A (2011) Fast removal of methylene blue from aqueous solution by adsorption onto chitosan-g-poly (acrylic acid)/attapulgite composite. Desalination 266:33–39. Doi:10.1016/j.desal.2010.07.065.

[4] Bulut Y and Karaer H (2015) Removal of methylene blue from aqueous solution by crosslinked chitosan-g-poly(acrylic acid)/bentonite composite. Chem Eng Commun 202:1635-1644. https://doi.org/10.1080/00986445.2014.968713.

[5] Palaniappan S, John A (2008) Polyaniline materials by emulsion polymerization pathway. Prog Polym Sci 33:732-758. Doi:10.1016/j.progpolymsci.2008.02.002.

[6] Ansari R, Samaneh, Alaei and Khah AM (2011) Application of polyaniline for removal of acid green 25 from aqueous solution. J Sci Ind Res 70:804-809.

[7] Baei MS, Babaee V, Pirouz F (2011) Preparation of polyaniline nanocomposites for removal of sulfate from wastewater. 2nd International Conference on Chemistry and Chemical Engineering 14:95.

[8] Olad A, Rashidzadeh A (2012) Poly(N-vinylpyrrolidone) modified polyaniline/Na^+-cloisite nanocomposite: Synthesis and characterization. Fiber Polym 13:16-20. DOI 10.1007/s12221-012-0016-0.

[9] Souza FG, Sirelli L, Michel RC, Soares BG, Herbst MH (2006) *In situ* polymerization of aniline in the presence of carbon black. J Appl Polym Sci 102:535-541. DOI:10.1002/app.24280.

[10] Mahanta D, Madras G, Radhakrishnan S, Patil S (2008) Adsorption of sulfonated dyes by polyaniline emeraldine salt and its kinetics. J Phys Chem 112:10153-10157. https://doi.org/10.1021/jp803903x.

[11] Kalotra S. and Mehta R (2020) Synthesis of polyaniline/clay nanocomposites by *in situ* polymerization and its application for the removal of Acid Green 25 dye from wastewater. Polymer Bulletin. 78:2439-2463. https://doi.org/10.1007/s00289-020-03222-3.

[12] Liu T, Li Y, Du Q, Sun J, Jiao Y, Yang G, Wang Z, Xia Y, Wang W, Wang K, Zhu H, Wu D (2012) Adsorption of methylene blue from aqueous solution by graphene. Colloids Surf B: Biointerfaces 90:197– 203. https://doi.org/10.1016/j.colsurfb.2011.10.019.

[13] Rida K, Bouraoui S, Hadnine S (2013) Adsorption of methylene blue from aqueous solution by kaolin and zeolite. Appl Clay Sci 83–84:99–105. DOI:10.1016/j.clay.2013.08.015.

[14] Wei C, Xu Z, Han F, Xu W, Gu J, Ou M, Xu X (2018) Preparation and characterization of poly(acrylic acid-co-acrylamide)/montmorillonite composite and its application for methylene blue adsorption. Colloid Polym Sci 296:653–667. https://doi.org/10.1007/s00396-018-4277-z.

[15] Yılmaz S, Zengin, A, Ecer U, Şahan,T (2019) Conversion from a natural mineral to a novel effective adsorbent: Utilization of pumice grafted with polymer brush for methylene blue decolorization from aqueous environments. Colloids Surf, A Physicochem Eng Asp 583:123961. https://doi.org/10.1016/j.colsurfa.2019.123961.

[16] Babazadeh M (2009) Aqueous dispersions of DBSA-doped polyaniline: One-pot preparation, characterization, and properties study. J Appl Polym Sci 113:3980–3984. https://doi.org/10.1002/app.30460.

[17] Sun F, Pan Y, Wang J, Wang Z, Hu C, Dong Q (2009) Synthesis of conducting polyaniline-montmorillonite nanocomposites *via* inverse emulsion polymerization in supercritical carbon dioxide. Polym Compos 31:163. https://doi.org/10.1002/pc.20783.

[18] Salem MA (2010) The role of polyaniline salts in the removal of direct blue 78 from aqueous solution: A kinetic study. React Funct Polym 70:707-714. Doi:10.1016/j.reactfunctpolym.2010.07.001.

[19] Kalaivasan N and Shafi SS (2010) Synthesis of various polyaniline/clay nanocomposites derived from aniline and substituted aniline derivatives by mechanochemical intercalation method. E-J Chem 7(4):1477-1483. https://doi.org/10.1155/2010/364680.

[20] Elsayed AH, Eldin MSM, Elsyed AM, Elazm AHA, Younes EM, Motaweh HA (2011) Synthesis and properties of polyaniline/ferrites nanocomposites. Int J Electrochem Sci 6:206-221.

[21] Kazim S, Ahmad S, Pfleger J, Plestil J, Joshi YM (2012) Polyaniline–sodium montmorillonite clay nanocomposites: Effect of clay concentration on thermal, structural, and electrical properties. J Mater Sci 47:420-428. DOI 10.1007/s10853-011-5815-y.

[22] Massoumi B and Mohammadi R (2013) Synthesis of nanostructured polyaniline *via* chemical oxidative polymerization: Investigation of morphology and conductivity of the prepared polymers. Polym Sci Ser B 55:593–600.

[23] Pande S, Swaruparani H, Bedre MD, Bhat R, Deshpande R, Venkataraman A (2012) Synthesis, characterization and studies of PANI-MMT nanocomposites. Nanosci Nanotechnol 2:90-98. DOI: 10.5923/j.nn.20120204.01.

[24] Benhebal H, Chaib M, Leonard AL, Crine M, Lambert SD (2014) Preparation of polyaniline-modified local clay and study of its sorption capacity. J Nanost Chem 4:98. DOI:10.1007/s40097-014-0098-x.

[25] Yeh JM, Liou SJ, Lai CY and Wu PC (2001) Enhancement of corrosion protection effect in polyaniline *via* the formation of polyaniline-clay nanocomposite materials. Chem Mater 13:1131-1136. Doi:10.1021/cm000938r.

[26] Stejskal J and Gilbert RG (2002) Polyaniline, preparation of a conducting polymer. Pure Appl Chem 74:857-867.

[27] Palaniappan S, John A, Amarnath CA, Rao VJ (2004) Mannich-type reaction in solvent free condition using reusable polyaniline catalyst. J Mol Catal A: Chem 218:47–53. Doi:10.1016/j.molcata.2004.04.010.

[28] Olad A (2011) Polymer/Clay Nanocomposites, advances in diverse industrial applications of nanocomposites, Dr. Boreddy Reddy (Ed.), ISBN: 978-953-307-202-9.

[29] ISO/TS27687 (2008) Nanotechnologies - Terminology and definitions for nano-objects – Nanoparticle, nanofibre, and nanoplate.

[30] Marquis DM, Guillaume E and Chivas-Joly C (2011) Properties of nanofillers in polymer, nanocomposites and polymers with analytical methods, Dr. John Cuppoletti (Ed.), ISBN: 978-953-307-352-1.

[31] Akpan EI, Shen X, Wetzel B, Friedrich K (2019) Design and synthesis of polymer nanocomposites. Polymer composites with functionalized nanoparticles 47-83. https://doi.org/10.1016/B978-0-12-814064-2.00002-0.

[32] Kumar AP, Depan D, Tomer NS, Singh RP (2009) Nanoscale particles for polymer degradation and stabilization – Trends and future prospective. Prog Polym Sci 34:479-515. DOI:10.1016/j.progpolymsci.2009.01.002.

[33] Sangamesha MA, Pushpalatha K, Shekar GL (2014) Synthesis and characterization of conducting polyaniline/copper selenide nanocomposites. J Adv Chem Sci 2:223-227.

[34] Karthikaikumar S, Karthikeyan M and Satheesh Kumar KK (2014) Removal of congo red dye from aqueous solution by polyaniline - montmorillonite composite. Chem Sci Rev Lett 2(8):606-614. ISSN 2278-6783. Article CS2320430911.

[35] Olad A and Azhar FF (2014) Eco-friendly biopolymer/clay/conducting polymer nanocomposite: characterization and its application in reactive dye removal. Fiber Polym 15:1321-1329. DOI 10.1007/s12221-014-1321-6.

[36] Ray S.S, Okamoto M (2003) Polymer/layered silicate nanocomposites: A review from preparation to processing. Prog Polym Sci 28:1539–1641. Doi:10.1016/j.progpolymsci.2003.08.002.

[37] Vijayakumar B, Anjana KO and Ranga Rao G (2015) Polyaniline/clay nanocomposites: preparation, characterization and electrochemical properties. IOP Conf Ser: Mater Sci and Eng 73:012112. Doi:10.1088/1757-899X/73/1/012112.

[38] Pavlidou S, Papaspyrides CD (2008) A review on polymer–layered silicate nanocomposites. Prog Polym Sci 33:1119–1198. https://doi.org/10.1016/j.progpolymsci.2008.07.008.

[39] Vergaro V, Abdullayev E, Lvov YM, Zeitoun A, Cingolani R, Rinaldi R, & Leporatti S (2010) Cytocompatibility and uptake of halloysite clay nanotubes. Biomacromolecules 11(3):820–826.. Doi: 10.1021/bm9014446.

[40] Kamble R, Ghag M, Gaikawad S, Panda BK (2012) Halloysite nanotubes and applications: A review. J Adv Scient Res 3:25-29.

[41] Halloysite clay [https://phantomplastics.com/functional-fillers/halloysite/ (Accessed on 12/08/2020)].

[42] Alexandre M, Dubois P (2000) Polymer-layered silicate nanocomposites: Preparation, properties and uses of a new class of materials. Mater Sci Eng R Rep 28:1-63. https://doi.org/10.1016/S0927-796X(00)00012-7.

[43] Saquing CD, Cheng TT, Aindow M and Erkey C (2004) Preparation of platinum/carbon aerogel nanocomposites using a supercritical deposition method. J Phys Chem B 108:7716-7722. Doi: 10.1021/jp049535v.

[44] Bakierska M, Chojnacka A, Swietosławski M, Natkanski P, Gajewska M, Rutkowska M and Molenda M (2017) Multifunctional Carbon aerogels derived by sol–gel process of natural polysaccharides of different botanical origin. Materials 10:1336. Doi: 10.3390/ma10111336.

[45] Carbon aerogel

(https://avax.news/educative/Carbon_aerogel_the_new_lightest_material.html).

[46] Shariff AM, Beshir DM, Bustam MA, and Maitra S (2010) Some studies on the synthesis and characterization of carbon aerogel. Trans Ind Ceram Soc 69:1-4. http://dx.doi.org/10.1080/0371750X.2010.11090822.

[47] Xu X, Zhou J, Nagaraju DH, Jiang L, Marinov VR, Lubineau G, Alshareef HN, and Oh M (2015) Flexible, highly graphitized carbon aerogels based on bacterial cellulose/lignin: Catalyst-

free synthesis and its application in energy storage devices. Adv Funct Mater 25:3193–3202. DOI: 10.1002/adfm.201500538.

[48] Hu E, Shang S, Tao X-M, Jiang S, Chiu K-L (2016) Regeneration and reuse of highly polluting textile dyeing effluents through catalytic ozonation with carbon aerogel catalysts. J Clean Prod 137:1055-1065. DOI: 10.1016/j.jclepro.2016.07.194.

[49] Zhao W, Zhu J, Wei W, Ma L, Zhu J and Xie J (2018) Comparative study of modified/non-modified aluminum and silica aerogels for anionic dye adsorption performance. RSC Adv 8:29129. DOI: 10.1039/c8ra05532g.

CHAPTER 2

LITERATURE REVIEW

In this chapter, the literature survey has been given on the synthesis and characterization of polyaniline (PANI) and PANI/clay nanocomposites, carbon aerogels (CA), and its nanocomposites. It mainly covers the literature on the adsorption of textile wastewater (Methylene blue and Acid green 25 dye) using PANI and PANI/MMT, CA and PANI/CA nanocomposites as an adsorbent. Currently, polymer/clay nanocomposites are emerging as the most prominent materials for wastewater treatment. Carbon aerogel is a new emerging material because of its extremely low density, thereby affording a large surface area.

2.1 Conducting Polymers

2.1.1 Polyaniline (PANI)

PANI is a highly conducting polymer synthesized through electrochemical and chemical methods **[1]**. PANI has been used as a cathode material for rechargeable batteries **[2].** PANI is also used in biomedical applications such as tissue engineering, drug delivery, neural, cardiac, and neural probes **[3, 4].** It has good electrical conductivity and therefore is used in numerous electrical devices, including sensors, electrochromic devices, light-emitting diodes, and supercapacitors **[3].** PANI can also be used to protect mild steel from corrosion **[5].**

Several reviews on polyaniline have been reported by many researchers, which cover the synthesis of polyaniline and its applications **[5-32]**.

Polyaniline salt and base powder have been synthesized in several studies using different catalysts such as hydrochloric acid, sulfuric acid, sodium lauryl sulphate, dodecylbenzene-sulfonic acid, and oxidizing agents such as ammonium persulfate, sodium persulfate, as shown in **Table 2.1**. From all these studies, it was concluded that the lower temperature is the most preferred temperature for the polymerization process because it gives a higher yield. A summary of the literature review on PANI synthesis is given in **Table 2.1**.

Table 2.1 A literature review on PANI salt and PANI base polymerization

Sr. No.	Monomer	Catalyst	Oxidizing agent	Reaction conditions for PANI salt	Reaction conditions for PANI base	References
1.	Aniline	HCl	Ammonium persulfate	T = 0°C Time = ~ 2 h Emeraldine salt (ES) powder dried at room temperature	Ammonium hydroxide T = room temperature Time = 3 h Emeraldine base (EB) powder dried for 48 h	**[33]**
2.	Aniline hydrochloride	-	Ammonium peroxydisulfate	T = room temperature (~18 – 24°C) Time = overnight ES powder dried in the air than in vacuum at 60°C	Not studied	**[34]**
3.	Aniline	HNO_3	Ammonium persulfate	T = 0°C Time = 24 h	Ammonium hydroxide	**[35]**

					T = room temperature Time = 24 h EB powder dried in a vacuum for 48 h	
4.	Aniline	HCl	Ammonium persulphate	Time = overnight	Ammonium hydroxide Time = overnight EB powder dried in desiccator = 24 h	**[36]**
5.	Aniline	H_2SO_4	Sodium persulfate	T = 5–10^oC Time = 4 h ES powder dried at 100^oC	Sodium hydroxide solution T = ambient temperature Time = 8 h EB powder dried at 100^oC	**[37]**
6.	Aniline	HCl	Ammonium persulfate	T = - 30 to ±1^oC Time = 6 h	Ammonium hydroxide T = - 30 to ±1^oC EB powder dried at 50^oC	**[38]**
7.	Aniline	HCl	Ammonium persulphate	T = below 5^oC.	Ammonium hydroxide solution T = below 5^oC Time = 24 h	**[39]**
8.	Aniline	Dodecylbenzene-sulfonic	Ammonium peroxysulfate	T = 0^oC Time = 6 h Dried ES powder	Not studied	**[40]**

		acid (DBSA)				
9.	Aniline	HCl	Ammonium persulfate	The reaction mixture was left stirring for 2 h at 0-5^{o}C and left unstirred overnight at room temperature ES powder dried at 50-60^{o}C	Sodium hydroxide T = room temperature Time = 2 h EB powder dried at 60^{o}C	**[41]**
10.	Aniline	Dodecylbenzene-sulfonic acid (DBSA)	Ammonium persulphate	T = room temperature Time = 24 h	Not studied	**[42]**
11.	Aniline	HCl	Ammonium persulfate	T = 0^{o}C ES powder at 60^{o}C	Not studied	**[43]**
12.	Aniline	HCl	Ammonium persulfate	T = 30^{o}C Time = 24 h	Ammonia solution T = room temperature Time = 3 h EB powder dried at 80^{o}C for 12 h	**[44]**
13.	Aniline	H_2SO_4, H_3PO_4 and HNO_3	Ammonium persulfate	T = 25^{o}C Time = 1 h ES powder dried at 60^{o}C overnight3	Not studied	**[45]**

14.	Aniline	HCl	Ammonium peroxysulfate	Ice bath Time = 24 h ES powder dried at 40^{o}C for 24 h	Ammonium hydroxide Ice bath Time = several hours, until pH reached 9 Dried EB powder for 24 h at 40^{o}C	**[46]**
15.	Aniline	H_2SO_4	KIO_3	T = room temperature Time = 4 h ES powder dried at room temperature	Not studied	**[47]**
16.	Aniline	1M HCl/LiCl or 1M CF_3COOH (Trifluoroacetic acid)	Ammonium persulphate	T = -15^{o}C -5^{o}C +5^{o}C Time = 2 h Dried ES powder foam	Ammonium hydroxide T = -15^{o}C -5^{o}C +5^{o}C Time = overnight Dried EB powder foam	**[48]**
17.	Aniline	H_2SO_4	Ammonium persulfate solution	Polymerization was carried out at a cold temperature ES powder dried for 2 days	Not studied	**[49]**
18.	Aniline	HCl	Ammonium peroxidisulphate	T = 0^{o}C Time = 10 h ES powder dried at 60^{o}C for 24 h	Not studied	**[50]**

19.	Aniline	HCl	Sodium persulfate	T = 25-30^{o}C Time = 4 h	Sodium hydroxide solution T = 25-30^{o}C Time = 4 h ES powder dried at 50^{o}C	**[51]**
20.	Aniline	HCl	Ammonium Persulfate	T = room temperature Time = 24 h	Ammonia solution Time = 4 h at room temperature	**[52]**
21.	Aniline	Sodium lauryl sulphate (SLS) and HCl	Ammonium persulfate	T = 0 ± 1^{o}C Time = 1h ES powder dried at 45^{o}C for 8 h	Not studied	**[53]**
22.	Aniline	HCl	Ammonium persulphate	T = - 0^{o}C ES powder dried at 60^{o}C	Not studied	**[54]**
23.	Aniline	HCl and SDS	Ammonium persulfate	T = 25^{o}C Time = 24 h ES powder dried at 60^{o}C for 24 h	Not studied	**[55]**
24.	Aniline	HCl	Ammonium peroxidisulphate	T = 5–10^{o}C Time = 3 h ES powder dried at 80^{o}C for 6 h	Not studied	**[56]**

2.1.2 Synthesis of polyaniline nanocomposites using various types of fillers (other than nanoclay)

Many researchers have explored the preparation of polyaniline nanocomposites by using different types of fillers. It is a well-accepted fact that the polymer interaction with the surface of the fillers will enhance the nanocomposite properties. That is the reason researchers are more interested in developing compatable nanocomposite materials for different applications.

Maser et al., [57] reported the *in-situ* fabrication of polyaniline/carbon nanotube and characterization of the composites. **Ramamurthy *et al.*, [38]** used a solution processing method to prepare polyaniline/multiwalled carbon nanotube composite and investigated their electrical and mechanical properties. The mechanical and thermal stability of polyaniline with 1% carbon nanotubes is greater than that of pure polyaniline and is suitable for electronic devices.

Ma *et al.*, [58] worked on the synthesis of polyaniline/TiO_2 through an *in-situ* polymerization method to investigate the gas-sensitivity behavior. **Wu *et al.*, [59]** synthesized PANI/Fe_2O_3 composite through an *in-situ* method with dodecylbenzene sulfonic acid (DBSA) and studied their conductivity and gas sensing behavior. **Wu *et al.*, [60]** prepared nanocomposites by synthesizing PANI with carbon black and investigating their microwave absorbing and electromagnetic properties. **Choudhury, [61]** reported the polymerization of polyaniline/silver nanocomposites to evaluate the AC conductivity, ethanol vapor sensitivity, and dielectric properties. **Kumar and Selvarajan, [62]** synthesized PANI/CeO_2 nanocomposites using microwave-assisted solution method and characterized with TEM, SEM, XRD, FTIR, and UV-Vis spectroscopy. They concluded that the nanocomposites that were created could be used to fabricate films or coatings.

Prasanna and Jayanna, [63] polymerized and studied the dielectric and AC conductivity properties of PANI/$CoFe_2O_4$ nanocomposites. The maximum conductivity was found with a $CoFe_2O_4$ amount of 60 wt% in PANI. For pure $CoFe_2O_4$, the maximum dielectric constant values were found at lower frequencies. **Fan *et al.*, [64]** polymerized graphene/polyaniline nanocomposite via *in-situ* polymerization and used it as electrode material to determine the electrochemical behavior of 4-aminophenol. **Elsayed *et al.*, [46]** worked on the synthesis (chemical method) and studied the properties of polyaniline/ferrite nanocomposites. **Ghatak *et al.*, [65]** reported the *in-situ* polymerization and characterization of prepared polyaniline/carbon nanotube composites.

Yerawar, [66] prepared polyaniline/zinc oxide by the use of *in-situ* chemical oxidative polymerization. They found that the conductivity of a composite containing 20% wt of zinc oxide is observed to be higher than that of polyaniline and all other composites. **Oh and Kim, [67]** have reported the synthesis of polyaniline/activated composites in the presence of carbon dodecyl benzenesulfonic acid (DBSA) through chemical oxidation polymerization. They study the effect of DBSA concentrations on polyaniline/activated composites. **Farbod *et al.*, [68]** studied the polymerization of functionalized and pure multiwall carbon nanotube/polyaniline composites. A study was performed to measure the glass transition temperature and electrical resistivity. **Li *et al.*, [69]** first prepared sandwich-like polyaniline/graphene nanosheets through chemical oxidation polymerization and then evaluated the electrochemical properties.

Zhao *et al.*, [70] reported the fabrication of a ternary sulfur/PANI/carbon black composite using a two-step thermal treatment for lithium-sulfur batteries. In sulfur/PANI/carbon black composites, PANI works as a connector among sulfur and carbon black; this improved the electrochemical

performance and reduced the active material loss in lithium-sulfur batteries. **Sedaghat and Golbaz, [71]** discussed the *in-situ* preparation of polyaniline/manganese dioxide nanocomposites, and results found an improvement in morphology compared to the pure PANI. **Zhou *et al.*, [72]** synthesized composite via oxidative polymerization method. As a result, the high relative strength and high conductivity were obtained in polyaniline/viscous fiber composite**. Xu and Xing, [73]** prepared polyaniline/zinc oxide using *in-situ* polymerization and used it as a photocatalyst for methylene blue dye degradation.

Polyaniline/copper selenide nanocomposite was prepared by **Sangamesha *et al.*, [54]**. The ordered structure of the polymer composite was shown by the XRD pattern. The obtained results suggest that the prepared nanocomposite could be used as a multifunctional material for various nanoelectronic devices. **Jayasudha *et al.*, [74]** synthesized polyaniline/silver nanocomposites through *in-situ* polymerization by varying 3% to 25% silver content. They studied the structural, electrical, and optical properties and also evaluated the DC electrical conductivity of nanocomposites.

Nadaf and Venkatesh, [75] used the oxidative polymerization method to fabricate polyaniline/copper oxide nanocomposites and characterized them by scanning electron and X-ray diffraction techniques. **Shendkar *et al.*, [76]** studied the supercapacitive performance of electrochemically polymerized polyaniline/cobalt hydroxide hybrid nanocomposites**. Olad and Gharekhani, [77]** polymerized polyaniline/activated carbon/polyvinyl alcohol nanocomposites with the help of *ex-situ* chemical synthesis method and use it as a supercapacitor electrode. Compared to the AC electrode, the results show that the nanocomposite electrode has a specific capacitance rise of more than 166 percent with 0.3 wt% of PANI amount.

Padmapriya *et al.*, [78] used emeraldine salt polyaniline-coated copper surface as a cathode material to investigate the hydrogen evolution reaction. The synthesis of polyaniline/cobalt chloride composites was successfully done by **Majhi *et al.*, [79]** by *in-situ* polymerization for supercapacitor application. They successfully improved the electrochemical performance and thermal properties of composites and use them for supercapacitor application as an electrode material. **Oliveira *et al.*, [80]** worked on the preparation of conductive films made by a combination of polyaniline, cellulose, and silver nanoparticles and improved their mechanical properties.

Zhang *et al.*, [81] reported the synthesis of $Ti_3C_2T_x$/co-doped PANI EMI shielding composite films via vacuum-assisted filtration method. These composite films have potential uses in high-tech fields where EMI shielding materials must be ultrathin and lightweight. **Biswas *et al.*, [82]** reported the synthesis of bismuth vanadate/graphene oxide/polyaniline via the hydrothermal method for visible-light photocatalysts performance. **Yanilmaz *et al.*, [83]** prepared flexible polyaniline/carbon nanofiber electrodes through sol-gel and electrospinning techniques for supercapacitor electrodes. **Aljafari *et al.*, [84]** prepared and studied the photoelectric and electrochromic properties of polyaniline-based redox-active gel material. **Mu *et al.*, [85]** polymerized cobalt (II) coordinated PANI electrodes through a facile electropolymerization and hydrothermal method for conversion devices and energy storage applications. **Yang *et al.*, [86]** use an *in-situ* polymerization method to develop graphene oxide/polyaniline nanocomposites. The author concluded that the coating of graphene oxide/polyaniline (4 wt %) nanocomposite won steel improved the corrosion protection efficiency compared to pure epoxy, polyaniline, and graphene oxide coating. The reported literature on PANI nanocomposites for various applications is summarized in **Table 2.2**.

Table 2.2 Literature summary on PANI nanocomposites (other than nanoclay) for various applications

Sr. No.	Polymer and their nanocomposite	Synthesis Method	Characterization techniques	Applications	References
1.	Polyaniline-coated electroactive paper actuators	Electrochemical	XRD, SEM, thickness measurement, actuation of bilayer and trilayer	Actuation behavior	**[87]**
2.	Polyaniline/ɤ-Al_2O_3	*In-situ* polymerization	FTIR, XRD, TGA, modulated differential scanning calorimetry	-	**[88]**
3.	Polyaniline/Nylon 6	Solvent casting	SEM, electrical conductivity, mechanical test, thermal stability studies, UV-Vis spectra	-	**[89]**
4.	Polyaniline/carbon nanotubes	*In-situ* polymerization	FTIR, SEM, TEM, galvanostatic charge/discharge, cyclic voltammetry, impedance, and cycle life measurements	Electrode material for supercapacitors	**[90]**
5.	Polyaniline/iron oxide nanoparticles	*In-situ* polymerization	TEM, TGA, FTIR, UV-Vis spectra,	Improve thermal stability	**[91]**

6.	Bacterial cellulose/polyaniline nanocomposites	*In-situ* polymerization	XRD, SAXS SEM, ATR-FTIR, TGA, electrical conductivity	Optical and electrical displays	**[92]**
7.	Polyaniline/silver	*In-situ* polymerization	UV-Vis spectra, AFM, SEM, XRD, dielectric measurements, and temperature-dependent resistivity	Improve electrical properties	**[93]**
8.	polyaniline/cerium(III)-nitrate-hexahydrate	*In-situ* polymerization	UV-Vis spectra, FTIR, DSC, SEM-EDX, dielectric measurements	Enhanced thermal and dielectric properties	**[94]**
9.	PANI/functionalized carbon nanofibers	*In-situ* mechanochemical polymerization	XRD, SEM, TEM, FTIR, UV-Vis spectra, DSC, TGA, electrochemical Measurements	Enhanced electrochemical capacitance	**[95]**
10.	Polyaniline-coated sulfur/conductive-carbon black composites	*In-situ* oxidative polymerization	XRD, SEM, TEM, FTIR, cyclic voltammetry, EIS spectra	As a cathode material for lithium/sulfur batteries	**[96]**
11.	Polyaniline-grafted reduced graphene oxide composite	*In-situ* chemical oxidative polymerization	FTIR, Raman spectra, XRD, XPS, FESEM, HR-TEM, TGA, cyclic voltammetry	Electrochemical Supercapacitors	**[97]**

12.	Polyaniline/carbon black	Layer-by layer assembly	TEM, SEM, Zeta potential, IR spectrum, magnetic property, and electrochemical tests	Electrode materials for supercapacitors	**[98]**
13.	Graphene/ polyaniline nanocomposite	Chemical oxidative polymerization	FTIR, XRD, BET, UV-Vis spectra, XPS, SEM	Enhanced sensitivity of ammonia sensor	**[99]**
14.	Hierarchical hollow spheres of Fe_2O_3 @polyaniline	Template-free method	SEM, HR-TEM, Raman spectra, BET, electrochemical measurements, electrochemical impedance spectroscopy	Lithium-ion battery anodes	**[100]**
15.	Reduced graphene oxide/polyaniline nanocomposites	Chemical oxidative polymerization	SEM, TEM, XPS, FTIR, IR	Supercapacitor	**[101]**
16.	Polyaniline/coated filter papers	Chemical oxidation polymerization	UV−Vis spectra, FTIR, TGA, SEM	Hybrid materials for dye adsorption	**[102]**
17.	Hierarchically nanostructured polyaniline/ functional multiwalled carbon	*In-situ* polymerization	SEM, TEM, FTIR, gas sensitivity analysis	High-Performance Gas Sensing	**[103]**

	nanotube nanocomposite				
18.	Polyaniline/graphene oxide composites	Physical mixture method	XRD, FTIR, SEM, DSC,	Aerospace	**[104]**
19.	3D Crumpled Graphene/Carbon Nanotube/Polyaniline Composites	Aerosol-spray process	SEM, TEM,EDS, XRD, FTIR, BET	Supercapacitors	**[105]**
20.	Core-shell polyaniline/ferrite composite	*In-situ* polymerization	XRD, XRF, FTIR, TEM, TGA, DTA	Magnetic properties	**[106]**
21.	Layer-by-layer sandwiched graphene/polyaniline nanorods/carbon nanotubes Heterostructure	*In-situ* polymerization and top-down step	XRD, XPS, N_2 adsorption-desorption, Raman spectroscopy, FESEM, and TEM	Supercapacitors electrodes	**[107]**
22.	3D porous polyaniline/reduced graphene oxide	Self-assembly	SEM, AFM, UV-Vis spectra, electrochemical measurements	High-performance Supercapacitors	**[108]**
23.	ɤ-Fe2O3-polyaniline nanocomposites	*In-situ* polymerization	XRD, FTIR, TGA, DTA, DSC, SEM, conductivity, and dielectric measurements	Capacitors	**[109]**

24.	Polyaniline/MnO_2 composites	Oxidation polymerization	FESEM, XRD, magnetometry studies, electrical conductivity	EMI Shielding	**[110]**
25.	Epoxy/poly(styrenesulfonate)-polyaniline/reduced graphene oxide	*In-situ* oxidative polymerization	XRD, FTIR, SEM, XPS spectra, differential scanning calorimetry (DSC), dynamic mechanical analyzer (DMA), Potentiodynamic polarization	Improvement of mechanical and anticorrosion properties	**[111]**
26.	Polyaniline nanofiber/multi walled carbon nanotubes composite	Interfacial polymerization	Raman spectra, FTIR, SEM, Impedance analysis, electrochemical tests	Supercapacitor electrode materials	**[112]**
27.	Bismuth vanadate/graphene oxide/polyaniline	Hydrothermal process	XRD, SEM, TEM, FTIR, UV- Vis spectra, DRS, XPS	Photocatalytic performance	**[82]**
28.	Laccase immobilized polyaniline/magnetic graphene composites	Hydrothermal synthesis	SEM, XRD, IR spectra, TEM, cyclic voltammetry and chronoamperometry	Detect hydroquinone in water	**[113]**
29.		*In-situ* polymerization	SEM, surface resistance test,		**[114]**

	Flexible polyaniline/nylon composites		dielectric constant, and loss tangent test	Dielectric properties and conductivity	
30.	Polyaniline/manganese dioxide nanoparticles	*In-situ* oxidative polymerization	XRD, FTIR, SEM, TEM, impedance analysis, thermogravimetry	Improved thermal stability and applied for electrode material applications	**[115]**
31.	Polyaniline@MIL-101/epoxy	*In-situ* polymerization	PXRD, FTIR, XPS, N_2 adsorption-desorption isotherms, SEM, EIS, anticorrosion performance measurements, TEM	Corrosion protection (metallic Anticorrosion)	**[116]**

2.2 PANI/clay nanocomposites

The polymer nanocomposite is a unique combination of a polymer (like polyethylene, polystyrene, polyamide, etc.) and nanoclays as a filler such as montmorillonite bentonite, halloysite, etc. Polymer/clay nanocomposite is a material with high surface area, high stability, high durability, and processability, and has unique characteristics such as good thermal, optical, mechanical, and electrical properties **[117, 118].** All these properties are making them the most preferred material for many applications. Recently, the development of polymer clay nanocomposites has gained a lot of interest for wastewater treatment.

The first polymer/clay nanocomposite (Nylon 6/clay hybrid) was prepared by the researchers of Toyota, Japan **[119-121].** The improvements in a range of material properties indicated that layered silicate material as a filler has a lot of potentials. Lately, plenty of other studies on nanocomposites has been published, involving several different polymer matrices and a variety of layered silicates. Montmorillonite clay is one of the most widely studied layered silicates. The development of PANI/clay nanocomposites can overcome the disadvantages of individual PANI and clay. The dispersion of clay into the PANI matrix increases the interfacial surface area and improves its properties.

2.2.1 Literature on synthesis and characterization of PANI/clay nanocomposites

Currently, polymer/clay nanocomposites are one of the most prominent materials in the research field. In recent years, there are many publications on polymer-based nanocomposites in different journals on different applications. Polymer/clay nanocomposites have been improved the numerous properties of an individual one.

Many different types of polymers and clays have been studied for the synthesis of nanocomposites. A fabrication of exfoliated polystyrene/MMT nanocomposites was reported by **Fu and Qutubuddin, [120]** using vinylbenzyldimethyldodecylammonium chloride surfactant via free radical polymerization. The thermal degradation temperature and dynamic modulus of exfoliated nanocomposites are greater than that of neat polystyrene. **Essawy *et al.*, [122],** modified MMT clay by using surfactants named cetylpyridinium chloride and cetyltrimethylammonium bromide. These modified clays were further used to prepare poly(methylmethacrylate) nanocomposites using *in-situ* emulsion and intercalative suspension polymerization. The nanocomposites showed

improvement in thermal stability. **Uthirakumar *et al.*, [123]** used (2,2-azobis{2-methyl-N-[2-acetoxy-(2-N,N,N-tributylammonium bromide)ethyl] propionamide} initiator to prepare exfoliated polystyrene/MMT nanocomposites and evaluated their electrochemical properties.

A study was investigated by **Wu *et al.*, [124]** to prepare PANI nanocomposites with synthetic mica clay through an *in-situ* polymerization method. As observed, the conductivity of the PANI/synthetic mica clay nanocomposite steadily increased with the addition of PANI. This increase was mainly appeared with 40.6 wt % of PANI content due to the phenomenon of intercalated PANI molecules percolating. Compared to PANI, the nanocomposites' degradation rate and temperature were observed to be reduced and increased, respectively. PANI was intercalated within the silicate mica clay galleries and allowing the basal spacing to extend as determined by WAXD patterns. The intercalation was also confirmed by FTIR, TEM, UV-Vis, AFM, and SEM techniques.

Sedlakova *et al.*, [125] described the synthesis of polystyrene/MMT-Na and poly(butyl methacrylate)/MMT-Na nanocomposites latexes via *in-situ* emulsion polymerization and modified MMT-Na clay with an MMT-QS coupling agent.

Ahmad *et al.*, [126] studied the comparison of polyimide/MMT nanocomposites prepared by two different techniques, i.e., solution dispersion and *in-situ* polymerization. They concluded that the *in-situ* polymerization provides a higher dispersion of MMT clay in polyimide matrices than the solution dispersion method. The thermal stability of polyamide/MMT nanocomposites is more as compared to pure polyimide. The results showed that thermal stability improved with the addition of OMMT.

In-situ polymerization was used to fabricate reinforced glass fiber epoxy loaded with MMT/aerosil by **Srinivasulu *et al.*, [127]**. They concluded that properties like tensile strength, flexural strength, flexural and tensile modulus have been enhanced up to four gm wt loading for both nanocomposites and decreased as the filler content was increased. These improvements in properties will make them the material used in marine, automobile, lightweight articles, and aerospace applications.

Mallakpour and Marziyeh, [128] have prepared biodegradable polyvinylpyrrolidone nanocomposites with modified AA-MMT clay (amino acid modified-montmorillonite). The results showed a slight improvement in heat stability as compared to conventional polyvinylpyrrolidone. **Assem *et al.*, [129]** reported the synthesis of Poly(diallyldimethylammonium chloride)/sodium bentonite clay nanocomposites by a solution-intercalation method. The authors study the effect of polymer concentration and molecular weight on its nanocomposites properties (like thermal, structural, and dielectric).

Djamaa *et al.*, [130] synthesized poly(acrylic acid)/organophilic MMT and poly(acrylic acid-co-styrene)/organophilic MMT nanocomposites through *in-situ* radical polymerization using an initiator named 2,2′ azobis(isobutyronitrile) for adsorption applications.

Arya and Sharma, [131] prepared and studied the enhancement of PEO–PVC/$LiPF_6$/MMMT (polyethylene oxide-polyvinyl chloride/Lithium hexafluorophosphate/modified montmorillonite) nanocomposite properties.

2.2.2 Literature on synthesis and characterization of PANI/MMT nanocomposites

Hoang and Holze, [132] reported the fabrication of PANI/MMT nanocomposites via *in situ* electrochemical polymerizations on a gold sheet electrode. The formation of nanocomposites was confirmed by FTIR and XRD analysis. The results of cyclic voltammetry analysis show that PANI and PANI/MMT were similar to each other under the same conditions. Conductivity Measurements of PANI/MMT nanocomposites indicating an order of magnitude smaller than PANI.

Olad and Rashidzadeh, [133] used an *in-situ* polymerization method to synthesize polyaniline/hydrophilic montmorillonite (Na-MMT) and polyaniline/organophilic montmorillonite (Cloisite 15A) nanocomposites and investigated their anticorrosion properties. The addition of MMT clay to a PANI matrix improves the anticorrosive properties of nanocomposites. Furthermore, the coatings of PANI/Na-MMT and PANI/OMMT (5 % (w/w) of nanocomposites in 3.5 % (w/w) NaCl and 1M H_2SO_4 solution) on iron samples shows better results than pure PANI.

Reena *et al.*, [134] use five different types of amphiphilic dopants (dodecylbenzene sulphonic acid, camphor sulphonic acid, para-toluene sulphonic acid, 2,6-naphthalene sulphonic acid, and stearic acid) to prepare PANI/Na^+ MMT nanocomposites through *in-situ* intercalative emulsion polymerization. They examined how dopants affected the nanocomposites morphology and characteristics, such as thermal stability, conductivity, and phase transition temperature.

Shakoor *et al.*, [135] fabricated PANI/MMT with 2:1 of monomer to oxidant ratio. They evaluated the impact of MMT content on nanocomposites' AC conductivity. In nanocomposites, the degree of interaction between MMT and PANI chains was highest with 1 % MMT, but it decreases

gradually with the further inclusion of MMT. It has been seen that if the amount of MMT increases, the low-frequency AC conductivities of PANI/MMT nanocomposites decreases.

Abdelkader *et al.*, [136] studied the synthesis of PANI with acid-exchanged montmorillonite clay (Maghnite-H^+) to enhance the thermal stability of pure PANI identified with two analysis: thermogravimetric and differential scanning calorimetry. Their findings suggested that Maghnite-H^+ could be used for polymer synthesis.

Vijayakumar *et al.*, [137] prepared and characterized PANI/smectite clay nanocomposites for their physicochemical properties. The thermal stability of PANI was found to be higher than PANI/smectite clay nanocomposites. The electrochemical studies using cyclic voltammetry revealed that even at higher scan frequencies, nanocomposites outperform pure PANI in terms of supercapacitance. Nanocomposites had specific capacitances of 415-455 Fg^{-1} when scanned at a rate of 10 mVs.

A mechanochemical intercalation method was used to prepared PANI (DBSA)/MMT nanocomposites by **Kalaivasan and Shafi, [138]** and studied the corrosion protection properties. The DBSA PANI/MMT coatings on C45 steel show better corrosion protection than conventional PANI when the molar ratio of DBSA and aniline is 1:7.

Zhang *et al.*, [139] worked on polyaniline/montmorillonite/epoxy coating by varying polyaniline/OMMT powder amount and studied the corrosion protection performance on steel.

Motlatle *et al.*, 140] prepared polyaniline/montmorillonite composite coated with epoxy resin and investigated their corrosion protection and mechanical properties. **Leon-Almazan *et al.*, [141]** used two different techniques (ultrasonication and mechanical agitation) and two doping acids,

i.e., dodecylbenzene sulfonic acid and hydrochloric acid, to prepare polyaniline/organomodified montmorillonite nanocomposites through oxidative polymerization method and studied to see the effect on morphology and electrical properties. They found improvement in electrical properties but did not observe any change in morphology.

Silva *et al.*, [142] synthesized polyaniline-organophilic montmorillonite (PANI-OMMT) via *in-situ* polymerization and polyvinyl alcohol/polyaniline-organophilic montmorillonite nanocomposite through the electrospinning method. They developed a material that can be used in environmental and gas sensor applications. **Meneses *et al.*, [143]** worked on the synthesis of polyaniline (emeraldine salt)/bentonite composites by the use of a mechanical mixing method and studied their AC conductivity properties.

Pinto *et al.*, [144] worked on synthesizing MMT-PANI/PS nanocomposites using the melt intercalation method. The author revealed that the glass transition temperature of MMT-PANI/PS was decreased as the quantity of MMT-PANI was increased. As clay dispersion improves, a conducting interphase forms, changing the polystyrene (PS) electrical behavior from insulating to diffusive, as measured by Electrochemical Impedance Spectroscopy. **Rahmouni and Belbachir, [145]** synthesized polyaniline-polyethylene oxide/Mag-H^+ (Algerian MMT) composite using cationic polymerization and studied their physical and chemical properties.

Abbas *et al.*, [146] reported the synthesis of Polyaniline/modified montmorillonite, polyiodoaniline/modified montmorillonite, and poly(ANI-co-2-IANI) modified montmorillonite through *in-situ* chemical polymerization. The successful synthesis was confirmed by FTIR, XRD, XRF, UV-Vis spectra, TEM, and cyclic voltammetry analysis. **Kenane *et al.*, [147]** prepared polyaniline/montmorillonite-cetyltrimethylammonium bromide, poly o-anisidine-co-

aniline/montmorillonite-cetyltrimethylammonium bromide, poly o-anisidine/montmorillonite-cetyltrimethylammonium bromide through oxidative chemical polymerization technique. They found that the prepared nanocomposites are electroactive and can be used in photovoltaic applications. A summary of PANI/MMT *in-situ* nanocomposites is given in **Table 2.3**.

Table 2.3 A literature review on PANI/clay nanocomposites prepared by *in-situ* polymerization

Sr. No.	Monomer and Clay	Catalyst	Oxidizing agent	Reaction condition	Final product	References
1.	Aniline and MMT clay	HCl	Ammonium persulfate	T = 5^{o}C Time = 3 h PCN salt powder dried at room temperature for 48 h PCN base powder was formed by adding ammonium hydroxide T = room temperature Time = 4 h PCN base powder dried at room temperature for 48 h	PANI/MMT dried at room temperature for 48 h	**[33]**
2.	Aniline monomer and NA^{+}-MMT clay	DBSA (dodecyl benzene sulfonic acid)	Ammonium persulfate	T = 25^{o}C	PANI-DBSA/MMT clay	**[148]**
3.	Aniline monomer	HCl	Ammonium persulfate	T = room temperature	PANI-MMT clay dried	**[149]**

	and An^+-MMT			Time = 24 h	under dynamic vacuum and stored in a desiccator	
4.	Aniline and Na^+-MMT clay	Camphorsulfonic acid and (-)HCSA	Ammonium persulfate	T = room temperature Time = 10 h	PANI/MMT dried in desiccator	**[150]**
5.	Aniline and Na^+-MMT clay	DBSA	Ammonium persulphate	T = room temperature Time = 24 h	DBSA-doped PANI/Na^+ – MMT	**[42]**
6.	Aniline monomer and pillared clay	HCl	Ammonium persulfate	T = 0^{o}C Time = Stirring 8 h and is kept overnight	PANI/PILC dried at 50^{o}C	**[151]**
7.	Aniline and Na^+ MMT clay	HCl	Ammonium persulfate	T = room temperature Time = 72 h	Dried PANI/clay	**[152]**
8.	Aniline and MMT clay	HCl	Ammonium peroxy-Disulphate	T = 0^{o}C Time = stirring 2 h and kept overnight	PANI/MMT dried at room temperature	**[153]**
9.	Aniline and illite clay	HCl	Ammonium persulfate	T = 4-6^{o}C Time = overnight	PANI/clay (illite) Dried at 50^{o}C	**[154]**
10.	Aniline and MMT clay	HCl	Hydrogen peroxide	T = 0-5^{o}C Time = 24 h	Dried PANI/MMT	**[155]**
11.	Aniline monomer	HCl	Ammonium persulfate	T = 0^{o}C at ice bath Time = 4 h	Dried PANI/MMT	**[156]**

	and NA^+-MMT clay				for 24 h at 80°C	
12.	Aniline free anilinium-MMT clay	H_2SO_4	Ammonium persulphate solution	T = room temperature	PANI/MMT dried for 4 h	**[49]**
13.	Aniline monomer and MMT clay	HCl	Ammonium persulfate	T = -4 and 0°C Time = 6 h	PANI/MMT dried at 60^0C for 24 h	**[157]**
14.	Aniline monomer and NA^+-MMT clay	HCl	Ammonium persulfate	T = 0°C Time = 14 h	PANI/MMT dried at 60^0C for 24 h	**[158]**
15.	Aniline and Na^+ MMT	HCl and CTAB (cetyltrimethylammonium bromide)	Ammonium Persulfate	T = 25°C Time = 24 h	PANI/MMT dried at 60°C for 24 h	**[159]**
16.	Aniline and CNT –COOH	HCl and HNO_3	Potassium persulfate	Time = 3 h	CNT/PANI dried at 40°C for 24 h	**[160]**
17.	Aniline monomer and OMMT clay	HCl and DBSA	Ammonium persulfate	T = 5°C Time = overnight	PANI/OMMT dried at room temperature for 72 h	**[141]**
18.	Aniline and MMT clay	Sulfuric Acid	Ammonium Persulfate	T = 0°C Time = 24 h	MMT/PANI Composites	**[161]**

19.	Aniline and MMT clay	HCl	Ammonium Persulfate	T = 5°C Time = 8 h	PANI/MMT nanocomposites	**[162]**
20.	Aniline and Indian clay	HCl	Potassium perdisulphate	T = ± 5°C Time = 24 h	Polyaniline-Indian clay nanocomposites	**[163]**

2.2.3 Literature on synthesis and characterization of PANI/HNT nanocomposites

Several reviews have been reported by the researchers on halloysite clay and polymer/halloysite clay nanocomposites such as **Joussein *et al.*, [164]; Du *et al.*, [165]; Yuan *et al.*, [166]; Yu *et al.*, [167]; Gaaz *et al.*, [168]; Kausar *et al.*, [169]; Papoulis, [170]; Danyliuk *et al.*, [171].**

There are a few literature reports about the fabrication of polyaniline/halloysite clay nanocomposites. The polymerization time in these studies is higher than in the present study. The different processing route in the present study gives the better nanocomposite.

Zhang *et al.*, [172] reported the synthesis of polyaniline/halloysite nanotubes through *in-situ* chemical polymerization. The authors used XRD, XPS, and TEM analyses to explore the impact of the polymerizing media acidity onto the halloysite nanotubes structure. The results show that as the HCl amount increased during the polymerization process, the nanocomposites conductivity also increased. **Tierrablanca *et al.*, [173]** synthesized environmentally friendly halloysite/hematin/polyaniline nanocomposites with thermal conductivity of 8.8×10^{-1} S/cm.

Zhou *et al.*, [174] investigated the fabrication of multi-pored polyaniline/halloysite nanocomposite by the use of *in-situ* mechanochemical polymerization method and the formation of nanocomposites was confirmed by FTIR, XRD, UV-Vis spectra, and TEM techniques.

Abolghasemi *et al.*,[175] fabricated polyaniline/halloysite nanotube via *in-situ* polymerization technique. They found that the prepared nanocomposite material may be utilized for solid-phase microextraction fiber coating. The results prove that polyaniline/halloysite fiber is an excellent adsorbent for phenolic compound extraction from water.

Yang *et al.*, [176] reported the fabrication of Ag nanoparticles/polyaniline/halloysite nanocomposites material for the utilization as H_2O_2 sensing. **Huang *et al.*, [177]** worked on the synthesis of halloysite/polyaniline nanocomposites material by two methods one is *in-situ* polymerization and another one is the layer-by-layer assembly method. The authors found that the prepared nanocomposites have a great potential for supercapacitors applications.

Zhou *et al.*, [178] synthesized polyaniline/halloysite nanocomposites by chemical oxidative polymerization method for application of the electrochemical sensor. **Noskov *et al.*, [179]** prepared halloysite/polyaniline nanocomposites via the chemical oxidative method for gas sensor applications.

2.3 Polymer/clay nanocomposites in wastewater treatment

In the last few years, nanocomposites have gained a lot of interest in wastewater treatment. The high surface area of nanocomposites is made them a suitable material for water purification. So far, polyaniline has been developed with various types of materials such as metal oxides, graphene,

multiwalled carbon nanotubes, carbon, zeolite, magnetite, sawdust, chitosan, hexagonal silica, chitin, etc. and effectively used for removing a variety of pollutants from industrial effluent. Many types of adsorbents have been investigated for heavy metal ions and dyes adsorption study, but they all have some limitations like high cost, processing, and disposal problems. Among all the adsorbent materials, nanocomposites are the most encouraging ones for pollutant treatment. The fabrication of polyaniline with different types of materials improved their adsorption capacities. The main factor that increased the adsorption capacity is the chemical and textural properties of nanocomposites. The next section will discuss the available literature on heavy metal ions and dye's adsorption through PANI/MMT-based adsorbents. In the present study, the focus is on Methylene blue and Acid green 25 dye adsorption.

2.3.1 PANI/MMT nanocomposites for heavy metal ions treatment

Chen *et al.*, [180] reported the adsorption of hexavalent chromium (Cr(VI)) using *in-situ* chemical oxidation polymerized PANI/MMT composite. At a temperature of 25°C, PANI/MMT showed a higher Cr(VI) adsorption efficiency of 308.6 mg/g.

Piri *et al.*, [181] synthesized polyaniline/modified clay nanocomposite and applied it for Pb(II) ions adsorption. The prepared nanocomposites exhibited 70.42 mg/g of adsorption efficiency. **Soltani *et al.*, [182]** investigated the synthesis and adsorption of Cu(II) ions using polyaniline/clay nanomaterials adsorbent. The highest removal of 22.77 mg/g was obtained at pH 6 and 25°C. **Ali *et al.*, [183]** prepared phytic acid doped polyaniline and polyaniline/montmorillonite composite for copper (II) ions adsorption. **P**-PANI has an adsorption capacity of 66.6 mg/g, whereas P-PANI/MMT composites have an adsorption capacity of 87 mg/g.

Several other studies reported the heavy metal ions treatment through polyaniline-based nanocomposites adsorbent such as **Li *et al.,* [184]** worked on adsorption treatment of Cr(VI) and Hg(II) through polyaniline composite prepared with humic acid. **Gu *et al.,* [185]** developed polyaniline/Fe_3O_4 nanocomposites via facile surface-initiated polymerization for hexavalent chromium (Cr(VI)) adsorption. **Javadian *et al.,* [186]** reported Ni(II) adsorption by using polyaniline/hexagonal mesoporous silica nanocomposite adsorbent. **Fang *et al.,* [187]** used polyaniline/coconut shell–activated carbon composites for Cu(II) adsorption. **Javadian *et al.,* [188]** prepared polyaniline/hexagonal mesoporous silica nanocomposite and used it as an adsorbent for Hg^{2+} ions adsorption. **Shyaa *et al.,* [189]** removed chromium (VI) from wastewater through polyaniline/zeolite nanocomposite adsorbent.

2.3.2 PANI/MMT nanocomposites for dye treatment

2.3.2.1 Adsorption of Methylene blue dye on PANI based nanocomposite adsorbents

Chowdhury *et al.,* [36] used chemically synthesized polyaniline (acid and base) for Methylene blue and Procion red dye removal. The results revealed that Methylene blue dye adsorbed more on basic PANI, and Procion red dye adsorbed more on acidic PANI. The adsorption equilibrium occurred within 2 h of contact time.

Keivani *et al*. [89] reported the adsorption behavior of PANI/sawdust nanocomposite in removing Methylene blue dye. The reduction in dye concentration was found to be 99.5 % in 30 min at pH 9. **Ayad and El-Nasr, [190]** worked on Methylene blue dye treatment through polyaniline nanotubes adsorbent. Complete removal was obtained in 20 min of contact time

Benhebal *et al.*, [191] investigated Methylene blue dye adsorption onto PANI/modified clay (kaolinite/illite) nanocomposites. A removal of 97.84 % was obtained in 20 min under optimized conditions (pH = 6, C_o = 10 mg/L, A = 1 g/L, T = 25°C).

PANI/$NiFe_2O_4$ (Polyaniline/nickel ferrite) nanocomposites have been developed by **Patil and Shrivastava, [192]** through the *in-situ* self-polymerization method and applied for Methylene blue dye adsorption. The maximum adsorption rate of 6.65 mg/g was achieved by the prepared adsorbent at pH 9. **Shahabuddin *et al.*, [193]** prepared polyaniline-coated graphene oxide@$SrTiO_3$ nanotube nanocomposites by *in-situ* oxidative polymerization and employed it to remove Methylene blue and Methyl orange dye effluent. The nanocomposite adsorbent removed 99 % of Methylene blue and 91 % of Methyl orange dye at pH 7 in 30 min at room temperature.

2.3.2.2 Adsorption of Methylene blue dye on PANI/MMT nanocomposite adsorbent

There is not much literature available for the treatment of Methylene blue dye on polyaniline/montmorillonite clay nanocomposite adsorbent. Only one study has been reported by **Mu *et al.*, [194].** They performed an adsorption study of Methylene blue, Congo red, and Brilliant green dye on well-defined, two-dimensional superparamagnetic clay(MMT and VMT)/polyaniline/Fe_3O_4 nanocomposites. The adsorbent gave a removal efficiency of 99.6 % for Methylene blue dye, 98.1 % for Congo red, and 96.2 % for Brilliant green dye within 60 min of contact time at 25°C. In **Table 2.4**, various adsorbents that have been used to remove Methylene blue dye are given.

Table 2.4 Different adsorbents used for Methylene blue dye adsorption

Sr. No.	Adsorbate	Adsorbent	Optimized conditions	Percentage removal /adsorption capacity	References
1.	Methylene blue	Montmorillonite clay	C_o = 100 mg/L C = 100 ml A = 0.1 g pH = 5.65 t = 60 min	58.2 mg/g	**[6]**
2.	Methylene blue	Carbon nanotubes	C_o = 10 mg/L A = 400 mg/L T = 310 K t = 120 min	132.6 mg/g	**[195]**
3.	Methylene blue	Graphene oxide	C_o = 0.33–3.3 mg/mL C = 5 ml A = 0.33 mg/ml pH = 7 t = 2 h T = 293 K	1.939 mg/mg	**[196]**
4.	Methylene blue	Lignocellulose-g-poly(acrylic acid)/montmorillonite hydrogel nanocomposites	C_o = 2500 mg/L C = 50 ml A = 50 mg pH = 5 T = 30°C t = 120 min	1994.38 mg/g	**[197]**
5.	Methylene blue	Graphene oxide/calcium alginate	C_o = 30-80 mg/L C = 50 ml A = 25 mg T = 25°C t = 5 h	181.81 mg/g	**[198]**
6.	Methylene blue	$ZnCl_2$ Activated Corn Husk Carbon	C_o = 40 and 65 mg/L C = 50 ml pH = 4	662.25mg/g	**[199]**

			A = 0.3 g/L t = 80 min T = 318 K	(removal more than 90%)	
7.	Methylene blue	Acid activated carbon Vitex Negundo Stem	C_o = 50 mg/L C = 50 ml A = 25 mg t = 45 min T = 30°C	85 %	**[200]**
8.	Methylene blue	Montmorillonite clay modified with iron oxide	C = 50 ml A = 0.1 g T = 333 K t = 4 h	71.12 mg/g	**[201]**
9.	Methylene blue	Annona squmosa seed	C_o = 50 mg/L C = 50 ml A = 0.2 g pH = 6 T = 27 ± 2°C	24.33 %	**[202]**
10.	Methylene blue	Walnut shells powder	C_o = 100 mg/L C = 50 ml A = 0.5 g/L T = 20°C pH = 6.8	178.9 mg/g	**[203]**
11.	Methylene blue	Carboxymethyl cellulose/k-carrageenan/activated montmorillonite	C_o = 25 ppm C = 50 ml A = 0.1 g T = 30°C pH = 6 t = 120 min	92 %	**[204]**
12.	Methylene blue	Kaolin	C_o = 80–150 mg/L C = 100 ml A = 0.5 g/L pH = 6 T = 25°C t = 120 min	52.76 mg/g 97.5% removal (100 mg/L)	**[205]**
13.			C_o = 50 mg/L		**[206]**

	Methylene blue	Hydroxyapatite sodium alginate (CaHAp-Alg)	C = 50 ml A = 1 g/L PH = 6<pH <7 T = 25°C t = <60 min for CaHAp, 30 min for CaHAp-Alg	77.510 mg/g of CaHAp and 142.850 mg/g of CaHAp-Alg	
14.	Methylene blue	MnO_2 nanosheets@montmorillonite	C_o = 10 mg/L C = 100 ml A = 0.1 g/L pH = 2 t = 5 min T = 30°C	97.7 % (363.63 mg/g)	**[207]**
15.	Methylene blue	Humic Acid covered Alumina	C_o = 50 mg/L C = 60 ml A = 1 g/L t = 50 min pH = 6 T = ambient temperature	50 % removal/capacity 25.17 mg/g	**[208]**
16.	Methylene blue	Algerian palygorskite	C_o = 10 mg/L C = 50 ml A = 50 mg t = 5min T = room temperature	97 %	**[209]**
17.	Methylene blue	EDTA-modified bentonite	C_o = 10-100 mg/L C = 50 ml pH = 2.3 A = 20 mg t = 120 min T = 30-50°C	160 mg/g	**[210]**
18.	Methylene blue	Poly(acrylic acid-co-styrene)/ OMMT clay nanocomposites	C_o = 50 mg/L pH = 3.6 A = 50 mg T = room temperature	74%	**[130]**

			t = 80 min		

2.3.2.3 Adsorption of Acid green 25 dye on PANI based nanocomposite adsorbents

Not much literature is available for the adsorption of Acid green 25 dye using polyaniline-based nanocomposite adsorbent. Only a few studies have been reported in this area, such as **Ansari *et al.*, [211]** investigated the adsorption efficiency of Acid green 25 dye on polyaniline/sawdust. The adsorbent removed 96 % of dye (50 mg/L) at pH 2 with 0.8 g of adsorbent in 60 min of contact time. **Ayad and El-Nasr, [212]** applied polyaniline nanotubes salt/silica composite for Acid green 25 adsorptions. The complete removal of 1.8 mg/L of dye was observed in 10 min with 0.05 g of adsorbent at 25°C. Adsorption was described best by the Langmuir model with a capacity of 6.896 mg/g.

Another adsorption study was performed by **Ansari and Dezhampanah, [213]** on polyaniline/sawdust composite. The adsorbent obtained a maximum AG25 adsorption capacity of 6.21 mg/g under the optimized conditions (C_o = 20-100 mg/L, A = 0.8 g, pH = 2, t = 60 min, T = room temperature). In **Table 2.5**, we have summarized the literature on the adsorption of AG25 dye using various types of adsorbents.

Table 2.5 Different adsorbents for Acid green 25 dye adsorption

Sr. No.	Adsorbate	Adsorbent	Optimized conditions	Percentage removal/ adsorption capacity	References
1.	Acid green 25		C_o = 50 mg/L C = 200 ml		**[214]**

		Sodium Alginate/titania nanoparticle	A = 0.5 g/L pH = 2 T = 25°C t = 20 min	Removal of more than 90 %	
2.	Acid green 25	Ananas comosus (L) activated carbon	C_o = 100 mg/L C = 200 mL A = 100 mg pH = 2 T = 25°C t = 90 min	Removal 94.2 %/ adsorption capacity 182.6 mg/g	**[215]**
3.	Acid green 25	Polyoxypropyle nediamine-modified chitosan (D_{2000}-Cs)	C_o = 18 mg/L C = 50 ml A = 20 mg pH = 3 T = 25°C t = 60 min	99.4 % removal and 44.5 mg/g adsorption capacity	**[216]**
4.	Acid green 25	Oxidized multiwalled carbon nanotubes	C_o = 30 mg/L C = 50 ml A = 0.025 g/L pH = 2 T = 25°C t = 15 min	>90%	**[217]**
5.	Acid green 25	Activated carbon-MnO_2 nanocomposite	C_o = 10 mg/L C = 50 mL A = 100 mg T = 30.2ºC t = 120 min	76.73 mg/g	**[218]**
6.	Acid green 25	Biosorbent (NaOH activated prunus dulcis)	C_o = 50 , 100, 200 mg/L A = 6 g/L pH = 2 t = 330 min T = 323 K	Removal 96.1 % - 82.03% Adsorption capacity 50.79 mg/g	**[219]**
7.					**[220]**

	Acid green 25	Kaolin (KM 20 and (KM 40)	C_o = 10, 20, 30, 40, 50, 60 mg/L C = 250 ml A = 0.6 g/L pH = 7 T = 26 ± 2°C T = 3 h	23.26 mg/g for KM 20 and 30.49 mg/g for KM 40	

2.3.2.4 Adsorption of Acid green 25 dye on PANI/MMT nanocomposite adsorbents

No study has been found single on the use of PANI/MMT adsorbent to treat Acid green 25 dye. In the present study, PANI/MMT nanocomposites have been used effectively to treat Acid green 25 dye. The available literature on AG25 dye adsorption using different adsorbents is summarized in **Table 2.5**.

2.3.3 Polyaniline based nanocomposite adsorbents for various textile dye adsorption

We have also summarized the adsorption data on PANI-based nanocomposite adsorbents for different textile dye removal in **Table 2.6.**

Table 2.6 Polyaniline based nanocomposite adsorbents for various textile dye adsorption

Sr. No.	Adsorbent	Adsorbate	Optimized conditions	Percentage removal/adsorption capacity	References
1.	Polyaniline salt	Sulfonated dyes	C_o = 100 ppm t = 1 h	Dye completely adsorbed	**[221]**

2.	Polyaniline salt	Direct blue 78	t = 1 h	The rate dropped as the concentration of DB78 and pH increased.	**[45]**
3.	Polyaniline/ hollow $MnFe_2O_4$ nanocomposite	Crystal violet	C_o = 5 ppm pH = 7 T = 25°C t = 15 min	75.6%	**[222]**
4.	Polyaniline/ sawdust	Methyl orange	C_o = 50 mg/L pH = 6 T = room temperature t = 60 min	89.1%	**[223]**
5.	Starch/polyaniline	Reactive dyes	pH = 3 T = 25°C t = 40 min	Reactive black 5 = 99%, Reactive violet 4 = 98%, and Decolorized of dye bath = 87%	**[224]**
6.	Polyaniline nanocomposite	Acid violet 49	C_o = 50 mg/L pH = 3.4 T = 30°C t = 50 min	91.96%	**[225]**
7.	Polyaniline/ MMT composite	Congo red	C_o = 40 mg/L T = 30°C t = 60 min	25.1 mg/g	**[226]**
8.	Starch/MMT/polyaniline	Reactive dye	C_o = 20 mg/L pH = 2-10	91.74 mg/g	**[227]**
9.	Polyaniline/ cerium oxide	Remazol red dye	C_o = 50 mg/L pH = 6.5 T = 25°C t = 40 min	99%	**[228]**
10.	Graphene oxide/polyaniline/manganese oxide ternary	Indigo carmine	C_o = 45.61 mg/L T = 30°C	Removal onto GO/PANI is 79.31 % GO/PANI > GO/PANI/Mn_2O_3	**[229]**

	nanocomposites			>PANI>PANI/MnO_2 (88.73, 76.40, 60.45 and 22.52 mg/g)	

2.4 Carbon aerogels

The synthesis of aerogel was first reported by **Kistler [230]** in 1931**.** The author discovered aerogel, made of silica, through a supercritical drying process. However, this process has some limitations like high manufacturing cost and is time-consuming. In 1968, Teichner made the procedure simpler using an organic precursor such as tetramethyl orthosilicate and solvent. Since 1970, aerogels have gained much interest from researchers. The focus has been on developing an aerogel with better drying technology.

Carbon aerogels are organic aerogels having the advantage of controlled micro and mesoporosity properties. The factors that affect the porosity in carbon aerogels are: curing and drying procedures, original ingredients, and carbonization conditions **[231]**. Carbon aerogels were first fabricated by **Pekala [232]** in 1989 from resorcinol and formaldehyde via a sol-gel polycondensation process. Carbon aerogels are classified into three categories, i.e., organic-based carbon aerogel, biomass-based carbon aerogel, and graphitic materials-based carbon aerogel. Organic-based carbon aerogel involves polymers, aromatics, and aldehydes, biomass-based carbon aerogel involves porous biomass and hydrated biomass, graphitic materials-based carbon aerogel involves graphene, carbonitride, carbon nanotube, and carbide.

2.4.1 Synthesis of carbon aerogels and its composites

Researchers have recently focused their attention on the production of aerogel materials. Because of the advantages of high surface area, porous structures, environmental compatibility, and electrical conductivity, carbon aerogel is the most favorable material for energy devices.

Zhang *et al.*, [233] prepared and claimed that silver dispersed carbon aerogels have strong antibacterial activity**. Saquing *et al.*, [234]** synthesized platinum/carbon aerogel nanocomposites by the supercritical deposition method**.**

A supercapacitive electrode material ZnO/carbon aerogel composite was developed by **Kalpana *et al.*, [235]**. **Fang and Binder, [236]** developed modified activated carbon aerogel with superior properties, which made this material more efficient for storing high energy in an electric double-layer capacitor. **Tsioptsias *et al.*, [237]** prepared chitin aerogels and carbon aerogels and study the effect of different parameters like temperature, pressure, gel concentration, and solvent.

A high surface area of porous carbon aerogels (619.26 m^2/g) has been prepared by **Shariff *et al.*, [238].** They further use it to treat heavy metal ions and toxic materials. **An *et al.*, [239]** produced polypyrrole/carbon aerogel composite and applied it as an electrode in supercapacitors. The results show an excellent performance by prepared composite in supercapacitors.

Lin *et al.*, [240] worked to synthesize metal hydride/carbon aerogel composites and identified their hydrogen storage ability. They found that the abilities of carbon aerogels for hydrogen adsorption were increased after the synthesis of CA with metal hydrides. A study was also performed by **Rejitha *et al.*, [241]** on carbon aerogel synthesis. They investigated the effect of catalysts on the synthesis of carbon aerogels and their physical properties. **Bakierska *et al.*, [242]** produced high conductivity and high surface area starch-based carbon aerogels, which can be used in energy applications.

Yan *et al.*, [243] reported the synthesis of carbon aerogels using three different catalysts (sodium carbonate, calcium hydroxide, and sodium hydroxide) via resorcinol and formaldehyde monomers polycondensation. Carbon aerogel made with sodium carbonate catalyst was superior to others in surface area, resistivity, pore size distribution, and structure. A study was performed by **Wang *et al.*, [244]** in which they found that the synthesis of carbon aerogels through the acidizing process can enhance the degree of graphitization. **Schwan and Ratke, [245]** synthesized flexible carbon aerogels that can be used for batteries and supercapacitors applications.

Ciszewski *et al.*, [246] worked to modify carbon aerogels by CNT, graphene, and graphene oxide for supercapacitor performance. Carbon aerogel and Ni-doped carbon aerogel were synthesized and examined as supercapacitor electrodes by **Wang *et al.*, [247].** They obtained Ni-doped carbon aerogels with improved supercapacitor performance than pure carbon aerogels.

Monolithic carbon aerogels composites synthesized by **Lu *et al.*, [248]** show potential for thermal protection in the aerospace field and lithium-sulfur batteries as an electrode material. **Guo *et al.*, [249]** produced highly stretchable carbon aerogels for smart robots, aerospace, and wearable device applications**. Wang *et al.*, [250]** produced carbon aerogels as potential electrode material in supercapacitor devices and investigated their electrochemical performance.

Many studies reported the work on the synthesis of carbon aerogels by the researchers such as **Maldonado-Hodar *et al.*, [251]**; **Cotet *et al.*, [252]; Czakkel *et al.* [253]; Lyu *et al.*, [254].** Some reviews are also reported, such as **Pekala *et al.*, [255]; Araby *et al.*, [256]; Torres *et al.*, [257].**

2.4.2 PANI/carbon aerogel

There are only a few literature studies available on polyaniline/carbon aerogel nanocomposites synthesis. In this field, **Xu *et al.*, [258]** used *in-situ* chemical oxidation to prepare polyaniline/carbon aerogel and improve their electrochemical properties. The authors found that the addition of carbon aerogel in the polyaniline improved the electrochemical properties.

An *et al.*, [259] produced polyaniline/carbon aerogel composite through chemical oxidation polymerization for supercapacitors. The authors worked on the electrochemical performance of the composites. **Jin *et al.*, [260] and Chen *et al.*, [261]** synthesized polyaniline/carbon aerogels composite successfully as an electrode material for supercapacitors applications. **Tang *et al.*, [262]** prepared and investigated the performance of polyaniline-coated activated carbon aerogel/sulfur composite for a lithium-sulfur battery. The fabrication of composite improved the electrochemical properties.

2.4.3 PANI/carbon aerogels for AG25 dye adsorption

There is no report available in the literature on carbon aerogels for AG25 dye adsorption. Carbon aerogels which have been reported in the literature, but these are limited to their use as the electrode material. Only a few studies are available on textile adsorption. Their porous structure adsorption efficiency has not been explored properly.

The literature review on different dye adsorption with carbon aerogel and its nanocomposites is presented in **Table 2.7.**

Table 2.7 A literature review of dye adsorption with carbon aerogel and its nanocomposites.

Sr. No.	Adsorbent	Adsorbate	Optimized conditions	Removal percentage (%)	Adsorption capacity	References

1.	Carbon aerogels	RBRX Dye	C_o = 400 – 1200 mg/L C = 100 mL A = 26.6 g Cell Voltage = 20V Air Flowrate = 0.4 L min^{-1} T = 30°C t = 30 min	96	Not studied	**[263]**
2.	Activated carbon aerogels	Basic blue 9 and Acid red 183	C_o of BB9 = 10 mg/L C_o of AR183 = 150 mg/L C = 500 mL A = 0.01 g T = 26°C t = 300 min	_	CA-K-900 (inactivated CA) adsorbed 200 mg/g BB9 and 280 mg/g AR183 CA-K-A1000 (activated CA) adsorbed 360 mg/g BB9 and 2650 mg/g AR183	**[264]**
3.	MCM41 and Carbon aerogel (MCA)	Basic yellow 87	C_o = 68.4 to 820.0 mg/L C = 50 mL A = 0.05 g T = 22°C, 42°C, 62°C t = 24 h	_	MCM41 = 169 mg/g and MCA = 178 mg/g	**[265]**
4.	Carbon xerogel	Phenol	C_o = 100-500 mg/L C = 50 mL A = 0.075 g T = 25°C	21.5 (A = 0.2 g)	32 mg/g	**[266]**

			t = 24 h			
5.	Carbon aerogels	Methylene blue	C_o = 150-400 mg/L C = 50 mL A = 50 mg T = 25ºC, 35ºC, 45°C t = 30 min	_	819.67 mg/g	**[267]**
6.	Composite maghemite/ hematite/ carbon aerogel nanostructures [Composite Fe_3O_4/ɣ-Fe_2O_3 nanorods (180N) and mesoporous ɣ-Fe_2O_3/ɣ-Fe_2O_3/CA structures (CA-180)]	Rhodamine B	C_o = 8 mg/L C = 100 mL A = 10 mg t = 12 h	3.3 % of 180N and 98.2% of CA-400	1.52 mg/g and 151.52 mg/g	**[268]**
7.	Graphene nanosheet / carbon composite aerogels	Methylene blue	C_o = 25 mg/L C = 30 mL A = 25 mg T = 25ºC t = 30 min	98	403 mg/g	**[269]**
8.	Flexible carbon fiber aerogel	Methylene blue	C_o = 10 -120 mg/L C = 50 mL A = 20 mg T = 25ºC, 27ºC, 45ºC, 55ºC t = 100 min	_	102.23 mg/g	**[270]**
9.	β-cyclodextri	Methylene blue	C_o = 60 mg/L C = 20 mL	94.5	166.67 mg/g	**[271]**

	n/activated carbon aerogels		A = 10 mg T = 30^{o}C t = 500 min			
10.	Porous carbon aerogel activated persulfate	Rhodamine B	C_o = 20 mg/L A = 0.2 g/L T = 25°C, 35°C, 45°C t = 60 min	100 with CA/PS 30.7 with PS 38.2 with CA	_	**[272]**
11.	Activated carbon aerogels	p-nitrophenol	C_o = 100 mg/L C = 25 mL A = 0.4 g/L T = 20^{o}C	96.2	613.34 mg/g	**[273]**
12.	N-doped carbon aerogel (alkaline peroxide mechanical pulp aerogels)	Rhodamine B	C_o = 5 g/L C = 5 mL A = 0.1 g t = 30 s	_	250 mg/g	**[274]**
13.	Carbon aerogels	Methylene blue	C_o = 50 to 500 mg/L T = 25°C, 35°C, and 45°C t = 1000 min	_	421.94 mg/g	**[275]**

From Table 2.7, it can be concluded that carbon aerogels have been used for different dye adsorption but have not yet been utilized as an adsorbent for AG25 dye adsorption. There are no such PANI/Aerogel nanocomposites in **Table 2.7**. Also, there is limited literature in which polyaniline is combined with carbon aerogel to prepare nanocomposites. The present study aims to prepare polyaniline/carbon aerogel nanocomposites for an anionic dye (AG25) adsorption. *The in-situ* polymerization method has been used for preparing nanocomposites.

From the above literature survey, it was observed that synthesis of polyaniline and polyaniline/montmorillonite clay nanocomposites have been reported by the researchers, but they are limited to supercapacitors electrode materials, anticorrosion properties, and sensors applications. Additionally, researchers have not explored the synthesis of polyaniline/carbon aerogels and their efficiency in removing AG25 dye. A few studies on the synthesis of polyaniline/carbon aerogels are available.

Based upon the literature survey, a few gaps have been identified.

2.5 Gaps in the literature

The following are the gaps in the literature:

Several studies have been reported in the literature on the synthesis and characterization of PANI/MMT clay nanocomposites. PANI/MMT has also been used for wastewater treatment, but there has been no study reporting PANI/MMT nanocomposites as an adsorbent for AG25 dye adsorption, and only one report is available on PANI/MMT clay nanocomposites for MB adsorption. In most of the research articles, authors have used PANI/MMT clay nanocomposites as a supercapacitor material, sensors, and corrosion protection applications and also use MMT to improve mechanical and thermal properties.

Similarly, reports are available on carbon aerogels synthesis, but only a few reports are available on PANI/CA nanocomposites synthesis. Also, the work has not been done on AG25 dye adsorption with PANI/CA nanocomposites.

In the present study, PANI/MMT nanocomposites have been synthesized and used as an adsorbent for AG25 (anionic dye) and MB (cationic dye) adsorption. Also, CA and PANI/CA

nanocomposites have been synthesized and used as adsorbents for AG25 (anionic dye) adsorption. This is the first study on AG25 adsorption with CA and PANI/CA adsorbents.

These gaps led to the framing of research objectives as given below:

2.6 Objectives

The following objectives have been set for the study

1. To synthesize polyaniline nanocomposites with varying amounts of clay.
2. To characterize the prepared polyaniline nanocomposites.
3. To impregnate *in-situ* aniline on a porous substrate.
4. To characterize nanocomposites synthesized in step three.
5. To evaluate the above material as an adsorbent for dye removal.

References

[1] Anand J, Palaniappan S and Sathyanarayana DN (1998) Conducting polyaniline blends and composites. Prog Polym Sci 23:993–1018.

[2] Shi H-Y, Ye Y-J, Liu K, Song Y and Sun X (2018) A long-cycle-life self-doped polyaniline cathode for rechargeable aqueous zinc batteries. Angew Chem Int Ed Engl 57(50):16359-16363. doi: 10.1002/anie.201808886.

[3] Zarrintaj P, Yazdi MK, Jouyandeh M, Saeb MR (2019) PANI-based nanostructures. Fundamentals and Emerging Applications of Polyaniline 121-130. https://doi.org/10.1016/B978-0-12-817915-4.00007-5.

[4] Boomi P, Poorani GP, Palanisamy S, Selvam S, Ramanathan G, Ravikumar S, Barabadi H, Prabu HG, Jeyakanthan J, Saravanan M (2019) Evaluation of antibacterial and anticancer potential of polyaniline bimetal nanocomposites synthesized from chemical reduction method. J Clust Sci. https://doi.org/10.1007/s10876-019-01530-x.

[5] Jangid NK (2019) Recent advancement in synthesis and properties of polyaniline. Int J Innov Res Sci Eng Technol 8(4):3751-3772. DOI:10.15680/IJIRSET.2019.0804019.

[6] Gurses A, Dogar C, Yalcm M, Acıkyıldız M, Bayrak R, Karaca S (2006) The adsorption kinetics of the cationic dye, methylene blue, onto clay. J Hazard Mater B131:217–228. doi:10.1016/j.jhazmat.2005.09.036.

[7] Syed AA and Dinesan MK (1991) Review: A polyaniline-A novel polymeric material. Talanta 38(8):815-837.

[8] Lux F (1994) Properties of electronically conductive polyaniline: a comparison between well-known literature data and some recent experimental findings. Polymer 35:2915-2936.

[9] Gospodinova N and Terlemezyan L (1998) Conducting polymers prepared by oxidative polymerization: polyaniline. Prog Polym Sci 23:1443–1484.

[10] Zhang D and Wang Y (2006) Synthesis and applications of one-dimensional nano-structured polyaniline: An overview. Mater Sci Eng B 134:9–19.

[11] Eftekhari A (2006) Synthesis of nanostructured large particles of polyaniline. Journal of Appl Polym Sci 102:6060–6063.

[12] Palaniappan S, John A (2008) Polyaniline materials by emulsion polymerization pathway. Prog Polym Sci 33:732–758.

[13] Crowley K, Smyth MR, Killard AJ, Morrin A (2013) Printing polyaniline for sensor applications. Chem Pap 67(8):771–780. DOI: 10.2478/s11696-012-0301-9. J Mater Sci 48:7708–7717. DOI 10.1007/s10853-013-7591-3.

[14] Gu H, Guo J, Wei S, Guo Z (2013) Polyaniline Nanocomposites with Negative Permittivity. J Appl Polym Sci 2230-2244. Doi: 10.1002/APP.39420.

[15] Shinde SS, A.Kher J (2014) A review on polyaniline and its noble metal composites. IJIRSET 3(9):16570-16576. DOI: 10.15680/IJIRSET.2014.0310023.

[16] Fratoddi I, Venditti I, Cametti C, Russo MV (2015) Chemiresistive polyaniline-based gas sensors: A mini review. Sens Actuators B: Chem 220:534-548. https://doi.org/10.1016/j.snb.2015.05.107.

[17] Razak SI Abd, Wahab IF, Fadil F, Dahli FN, Md Khudzari AZ and Adeli H (2015) A review of electrospun conductive polyaniline based nanofiber composites and blends: processing features, applications, and future directions. Adv Mater Sci Eng Article ID 356286:19. http://dx.doi.org/10.1155/2015/356286.

[18] Wang H, Lin J, Shen ZX (2016) Polyaniline (PANi) based electrode materials for energy storage and conversion. J Sci: Adv Mater Devices 1:225-255.

[19] Sen T, Mishra S and Shimpi NG (2016) Synthesis and sensing applications of polyaniline nanocomposites: a review. RSC Adv 6:42196-42222.

[20] Lai J, Yi Y, Zhu P, Shen J, Wu K, Zhang L, Liu J (2016) Polyaniline-based glucose biosensor: A review. J Electroanal Chem 782:138–153.

[21] Tanguy NR, Thompson M, Yan N (2018) A review on advances in application of polyaniline for ammonia detection. Sens Actuators B 257:1044–1064.

[22] Banerjee J, Dutta K, Kader MB, Nayak SK (2019) An overview on the recent developments in polyaniline-based supercapacitors. Polym Adv Technol 30(8):1902-1921. https://doi.org/10.1002/pat.4624.

[23] Shoaie N, Daneshpour M, Azimzadeh M, Mahshid S, Khoshfetrat SM, Jahanpeyma F, Gholaminejad A, Omidfar K, Foruzandeh M (2019) Electrochemical sensors and biosensors based on the use of polyaniline and its nanocomposites: a review on recent advances. Microchimica Acta 186:465. https://doi.org/10.1007/s00604-019-3588-1.

[24] Luo Y, Guo R, Li T, Li F, Liu Z, Zheng M, Wang B, Yang Z, Luo H and Wan Y (2019) Application of polyaniline for Li-Ion batteries, lithium–sulfur batteries, and supercapacitors. ChemSusChem 12:1591–1611. DOI:10.1002/cssc.201802186.

[25] Liao G, Li Q, Xu Z (2019) The chemical modification of polyaniline with enhanced properties: A review. Prog Org Coat 126:35–43.

[26] Cho S, Lee JS and Joo H (2019) Recent developments of the solution-processable and highly conductive polyaniline composites for optical and electrochemical applications. Polymers 11:1965. doi:10.3390/polym11121965.

[30] Zujovic Z, Kilmartin PA and Travas-Sejdic J (2020) The applications of solid-state NMR to conducting polymers. The special case on polyaniline. Molecules 25:444 doi:10.3390/molecules25030444.

[31] Li Z and Gong L (2020) Research Progress on Applications of Polyaniline (PANI) for Electrochemical Energy Storage and Conversion. Materials 13(3):548. https://doi.org/10.3390/ma13030548.

[32] Kazemi F, Naghib SM, Zare Y and Rhee KY (2020) Biosensing applications of polyaniline (PANI)-based nanocomposites: A review. Polym Rev 449:701. https://doi.org/10.1080/15583724.2020.1858871.

[33] Yeh JM, Liou SJ, Lai CY and Wu PC (2001) Enhancement of corrosion protection effect in polyaniline via the formation of polyaniline-clay nanocomposite Materials. Chem Mater 13:1131-1136.

[34] Stejskal J and Gilbert RG (2002) Polyaniline, preparation of a conducting polymer. Pure Appl Chem 74:857-867.

[35] Chen CH (2003) Thermal and morphological studies of chemically prepared emeraldine-base-form polyaniline powder. J Appl Polym Sci 89:2142–2148.

[36] Chowdhury AN, Jesmeen SR, Hossain MM (2004) Removal of dyes from water by conducting polymeric adsorbent. Polym Adv Technol 15:633–638.

[37] Palaniappan S, John A, Amarnath CA, Rao VJ (2004) Mannich-type reaction in solvent free condition using reusable polyaniline catalyst. J Mol Catal A: Chem 218:47–53.

[38] Ramamurthy PC, Harrell WR, Gregory RV, Sadanadan B, Rao AM (2004) mechanical and electrical properties of solution-processed polyaniline multiwalled carbon nanotube composite films. J Electrochem Soc 151:502–506.

[39] Acevedo DF, Salavagione HJ, Miras MC, Barbero CA (2005) Synthesis, properties and applications of functionalized polyanilines. J Braz Chem Soc. https://doi.org/10.1590/S010350532 00500 0200020.

[40] Souza FG, Sirelli L, Michel RC, Soares BG, Herbst MH (2006) In situ polymerization of aniline in the presence of carbon black. J Appl Polym Sci 102:535-541.

[41] Ansari R (2006) Application of polyaniline and its composites for adsorption/recovery of chromium (VI) from aqueous solutions. Acta Chim Slov 53(1):88–94.

[42] Chang KC, Jang GW, Peng CW, Lin CY, Shieh JC, Yeh JM, Yang JC, Li WT (2007) Comparatively electrochemical studies at different operational temperatures for the effect of nanoclay platelets on the anticorrosion efficiency of DBSA-doped polyaniline/Na+–MMT clay nanocomposite coatings. Electrochim Acta 52:5191–5200.

[43] Simoes FR, Bulhoes LOS, Pereira EC (2009) Synthesis and characterization of conducting composites of polyaniline and carbon black with high thermal stability. Polimeros 19:54–57.

[44] Babazadeh M (2009) Aqueous dispersions of DBSA-doped polyaniline: one-pot preparation, characterization, and properties study. J Appl Polym Sci 113:3980–3984.

[45] Salem MA (2010) The role of polyaniline salts in the removal of direct blue 78 from aqueous solution: A kinetic study. React Funct Polym 70:707-714.

[46] Elsayed AH, Mohy Eldin MS, Elsyed AM, Abo Elazm AH, Younes EM, Motaweh HA (2011) Synthesis and properties of polyaniline/ferrites nanocomposites. Int J Electrochem Sci 6:206–221.

[47] Baei MS, Babaee V, Pirouz F (2011) Preparation of polyaniline nanocomposites for removal of sulfate from wastewater. 2nd International Conference on Chemistry and Chemical Engineering 14:95.

[48] Chauhan NPS, Ameta R, Ameta R, Ameta SC (2011) Thermal and conducting behaviour of emeraldine base (EB) form of polyaniline (PANI). Indian J Chem Technol 18(2):118–122.

[49] Pande S, Swaruparani H, Bedre MD, Bhat R, Deshpande R, Venkataraman A (2012) Synthesis, characterization and studies of PANI-MMT nanocompoisites. Nanosci Nanotechnol 2:90-98.

[50] Kavitha B, Siva Kumar K, Narsimlu N (2013) Synthesis and characterization of polyaniline nanofibers. Indian J Pure Ap Phy 51(3):207–209.

[51] Boddula R and Srinivasan P (2014) Emeraldine Base form of polyaniline nanofibers as new, economical, green, and efficient catalyst for synthesis of Z-Aldoximes. J Catal 2014:6.

[52] Wasu MB, Raut AR (2014) Synthesis and characterization of polyaniline based conducting polymers. J Chem Chem Sci 4(2):90–97.

[53] Sharma D, Kaith BS, Rajput J (2014) Single step in situ synthesis and optical properties of polyaniline/ZnO nanocomposites. Sci World J. https://doi.org/10.1155/2014/904513.

[54] Sangamesha MA, Pushpalatha K, Shekar GL (2014) Synthesis and characterization of conducting polyaniline/copper selenide nanocomposites. J Adv Chem Sci 2:223-227.

[55] Bavio MA, Acosta GG, Kessler T (2014) Polyaniline and polyaniline-carbon black nanostructures as electrochemical capacitor electrode materials. Int J Hydrog Energy 39:8582–8589.

[56] Najim TS, Salim AJ (2017) Polyaniline nanofibers and nanocomposites: Preparation, characterization, and application for Cr(VI) and phosphate ions removal from aqueous solution. Arab J Chem 10:S3459–S3467. https://doi.org/10.1016/j.arabjc.2014.02.008.

[57] Maser WK, Benito AM, Callejas MA, Seeger T, Martinez MT, Schreiber J, Muszynski J, Chauvet O, Osvath Z, Koos AA, Biro LP (2003) Mater Sci Eng C 23:87–91.

[58] Ma X, Wang M, Li G, Chena H, Bai R (2006) Preparation of polyaniline–TiO_2 composite film with in situ polymerization approach and its gas-sensitivity at room temperature. Mater Chem Phys 98:241–247.

[59] Ma X, Wang M, Li G, Chena H, Bai R (2006) Preparation of polyaniline–TiO_2 composite film with in situ polymerization approach and its gas-sensitivity at room temperature. Mater Chem Phys 98:241–247.

[60] Wu KH, Ting TH, Wang GP, Ho WD, Shih CC (2008) Effect of carbon black content on electrical and microwave absorbing properties of polyaniline/carbon black nanocomposites. Polym Degrad Stab 93:483-488.

[61] Choudhury A (2009) Polyaniline/silver nanocomposites: Dielectric properties and ethanol vapour sensitivity. Sens Actuators B 138:318–325.

[62] Kumar E and Selvarajan P (2010) Synthesis and studies of PANI/cerium dioxide nanocomposites. J Exp Sci 1:11-14.

[63] Prasanna GD and Jayanna HS (2011) In situ synthesis, characterization and frequency dependent AC conductivity of polyaniline/$CoFe_2O_4$ nanocomposites. J Adv Dielectr 1(3):357-362.

[64] Fan Y, Liu J-H, Yang C-P, Yu M, Liu P (2011) Graphene–polyaniline composite film modified electrode for voltammetric determination of 4-aminophenol. Sens Actuators B 157:669–674.

[65] Ghatak S, Chakraborty G, Meikap AK, Woods T, Babu R, Blau WJ (2011) Synthesis and characterization of polyaniline/carbon nanotube composites. J Appl Polym Sci 119:1016–1025.

[66] Yerawar GR (2012) Characterization of chemically synthesized polyaniline-zinc oxide nanocomposites. Der Pharma Chemica 4(3):1288-1291.

[67] Oh M and Kim S (2012) Effect of dodecyl benzene sulfonic acid on the preparation of polyaniline/activated carbon composites by in situ emulsion polymerization. Electrochim Acta 59:196–201.

[68] Farbod M, Tadavani SK (2012) Electrical properties and glass transition temperature of multiwalled carbon nanotube/polyaniline composites. J Non-Cryst Solids 358:1339–1344.

[69] Li Y, Peng H, Li G, Chen K (2012) Synthesis and electrochemical performance of sandwich-like polyaniline/graphene composite nanosheets. Eur Polym J 48:1406–1412.

[70] Zhao X, Kim J-K, Ahn H-J, Cho K-K, Ahn J-H (2013) A ternary sulfur/polyaniline/carbon composite as cathode material for lithium sulfur batteries. Electrochim Acta 109:145– 152. http://dx.doi.org/10.1016/j.electacta.2013.07.067.

[71] Sedaghat S and Golbaz F (2013) In situ oxidative polymerization of aniline in the presence of manganese dioxide and preparation of polyaniline/MnO_2 nanocomposite. J Nanostructure Chem 3:65.

[72] Zhou B, Wang N, Zhang X, Wang Y, Xiong J and Yan X (2013) In situ polymerization of polyaniline/viscose fiber. Appl Mech Mater 367:7-11.

[73] Xu H and Xing J-W (2013) Preparation of ZnO/PANI nanocomposite and study on its photocatalytic properties. Adv Mater Res 716:368-372. doi:10.4028/www.scientific.net/AMR.716.368.

[74] Jayasudha S, Priya L, Vasudevan KT (2014) Preparation and characterization of Polyaniline/Ag nanocomposites. Int J Chem Tech Res 6(3):1821–1823.

[75] Nadaf LI, Venkatesh KS (2015) Polyaniline-copper oxide nano-composites: Synthesis and characterization. Mat Sci Res India 12(2):108–111. https://doi.org/10.13005/msri/120204.

[76] Shendkar JH, Zate M, Tehare K, Jadhav VV, Mane RS, Naushad M, Yun JM, Kim KH (2016) Polyaniline-cobalt hydroxide hybrid nanostructures and their supercapacitor studies. Mater Chem Phys 180:226-236.

[77] Olad A and Gharekhani H (2016) Study on the capacitive performance of polyaniline/activated carbon nanocomposite for supercapacitor application. J Polym Res 23:147. DOI: 10.1007/s10965-016-1031-4.

[78] Padmapriya S, Harinipriya S, Jaidev K, Sudha V, Kumar D, Pal S (2017) Storage and evolution of hydrogen in acidic medium by polyaniline. Int J Energy Res 1–14. DOI: 10.1002/er.3920.

[79] Majhi M, Choudhary RB, Thakur AK, Omar FS, Duraisamy N, Ramesh K, Ramesh S (2018) $CoCl_2$-doped polyaniline composites as electrode materials with enhanced electrochemical performance for supercapacitor application. Polym Bull 75:1563–1578. https://doi.org/10.1007/s00289-017-2112-1.

[80] Oliveira RDS, Bizeto MA, Camilo FF (2018) Production of self-supported conductive films based on cellulose, polyaniline and silver nanoparticles. Carbohydr Polym 199 (2018) 84–91.

[81] Zhang Y, Wang L, Zhang J, Song P, Xiao Z, Liang C, Qiu H, Kong J, Gu J (2019) Fabrication and investigation on the ultra-thin and flexible Ti_3C_2Tx/co-doped polyaniline electromagnetic interference shielding composite films. Compos Sci Technol 183:107833.

[82] Biswas MRUD, Ho BS, Oh W-C (2019) Eco-friendly conductive polymer-based nanocomposites, $BiVO_4$/graphene oxide/polyaniline for excellent photocatalytic performance. Polym Bull. https://doi.org/10.1007/s00289-019-02973-y.

[83] Yanilmaz M, Dirican M, Asir AM, Zhanga X (2019) Flexible polyaniline-carbon nanofiber supercapacitor electrodes. J Energy Storage 24:100766. https://doi.org/10.1016/j.est.2019.100766.

[84] Aljafari B, Indrakar SK, Ram MK, Biswas PK, Stefanakos E and Takshi A (2019) A polyaniline-based redox-active composite gel electrolyte with photo-electric and electrochromic properties. ChemElectroChem 6:5888–5895. DOI: 10.1002/celc.201901850.

[85] Mu Y, Ruan C, Li P, Xu J, Xie Y (2020) Enhancement of electrochemical performance of cobalt (II) coordinated polyaniline: A combined experimental and theoretical study. Electrochim Acta 338:135881. https://doi.org/10.1016/j.electacta.2020.135881.

[86] Yang S, Zhu S and Hong R (2020) Graphene oxide/polyaniline nanocomposites used in anticorrosive coatings for environmental protection. Coatings 10:1215. doi:10.3390/coatings10121215.

[87] Kim J, Yun S-R, Deshpande SD (2007) Synthesis, characterization and actuation behavior of polyaniline-coated electroactive paper actuators. Polym Int 56:1530–1536. https://doi.org/10.1002/pi.2297.

[88] Qi YN, Xu F, Ma HJ, Sun LX, Zhang J and Jiang T (2008) Thermal stability and glass transition behavior of PANI/ɣ-Al_2O_3 composites. J Therm Anal Calorim 91(1):219–223.

[89] Keivani MB, Zare K, Aghaie H and Ansari R (2009) Removal of methylene blue dye by application of polyaniline nano composite from aqueous solutions. J Phys Theor Chem 6(1):50-56.

[90] Zheng L, Wang X , An H, Wang X, Yi L and Bai L (2010) The preparation and performance of flocculent polyaniline/carbon nanotubes composite electrode material for supercapacitors. J Solid State Electrochem. Doi: 10.1007/s1000801011318.

[91] Khan A, Aldwayyan AS, Alhoshana, M and Alsalhi M (2010) Synthesis by in situ chemical oxidative polymerization and characterization of polyaniline/iron oxide nanoparticle composite. Polym Int 59:1690–1694. DOI 10.1002/pi.2908.

[92] Marins JA, Soares BG, Dahmouche K, Ribeiro SJL, Barud H, Bonemer D (2011) Structure and properties of conducting bacterial cellulose-polyaniline nanocomposites. Cellulose 18:1285–1294. DOI 10.1007/s10570-011-9565-4.

[93] Alam F, Ansari SA, Khan W, Khan ME and Naqvi AH (2012) Synthesis, structural, optical and electrical properties of in-situ synthesized polyaniline/silver nanocomposites. Funct Mater Lett 5(3):1250026. DOI: 10.1142/S1793604712500269.

[94] Ozkazanc E, Zor S, Ozkazanc H, Guney HY, Abaci U (2012) Synthesis, characterization and dielectric behavior of (ES)-form polyaniline/cerium(III)-nitrate-hexahydrate composites. Mater Chem Phys 133:356– 362.

[95] Du X, Liu HY, Cai G, Mai YW and Baji A (2012) Use of facile mechanochemical method to functionalize carbon nanofibers with nanostructured polyaniline and their electrochemical capacitance. Nanoscale Res Lett 7:111. http://www.nanoscalereslett.com/content/7/1/111.

[96] Li G-C, Li G-R, Ye S-H, and Gao X-P (2012)A Polyaniline-coated sulfur/carbon composite with an enhanced high-rate capability as a cathode material for lithium/sulfur batteries. Adv Energy Mater 2:1238–1245. DOI: 10.1002/aenm.201200017.

[97] Kumar NA, Choi H-J, Shin YR, Chang DW, Dai L and Baek J-B (2012) Polyaniline-grafted reduced graphene oxide for efficient electrochemical supercapacitors. ACS Nano 6(2):1715–1723.

[98] Mu B, Liu P, Wang A (2013) Synthesis of polyaniline/carbon black hybrid hollow microspheres by layer-by-layer assembly used as electrode materials for supercapacitors. Electrochim Acta 88:177– 183.

[99] Wu Z, Chen X, Zhu S, Zhou Z, Yao Y, Quan W, Bin Liu B (2013) Enhanced sensitivity of ammonia sensor using graphene/polyaniline nanocomposite. Sens Actuators B 178:485– 493.

[100] Jeong J-M, Choi BG, Lee SC, Lee KG, Chang S-J, Han Y-K, Lee YB, Lee HU, Kwon S, Lee G, Lee C-S, Huh Y-S (2013) Hierarchical Hollow spheres of Fe_2O_3@polyaniline for lithium ion battery anodes. Adv Mater. DOI: 10.1002/adma.201302710.

[101] Salunkhe RR, Hsu S-H, Wu KCW and Yamauchi Y (2014) Large-scale synthesis of reduced graphene oxides with uniformly coated polyaniline for supercapacitor applications. ChemSusChem 7:1551 – 1556.

[102] Majumdar S, Saikia U and Mahanta D (2015) Polyaniline-coated filter papers: Cost effective hybrid materials for adsorption of dyes. J Chem Eng Data 60:3382−3391. DOI: 10.1021/acs.jced.5b00645.

[103] Wan P, Wen X, Sun C, Chandran BK, Zhang H, Sun X and Chen X (2015) Flexible transparent films based on nanocomposite networks of polyaniline and carbon nanotubes for high-performance gas sensing. Small 11(40):5409–5415.

[104] Vargas LR, Poli AK, Dutra RDCL, Souza CBD, Baldan MR, Gonçalves ES (2017) Formation of composite polyaniline and graphene oxide by physical mixture method. J Aerosp Technol Manag 9(1):29-38. doi: 10.5028/jatm.v9i1.697.

[105] Jo EH, Jang HD, Chang H, Kim SK, Choi JH and Lee CM (2017) 3D network-structured crumpled graphene/carbon nanotube/polyaniline composites for supercapacitors. ChemSusChem 10:2210 – 2217. DOI:10.1002/cssc.201700212.

[106] Donescu D, Fierascu RC, Ghiurea M, Manaila-Maximean D, Nicolae CA, Somoghi R, Spataru CI, Stanica N, Raditoiu V, Vasile E (2017) Synthesis and magnetic properties of inverted core-shell polyaniline-ferrite composite. Appl Surf Sci 414:8–17.

[107] Liu P, Yan J, Gao X, Huang Y, Zhang Y (2018) Construction of layer-by-layer sandwiched graphene/polyaniline nanorods/carbon nanotubes heterostructure for high performance supercapacitors. Electrochim Acta 272.

[108] Wu J, Zhang Q, Wang J, Huang X and Bai H (2018) A self-assembly route to porous polyaniline/reduced graphene oxide composite materials with molecular-level uniformity for high-performance supercapacitors. Energy Environ Sci 11:1280-1286. DOI: 10.139/C8EE00078F.

[109] Mallikarjuna NN, Manohar SK, Kulkarni PV, Venkataraman A, Aminabhavi TM (2015) Novel high dielectric constant nanocomposites of polyaniline dispersed with γ-Fe_2O_3 nanoparticles. J Appl Polym Sci 97:1868–1874.

[110] Pal R, Goyal SL, Gupta V and Rawal I (2019) MnO_2-Magnetic core-shell structured polyaniline dependent enhanced EMI shielding effectiveness: A study of VRH conduction. ChemistrySelect 4:9194 –9210. DOI: 10.1002/slct.201901199.

[111] Lin Y-T, Don T-M, Wong C-J, Meng F-C, Lin Y-J, Lee S-Y, Lee C-F, Chiu W-Y (2019) Improvement of mechanical properties and anticorrosion performance of epoxy coatings by the introduction of polyaniline/graphene composite. Surf Coat Technol 374:1128–1138.

[112] Xiong S, Zhang X, Wang R, Lu Y, Li H, Liu J, Li S, Qiu Z, Wu B, Chu J, Wang X, Zhang R, Gong M, Chen Z (2019) Preparation of covalently bonded polyaniline nanofibers/carbon nanotubes supercapacitor electrode materials using interfacial polymerization approach. J Polym Res 26: 90. https://doi.org/10.1007/s10965-019-1749-x.

[113] Lou C, Jing T, Zhou J, Tian J, Zheng Y, Wang C, Zhao Z, Lin J, Liu H, Zhao C, Guo Z (2020) Laccase immobilized polyaniline/magnetic graphene composite electrode for detecting hydroquinone. Int J Biol Macromol 149:1130-1138. doi: 10.1016/j.ijbiomac.2020.01.248.

[114] Liu Y, Sun J and Zhao X (2020) The study on the dielectric properties and conductivity of polyaniline/nylon composites. J Text Inst 111:1697-1704. https://doi.org/10.1080/00405000.2020.1743478.

[115] Vijayalakshmi S, Kumar E and Nithya S (2020) Investigation on polyaniline with manganese dioxide nanostructure by using an in situ oxidative polymerization method. Ionics 26:839–848. https://doi.org/10.1007/s11581-019-03207-x.

[116] Ren B, Li Y, Meng D, Li J, Gao S, Cao R (2020) Encapsulating polyaniline within porous MIL-101 for high-performance corrosion protection. J Colloid Interface Sci 579:842–852.

[117] Zeng QH, Yu AB, Lu GQ (Max) and Paul DR (2005) Clay-based polymer nanocomposites: Research and commercial development. J Nanosci Nanotechnol 5:1574–1592.

[118] Omanovic-Miklicanin E, Badnjevic A, Kazlagic A, Hajlovac M (2020) Nanocomposites: a brief review. Health and Technology 10:51–59. https://doi.org/10.1007/s12553-019-00380-x.

[119] Usuki A, Kojima Y, Kawasumi M, Okada A, Fukushima Y, Kurauchi T, and Kamigaito O (1993) Synthesis of nylon 6-clay hybrid. J Mater Res 8(5):1179-1184.

[120] Fu X and Qutubuddin S (2001) Polymer–clay nanocomposites: exfoliation of organophilic montmorillonite nanolayers in polystyrene. Polymer 42:807–813.

[121] Okamoto M and Ray SS (2004) Polymer/Clay Nanocomposites. Encyclopedia of Nanoscience and Nanotechnology 8:1–52.

[122] Essawy H, Badran A, Youssef A, Abd El-Hakim AE-F (2014) Synthesis of poly(methylmethacrylate)/montmorillonite nanocomposites via in situ intercalative suspension and emulsion polymerization. Polym Bull 53, 9–17. DOI 10.1007/s00289-004-0312-y

[123] Uthirakumar P, Song M-K, Nah C, Lee Y-S (2005) Preparation and characterization of exfoliated polystyrene/clay nanocomposites using a cationic radical initiator-MMT hybrid. Eur Polym J 41:211–217.

[124] Wu C-S, Huang Y-J, Hsieh T-H, Huang P-T, Hsieh B-Z, Han Y-K, Ho K-S (2008) Studies on the conducting nanocomposite prepared by in situ polymerization of aniline monomers in a neat (aqueous) synthetic mica clay. J Polym Sci A Polym Chem, 46:1800–1809.

[125] Sedlakova Z, Plestil J, Baldrian J, Slouf M, Holub P (2009) Polymer-clay nanocomposites prepared via in situ emulsion polymerization. Polym Bull 63:365–384. DOI 10.1007/s00289-009-0097-0.

[126] Ahmad MB, Gharayebi Y, Salit MS, Hussein MZ and Shameli K (2011) Comparison of in situ polymerization and solution-dispersion techniques in the preparation of polyimide/montmorillonite (MMT) nanocomposites. Int J Mol Sci 12:6040-6050. doi:10.3390/ijms12096040.

[127] Srinivasulu R, Madhusudan S, Kumar MA, Murthy VN, Kartikeyan N (2013) Synthesis and characterization of polymer nanocomposites filled with nanoclay/aerosil on mechanical and thermal properties. Int J Nanomater Biostructures 3(4):51-56.

[128] Mallakpour S and Khani M (2016) Characterization of nanocomposite laminates fabricated from aqueous dispersion of polyvinylpyrrolidone and L-leucine amino acid modified-montmorillonite. Polym Bull 73:2677–2688. DOI 10.1007/s00289-016-1614-6.

[129] Assem Y, Khalaf AI, Rabia AM, A. A. Yehia AA, Zidan TA (2017) Poly(diallyldimethylammonium chloride)/clay nanocomposites: effect of molecular weight and concentration of polymer on the structural, thermal, and dielectric properties. Polym Bull 74:3015–3026. DOI 10.1007/s00289-016-1873-2.

[130] Djamaa Z, Lerari D, Mesli A, Bachari K (2019) Poly(acrylic acid-co-styrene)/clay nanocomposites: efficient adsorbent for methylene blue dye pollutant. Int J Plast Technol 23(1):110–121. https://doi.org/10.1007/s12588-019-09237-4.

[131] Arya A and Sharma AL (2020) Investigation on enhancement of electrical, dielectric and ion transport properties of nanoclay-based blend polymer nanocomposites. Polym Bull 77:2965–2999. https://doi.org/10.1007/s00289-019-02893-x.

[132] Hoang HV and Holze R (2006) Electrochemical synthesis of polyaniline/montmorillonite nanocomposites and their characterization. Chem Mater 18:1976-1980.

[133] Olad A and Rashidzadeh A (2008) Preparation and anticorrosive properties of PANI/Na-MMT and PANI/O-MMT nanocomposites. Prog Org Coat 62:293–298.

[134] Reena VL, Sudha JD, Pavithran C (2009) Role of Amphiphilic dopants on the shape and properties of electrically conducting polyaniline-clay nanocomposite. J Appl Polym Sci 113:4066–4076.

[135] Shakoor A, Rizvi TZ, Nawaz A (2011) Raman spectroscopy and AC conductivity of polyaniline montmorillonite (PANI–MMT) nanocomposites. J Mater Sci: Mater Electron 22:1076–1080. DOI 10.1007/s10854-010-0262-0.

[136] Abdelkader R, Amine H, and Mohammed B (2012) Thermally stable forms of pure polyaniline catalyzed by an acid-exchanged montmorillonite clay called Maghnite-H+ as an effective catalyst. Int J Polym Sci Article ID 846710:7. doi:10.1155/2012/846710.

[137] Vijayakumar B, Anjana KO and Rao GR (2015) Polyaniline/clay nanocomposites: preparation, characterization and electrochemical properties. IOP Conf. Series: Mater Sci Eng 73:012112. doi:10.1088/1757-899X/73/1/012112.

[138] Kalaivasan N, Shafi SS (2017) Enhancement of corrosion protection effect in mecnochemically synthesized Polyaniline/MMT clay nanocomposites. Arab J Chem 10:S127–S133.

[139] Zhang Y, Shao Y, Shi Q, Li P (2017) Effect of polyaniline/montmorillonite content on the corrosion protection of epoxy coating. Anti-Corros Methods Mater 64:75 – 82. http://dx.doi.org/10.1108/ACMM-03-2015-1511.

[140] Motlatle AM, Ray SS, Scrib M (2018) Polyaniline-clay composite-containing epoxy coating with enhanced corrosion protection and mechanical properties. Synth Met 245:102–110.

[141] Leon-Almazan CMD, Estrada-Moreno IA, Páramo-Garcia U, Rivera-Armenta,JL (2018) Polyaniline/clay nanocomposites. A comparative approach on the doping acid and the clay spacing technique. Synth Met 236:61–67.

[142] Silva DBRS, Junior LPC, Aguiar MFD, Melo CPD, Alves KGB (2018) Preparation and characterization of nanofibers of polyvinyl alcohol/polyaniline-montmorillonite clay. J Mol Liq 272:1070–1076.

[143] Meneses XB, Rillera AS, Dahonog LA and Tapia AKG (2018) Conduction in polyaniline-emeraldine salt/bentonite composites using impedance spectroscopy. Key Eng Mater 775:63-67. doi:10.4028/www.scientific.net/KEM.775.63.

[144] Pinto CP, Pachekoski WM, Dalmolin C, Becker D (2019) Plasticizer effect and electronic diffusive behavior of polyaniline-modified clay in polystyrene nanocomposites. Polym Compos. DOI 10.1002/pc.24594.

[145] Rahmouni A and Belbachir M (2019) Molecular structure of PANI and its homologue PANI–PEO2000 catalyzed by Maghnite-H+ (Algerian MMT): synthesis, characterization and physical and chemical properties. Polym Bull 76:4677–4701. https://doi.org/10.1007/s00289-018-2620-7.

[146] Abbas M, Hachemaoui A, Yahiaoui A, Mourad A-H.I, Belfedal A and Cherupurakal N (2020) Chemical synthesis of nanocomposites via *in-situ* polymerization of aniline and iodoaniline using exchanged montmorillonite. Polymers and Polymer Composites 1–10.

[147] Kenane A, Galca A-C, Matei E, Yahiaoui A, Hachemaoui A, Benkouider AM, Bartha C, Istrate MC, Galatanu M, Rasoga O, Stanculescu A (2020) Synthesis and characterization of conducting aniline and o-anisidine nanocomposites based on montmorillonite modified clay. Appl Clay Sci 184 (2020) 105395.

[148] Kim BH, Jung JH, Hong SH, Joo J (2002) Nanocomposite of polyaniline and Na+-montmorillonite clay. Macromolecules 35:1419–1423.

[149] Nascimento GM, Constantino VRL, Landers R, Temperini MLA (2004) Aniline polymerization into montmorillonite clay: a spectroscopic investigation of the intercalated conducting polymer. Macromolecules 37:9373–9385.

[150] Nascimento GM, Constantino VRL, Landers R, Temperini MLA (2006) Spectroscopic characterization of polyaniline formed in the presence of montmorillonite clay. Polymer 47:6131–6139.

[151] Binitha NN, Sugunan S (2008) Polyaniline/pillared montmorillonite clay composite nanofibers. J Appl Polym Sci 107:3367–3372.

[152] Kalaivasan N, Shafi SS (2010) Synthesis of various polyaniline/clay nanocomposites derived from aniline and substituted aniline derivatives by mechanochemical intercalation method. E-J Chem 7(4):1477–1483.

[153] Narayanan BN, Koodathil R, Gangadharan T, Yaakob Z, Saidu FK, Chandralayam S (2010) Preparation and characterization of exfoliated polyaniline/montmorillonite nanocomposites. Mater Sci Eng B 168:242–244.

[154] Srivastava N, Singh Y, Singh RA (2011) Preparation of intercalated polyaniline/clay nanocomposite and its exfoliation exhibiting dendritic structure. Bull Mater Sci 34:635–638.

[155] Binitha N, Suraja V, Yaakob Z, Sugunan S (2011) Synthesis of polyaniline-montmorillonite nanocomposites using H_2O_2 as the oxidant. Sains Malays 40(3):215–219.

[156] Kazim S, Ahmad S, Pfleger J, Plestil J, Joshi YM (2011) Polyaniline–sodium montmorillonite clay nanocomposites: effect of clay concentration on thermal, structural, and electrical properties. J Mater Sci 47:420–428.

[157] Baldissera AF, Souza JF, Ferreira CA (2013) Synthesis of polyaniline/clay conducting nanocomposites. Synth Met 183:69–72.

[158] Deng S, Guang Li G (2013) structural features and microwave absorbing properties of polyaniline montmorillonite composites prepared by in-situ. J Fiber Bioeng Informat 6(1):33–40.

[159] El-Ghaffar MA, Youssef AM, Abd El-Hakim AA (2015) Polyaniline nanocomposites via in situ emulsion polymerization based on montmorillonite: preparation and characterization. Arab J Chem 8(6):771–779. https://doi.org/10.1016/j.arabjc.2014.01.001.

[160] Nguyen VH, Shim JJ (2015) Green synthesis and characterization of carbon nanotubes/polyaniline nanocomposites. J Spectrosc. https://doi.org/10.1155/2015/297804.

[161] Yamabe K, Goto H (2018) Synthesis and surface observation of montmorillonite/polyaniline composites. J Compos Sci 2:15. https://doi.org/10.3390/jcs2010015.

[162] Hattab Y, Benharrats N (2019) Electrical and thermal properties of PANI–Mmt nanocomposites in strongly acidic aqueous media. SN Appl Sci 1:750. https://doi.org/10.1007/s42452-019-0703-1.

[163] Suneetha RRB, Kulandaivel S, Vedhi C (2020) Synthesis, characterization and electrochemical application of hybrid nanocomposites of polyaniline with novel clay mineral. Mater Today: Proc. doi:10.1016/j.matpr.2020.07.211.

[164] Joussein E, Petit S, Churchman J, Theng B, Righi D and Delvaux B (2005) Halloysite clay minerals - a review. Clay Minerals. 40:383-426. DOI: 10.1180/0009855054040180.

[165] Du M, Guo B and Jia D (2010) Newly emerging applications of halloysite nanotubes: a review. Polym Int. 59:574–582. DOI 10.1002/pi.2754.

[166] Yuan P, Tan D, Annabi-Bergaya F (2015) Properties and applications of halloysite nanotubes: recent research advances and future prospects. Applied Clay Science 112–113:75–93. http://dx.doi.org/10.1016/j.clay.2015.05.001.

[167] Yu L, Wang H, Zhang Y, Zhang B and Liu J (2016) Recent advances in halloysite nanotube derived composites for water treatment. Environmental Science Nano. 3:28-44. DOI: 10.1039/c5en00149h.

[168] Gaaz T.S, Sulong A.B, Kadhum A.A.H, Al-Amiery A.A, Nassir M.H and Jaaz A.H (2017) The Impact of Halloysite on the Thermo-Mechanical Properties of Polymer Composites. Molecules. 22:838. doi:10.3390/molecules22050838.

[169] Kausar A (2018) Review on Polymer/Halloysite Nanotube Nanocomposite. Polymer-Plastics Technology and Engineering. 57:548-564. https://doi.org/10.1080/03602559.2017.1329436.

[170] Papoulis D (2019) Halloysite based nanocomposites and photocatalysis: A Review. Applied Clay Science 168:164–174. https://doi.org/10.1016/j.clay.2018.11.009.

[171] Danyliuk N, Tomaszewska J, Tatarchuk T (2020) Halloysite nanotubes and halloysite-based composites for environmental and biomedical applications. Journal of Molecular Liquids 309:113077. https://doi.org/10.1016/j.molliq.2020.113077.

[172] Zhang L, Wang T, Liu P (2008) Polyaniline-coated halloysite nanotubes via in-situ chemical polymerization. Appl Surf Sci 255:02091–2097. doi:10.1016/j.apsusc.2008.06.187.

[173] Tierrablanca E, Romero-Garcia J, Roman P, Cruz-Silva R (2010) Biomimetic polymerization of aniline using hematin supported on halloysite nanotubes. Applied Catalysis A: General 381:267–273. doi:10.1016/j.apcata.2010.04.021.

[174] Zhou C, Du X, Liu Z, Mai Y.W, Ringer S.P (2011) Multi-holed clay nanotubes and their modification with a polyaniline nanolayer. J Mater Sci. 46:446–450. DOI 10.1007/s10853-010-4909-2.

[175] Abolghasemi M.M, Arsalani N, Yousefi V, Arsalani M, Piryaei M (2016) Fabrication of polyaniline-coated halloysite nanotubes by in situ chemical polymerization as a solid-phase microextraction coating for the analysis of volatile organic compounds in aqueous solutions. Journal of Separation Science. 39:956–963. DOI 10.1002/jssc.201500839.

[176] Yang Z, Zheng X and Zheng J (2016) Non-enzymatic sensor based on a glassy carbon electrode modified with Ag nanoparticles/polyaniline/halloysite nanotube nanocomposites for hydrogen peroxide sensing. RSC Advances. DOI: 10.1039/C6RA06366G.

[177] Huang H, Yao J, Chen H, Zeng X, Chen C, She X, Li L (2016) Facile preparation of halloysite/polyaniline nanocomposites via in situ polymerization and layer-by-layer assembly with good supercapacitor performance. Journal of Materials Science. 51:4047–4054. DOI 10.1007/s10853-016-9724-y.

[178] Zhou T, ZhaoY, Han W, Xie H, Li C and Yuan M (2017) Enhanced solvent-free selective oxidation of cyclohexene to 1,2-cyclohexanediol by polyaniline@halloysite nanotubes. Journal of Materials Chemistry A. 5:18230-18241. https://doi.org/10.1039/C7TA02605F.

[179] Noskov Y, Ogurtsov N, Bliznyuk V, Lvov Y, Myronyuk I and Pud A (2021) Synthesis and properties of core–shell halloysite–polyaniline nanocomposites. Applied Nanoscience. https://doi.org/10.1007/s13204-021-01812-9.

[180] Chen J, Hong X, Zhao Y and Zhang Q (2014) Removal of hexavalent chromium from aqueous solution using exfoliated polyaniline/montmorillonite composite. Water Sci Technol 70(4):678-684. DOI:10.2166/wst.2014.277.

[181] Piri S, Zanjani ZA, Piri F, Zamani A, Yaftian M and Davari M (2016) Potential of polyaniline modified clay nanocomposite as a selective decontamination adsorbent for Pb(II) ions from contaminated waters; kinetics and thermodynamic study. J Environ Health Sci Eng 14:20. DOI 10.1186/s40201-016-0261-z.

[182] Soltani H, Belmokhtar A, Zeggal FZ, Benyoucef A, Bousalem S, Bachari K (2019) Copper(II) removal from aqueous solutions by PANI-clay hybrid material: fabrication, characterization, adsorption and kinetics study. J Inorg Organomet Polym Mater 29:841–850.

[183] Ali MB, Wang F, Boukherroub R, Lei W, Xia M (2019) Phytic acid-doped polyaniline nanofibers-clay mineral for efficient adsorption of copper (II) ions. Journal of Colloid and Interface Science 553:688–698.

[184] Li Q, Sun L, Zhang Y, Qian Y, Zhai J (2011) Characteristics of equilibrium, kinetics studies for adsorption of Hg(II) and Cr(VI) by polyaniline/humic acid composite. Desalination 266:188-194. https://doi.org/10.1016/j.desal.2010.08.025.

[185] Gu H, Rapole SB, Sharma J, Huang Y, Cao D, Colorado HA, Luo Z, Haldolaarachchige N, Young DP, Walters B, Wei S, Guo Z (2012) Magnetic polyaniline nanocomposites toward toxic hexavalent chromium removal. RSC Advances 2:11007–11018. DOI: 10.1039/c2ra21991c.

[186] Javadian H, Vahedian P, Toosi M (2013) Adsorption characteristics of Ni(II) from aqueous solution and industrial wastewater onto polyaniline/HMS nanocomposite powder. Appl Surf Sci 284:13-22. https://doi.org/10.1016/j.apsusc.2013.06.111.

[187] Fang X, Xu X, Wang S, and Wang D (2013) Adsorption kinetics and equilibrium of Cu(II) from aqueous solution by polyaniline/coconut shell–activated carbon composites. J Environ Eng 139(10):1279-1284.

[188] Javadian H, Ghaemy M, Taghavi M (2014) Adsorption kinetics, isotherm, and thermodynamics of Hg^{2+} to polyaniline/hexagonal mesoporous silica nanocomposite in water/wastewater. J Mater Sci 49:232–242. DOI 10.1007/s10853-013-7697-7.

[189] Shyaa AA, Hasan OA, Abbas AA (2015) Synthesis and characterization of polyaniline/zeolite nanocomposite for the removal of chromium(VI) from aqueous solution. J Saudi Chem Soc 19:101–107. http://dx.doi.org10.1016/j.jscs.2012.01.001.

[190] Ayad MM and El-Nasr AA (2010) Adsorption of cationic dye (methylene blue) from water using polyaniline nanotubes base. J Phys Chem C 114:14377–14383. Doi: 10.1021/jp103780w.

[191] Benhebal H, Chaib M, Leonard AL, Crine M, Lambert SD (2014) Preparation of polyaniline-modified local clay and study of its sorption capacity. J Nanost Chem 4:98.

[192] Patil MR and Shrivastava VS (2016) Adsorptive removal of methylene blue from aqueous solution by polyaniline nickel ferrite nanocomposite: a kinetic approach. Desalin Water Treat 57(13):5879-5887.

[193] Shahabuddin S, Sarih NM, Kamboh MA, Nodeh HR, Mohamad S (2016) Synthesis of polyaniline coated graphene Oxide@SrTiO3 nanocube nanocomposites for enhanced removal of carcinogenic dyes from aqueous solution. Polymers 8(9):305.

[194] Mu B, Tang J, Zhang L, Wang A (2016) Preparation, characterization and application on dye adsorption of a well-defined two-dimensional superparamagnetic clay/polyaniline/Fe_3O_4 nanocomposite. Appl Clay Sci 132–133:7–16. http://dx.doi.org/10.1016/j.clay.2016.06.005.

[195] Shahryari Z, Goharrizi AS and Azadi M (2010) Experimental study of methylene blue adsorption from aqueous solutions onto carbon nano tubes. Int J Water Resour Environ Eng 2(2):016-028.

[196] Zhang W, Zhou C, Zhou W, Lei A, Zhang Q, Wan Q, Zou B (2011) Fast and considerable adsorption of methylene blue dye onto graphene oxide. Bull Environ Contam Toxicol (2011) 87:86–90. DOI 10.1007/s00128-011-0304-1.

[197] Shi Y, Xue Z, Wang X, Wang L, Wang A (2013) Removal of methylene blue from aqueous solution by sorption on lignocellulose-g-poly(acrylic acid)/montmorillonite three-dimensional cross-linked polymeric network hydrogels. Polym Bull 70:1163–1179. DOI 10.1007/s00289-012-0898-4.

[198] Li Y, Du Q, Liu T, Sun J, Wang Y, Wu S, Wang Z, Xia Y, Xia L (2013) Methylene blue adsorption on graphene oxide/calcium alginate composites. Carbohydr Polym 95:501– 507.

[199] Khodaie M, Ghasemi N, Moradi B and Rahimi M (2013) Removal of methylene blue from wastewater by adsorption onto $ZnCl_2$ activated corn husk carbon equilibrium studies. J Chem Article ID 383985:6. http://dx.doi.org/10.1155/2013/383985.

[200] Kavitha K and Senthamilselvi MM (2014) Adsorptive removal of methylene blue using the natural adsorbent-Vitex Negundo Stem. Int J Curr Res Aca Rev 2(9):270-280.

[201] Cottet L, Almeida CAP, Naidek N, Viante MF, Lopes MC, Debacher NA (2014) Adsorption characteristics of montmorillonite clay modified with iron oxide with respect to methylene blue in aqueous media. Appl Clay Sci 95:25-31.

[202] Santhi T, Manonmani S, Vasantha VS, Chang YT (2016) A new alternative adsorbent for the removal of cationic dyes from aqueous solution. Arab J Chem 9:S466–S474.

[203] Miyah Y, Lahrichi A, Idrissi M, Khalil A, Zerrouq F (2018) Adsorption of methylene blue dye from aqueous solutions onto walnut shells powder: Equilibrium and kinetic studies. Surf Interfaces. doi: 10.1016/j.surfin.2018.03.006.

[204] Liu C, Omer AM, Ouyang X-K (2018) Adsorptive removal of cationic methylene blue dye using carboxymethyl cellulose/k-carrageenan/activated montmorillonite composite beads: Isotherm and kinetic studies. Int J Biol Macromol 106:823-833. https://doi.org/10.1016/j.ijbiomac.2017.08.084.

[205] Mouni L, Belkhiri L, Bollinger J-C, Bouzaza A, Aymen Assadi A, Tirri A, Dahmoune F, Madani K, Remini H (2018) Removal of Methylene Blue from aqueous solutions by adsorption on Kaolin: Kinetic and equilibrium studies. Appl Clay Sci153:38–45.

[206] Guesmi Y, Agougui H, Lafi R, Jabli M, Hafiane A (2018) Synthesis of hydroxyapatite-sodium alginate via a co-precipitation technique for efficient adsorption of Methylene Blue dye. J Mol Liq 249:912–920. https://doi.org/10.1016/j.molliq.2017.11.113.

[207] He Y, Jiang DB, Chen J, Jiang DY, Zhang YX (2018) Synthesis of MnO_2 nanosheets on montmorillonite for oxidative degradation and adsorption of methylene blue. J Colloid Interface Sci 510:207–220. https://doi.org/10.1016/j.jcis.2017.09.066.

[208] Akbour RA, Ouachtak H, Jada A, Akhouairi S, Addi AA, Douch J, Hamdani M (2018) Humic acid covered alumina as adsorbent for the removal of organic dye from coloured effluents. Desalin Water Treat 112:207–217. doi: 10.5004/dwt.2018.22006.

[209] Youcef LD, Belaroui LS, Lopez-Galindo A (2019) Adsorption of a cationic methylene blue dye on an Algerian palygorskite. Appl Clay Sci 179:105145. https://doi.org/10.1016/j.clay.2019.105145.

[210] De Castro MLFA, Abad MLB, Sumalinog DAG, Abarca RRM, Paoprasert P, de Luna MDG (2018) Adsorption of Methylene Blue dye and Cu(II) ions on EDTA-modified bentonite: Isotherm, kinetic and thermodynamic studies. Sustain Environ Res 28:197-205.

[211] Ansari R, Samaneh, Alaei and Khah AM (2011) Application of polyaniline for removal of acid green 25 from aqueous solution. J Sci Ind Res 70:804-809.

[212] Ayad MM and El-Nasr AA (2012) Anionic dye (acid green 25) adsorption from water by using polyaniline nanotubes salt/silica composite. J Nanostructure Chem 3:3.

[213] Ansari R and Dezhampanah H (2013) Application of polyaniline/sawdust composite for removal of acid green 25 from aqueous solutions: kinetics and thermodynamic studies. Eur Chem Bull 2:220-225.

[214] Mahmoodi NM, Hayati B, Arami M, Bahrami H (2011) Preparation, characterization and dye adsorption properties of biocompatible composite (alginate/titania nanoparticle). Desalination 275:93-101. https://doi.org/10.1016/j.desal.2011.02.034.

[215] Parimalam R, Raj V, Sivakumar P (2012) Removal of acid green 25 from aqueous solution by adsorption. E-J Chem 9:1683–1698.

[216] Salahuddin NA, Ayad MM, Essa ME (2015) Modified chitosan for efficient dye adsorption in low acid media. Int J Mater Chem 5:54-63.

[217] Sobhanardakani S, Zandipak R (2015) Removal of anionic dyes (Direct Blue 106 and Acid Green 25) from aqueous solutions using oxidized multi-walled carbon nanotubes. Iran J Health Sci 3(3):48–57.

[218] Sathya M, Kumar PE, Santhi M and Muralidharan B (2018) Removal of acid green 25 dye by using activated carbon prepared from passiflorafoetida[PAC-MnO_2-NC]nanocomposite in batch adsorption-kinetic study. Rasayan J Chem 11(4):1741-1749. http://dx.doi.org/10.31788/RJC.2018.1144029.

[219] Jain SN, Gogate PR (2018) Efficient removal of Acid Green 25 dye from wastewater using activated Prunus Dulcis as biosorbent: batch and column studies. J Environ Manag 210:226–238.

[220] Yap PW, Priyaa V (2019) Removal of crystal violet and acid green 25 from water using kaolin. Mater Sci Eng 495:012052. https://doi.org/10.1088/1757-899X/495/1/012052.

[221] Mahanta D, Madras G, Radhakrishnan S, Patil S (2008) Adsorption of sulfonated dyes by polyaniline emeraldine salt and its kinetics. J Phys Chem 112:10153-10157.

[222] Rahimi R, Kerdari H, Rabbani M (2010) Adsorptive removal of crystal violet (CV), a carcinogenic textile dye, from aqueous solution by conducting polyaniline/hollow manganese ferrite nanocomposites. ECSOC-14. https://www.researchgate.net/publication/228525238.

[223] Ansari R, Mosayebzadeh Z (2011) Application of polyaniline as an efficient and novel adsorbent for azo dyes removal from textile wastewaters. Chemical Papers 65(1):1–8.

[224] Janaki V, Vijayaraghavan K, Oh BT, Lee KJ, Muthuchelian K, Ramasamy AK, Kannan SK (2012) Starch/polyaniline nanocomposite for enhanced removal of reactive dyes from synthetic effluent. Carbohydr Polym 90:1437–1444.

[225] Baseri JR, Palanisamy PN and Sivakumar P (2012) Application of polyaniline nano composite for the adsorption of acid dye from aqueous solutions. E-J of Chem 9(3):1266-1275. https://doi.org/10.1155/2012/415234.

[226] Karthikaikumar S, Karthikeyan M, Satheesh Kumar KK (2014) Removal of congo red dye from aqueous solution by polyaniline- montmorillonite composite. Chem Sci Rev Lett 2(8):606–614.

[227] Olad A, Azhar FF (2014) Eco-friendly biopolymer/clay/conducting polymer nanocomposite: characterization and its application in reactive dye removal. Fiber Polym 15:1321–1329.

[228] Khairy M, Kamal R, Amin NH, Mousa MA (2016) Kinetics and isotherm studies of Remazol Red adsorption onto polyaniline/cerium oxide nanocomposites. J Bas Environ Sci 3:123–132.

[229] Gemeay AH, Elsharkawy RB, Aboelfetoh EF (2018) Graphene oxide/polyaniline/manganese oxide ternary nanocomposites, facile synthesis, characterization, and application for indigo carmine removal. J Polym Environ 26:655–669.

[230] Kistler SS (1931) Coherent expanded aerogels and jellies. Nature 127(3211):741. doi: 10.1038/127741a0.

[231] Moreno-Castilla C and Maldonado-Hodar FJ (2005) Carbon aerogels for catalysis applications: An overview. Carbon 43:455–465.

[232] Pekala RW (1989) Organic aerogels from the polycondensation of resorcinol with formaldehyde. J Mater Sci 24:3221 3227.

[233] Zhang S, Fu R, Wu D, Xu W, Ye Q, Chen Z (2004) Preparation and characterization of antibacterial silver-dispersed activated carbon aerogels. Carbon 42:3209–3216.

[234] Saquing CD, Cheng TT, Aindow M and Erkey C (2004) Preparation of platinum/carbon aerogel nanocomposites using a supercritical deposition method. J Phys Chem B 108:7716-7722. Doi:10.1021/jp049535v.

[235] Kalpana D, Omkumar KS, Kumar SS, Renganathan NG (2006) A novel high power symmetric ZnO/carbon aerogel composite electrode for electrochemical supercapacitor. Electrochim Acta 52:1309–1315. doi:10.1016/j.electacta.2006.07.032.

[236] Fang B and Binder L (2006) A modified activated carbon aerogel for high-energy storage in electric double layer capacitors. J Power Sources 163 (2006) 616–622. doi:10.1016/j.jpowsour.2006.09.014.

[237] Tsioptsias C, Michailof C, Stauropoulos G, Panayiotou C (2009) Chitin and carbon aerogels from chitin alcogels. Carbohydr Polym 76,:535–540. doi:10.1016/j.carbpol.2008.11.018.

[238] Shariff AM, Beshir DM, Bustam MA and Maitra S (2010) Some studies on the synthesis and characterization of carbon aerogel. Trans Ind Ceram Soc 69:1-4 http://dx.doi.org/10.1080/0371750X.2010.11090822.

[239] An H, Wang Y, Wang X, Zheng L, Wang X, Yi L, Bai L, Zhang X (2010) Polypyrrole/carbon aerogel composite materials for supercapacitor. J Power Sources 195:6964–6969. doi:10.1016/j.jpowsour.2010.04.074.

[240] Lin KS, Mai Y-J, Chiu SW, Yang JH and Chan SLI (2012) Synthesis and characterization of metal hydride/carbon aerogel composites for hydrogen storage. J Nanomater Article ID 201584, 9 pages. doi:10.1155/2012/201584.

[241] Rejitha KS, Abraham PA, Panicker NPR, Jacob KS, Pramanik NC (2013) Role of catalyst on the formation of resorcinol-furfural based carbon aerogels and its physical properties. Advances in Nanoparticles 2:99-103. http://dx.doi.org/10.4236/anp.2013.22017.

[242] Bakierska M, Molenda M, Majda D, Dziembaj R (2014) Functional starch based carbon aerogels for energy applications. Procedia Eng 98:14-19.. https://doi.org/10.1016/j.proeng.2014.12.481.

[243] Yan M-F, Zhang L-H, He R, Liu Z-F (2015) Synthesis and characterization of carbon aerogels with different catalysts. J Porous Mater 22:699–703. DOI 10.1007/s10934-015-9942-8.

[244] Wang S, Yan M, Li H, Zhang L and Liu Z (2015) Synthesis and characterization of carbon aerogels with acidizing process. IC3ME 2015 407-411.

[245] Schwan M and Ratke L (2016) Flexible carbon aerogels. C 2:22. https://doi.org/10.3390/c2030022.

[246] Ciszewski M, Szatkowska E, Koszorek A, Majka M (2017) Carbon aerogels modified with graphene oxide, graphene and CNT as symmetric supercapacitor electrodes. J Mater Sci: Mater Electron 28:4897–4903. DOI 10.1007/s10854-016-6137-2.

[247] Wang S, Yan M, Liu H, Xu Y, Zhang L, Liu Z (2017) Preparation and characterization of Ni-doped carbon aerogel for supercapacitor. Mater Sci Eng 167:012014. doi:10.1088/1757-899X/167/1/012014.

[248] Lu S, Guo H, Zhou Y, Liu Y, Jin Z, Liu B, Zhou Y (2017) The monolithic carbon aerogels and aerogels composites for electronics and thermal protection applications. AIP Conf Proc 1884:030004-1–030004-4. doi: 10.1063/1.5002514.

[249] Guo F, Jiang Y, Xu Z, Xiao Y, Fang B, Liu Y, Gao W, Zhao P, Wang H and Gao C (2018) Highly stretchable carbon aerogels. Nat Commun 9:881. DOI: 10.1038/s41467-018-03268-y.

[250] Wang J, Angnes L and Tobias H (1993) Carbon aerogel composite electrodes. Anal Chem 65:2300-2303.

[251] Maldonado-Hodar FJ, Ferro-Garcia MA, Rivera-Utrilla J, Moreno-Castilla C (1999) Synthesis and textural characteristics of organic aerogels, transition-metal-containing organic aerogels and their carbonized derivatives. Carbon 37:1199–1205.

[252] Cotet LC, Danciu AV, Cosoveanu AV, Popescu LC, Roig AA and Molins E (2007) Synthesis of meso- and macroporous carbon aerogels. Revue Roumaine de Chimie 52(11):1077–1081.

[253] Czakkel O, Geissler E, Szilagyi IM, Szekely E, Laszlo K (2009) Cu-doped resorcinol–formaldehyde (RF) polymer and carbon aerogels. J Colloid Interface Sci 337:513–522. doi:10.1016/j.jcis.2009.05.059.

[254] Lyu S, Chen Y, Han S, Guo L, Chen Z, Lu Y, Chen Y, Yang N and Wang S (2018) Layer-by-layer assembled polyaniline/carbon nanomaterial-coated cellulosic aerogel electrodes for high-capacitance supercapacitor applications. RSC Adv 8:13191. DOI: 10.1039/c8ra01754a

[255]Pekala RW, Mayer ST, Kaschmitter JL, and Kong FM (1994) Carbon aerogels: an update on structure, properties, and applications. Sol-Gel Processing and Applications 369:377.

[256] Araby S, Qiu A, Wang R, Zhao Z, Wang C-H and Ma J (2016) Aerogels based on carbon nanomaterials. J Mater Sci 51:9157–9189.

[257] Torres CEIT, Quezada TESQ, Kharissova OV, Kharisov KBI, de la Fuente MID (2021) Carbon-based aerogels and xerogels: Synthesis, properties, oil sorption capacities, and DFT simulations. J Environ Chem Eng 9:104886. https://doi.org/10.1016/j.jece.2020.104886.

[258] Xu F, Zheng G, Wu D, Liang Y, Lia Z and Fu R (2010) Improving electrochemical performance of polyaniline by introducing carbon aerogel as filler. Phys Chem 12:3270–3275.

[259] An H, Wang Y, Wang X, Li N and Zheng L (2010) The preparation of PANI/CA composite electrode material for supercapacitors and its electrochemical performance. J Solid State Electrochem 14:651–657. DOI 10.1007/s10008-009-0835-0.

[260] Jin Z, Zhao D, Li B, Ren X, Yan S, Qin C and Li R (2012) Hybrid supercapacitors based on polyaniline and carbon aerogels composite electrode materials. Adv Mater Res Vols. 391-392:18-22. doi:10.4028/www.scientific.net/AMR.391-392.18.

[261] Chen F, Gui D, Ding S, Zhu Y, Liu L (2012) Carbon aerogel /polyaniline composite as supercapacitors packaging applications. 2012 International Conference on Electronic Packaging Technology & High Density Packaging 254-257.

[262] Tang Z, Jiang J, Liu S, Chen L, Liu R, Zheng B, Fu R and Wu D (2017) Polyaniline-coated activated carbon aerogel/sulfur composite for high performance lithium-sulfur battery. Nanoscale Res Lett 12:617. DOI 10.1186/s11671-017-2372-6.

[263] Wu X, Yang X, Wu D, Fu R (2008) Feasibility study of using carbon aerogel as particle electrodes for decoloration of RBRX dye solution in a three-dimensional electrode reactor. Chem Eng J 138:47–54. doi:10.1016/j.cej.2007.05.027.

[264] Ling, S.K., Tian, H.Y., Wang, S., Rufford, T., Zhu, Z.H., Buckley, C.E. (2011). KOH catalysed preparation of activated carbon aerogels for dye adsorption, J. Colloid Interface Sci., 357, 157–162. doi:10.1016/j.jcis.2011.01.092.

[265] Wu X, Hui KN, Hui KS, Lee S.K, Zhou W, Chen R, Hwang DH, Cho YR, Son YG (2012) Adsorption of basic yellow 87 from aqueous solution onto two different mesoporous adsorbents. Chem Eng J 180:91– 98. doi:10.1016/j.cej.2011.11.009.

[266] Rodrigues LA, Campos TMB, Alvarez-Mendes MO, Coutinho ADR., Sakane KK, Thim GP (2012) Phenol removal from aqueous solution by carbon xerogel. J Sol-Gel Sci Technol 63: 202–210. DOI 10.1007/s10971-012-2745-3.

[267] Ren T, Han Y, Zhang M, Zhang B, Gou X (2014) Formation of carbon aerogels from glucose and as adsorbents for removal of methylene blue. J Mater Sci Res 3, 74-81. http://dx.doi.org/10.5539/jmsr.v3n2p74.

[268] Lin, Y-F., Chang, C-Y. (2015). Design of composite maghemite/hematite/carbon aerogel nanostructures with high performance for organic dye removal, Sep. Purif. Technol., 149, 74–81. http://dx.doi.org/10.1016/j.seppur.2015.05.025.

[269] Sun W, Du A, Zhou B, Shen J, Huang S, Tang J (2016) Ultra-low-density GNS/CA composite aerogels with ultra-high specific surface for dye removal J Sol-Gel Sci Technol 80:68–76. DOI 10.1007/s10971-016-4047-7.

[270] Li, Z., Jia, Z., Ni, T., Li, S. (2017). Adsorption of methylene blue on natural cotton based flexible carbon fiber aerogels activated by novel air-limited carbonization method, J. Mol. Liq., 242, 747–756. doi: 10.1016/j.molliq.2017.07.06.

[271] Zhou K, Yanhui Li Y, Li Q, Du Q, Wang D, Sui K, Wang C, Li H and Xia Y (2018) Kinetic, isotherm and thermodynamic studies for removal of Methylene blue using β-cyclodextrin/activated carbon aerogels. J Polym Environ 26:3362–3370. https://doi.org/10.1007/s10924-018-1219-2.

[272] Jiang, L., Zhang, Y., Zhou, M., Liang, L., Li, K. (2018). Oxidation of Rhodamine B by persulfate activated with porous carbon aerogel through a non-radical mechanism, J. *Hazard Mater.*, 358, 53–61. https://doi.org/10.1016/j.jhazmat.2018.06.048.

[273] Li, K., Zhou, M., Liang, L., Jiang, L., Wang, W. (2019). Ultrahigh-surface-area activated carbon aerogels derived from glucose for high-performance organic pollutants adsorption, J. Colloid Interface Sci. 546, 333–343. https://doi.org/10.1016/j.jcis.2019.03.076.

[274] Lei E, Li W, Sun J, Wu Z and Liu S (2019) N-doped carbon aerogels obtained from APMP fiber aerogels saturated with rhodamine dye and their application as supercapacitor electrodes. Appl Sci 9(4):618. https://doi.org/10.3390/app9040618.

[275] Lv D, Li Y, Wang L (2020) Carbon aerogels derived from sodium lignin sulfonate embedded in carrageenan skeleton for methylene-blue removal. Int J Biol Macromol 148:979–987. https://doi.org/10.1016/j.ijbiomac.2020.01.136.

CHAPTER 3

MATERIALS AND METHODS

This chapter describes the materials, experimental set-up, and equipment used for the synthesis of polyaniline (PANI), polyaniline/montmorillonite clay (PANI/MMT), polyaniline/halloysite clay (PANI/HNT), and polyaniline/carbon aerogel (PANI/CA) nanocomposites. Materials and experimental set-up are discussed in **Sections 3.1 and 3.2**. **Section 3.3** is about the equipment used for material synthesis. The details about the characterization techniques are also discussed in this chapter and given in **Section 3.4**.

3.1 Materials

Aniline (ACS reagent, ≥ 99.5 % purity) (IUPAC name: Phenylamine), Hydrochloric acid (HCl), Ammonium persulfate (AR, ≥ 98.5 % purity, chemical formula: $(NH_4)_2S_2O_8$), IUPAC name: diazanium; sulfonatooxy sulfate) and Montmorillonite clay (chemical formula: $(Na,Ca)_{0.33}(Al,Mg)_2(Si_4O_{10})(OH)_2 \cdot NH_2O$)) was purchased from Sigma Aldrich, India. Acetone (2-propanone) and NMP (1-Methyl-2-pyrrolidone) were purchased from LOBA Chemicals, India. Halloysite nanoclay (product no: 685445) was purchased from Sigma Aldrich. Carbon aerogel powder was purchased from China. The Acid green 25 dye (anionic, CI. No.61570, molecular weight: 622.58 g/mol) was also purchased from Sigma Aldrich. Methylene blue dye (analytical grade, M9140 was purchased from Sigma Aldrich. All the solutions for synthesis and adsorption study were prepared using distilled water.

3.1.1 Aniline (monomer)

Aniline was used as a monomer for the synthesis of PANI and its nanocomposites. Aniline is soluble in water. The characteristics details of aniline are shown in **Table 3.1**.

Table 3.1 Characteristics details of aniline

Monomer	Linear Formula	Molecular Weight	Structure
Aniline	$C_6H_5NH_2$	93.13 g/mol	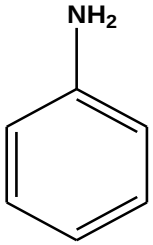

3.1.2 Oxidizing agent

Ammonium persulfate was used as an oxidizing agent in the polymerization process. It is also known as ammonium peroxodisulfate. The characteristics details about ammonium persulfate are shown in **Table 3.2**.

Table 3.2 Characteristics details of ammonium persulfate

Oxidizing agent	Linear Formula	Molecular Weight	Structure
Ammonium persulfate	$(NH_4)_2S_2O_8$	228.20 g/mol	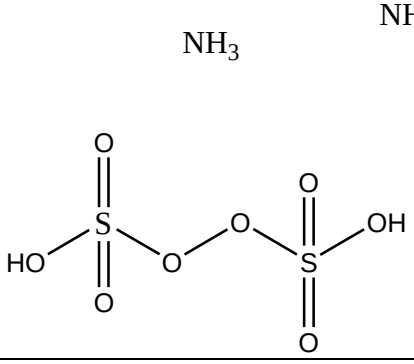

3.2 Experimental set-up for synthesis

The material synthesis was performed in four steps. The first step is homogenization, the second step is ultrasonication (sonicator probe), and the third step is polymerization using a magnetic stirrer, followed by the last fourth step: filtration and drying. **Figure 3.1** depicts the experimental setup used to polymerize PANI and its nanocomposites.

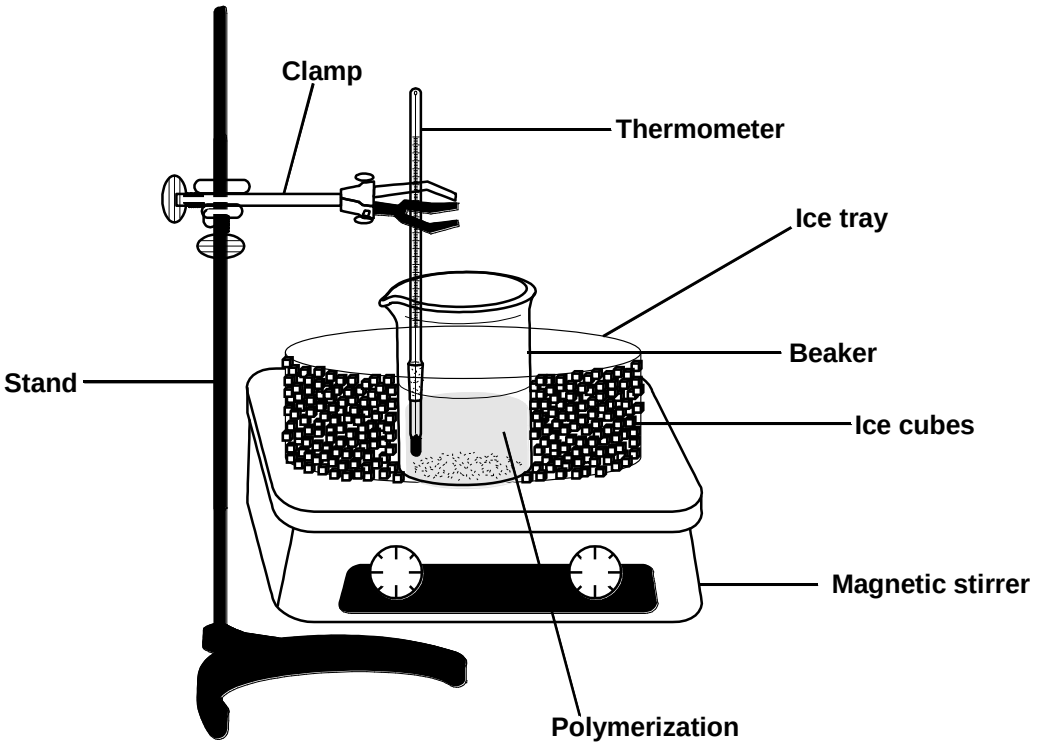

Figure 3.1 Synthesis set-up

3.3 Equipment used for synthesis

3.3.1 Homogenizer and probe sonicator

In the present study, the IKA®T18 digital ultra turrax® homogenizer and JYD-750L probe sonicator have been used for material dispersion and are shown in **Figure 3.2**. Homogenizer has been used to produce a uniform suspension in an aqueous medium at 10,000 rpm. Regarding the probe sonicator, the sonication was performed at 80 % amplitude with a power of 750W and operating at 20 kHz frequency. In nanotechnology, a probe sonicator is widely used to disperse nanoparticles at the nanoscale in liquid. It is the most efficient and effective technique for nanoparticle dispersion in an aqueous medium. A probe sonicator breaks down colloidal particle aggregates of micron size to the nanoscale level.

Homogenizer **Probe sonicator**

Figure 3.2 Homogenizer and probe sonicator

3.3.2 Magnetic stirrer

The material synthesis was performed using a magnetic stirrer at a constant temperature. The polymerization temperature was controlled through ice cubes. The IKA® C- MAG HS4 digital magnetic stirrer was used for the polymerization process, as shown in **Figure 3.3**.

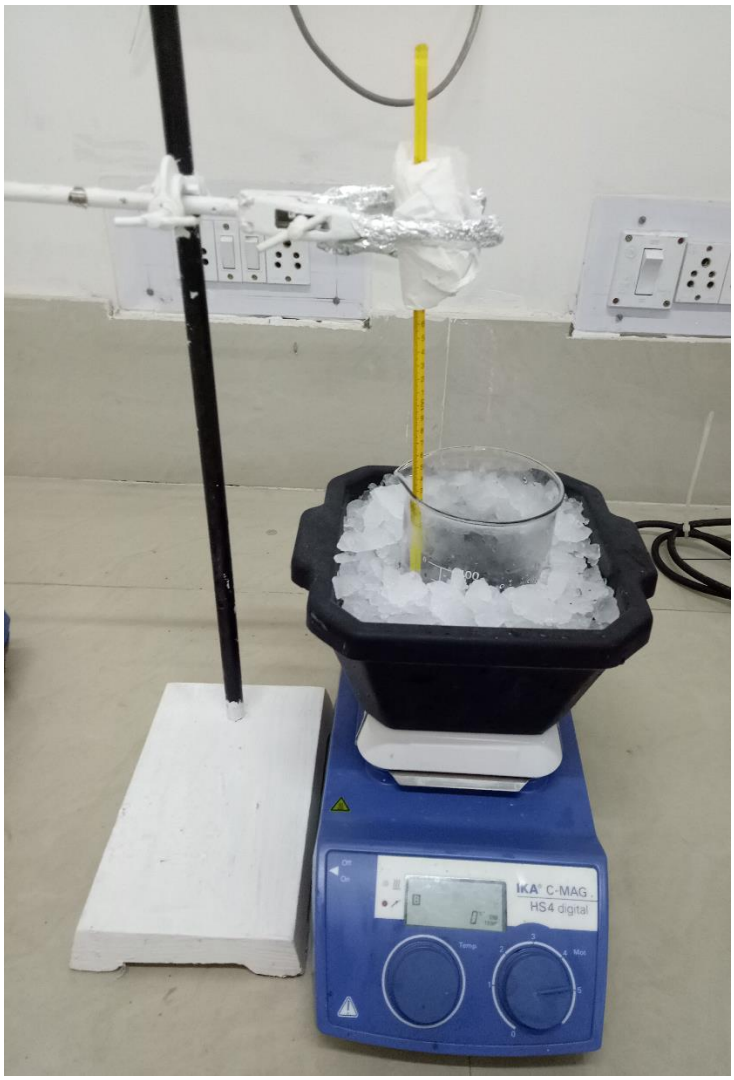

Figure 3.3 Magnetic stirrer

3.3.3 Vacuum filter

Vacuum filtration is a method to separate solids from liquids at a fast rate. In the present study, vacuum filtration **(Figure 3.4)** has been used to obtain the polymers and nanocomposites after the polymerization process. The obtained solid material was washed with 1M HCl, acetone, and distilled water using a vacuum filter to remove the impurities.

Figure 3.4 Vacuum filtration

3.3.4 Vacuum oven

In the present study, the BIONICS Scientific vacuum oven was used. The drying of the filtered solid material was performed at a temperature of 50°C under a vacuum. Vacuum drying is more effective in removing moisture in less time than in an ordinary oven.

3.4 Characterization techniques

Characterization of PANI, PANI/MMT, PANI/MMT, CA, and PANI/CA nanocomposites was done by Scanning electron microscopy (SEM), Field emission scanning electron microscope

(FESEM), Fourier transform infrared spectroscopy (FTIR), X-ray diffraction (XRD), BET (Brunauer Emmett Teller) analysis, UV-Vis spectroscopy, and HRTEM (High-Resolution Transmission Electron Microscope) techniques.

3.4.1 Fourier transform infrared spectra

The FTIR spectra were determined by Perkin Elmer Spectrum RX1 using KBr pellets with the scanning range 4000-450 cm^{-1}. Fourier transform infrared spectra were used to obtain the specific bands of the prepared samples.

3.4.2 X-ray diffractometer

X-ray diffractometer was done by PanAlytical XPERT-PRO ((Netherland) with a wavelength of 1.541 A° (operated at 40 mA, 45 kV). The XRD patterns were used to identify the interlayer spacing of clay in nanocomposite samples. It identified the crystallinity and structure of all the samples. XRD analysis of PANI, PANI/MMT, and PANI/HNT was done in the 2Θ range of 3 to 70º. CA and PANI/CA XRD was performed in the 2Θ range of 10 to 60º.

3.4.3 Scanning electron microscopy investigation and Field emission scanning electron microscopy investigation

Scanning electron microscopy was recorded using an instrument JEOL (JSM-6510 LV) to observe the prepared samples' surface morphology. The Field emission scanning electron microscopy was performed using Hitachi (HI-0876-0003).

3.4.4 High-resolution transmission electron microscope

A high-resolution transmission electron microscope (HRTEM) was performed using JEOL (JEM 2100 Plus). The HRTEM technique is generally used to identify the nanocomposite structure of a nanoscale.

3.4.5 Brunauer Emmett Teller

BET analysis was done to find the surface area and the pore size distribution of the samples. The equipment used for BET analysis was Microtec Belsorp Mini–II (Japan) and NOVA touch 2LX.

3.4.6 UV-Vis spectroscopy

UV-Vis spectra were recorded using PerkinElmer UV WinLab by dissolving the samples in NMP (N-methyl -2-pyrrolidone) solvent.

In the next chapter, the synthesis procedure of polyaniline and its nanocomposites have been discussed. The characterization results are discussed in **Chapter 4**.

CHAPTER 4

SYNTHESIS OF POLYANILINE AND ITS NANOCOMPOSITES

Polyaniline (PANI), polyaniline/montmorillonite clay (PANI/MMT), polyaniline/halloysite clay (PANI/HNT), polyaniline/carbon aerogel (PANI/CA) nanocomposites have been synthesized successfully through the *in-situ* polymerization method. The synthesis procedure is described in **Sections 4.1, 4.2, and 4.3**. The results and discussion of PANI and PANI/MMT, CA and PANI/CA, HNT, and PANI/HNT are presented in **Section 4.4**. Finally, conclusions are summarized in **Section 4.5**.

4.1 Synthesis of polyaniline and polyaniline/montmorillonite clay (PANI/MMT) nanocomposites

PANI and PANI/MMT clay nanocomposites were synthesized at two different temperatures of 0°C and 20^{o}C. *In-situ* polymerization method was used to synthesize PANI/MMT nanocomposites using HCl as a catalyst and ammonium persulfate as an oxidizing agent. The molar ratio of monomer/oxidant was 1:1, and the polymerization was done at 0^{o}C and 20^{o}C. The synthesis route and schematic diagram for the formation of PANI/MMT nanocomposites are presented in **Figures 4.1 (a, b),** respectively.

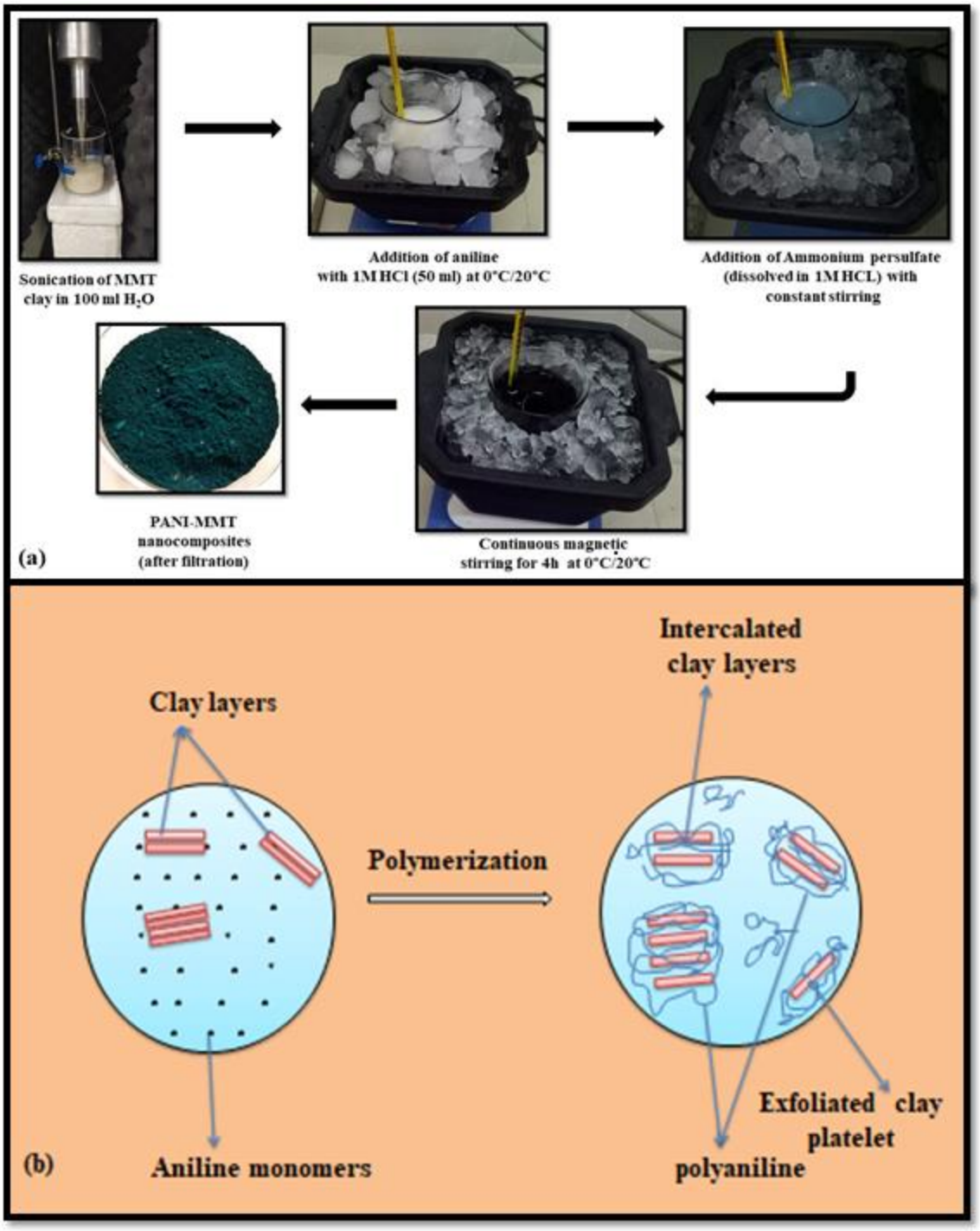

Figure 4.1 (a) Synthesis route (b) Schematic diagram depicting the *in-situ* polymerization of PANI/MMT nanocomposites.

The PANI/MMT nanocomposites were synthesized as per the experimental procedure described in the literature **[1, 2]**, with some modifications. To synthesize PANI/MMT clay nanocomposites, MMT clay (0, 1, 1.5, and 2 w/v %) was dispersed in distilled water (100 ml) and sonicated for 10 min using an ultrasonicator probe to achieve nanodispersion of clay. After the dispersion of the MMT clay, magnetic stirring was used to prepare PANI/MMT nanocomposites. A solution of 2 ml aniline in 1M HCl was added slowly to the above MMT clay suspension over a period of 5 min, with magnetic stirring, and the mixture was further stirred for another 20 min at 0^{o}C. Five grams of ammonium persulfate (oxidizing agent APS dissolved in 1 M HCl) was added slowly over a period of 10 min to the above suspension. For polymerization at 0^{o}C, the suspension was stirred continuously for 4 h at 0^{o}C to ensure the completion of the reaction. After the polymerization process, a dark green color precipitate of PANI/MMT clay nanocomposite was obtained. This product was obtained using vacuum filtration, and it was washed with 1M HCl, distilled water, and acetone to remove ammonium persulfate and other impurities. The obtained solid nanocomposite material was dried overnight under vacuum at 50^{o}C.

For the polymerization done at 20^{o}C, the mixture was continuously stirred at 20^{o}C for 2 h, and the reaction for the synthesis of nanocomposite was continued for 24 h without agitation to complete the polymerization.

The same procedure was adopted to prepare polyaniline (PANI), but herein MMT clay was not added.

4.2 Synthesis of polyaniline and polyaniline/halloysite clay (PANI/HNT) nanocomposites

PANI/HNT nanocomposite was prepared using the procedure adopted for PANI/MMT nanocomposite synthesis, wherein MMT clay was replaced by the HNT clay.

4.3 Synthesis of polyaniline/carbon aerogel (PANI/CA) nanocomposites

A number of experiments were performed at 0^{o}C to prepare PANI/CA nanocomposites by varying CA content from 0.1 to 0.5 g. Finally, the CA content of 0.2 g was selected to prepare PANI/CA nanocomposites for all further studies. The synthesis route and schematic diagram for the formation of PANI/CA nanocomposites are depicted in **Figures 4.2 (a, b),** respectively, and are as follows:

An *in-situ* polymerization was carried out to synthesize PANI/CA nanocomposite at 0^{o}C **(Figure 4.2)**. A homogenizer and an ultrasonicator probe were used for particle dispersion. To synthesize PANI/CA nanocomposite, 100 ml distilled water was taken in a beaker, and a 0.2 g of carbon aerogel was added to it. A solution of aniline and HCl was prepared separately in a 50 ml beaker. Afterward, the solution of distilled water and CA was homogenized for 10 min at 10,000 rpm. A suspension of aniline and HCl was slowly added during homogenization. An ultrasonicator probe sonicated this mixture for 10 min. The solution was again homogenized and sonicated for 10 min for good particle size dispersion. After the dispersion of the particles, the reaction was further carried out using a magnetic stirrer at 0^{o}C. The ammonium persulfate solution (5 g + 50 ml HCl) was added under constant stirring, and subsequently, the solution was stirred continuously for 4 h at 0^{o}C. After 4 h, the polymerization process was complete, and the product was filtered and washed with the help of HCl (1M), distilled water, and acetone. The synthesized product was dried overnight at 50^{o}C in a vacuum oven.

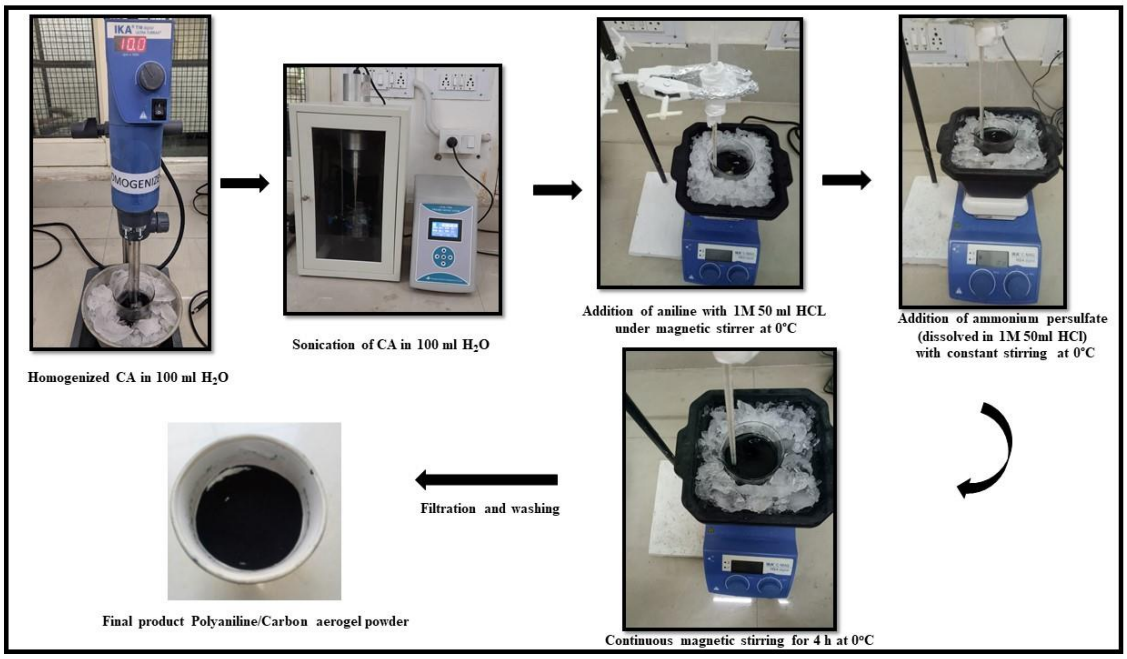

(a)

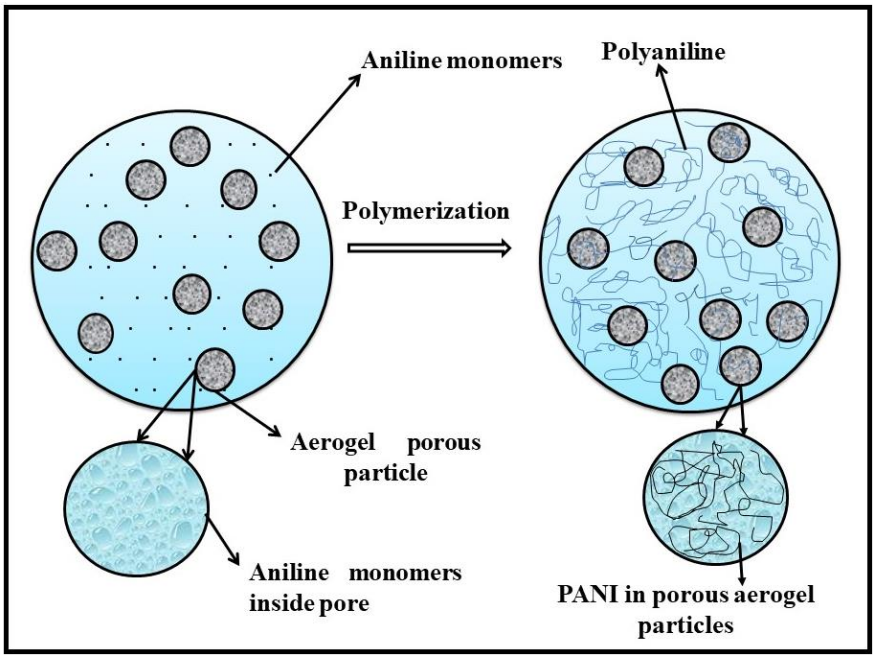

(b)

Figure 4.2 (a) Synthesis route and (b) Schematic diagram representing the *in-situ* polymerization of PANI/CA nanocomposites.

4.4 Results and discussion

4.4.1 PANI and PANI/MMT nanocomposites

PANI and PANI/MMT nanocomposites were characterized by FTIR, SEM, FESEM, XRD, BET, UV-Vis spectra, and HRTEM analysis.

A number of experiments were performed at 0^{o}C and 20^{o}C by using ammonium persulfate as an oxidizing agent. The nano-clay concentration w/v (%) was varied from 0, 1, 1.5 and 2.0. We have selected the lower temperatures (0^{o}C) for the adsorption experimental study, and one of the criteria adopted for the selection of temperature was lower polymerization time. Thus, PANI and PANI/MMT nanocomposites synthesized at 0^{o}C with 1 w/v (%) clay, were selected as adsorbents for adsorption experiments of AG25 dye.

4.4.1.1 Fourier transform infrared (FTIR) spectroscopic analysis

All the functional groups of the products have been identified by FTIR spectroscopy. FTIR spectra of PANI, MMT, and PANI/MMT nanocomposites constituting various clay contents, synthesized at lower and higher temperatures of 0^{o}C and 20^{o}C, respectively are depicted in **Figures 4.3 (a, b)**. The peaks at 3621 cm^{-1} and 3411 cm^{-1} (O-H stretching), 1016 cm^{-1} and 1101 cm^{-1} (Si-O stretch), 1633 cm^{-1} (H–O–H bending, 917 cm^{-1} (Al-OH bending), 701 cm^{-1} (Al-Mg-OH stretching), 534 cm^{-1} and 472 cm^{-1} (bands resulting from Si–O–Al and Si–O–Si bending) are explored in FTIR spectrum of pure MMT clay. The peaks at 3621 cm^{-1} and 3411 cm^{-1} These bands have also been reported by other researchers **[2-7].** The absorption bands of 0^{o}C PANI located at 1556 cm^{-1} and 1485 cm^{-1} can be attributed to the C=C stretch occurring in quinoid and benzenoid ring structure. **[8-10]**. The C-N bend in PANI results in the characteristic peak at 1303 cm^{-1}. **[8, 9]**. The presence of band at 1144 cm^{-1} is ascribed to the formation of $^{+}$HN=Q=NH^{+} framework **[9]**. The formation

of distinct bands of PANI and MMT clay can be visualized in spectra of PANI/MMT clay nanocomposites in both cases (prepared at either 0°C or 20°C temperature with varying amounts of MMT clay). The FTIR spectra of 0°C and 20°C are almost identical with a very small shift of peaks, and the peak intensity of 0°C spectra is higher as compared to 20°C spectra of nanocomposite samples. The FTIR spectra of 20°C prepared samples are shown in **Figure 4.3 (b)**.

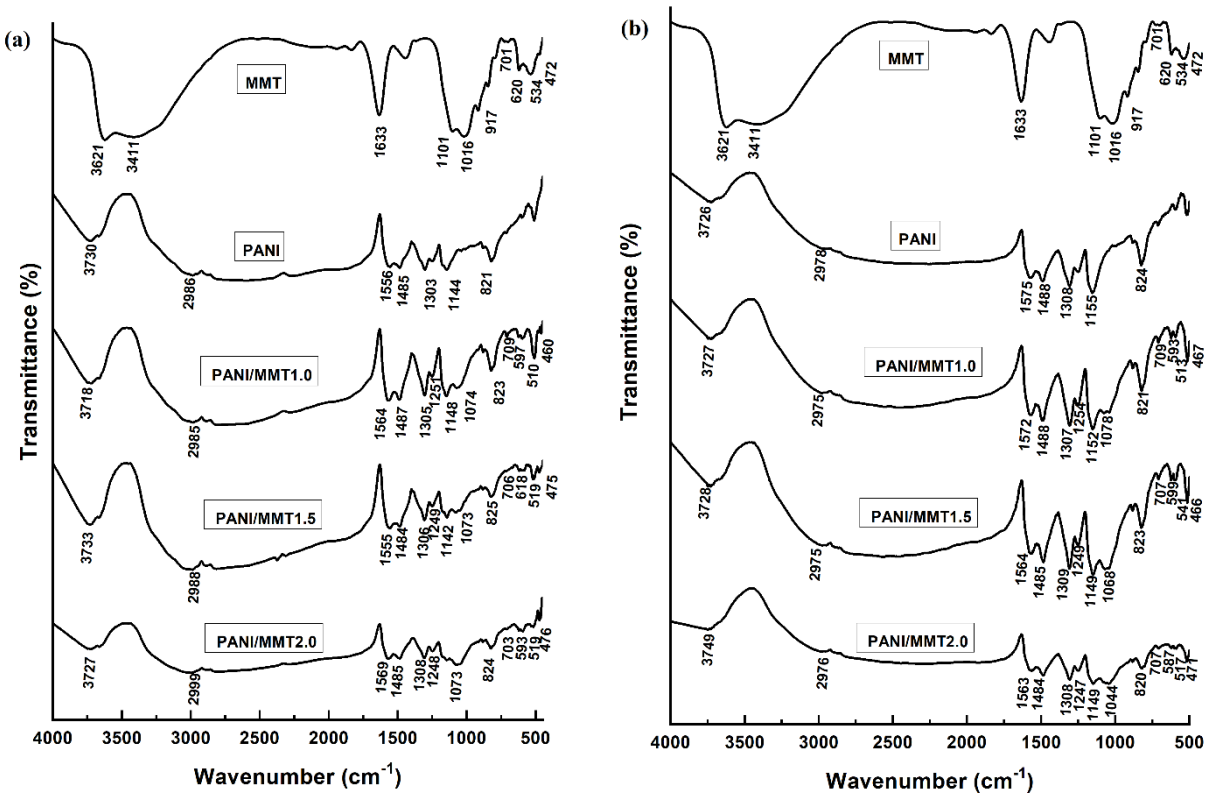

Figure 4.3 FTIR spectra of MMT, PANI, PANI/MMT1.0, PANI/MMT1.5, and PANI/MMT2.0 prepared at (a) 0°C and (b) 20°C.

The Si-O band of MMT in PANI/MMT spectra at 1074 cm^{-1} gives confirmation for successful intercalation of PANI into the MMT clay galleries **[2, 11]**. However, intercalation of MMT platelet was confirmed by WAXS and HRTEM studies, as described in the following section. The FTIR spectroscopy confirmed the chemical interaction of the MMT clay layers with the PANI chains.

4.4.1.2 X-ray diffraction (XRD) analysis

The XRD characterization was carried out to determine the insertion of PANI chains into the MMT clay interlayer space. XRD analysis was done in the *2Θ* range of 3 to 70°. The XRD patterns of MMT clay and the products (PANI and PANI/MMT) prepared by *in-situ* polymerization at 0, 1, 1.5, and 2.0 w/v (%) clay loadings are presented in **Figure 4.4**.

The PANI synthesized at 0°C exhibited sharp peaks at *2Θ* = 25.23°, and two more peaks were observed at 20.94°, 14.9°, and that indicates its crystalline nature **[12, 13].** PANI prepared at 20°C shows diffraction peaks at 2Θ = 14.70°, 20.41°, 25.58°, which shows the crystalline structure of the PANI **[1, 12, 14, 15]**. Thus, the XRD spectrum of PANI obtained at 0°C, and 20°C shows similar peaks. The spectrum of pure MMT showed a d_{001} peak at *2Θ* = 6.08°, corresponding to d-spacing of 14.52 A°. Wide and expanded angle XRD patterns of PANI, MMT, and PANI/MMT clay nanocomposites synthesized at 0°C are shown in **Figures 4.4 (a, b)**. The values for PANI/MMT nanocomposites are presented in **Table 4.1**. All the samples of nanocomposites are intercalated and not exfoliated. Similar XRD results are obtained for 20°C nanocomposite samples **(Figure 4.4(c)),** and the values for 20°C samples are presented in **Table 4.2**. The almost same values in Tables 4.1 and 4.2 indicate that the extent of intercalation of MMT by PANI polymer chains is the same in the nanocomposites prepared at 0°C and 20°C.

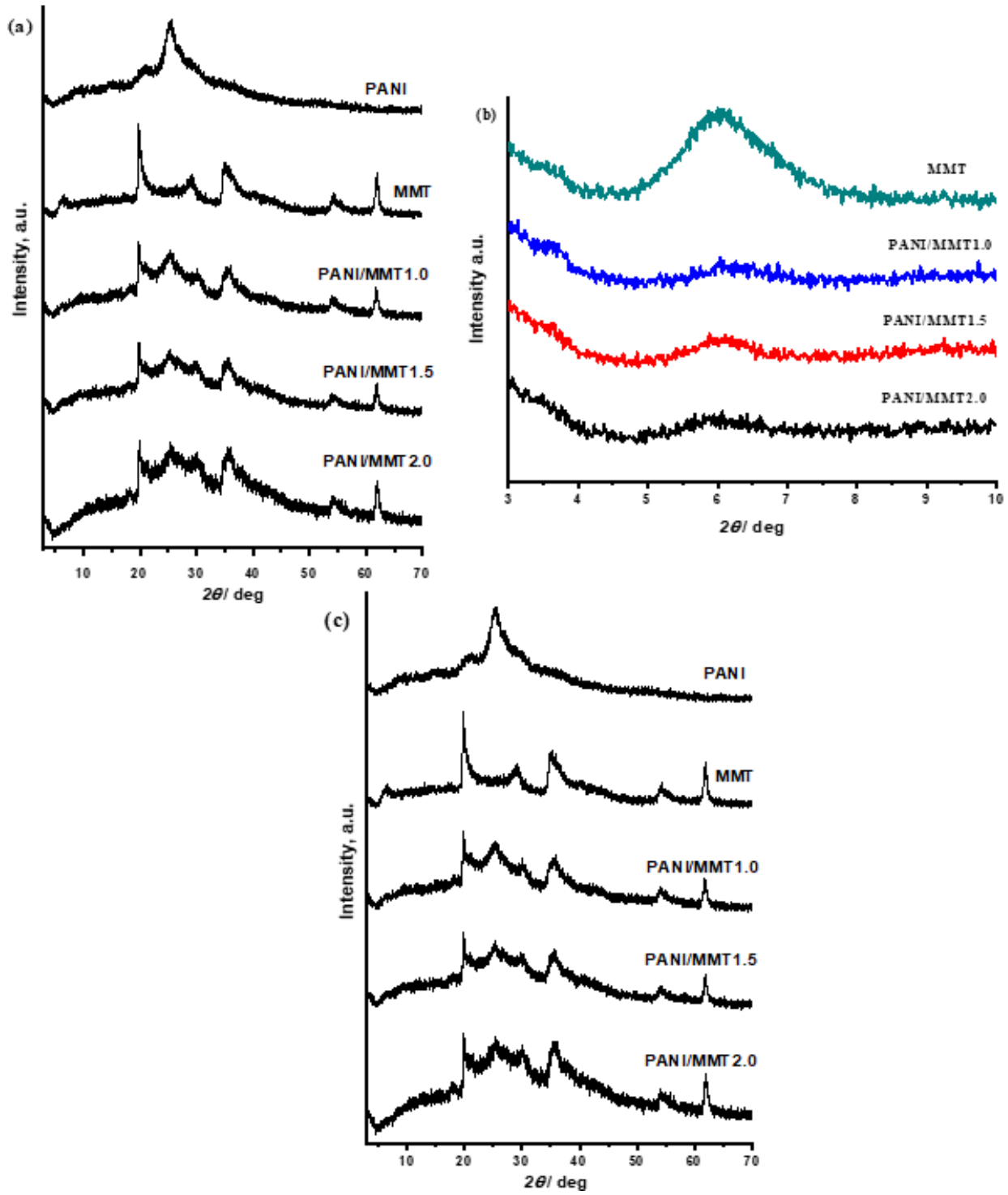

Figure 4.4 (a) Wide-angle and (b) Expanded angle XRD patterns of PANI, MMT, and its nanocomposites prepared at 0°C, (c) XRD pattern of PANI and nanocomposites prepared at 20°C.

Table 4.1 XRD data of MMT and PANI/MMT nanocomposites prepared at 0°C

Component	2Θ	d_{001} spacing (A°)
MMT	6.08	14.52
PANI/MMT1.0	6.28	14.05
PANI/MMT1.5	6.01	14.67
PANI/MMT2.0	5.97	14.78

Table 4.2 XRD pattern of MMT and PANI/MMT nanocomposites prepared at 20°C

Component	2Θ	d_{001} spacing (A°)
MMT	6.08	14.52
PANI/MMT1.0	6.27	14.08
PANI/MMT1.5	6.09	14.50
PANI/MMT2.0	5.98	14.75

4.4.1.3 UV-Vis spectroscopy analysis

The UV-Vis spectra of pure PANI and PANI-MMT clay nanocomposites synthesized at 0° and 20°C are displayed in **Figure 4.5**. The N-methyl-2-pyrrolidone solvent was used to dissolve all of the samples and absorption bands were analyzed by UV-Vis spectroscopy.

The UV-Vis spectrum of pure PANI synthesized at 0°C exhibits two absorption bands at around 332 nm and 638 nm wavelength, that are ascribed to the benzoid ring's π-π* transition besides exciton transitions in the quinoid ring **[16-21]**. These bands indicate that the PANI is in an emeraldine conducting state. The characteristics absorption bands of PANI-MMT nanocomposites were found at 324 nm and 626 nm for PANI/MMT1.0; 322 nm and 628 nm for PANI/MMT1.5; and 322-326 nm and 623-628 nm for PANI/MMT2.0. The benzoid ring's π-π* transition is ascribed to the spectral peak at 322-326 nm. The absorption peak at around 623-628 nm is due to the excitation transition from benzenoid ring to quinoid ring **[17, 20, 21].** The absorption bands of

PANI and PANI-MMT nanocomposites (0, 1, 1.5, 2 w / v %) synthesized at 20^{o}C are very similar to those synthesized at 0^{o}C. For 20^{o}C, two bands were obtained at 331 nm and 633 nm for pure PANI that can be ascribed to π-π* transition of benzoid ring and exciton transitions in the quinoid ring. The UV absorption peaks were found at 330 nm and 630 nm for PANI/MMT1.0, 324 nm and 624 nm for PANI/MMT1.5, 322-326 nm, and 623-628 nm for PANI/MMT2.0. In polyaniline/MMT nanocomposites samples, the adsorption bands shifted slightly to a lower wavelength, indicating the MMT clay and polyaniline interaction.

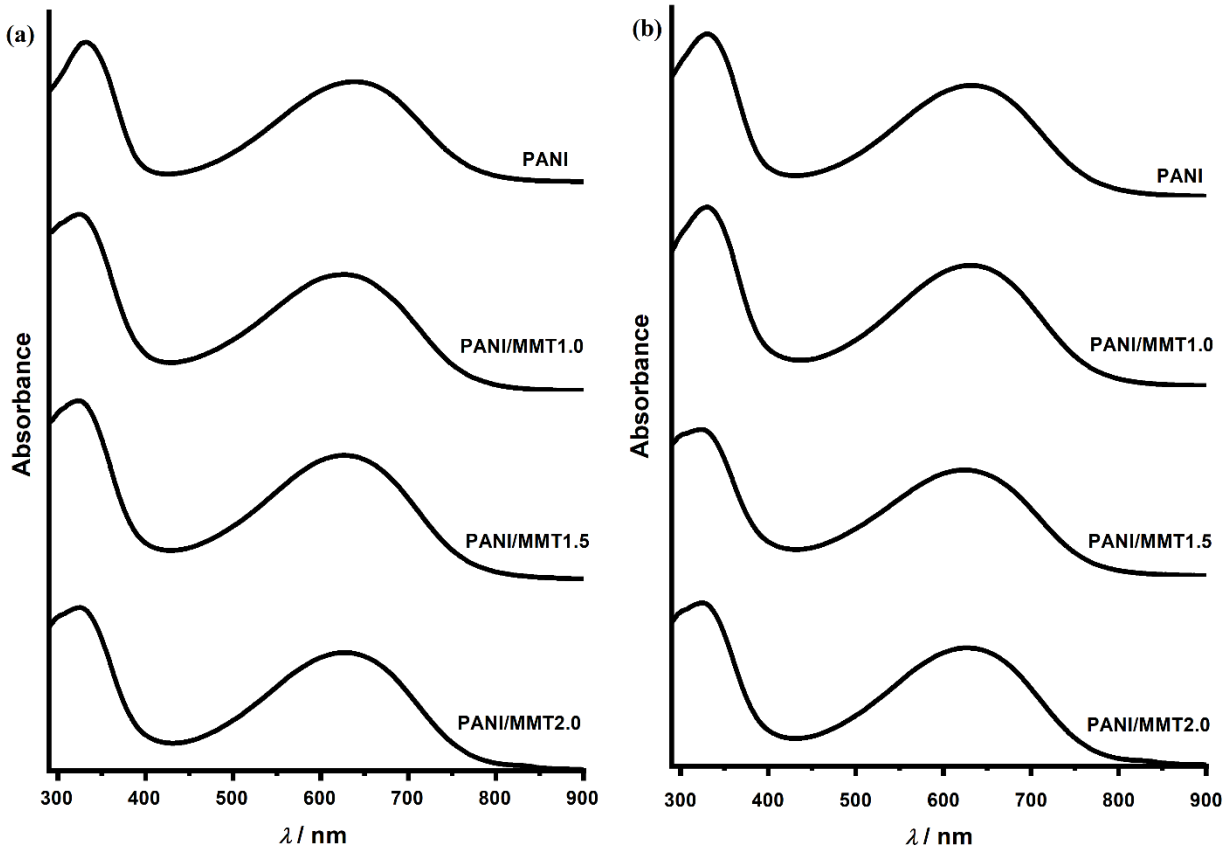

Figure 4.5 UV-VIS spectra of PANI and PANI/MMT prepared at (a) 0^{o}C and (b) 20^{o}C.

Thus, all these results (FTIR, XRD, and UV-vis spectra) were almost similar for the three compositions of PANI/MMT nanocomposites. Hence, the nanocomposites containing the least *e.g.* 1 w/v (%) amount of clay was selected for all further characterization studies. The 1 w/v (%) clay was selected to save on the cost of nanofiller to prepare nanocomposites for further adsorption studies.

4.4.1.4 Scanning electron microscopic and Field emission scanning electron microscopy

PANI (emeraldine salt) and PANI/MMT nanocomposites morphology was studied through SEM analysis. The SEM images of pure MMT clay showed a layered structure. The morphology of the pure PANI sample synthesized at 0°C and 20°C confirms that the prepared PANI has a granular texture, but the morphology of PANI/MMT nanocomposites was not clearly seen in SEM micrographs for both temperatures (0^oC and 20^oC), so FESEM analysis was done.

The FESEM images of pure PANI and PANI/MMT nanocomposites with 1 w/v (%) clay prepared at 0^oC and 20^oC are shown in **Figure 4.6**. The granular structure of PANI is identified in **Figures 4.6 (a, c)**. There is a significant difference in morphology of PANI and PANI/MMT nanocomposites (for both 0^oC and 20^oC temperature). In **Figures 4.6 (b, d)**, it can be clearly seen that the polymerization mainly occurred between the clay layers. **Figure 4.6(b)** is the FESEM image of PANI/MMT nanocomposites prepared at 0^oC, and **Figure 4.6(d)** shows the FESEM image of PANI/MMT nanocomposites prepared at 20^oC.

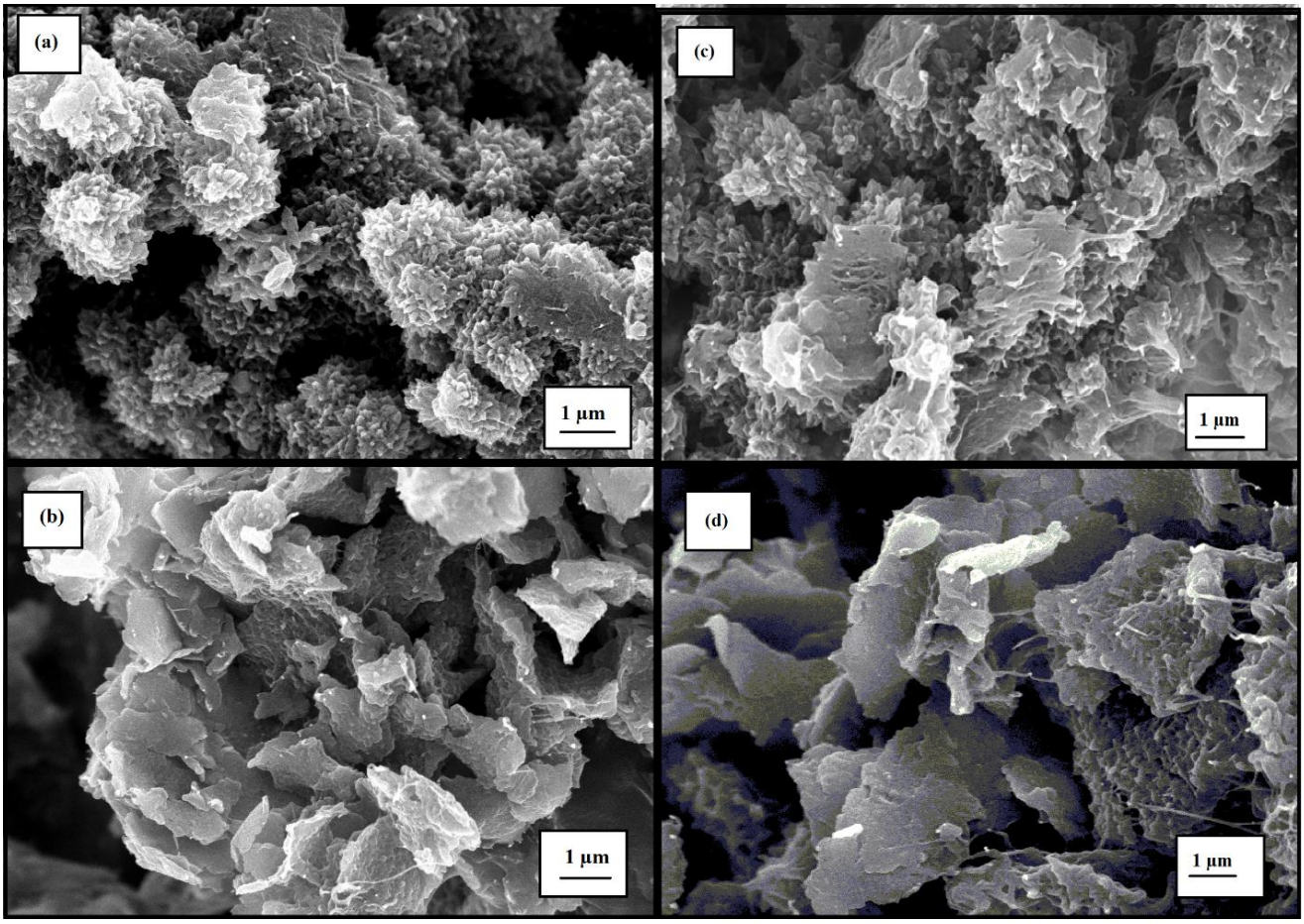

Figure 4.6 FESEM images of (a) PANI and (b) PANI/MMT nanocomposites prepared at 0^{o}C, (c) PANI, and (d) PANI/MMT samples prepared at 20^{o}C.

4.4.1.5 High-resolution transmission electron microscope

HRTEM analysis has been used to identify the internal structure of the PANI/MMT nanocomposites. **Figures 4.7 (a, b)** shown the HRTEM images of PANI/MMT nanocomposites synthesized by *in-situ* polymerization at 0^{o} and 20^{o}C. The clay platelets are represented by black lines, and the polymer matrix is represented by a grey/white surface. The HRTEM images of nanocomposites show that the nanocomposites consist of a silicate layers, and these MMT silicate

layers are intercalated within the PANI matrix. HRTEM analysis confirms the intercalated structure of PANI/MMT nanocomposites.

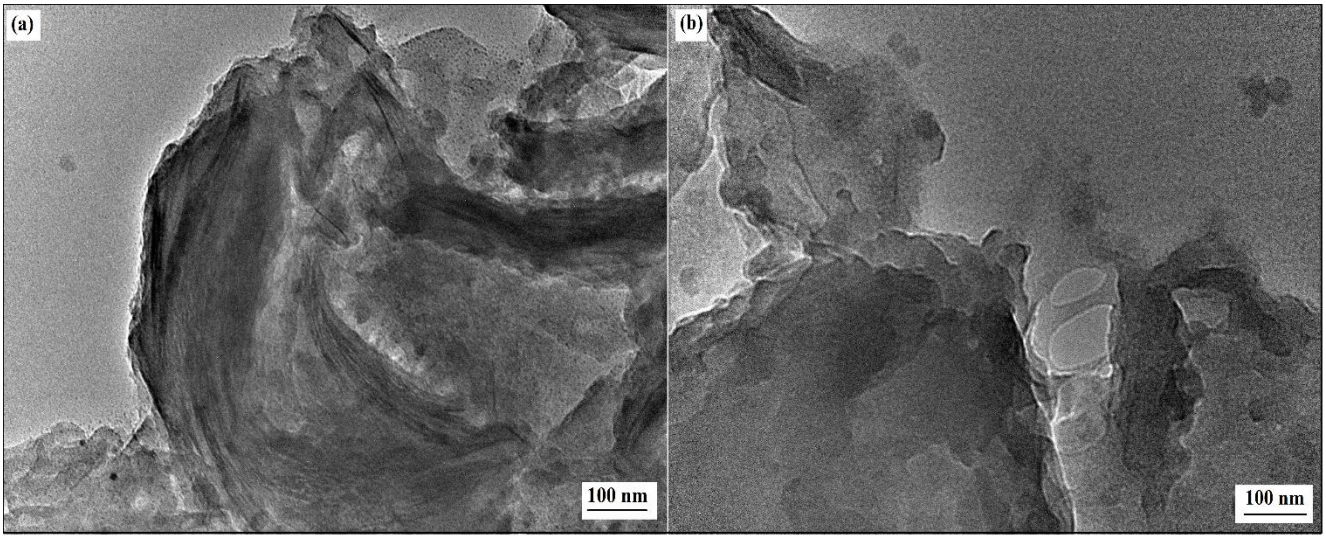

Figure 4.7 HRTEM images of PANI/MMT nanocomposites

4.4.1.6 Brunauer Emmett Teller

The surface area and pore size of pure PANI and PANI/MMT nanocomposites (0°C) were analyzed by BET analysis and are summarized in **Table 4.3**. The pore size distribution and nitrogen adsorption/desorption curves of PANI and PANI/MMT are shown in **Figures 4.8 (a, b) and Figures 4.8 (c, d)**. PANI affords a porous morphology. MMT clay morphology is less porous and has a less specific surface area, as find out from BET measurements as given in **Table 4.3**. However, the adsorption behavior of PANI/MMT is better than pure PANI. The nanocomposite surface area is lesser than that of PANI, possibly due to the presence of millions of nano-dispersed clay particles that block the pores in the PANI sample. This is so because MMT platelets, when dispersed at nano-level, possess a very large surface area, and hence, PANI/MMT would use their complementary properties to form adsorption.

From **Figure 4.8**, it can be observed that the nitrogen adsorption/desorption of PANI and PANI/MMT samples showed type II isotherms as per the IUPAC classification **[22]**. Furthermore, the plots indicate that PANI and PANI/MMT have a mesopore morphology (pore diameter lies between 2-50 nm).

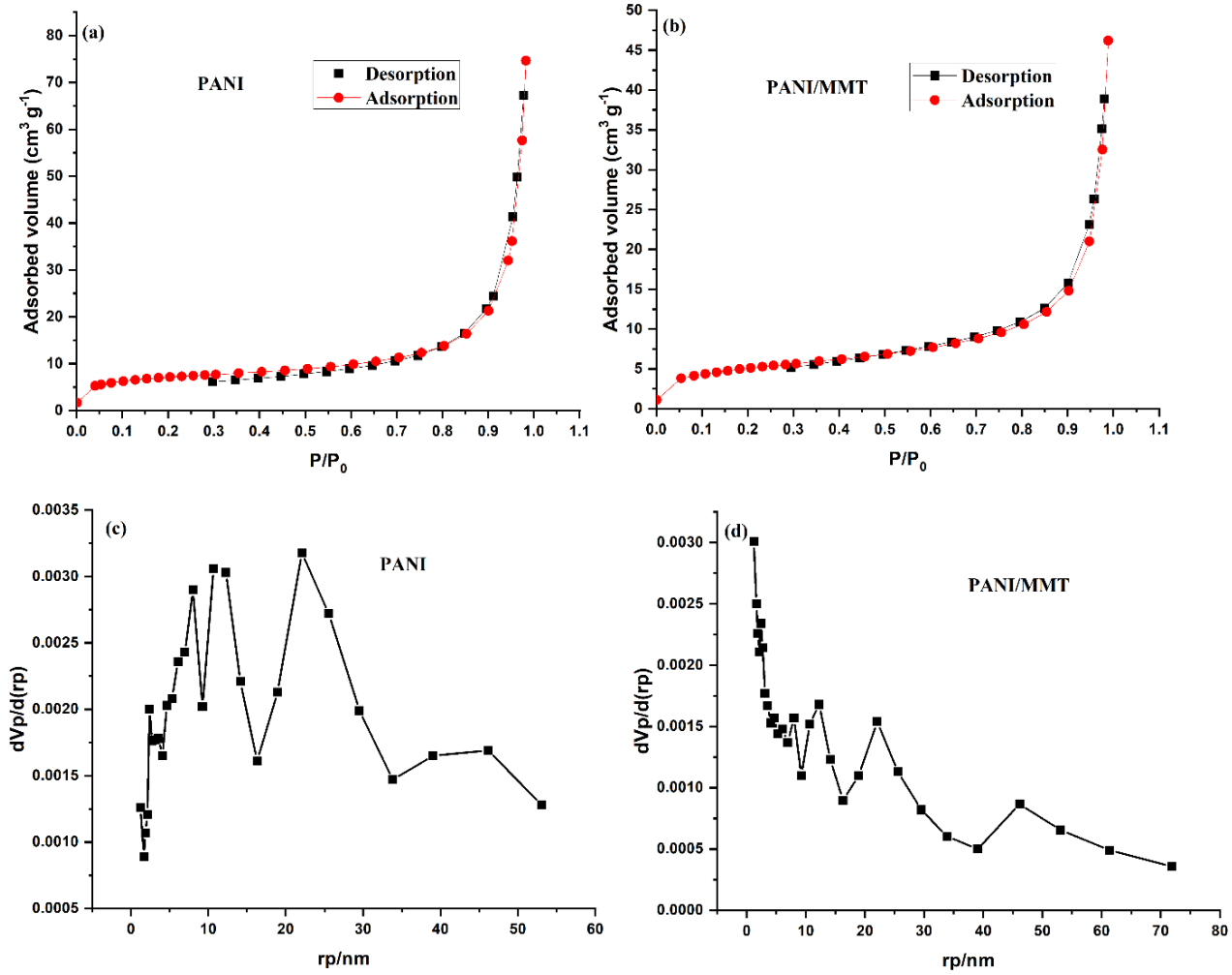

Figure 4.8 (a, b) Nitrogen adsorption/desorption isotherm and (c, d) pore size distribution curve of PANI and PANI/MMT.

Table 4.3 Specific **s**urface area of PANI and its nanocomposites

Samples	Pore diameter (nm)	Pore volume (cm^3/g)	BET (m^2/g)
PANI	17.55	0.12	26.32
PANI/MMT	15.63	0.07	18.28

4.4.2 CA and PANI/CA nanocomposites

Polyaniline/carbon aerogel (PANI/CA) nanocomposites have been synthesized via *in-situ* polymerization. Four distinct approaches were used to examine the morphology and structure of PANI/CA and CA powder, i.e. FTIR, XRD, BET analysis, and FESEM.

4.4.2.1 Brunauer–Emmett–Teller (BET)

The textural properties of CA and PANI/CA were examined using the BET method. From BET, the specific surface area and pore size distribution of both samples (PANI/CA and CA) were calculated at 77 K with nitrogen adsorption/desorption. The nitrogen adsorption/desorption curve of CA and PANI/CA are shown in **Figures 4.9(a, b),** and pore size distribution curves are shown in **Figures 4.9 (c, d)**. The surface area of pure CA powder was 2025.4 m^2/s, and for PANI/CA, it decreased to only 61.27 m^2/s for PANI/CA powder, as illustrated in **Table 4.4**. The surface area of the pure carbon aerogel sample was much higher than the nanocomposite sample. The high surface area of CA shows an excellent porous structure. The addition of PANI to carbon aerogel decreased the surface area of the nanocomposite sample due to PANI micropore blockage in the CA, as borne out by FESEM images shown later. The pore diameter and pore volume of CA were as high as 4.0 nm and 2.03 $cm^{3/}g$. For PANI/CA nanocomposites, it decreased to 0.71 nm and 0.15 cm^3/g, respectively.

Additionally, from **Figures 4.9(a, b),** it can be observed that the nitrogen adsorption/desorption of both CA and PANI/CA samples showed type IV isotherms as per the IUPAC classification **[22]**. This indicates that CA has a mesopores morphology (2-50 nm) and PANI/CA has a micropores morphology (< 2 nm).

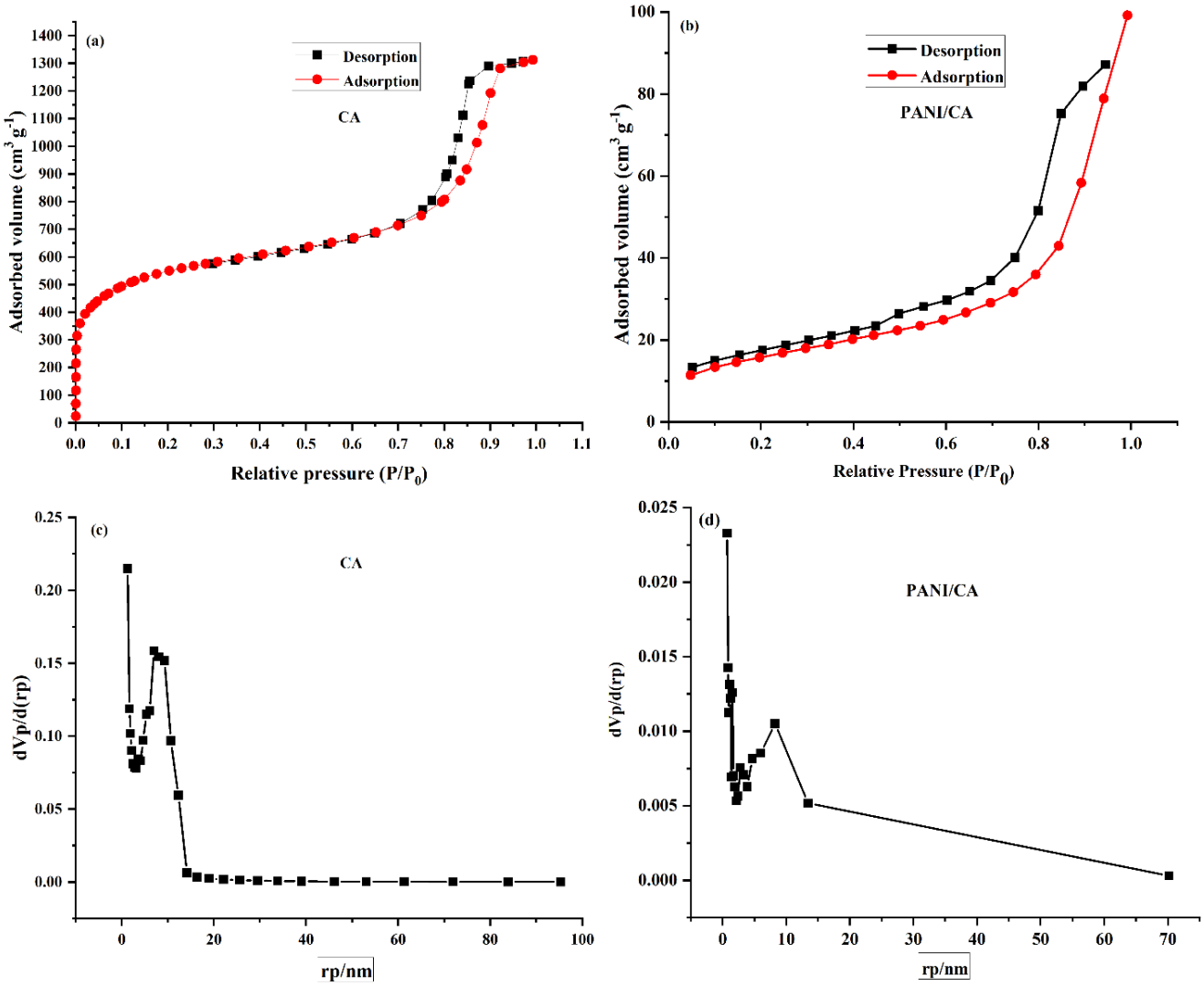

Figure 4.9 (a, b) Nitrogen Adsorption/Desorption isotherm and (c, d) pore size distribution curve of CA and PANI/CA.

Table 4.4 BET analysis results of CA and PANI/CA

Sample	BET (m^2/s)	Pore diameter (nm)	Pore volume (cm^3/g)
Carbon aerogel	2025.4	4.00	2.03
PANI/carbon aerogel	61.27	0.71	0.15

4.4.2.2 Fourier-transform infrared spectroscopy investigation

FTIR spectrum results for CA powder as well as PANI/CA nanocomposite are shown in Figure 4.10. In the FTIR spectra of CA, a broad absorption peak is observed at 3441.7 cm^{-1}, which is associated with –OH (hydroxide group) stretching. The vibration stretching of C=C is confirmed by 1631 cm^{-1} band; the C-N stretch band is located at 1116 cm^{-1}**[23, 24]**. In the spectra of PANI/CA, new absorption bands are confirmed due to PANI loading in the CA shown in **Figure 4.10**. In PANI/CA sample, peaks are detected at 3403 cm^{-1} correspondings to N-H stretch and 2924.5 cm^{-1} correspondings to C-H stretching **[25]**. The band at 1474.1 cm^{-1} and 1544.6 cm^{-1} corresponds to the benzenoid and quinoid ring (C=C stretching) that indicates the existence of polyaniline doped structures **[25-27].** The wavelength at 1296.1 cm^{-1} and 1240 cm^{-1} are accredited to C-N stretching **[25, 26, 28]**. C-H in-plane bend is represented by the peak at 1116.9 cm^{-1} and C-H out-of-plane bend is represented by the peak at 796.8 cm^{-1} **[25-28]**. These peaks confirm that PANI/CA nanocomposite has been successfully synthesized.

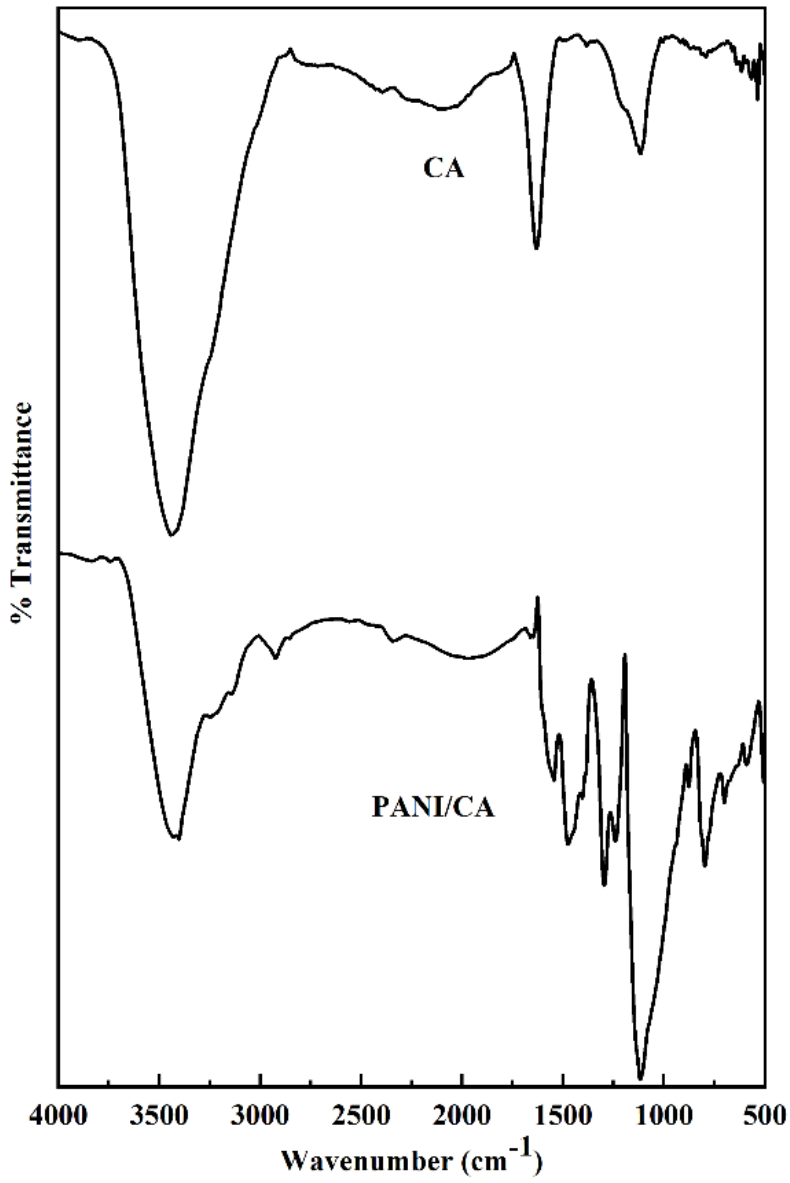

Figure 4.10 FTIR spectra of CA and PANI/CA nanocomposites.

4.4.2.3 X-ray diffraction investigation

XRD analysis results of carbon aerogel and PANI/CA powder are given in **Figure 4.11**. Two broad peaks of carbon aerogel identified at 22.98° and 43.41° can be attributed to graphite carbon. This shows that carbon is a crystalline substance and has a graphitic structure **[29-36]**. These two peaks are the typical carbon aerogel peaks. The XRD peaks of PANI/CA 15.28°, 20.77°, 25.55°, and

43.00° corresponds to d-spacing values of 5.79 A°, 4.27 A°, 3.48 A°, and 2.10 A°, respectively **[37-40]**. Therefore, all these peaks were indicating the existence of PANI in the CA.

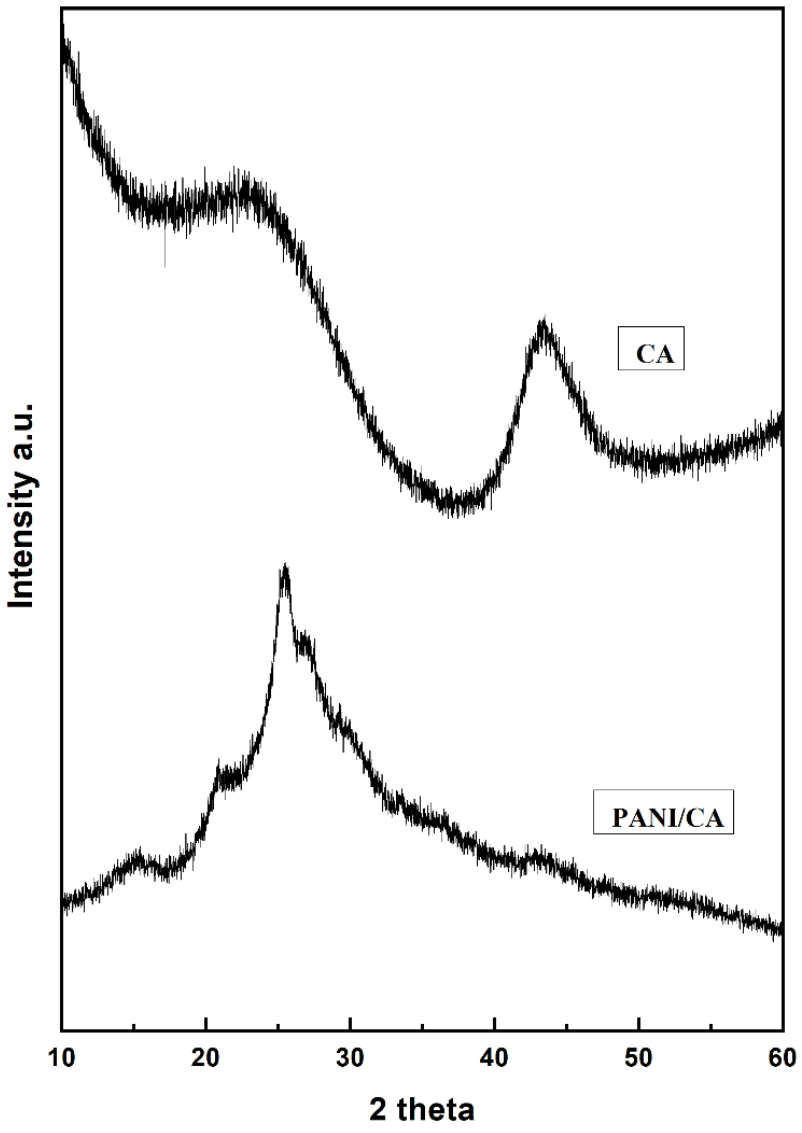

Figure 4.11 XRD pattern of Carbon and PANI/carbon aerogel.

4.4.2.4 Field Emission Scanning Electron Microscopy

The investigation of FESEM for CA and PANI/CA powder was done at low and high magnifications, as depicted in **Figure 4.12**. In **Figures 4.12 (a, b)**, the porous network structure of

CA can be easily seen. The morphology of the PANI/CA sample is shown in **Figures 4.12 (c, d)**. After the fabrication of CA with PANI polymer, the morphology drastically changes, which indicates the coating of CA with PANI. **Figures 4.12 (c, d)** show that the PANI has been deposited evenly on the porous CA material. CA pores have been covered by PANI polymer. The porous structure of CA is clearly more beneficial for the adsorption process.

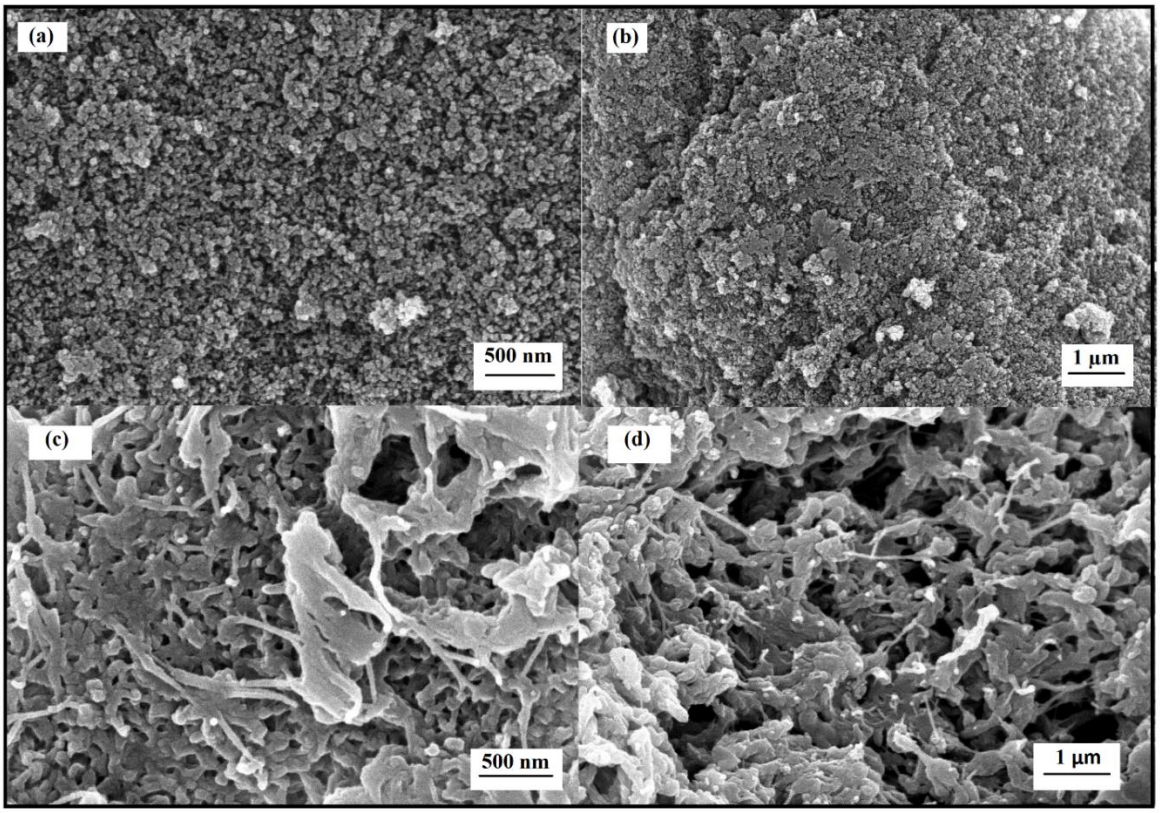

Figure 4.12 FESEM images of (a, b) CA and (c, d) PANI/CA.

4.4.3 PANI and PANI/HNT nanocomposites

Characterization of PANI/HNT nanocomposites has been analyzed using techniques like X-ray diffraction (XRD), Fourier transforms infrared spectroscopy (FTIR), and Field emission scanning electron microscopy (FESEM).

4.4.3.1 Fourier transform infrared spectroscopy (FTIR) investigation

Figure 4.13 shows the FTIR bands of pure HNT, PANI, besides PANI/HNT nanocomposites. FTIR spectra of PANI/HNT exhibiting characteristic peaks of HNT and pure PANI. In the spectra of pure HNT, the absorbed water bands are observed at 3435 cm^{-1} and 1650 cm^{-1}**[41]**. Si-O stretch can be assigned to the characteristic band at 1025 cm^{-1}. The vibration peak occurrence at 908 cm^{-1} is reason being the presence of O-H bends in inner hydroxyl groups. Two more bands are observed at 528 and 464 cm^{-1}, corresponding to Al-O-Si and Si-O-Si bending vibration **[42]**. The low-intensity peaks at 2924 cm^{-1} and 2853 cm^{-1} are accredited to symmetric and asymmetric stretchs of $–CH_2$ groups **[43]**. Compared to pristine HNT, HNT coated with PANI shows some additional peaks at 1565 and 1473 cm^{-1} (C=C stretching vibrations) attributed to quinonoid and benzenoid ring structures **[44]**. Two more crests appeared at 1384, and 1117 cm^{-1} corresponds to C-N stretch and C-H plane bending vibration **[35]**. These peaks are indicative of the deposits of PANI on the HNT sample.

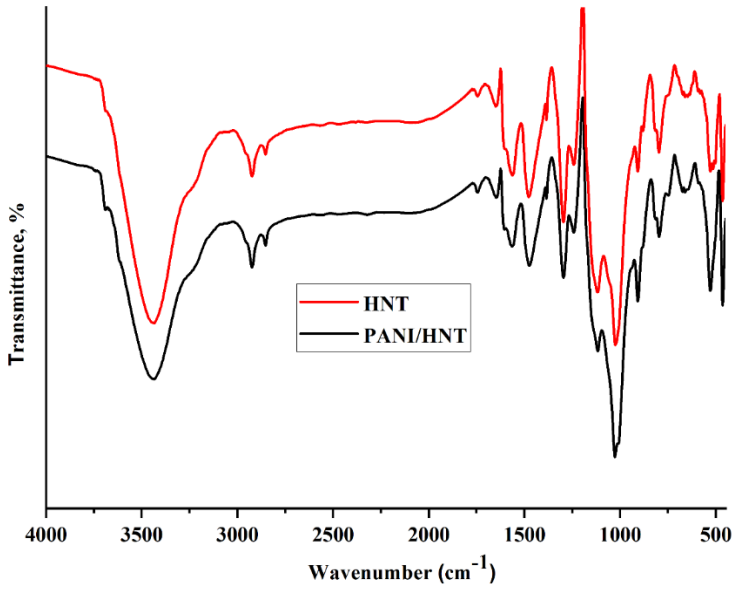

Figure 4.13 FTIR spectra of HNT and its nanocomposites

4.4.3.2 X-ray diffraction investigation

XRD spectra of pure HNT, PANI, and PANI/HNT nanocomposites is presented in **Figure 4.14**. the XRD study was performed in the range of 2Θ = 3 to 70°. Pure HNT XRD spectra showed typical diffraction peaks at 2Θ = 12.39, 19.91°, and 24.91° **[41, 45, 46]** corresponding to d-spacing of 7.13 A°, 4.45A° and 3.57A°, respectively. In the XRD spectra of PANI/HNT, the diffraction peaks intensity decreases and slightly shifted towards the right (12.41°, 19.94°, and 24.94°) and the reason is due to the interaction of the polymer chain with the HNT clay galleries. The nanocomposite spectra is almost identical to the HNT sample, indicating that its structure has been retained.

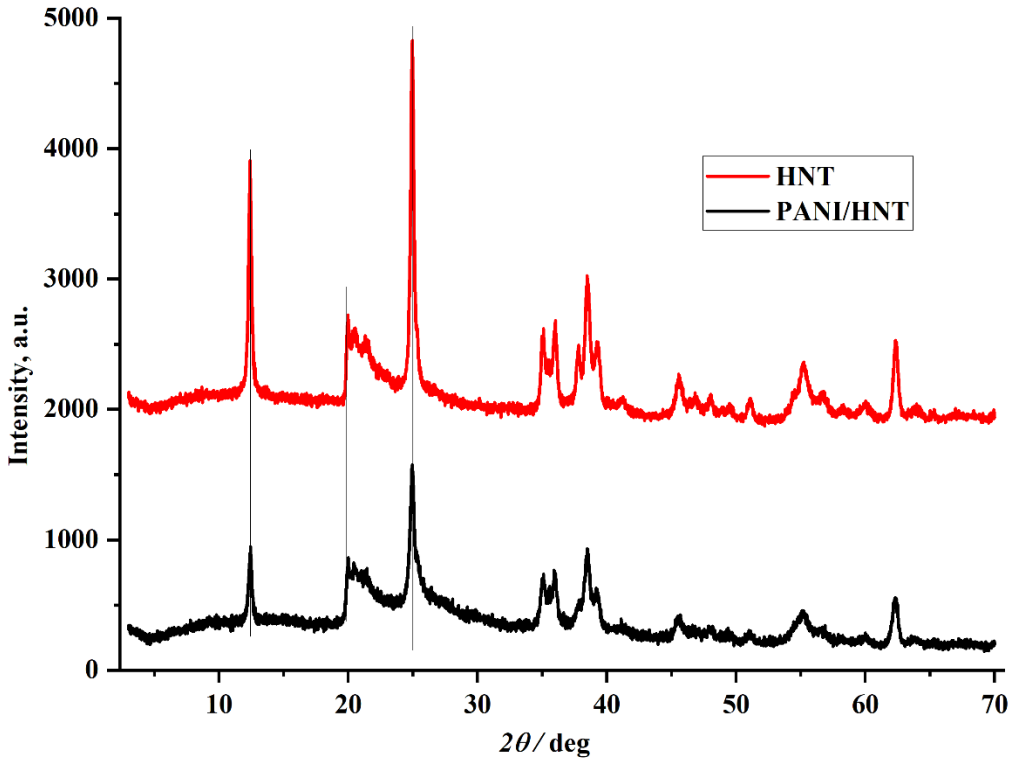

Figure 4.14 XRD of pure HNT and its nanocomposites

4.4.3.3 Field emission scanning electron microscopy investigation

PANI/HNT nanocomposite morphology was characterized by FESEM analysis. The higher and lower resolution FESEM images of PANI/HNT nanocomposite are shown in **Figure 4.15**. In the FESEM analysis of PANI/HNT **(Figures 4.15 (a, b))**, it can be seen that the tubular shape of the HNT surface was coated with PANI, suggesting the formation of the nanocomposite. FESEM results demonstrate that the halloysite clay has successfully interacted with PANI through an *in-situ* polymerization process.

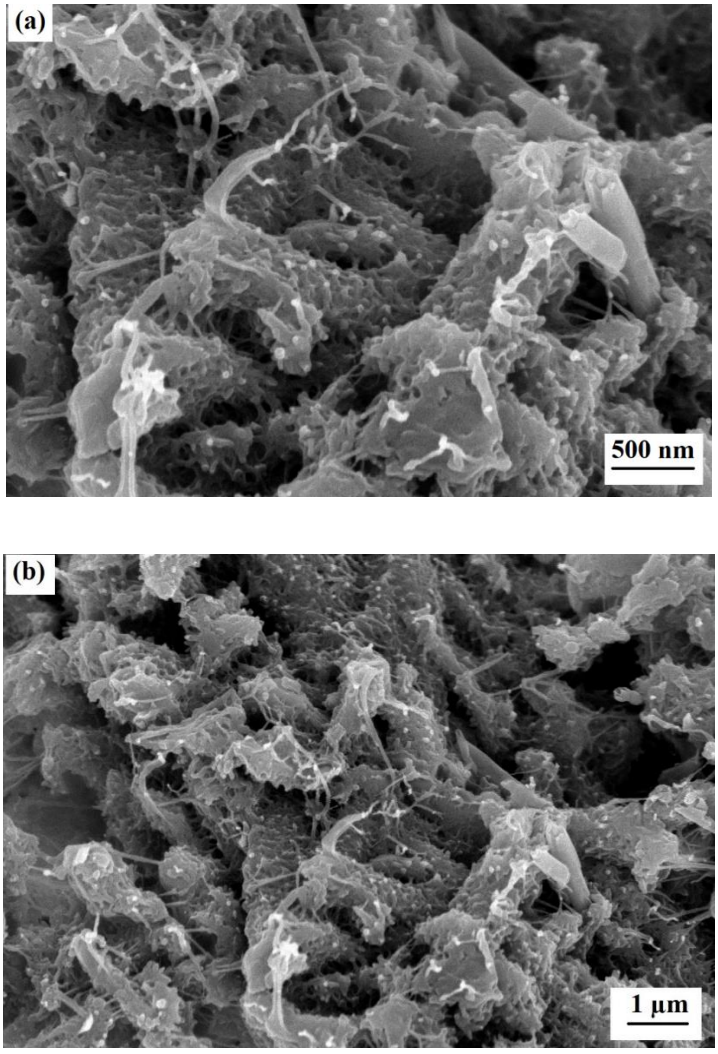

Figure 4.15 FESEM images of PANI/HNT nanocomposites

4.5 Conclusion

Polyaniline (PANI), polyaniline/montmorillonite clay (PANI/MMT), and polyaniline/carbon aerogel (PANI/CA) nanocomposites were successfully obtained by *in-situ* polymerization using ammonium persulfate as an oxidizing agent. Characterization techniques confirmed the successful fabrication of PANI, PANI/MMT, and PANI/CA nanocomposites. Further, polyaniline, polyaniline/montmorillonite clay nanocomposites, carbon aerogel powder, and polyaniline/carbon aerogel nanocomposites have been used for the remediation of Acid green 25 (AG25), an anionic dye and are discussed in **Chapters 5 and 6**.

References

[1] Sangamesha MA, Pushpalatha K, Shekar GL (2014) Synthesis and characterization of conducting polyaniline/copper selenide nanocomposites. Indian J Adv Chem Sci 2(3):223-227.

[2] Kazim S, Ahmad S, Pfleger J, Plestil J, Joshi YM (2011) Polyaniline–sodium montmorillonite clay nanocomposites: effect of clay concentration on thermal, structural, and electrical properties. J Mater Sci 47:420–428. DOI: 10.1007/s10853-011-5815-y.

[3] El-Ghaffar MA, Youssef AM, Abd El-Hakim AA (2015) Polyaniline nanocomposites *via in-situ* emulsion polymerization based on montmorillonite: Preparation and characterization. Arab J Chem 8(6):771-779. https://doi.org/10.1016/j.arabjc.2014.01.001.

[4] Olad A and Azhar FF (2014) Eco-friendly biopolymer/clay/conducting polymer nanocomposite: characterization and its application in reactive dye removal. Fiber Polym 15:1321-1329. DOI 10.1007/s12221-014-1321-6.

[5] Zehhaf A, Morallon E, Benyoucef A (2013) Polyaniline/montmorillonite nanocomposites obtained by *in-situ* intercalation and oxidative polymerization in cationic modified-clay (sodium, copper and iron). J Inorg Organomet Polym Mater 23:1485-1491. DOI:10.1007/s10904-013-9953-3.

[6] HambateGomdje V, Rahman AN, Wahabou A, BenoitLoura and Chtaini A (2017) Synthesis of organoclay and its applications in electrochemical detection of paracetamol. Der Chemica Sinica 8(1):206-217.

[7] Tyagi B, Chudasama CD, Jasra RV (2006) Determination of structural modification in acid activated montmorillonite clay by FT-IR spectroscopy. Spectrochim Acta A 64:273–278. DOI: 10.1016/j.saa.2005.07.018.

[8] Pande S, Swaruparani H, Bedre MD, Bhat R, Deshpande R, Venkataraman A (2012) Synthesis, characterization and studies of PANI-MMT nanocomposites. Nanosci Nanotechnol 2:90-98. DOI:10.5923/j.nn.20120204.01.

[9] Baldissera AF, Souza JF, Ferreira CA (2013) Synthesis of polyaniline/clay conducting nanocomposites. Synth Met 183:69-72. Doi:10.1016/j.synthmet.2013.09.022.

[10] Gomes EC, Oliveira MAS (2012) Chemical polymerization of aniline in hydrochloric acid (HCl) and formic acid (HCOOH) media. Differences between the two synthesized polyanilines. Am J Polym Sci 2:5-13. DOI:10.5923/j.ajps.20120202.02.

[11] Cole KC (2008) Use of infrared spectroscopy to characterize clay intercalation and exfoliation in polymer nanocomposites. Macromolecules 41:834-843. Doi: 10.1021/ma0628329.

[12] Binitha N, Suraja V, Yaakob Z, Sugunan S (2011) Synthesis of polyaniline-montmorillonite nanocomposites using H_2O_2 as the oxidant. Sains Malays 40(3):215-219.

[13] Qiu M, Zhang Y, Wen B (2018) Facile synthesis of polyaniline nanostructures with effective electromagnetic interference shielding performance. J Mater Sci - Mater El 29:10437-10444. Doi:101007/s10854-018-9100-6.

[14] Binitha NN, Sugunan S (2008) Polyaniline/pillared montmorillonite clay composite nanofibers. J Appl Polym Sci 107:3367–3372. DOI 10.1002/app.27353.

[15] Nadaf LI, Venkatesh KS (2015) Polyaniline-copper oxide nanocomposites: Synthesis and characterization. Mat Sci Res India 12(2):108-111. http://dx.doi.org/10.13005/msri/120204.

[16] Sui X, Chu Y, Xing S, Liu C (2004) Synthesis of PANI/AgCl, PANI/$BaSO_4$ and PANI/TiO_2 nanocomposites in CTAB/hexanol/water reverse micelle. Mater Lett 58:1255-1259. DOI:10.1016/j.matlet.2003.09.035.

[17] Chang KC, Jang GW, Peng CW, Lin CY, Shieh JC, Yeh JM, Yang JC, Li WT (2007) Comparatively electrochemical studies at different operational temperatures for the effect of nanoclay platelets on the anticorrosion efficiency of DBSA-doped polyaniline/Na^+–MMT clay nanocomposite coatings. Electrochimica Acta 52:5191–5200.

[18] Vivekanandan J, Ponnusamy V, Mahudeswaran A, Vijayanand PS (2011) Synthesis, characterization and conductivity study of polyaniline prepared by chemical oxidative and electrochemical methods. Arch Appl Sci Res 3(6):147-153. https://www.researchgate.net/publication/267383132.

[19] Jayasudha S, Priya L, Vasudevan KT (2014) Preparation and characterization of polyaniline/Ag nanocomposites. Int J Chem Tech Res 6(3):1821-1823.

[20] Yoshimoto S, Ohashi F, Kameyama T (2005) Characterization and thermal degradation studies on polyaniline-intercalated montmorillonite nanocomposites prepared by a solvent-free mechanochemical route. J Polym Sci B. 43:2705-2714. DOI: 10.1002/polb.20561.

[21] Sun F, Pan Y, Wang J, Wang Z, Hu C, Dong Q (2009) Synthesis of conducting polyaniline-montmorillonite nanocomposites via inverse emulsion polymerization in supercritical carbon dioxide. Polym. Compos. 31:163. https://doi.org/10.1002/pc.20783.

[22] Sing KSW (1982) Reporting physisorption data for gas/solid systems with special reference to the determination of surface area and porosity. Pure Appl Chem 54:2201—22l8. DOI: 10.1351/pac198254112201.

[23] Tsioptsias C, Michailof C, Stauropoulos G, Panayiotou C (2009) Chitin and carbon aerogels from chitin alcogels. Carbohydr Polym 76:535–540. Doi:10.1016/j.carbpol.2008.11.018.

[24] Abolhasani S, Ahmadpour A, Bastami TR, Yaqubzadeh A (2019) Facile synthesis of mesoporous carbon aerogel for the removal of ibuprofen from aqueous solution by central composite experimental design (CCD). J Mol Liq 281:261–268. Doi:10.1016/j.molliq.2019.02.084.

[25] Sampreeth T, Al-Maghrabi MA, Bahuleyan BK. and Ramesan MT (2018) Synthesis, characterization, thermal properties, conductivity and sensor application study of polyaniline/cerium-doped titanium dioxide nanocomposites. J Mater Sci 53:591–603. DOI 10.1007/s10853-017-1505-8.

[26] Xu F, Zheng G, Wu D, Liang Y, Lia Z. and Fu R (2010) Improving electrochemical performance of polyaniline by introducing carbon aerogel as filler. Phys Chem 12:3270–3275. DOI: 10.1039/b917677b.

[27] Waware US, Summers GJ, Hamouda AMS., and Rashi M (2018) Synthesis and characterization of polyaniline, poly(3-fluoroaniline), and poly(aniline-co-3- fluoroaniline) derivatives obtained by chemical oxidative polymerization methods. Polym Plast Technol Eng 57:1015–1025. https://doi.org/10.1080/03602559.2017.1370108.

[28] El-Sayed NS, Abd El-Aziz ME, Kamel S, Turky G (2018) Synthesis and characterization of polyaniline/tosylcellulose stearate composites as promising semiconducting materials. Synth Met 236:44–53. https://doi.org/10.1016/j.synthmet.2018.01.001.

[29] Rejitha KS, Abraham PA, Panicker NPR, Jacob KS, Pramanik NC (2013) Role of catalyst on the formation of resorcinol-furfural based carbon aerogels and its physical properties. Advances in Nanoparticles 2:99-103. http://dx.doi.org/10.4236/anp.2013.22017.

[30] Bakierska M, Molenda M, Majda D, Dziembaj R (2014) Functional starch based carbon aerogels for energy applications. Procedia Eng 98:14 – 19. Doi: 10.1016/j.proeng.2014.12.481.

[31] Wang S, Yan M, Liu H, Xu Y, Zhang L, Liu Z (2017) Preparation and characterization of Ni-doped carbon aerogel for supercapacitor. Mater Sci Eng 167:012014. Doi:10.1088/1757-899X/167/1/012014.

[32] Yan MF, Zhang LH, He R, Liu ZF (2015) Synthesis and characterization of carbon aerogels with different catalysts. J Porous Mater 22:699–703. DOI 10.1007/s10934-015-9942-8.

[33] Yan YXM and Liu Z (2017) Synthesis and characterization carbon nanotubes doped carbon aerogels. IOP Conf Series: Mater Sci Eng 275:012006. Doi:10.1088/1757-899X/275/1/012006.

[34] Alex AS, Ananda Lekshmi MS, Sekkar V, John B, Gouri C, Ilangovan SA (2017) Microporous carbon aerogel prepared through ambient pressure drying route as anode material for lithium ion cells. Polym Adv Technol 28:1945–1950. DOI: 10.1002/pat.4085.

[35] Hu F, Xu J, Zhang S, Jiang J, Yan B, Gu Y, Jiang M, Lin S and Chen S (2018) Core/shell structure halloysite/polyaniline nanotubes with enhanced electrochromic properties. J Mater Chem C 6:5707-5715. DOI: 10.1039/C8TC01163J.

[36] Li K, Zhou M, Liang L, Jiang L, Wang W (2019) Ultrahigh-surface-area activated carbon aerogels derived from glucose for high-performance organic pollutants adsorption. J Colloid Interface Sci. 546:333–343. https://doi.org/10.1016/j.jcis.2019.03.076.

[37] Patil PT, Anwane R.S, Kondawar SB (2015) Development of electrospun polyaniline/ZnO composite nanofibers for LPG sensing. Procedia Mater Sci 10:195 – 204. DOI: 10.1016/j.mspro.2015.06.041.

[38] Mezgebe MM, Yan Z, Wei G, Gong S, Zhang F, Guang S, Xu H (2017) 3D graphene-Fe_3O_4 polyaniline, a novel ternary composite for supercapacitor electrodes with improved

electrochemical properties. Mater Today Energy 5:164-172. http://dx.doi.org/10.1016/j.mtener.2017.06.007.

[39] Ajeel KI, Kareem QS (2019) Synthesis and characteristics of polyaniline (PANI) filled by graphene (PANI/GR) nano-films. IOP Conf. Series: Journal of Physics: Conf. Series 1234:012020. Doi:10.1088/1742-6596/1234/1/012020.

[40] Liu Y, Song L, Du L, Gao P, Liang N, Wu S, Minami T, Zang L, Yu C, and Xu X (2020) Preparation of polyaniline/emulsion microsphere composite for efficient adsorption of organic dyes. Polym 12:167. Doi:10.3390/polym12010167.

[41] Tan WL, Salehabadi A, Mohd Isa MH, Abu Bakar M, Abu Bakar NHH (2016) Synthesis and physicochemical characterization of organomodified halloysite/epoxidized natural rubber nanocomposites: A potential flame-resistant adhesive. J Mater Sci. 51:1121–1132. DOI 10.1007/s10853-015-9443-9.

[42] Lun H, Ouyang J, Yang JH (2014) Natural halloysite nanotubes modified as an aspirin carrier. RSC Advances. 4:44197–44202. DOI: 10.1039/c4ra09006c.

[43] Molaei A, Amadeh A, Yari M, Afshar MR (2016) Structure, apatite inducing ability, and corrosion behavior of chitosan/halloysite nanotube coatings prepared by electrophoretic deposition on titanium substrate. Mater Sci Eng C. 59:740–747. http://dx.doi.org/10.1016/j.msec.2015.10.073.

[44] Abolghasemi MM, Arsalani N, Yousefi V, Arsalani M, Piryaei M (2016) Fabrication of polyaniline-coated halloysite nanotubes by *in situ* chemical polymerization as a solid-phase microextraction coating for the analysis of volatile organic compounds in aqueous solutions. J Sep Sci 39:956–963. DOI 10.1002/jssc.201500839.

[45] Paran SMR, Naderi G, and Ghoreishy MHR (2016) Novel nanotube reinforces for safer polyamide-6-based nanocomposites. Society of Plastics Engineers. DOI: 10.2417/spepro.006390.

[46] Almasri DA, Saleh NB, Atieh MA, McKay G & Ahzi S (2019) Adsorption of phosphate on iron oxide doped halloysite nanotubes. Sci Rep 9:3232. https://doi.org/10.1038/s41598-019-39035-2.

CHAPTER 5

ADSORPTION STUDY OF ACID GREEN 25 DYE ON POLYANILINE/MONTMORILLONITE ADSORBENT

This chapter deals with the adsorption of AG25 dye using PANI and PANI/MMT nanocomposite as adsorbents. The prepared PANI and PANI/MMT nanocomposites (prepared at 0^{o}C) were studied for their adsorption behavior.

5.1 Adsorption study

5.1.1 Preparation of the stock solution and finding the maximum wavelength of AG25 dye

A stock solution was prepared by diluting one gram of AG25 dye in one liter of distilled water. The maximum wavelength of 642 nm was identified by the calibration curve (10 to 60 mg/L). The calibration curve of AG25 dye is presented in **Figure 5.1**.

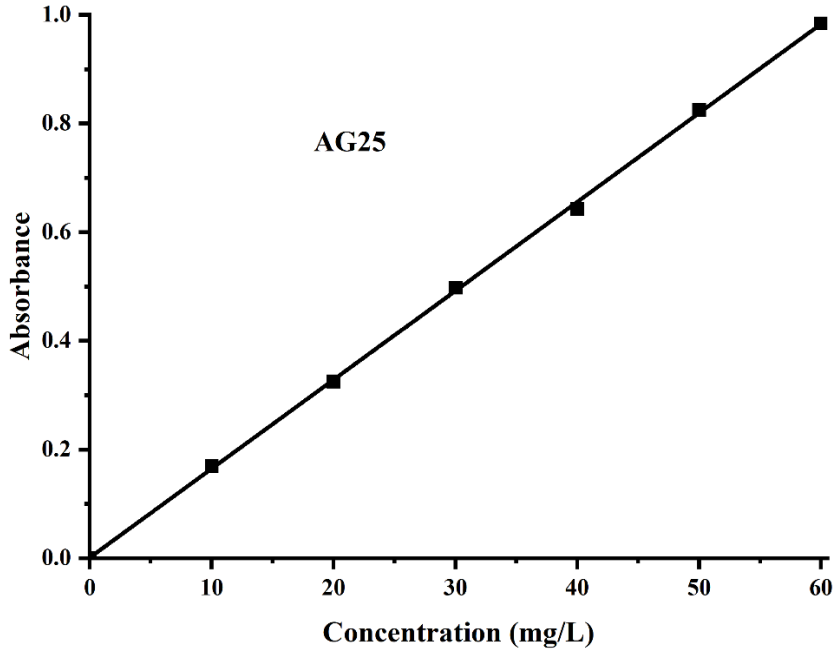

Figure 5.1 Calibration curve of AG25 dye

5.1.2 Batch adsorption

Adsorption studies were done by diluting a stock solution of Acid green 25 dye (1g/L) into different dye concentrations solutions (50-200 mg/L). The parameters studied were: effect of dye solution temperature (20 to 50^{o}C), adsorbent dose (0.008-0.6 g), initial AG25 dye concentration (50-200 mg/L), time (0-60 min) and pH (2-10). For the adsorption study, 100 mL of various initial dye concentration solutions were prepared along with a fixed amount of adsorbent. The experiments were carried out in an incubator shaker at 180 rpm for 60 min at pH 6 by varying temperatures from 20 to 50^{o}C.

The percentage of dye removal was calculated by:

$$\% \text{ removal} = 100(C_o - C_e)/C_o \quad (1)$$

Where C_o = initial concentration of AG25 dye

C_e = equilibrium concentration (mg/L) of AG25 dye

The equilibrium capacity of the dye was calculated by:

$$q_e = (C_o - C_e)V/m \quad (2)$$

Where q_e (mg/g) = amount of AG25 adsorbed at equilibrium per unit mass of adsorbent. V = volume (L) of AG25 dye solution. m = mass (g) of adsorbent.

5.2 Results and Discussion

5.2.1 Effect of pH

The interaction between the adsorbate and the adsorbent is considerably affected by dye aqueous solution pH. The chemistry of adsorbate solution, ionization degree of adsorbate molecules, and

the surface charge of adsorbent are strongly affected by the pH of dye solution **[1, 2]**. The pH effect on AG25 dye adsorption was examined on pure PANI and PANI/MMT by varying pH values in the range of 2 to 10. The dye solution's pH was varied using 1 molar HCl & 1 molar NaOH solutions, and the study was conducted with a starting 50 mg/L of AG25 dye concentration, a contact duration of 60 minutes, and a temperature of 20°C with a stirrer speed of 180 rpm.

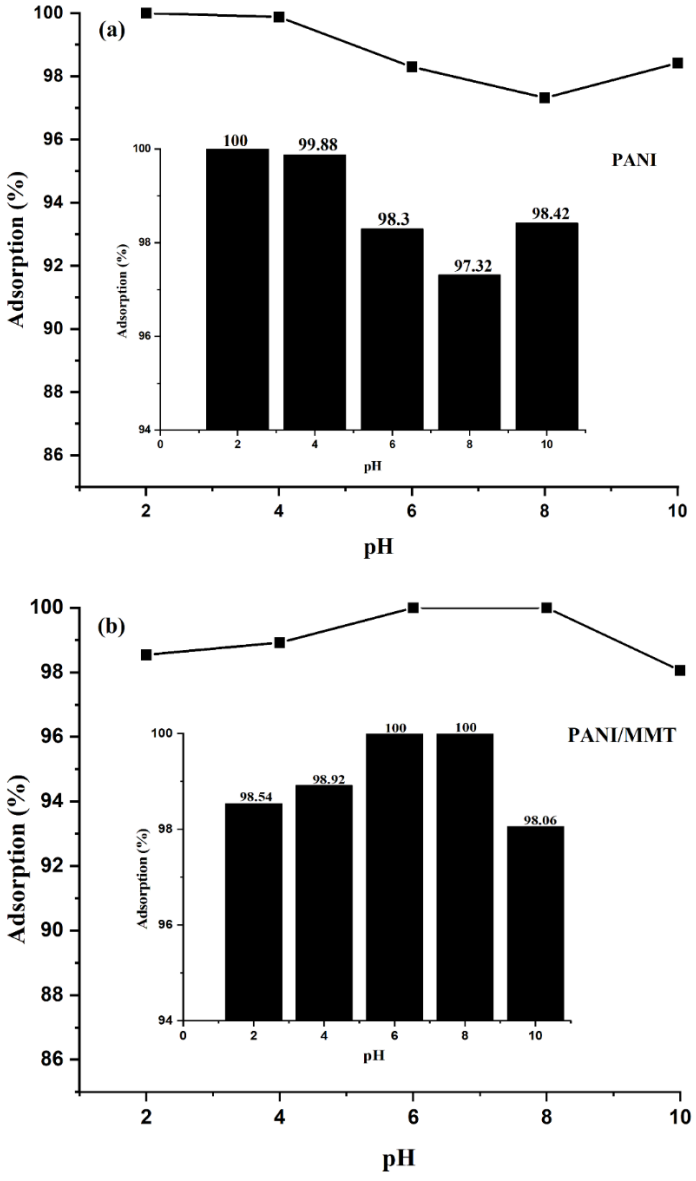

Figure 5.2 pH effect on AG25 dye removal.

The adsorption data of PANI in **Figure 5.2(a)** show that greater removal of AG25 dye was observed at lower pH values. The maximum adsorption of AG25 dye was obtained at pH = 2 (100% removal within 10 min), and the minimum adsorption was observed at pH = 8 (97.32%). The adsorption of AG25 dye was stable after a short interval time (15 min). In **Figure 5.2(a)**, it can be seen that there is no significant difference in adsorption between pH 2 (100%), pH 4 (99.88%), and pH 6 (98.33%), and so pH 6 was selected as an optimum pH for the adsorption study of AG25 dye. For PANI/MMT **(Figure 5.2(b))**, the maximum removal of AG25 dye was obtained at pH = 6 (100%), and the minimum adsorption was observed at pH = 10 (98.06%).

5.2.2 Effect of adsorbent dose

The adsorbent dosage effect was investigated for pure PANI and PANI/MMT for AG25 dye adsorption by taking various amounts of adsorbent (0.08 to 0.6 g) at 20°C with 50 mg/L of initial dye concentration for a duration of 60 min. The data of the effect of adsorbent are plotted between time vs. percentage removal and are displayed in **Figure 5.3**. After the dose of 0.4 g, there is hardly any difference in % removal for higher amounts **(Table 5.1)**. Hence, to use the lowest adsorbent amount, an adsorbent amount of 0.4 g was selected for further adsorption study of AG25 dye. However, when the amount of adsorbent increased, the extent of AG25 dye adsorbed also increased, this is mostly owing to the presence of more active adsorbent sites which can interact with the solution of the anionic dye **[3-5]**.

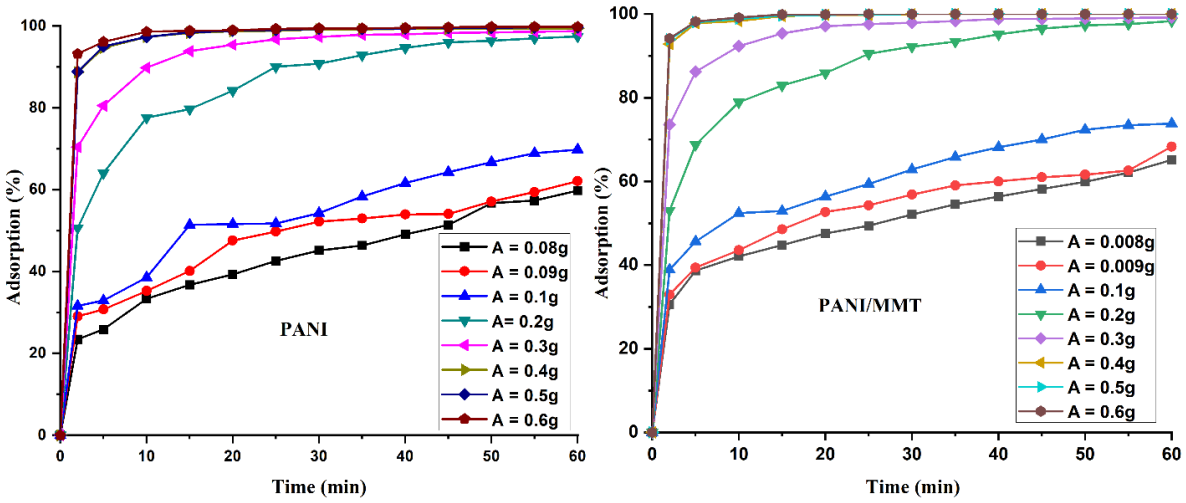

Figure 5.3 Effect of adsorbent amount (pH = 6, C_o = 50 mg/L, T = 20°C).

Table 5.1 Effect of PANI and PANI/MMT adsorbent dose

Adsorbent dose	**0.08g**	**0.09g**	**0.1g**	**0.2g**	**0.3g**	**0.4g**	**0.5g**	**0.6g**
% removal (PANI)	59.76%	62.08%	69.76%	97.44%	98.66%	99.4%	99.64%	99.76%
% removal (PANI/MMT)	65.14%	68.3%	73.8%	98.3%	99.16%	100%	100%	100%

5.2.3 Effect of initial dye concentration

Initial AG25 dye concentration effect with PANI and PANI/MMT nanocomposite adsorbents was studied. The C_o values were varied from 50 to 200 mg/L at a temperature of 20°C, optimized pH 6 and adsorbent amount of 0.4 g. **Figures 5.4(a, b)** illustrates the AG25 dye concentration effect onto PANI as well as PANI/MMT samples adsorption. Adsorption kinetics have been compared for pure PANI and PANI/MMT with a 50 mg/L dye concentration, in **Figure 5.4(c)**. Pure PANI

removed 94.64%, and PANI/MMT removed 97.82% of the dye within 5 min at 50 mg/L of AG25 dye. Also, within 30 min the PANI/MMT sample removed 100% and pure PANI salt sample removed 99.16% of the anionic dye (C_o = 50 mg/L, pH = 6, adsorbent = 0.4 g, T = 20°C). Since the adsorption occurs at a very fast rate, i.e., in a very short time period, the same data were plotted on a semi-log figure (the inset in **Figure 5.4(c)** to illustrate the adsorption behavior at short times. It can be seen that even at 1 min, the adsorption for PANI and PANI/MMT is about 88% and 93%, respectively.

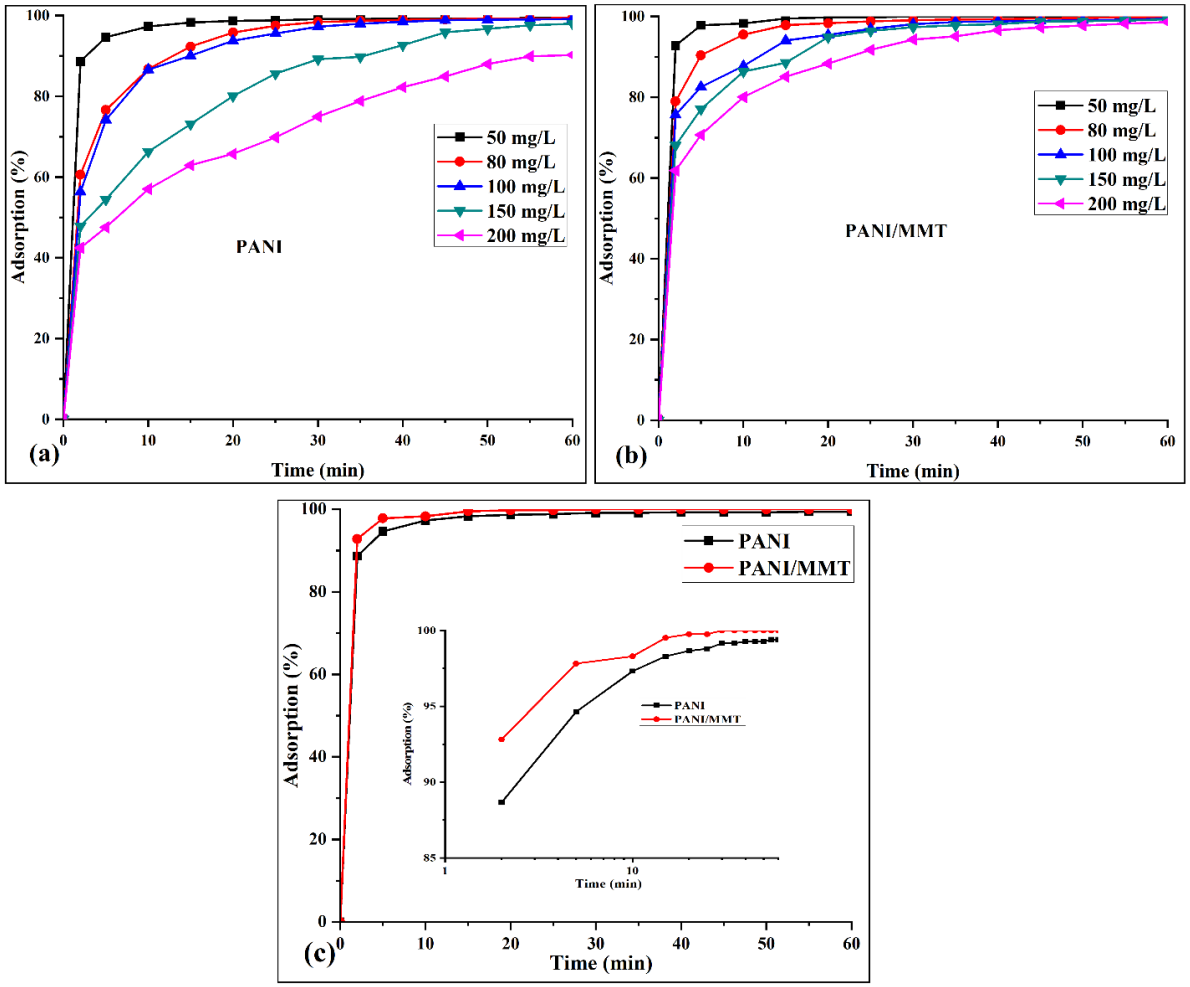

Figure 5.4 Initial dye concentration effect on AG25 dye elimination by (a) PANI, (b) PANI/MMT adsorbent (T = 20°C, pH = 6, C_o = 50-200 mg/L, t = 60 min), (c) is the comparison of PANI and PANI/MMT adsorption data (50 mg/L).

The results indicate that PANI/MMT nanocomposite efficiency as an adsorbent is higher than that of pure PANI. However, in the comparison of adsorption behavior at different initial dye concentrations, the removal efficiency of samples decreased by increasing the AG25 dye concentration. This may be attributed to the saturation of the adsorbent sites for removal of the dye molecules **[4, 6]**.

5.2.4 Effect of temperature

The effect of temperature was also studied for the removal of AG25 dye at 20°, 35°, 45° and 50°C (conditions: C_o = 50–200 mg/L, pH = 6, adsorbent = 0.4 g, t = 30 min). The effect of temperature on adsorption by PANI and PANI/MMT for AG25 dye removal is shown in **Figure 5.5**. The results indicate that the percentage removal by PANI is less than the removal by PANI/MMT nanocomposite, and removal of AG25 dye increases as the dye solution temperature rises from 20° to 50°C **[7]**. The higher adsorption by the nanocomposite is due to the nano dispersed clay platelets, the outer layer of which has a negative charge.

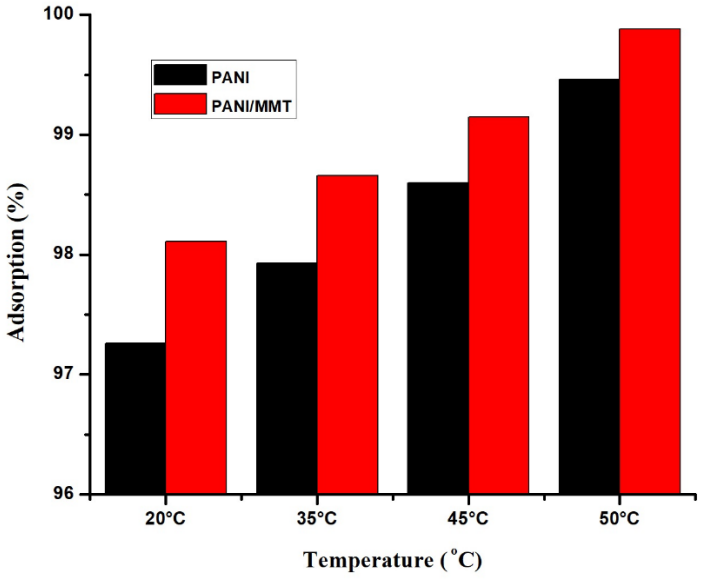

Figure 5.5 Comparison of PANI with PANI/MMT adsorption for AG25 dye removal (C_o = 50 mg/L, pH = 6, adsorbent amount = 0.4 g, t = 30 min).

5.2.5 Adsorption kinetics

There are different models available to evaluate the adsorption kinetic data. The adsorption kinetics study of AG25 dye was done using a pseudo-first order kinetic model as well as a pseudo-second order model. Pseudo-first order equation can be written by **[8]**

$$\log(q_e - q_t) = logq_e - k_f t/2.303 \qquad (3)$$

Where, q_e (mg/g) = amount of dye adsorbed at equilibrium; q_t (mg/g) = amount of dye adsorbed at time *t*; k_f (min^{-1}) = rate constant; *t* (min) = time.

The maximum adsorption time was taken to be 60 min, wherein the percentage of dye removal was more than 99% for all initial dye concentrations studied. The experimental data did not fit in pseudo-first order kinetic model **(Tables 5.2 and 5.4)**. Therefore, the first-order model is not a suitable model for the adsorption kinetic study of AG25 dye, as shown in **Figures 5.6 and 5.8**. Then, the pseudo-second kinetic model was tested for adsorption at different temperatures (20 to 50 °C) and different initial dye concentrations (50–200 mg/L). The equation for pseudo-second order model can be written as **[8]**:

$$\frac{t}{q_t} = \frac{1}{k_2 qe^2} + \frac{t}{qe} \qquad (4)$$

Where, k_2 = pseudo-second order rate constant.

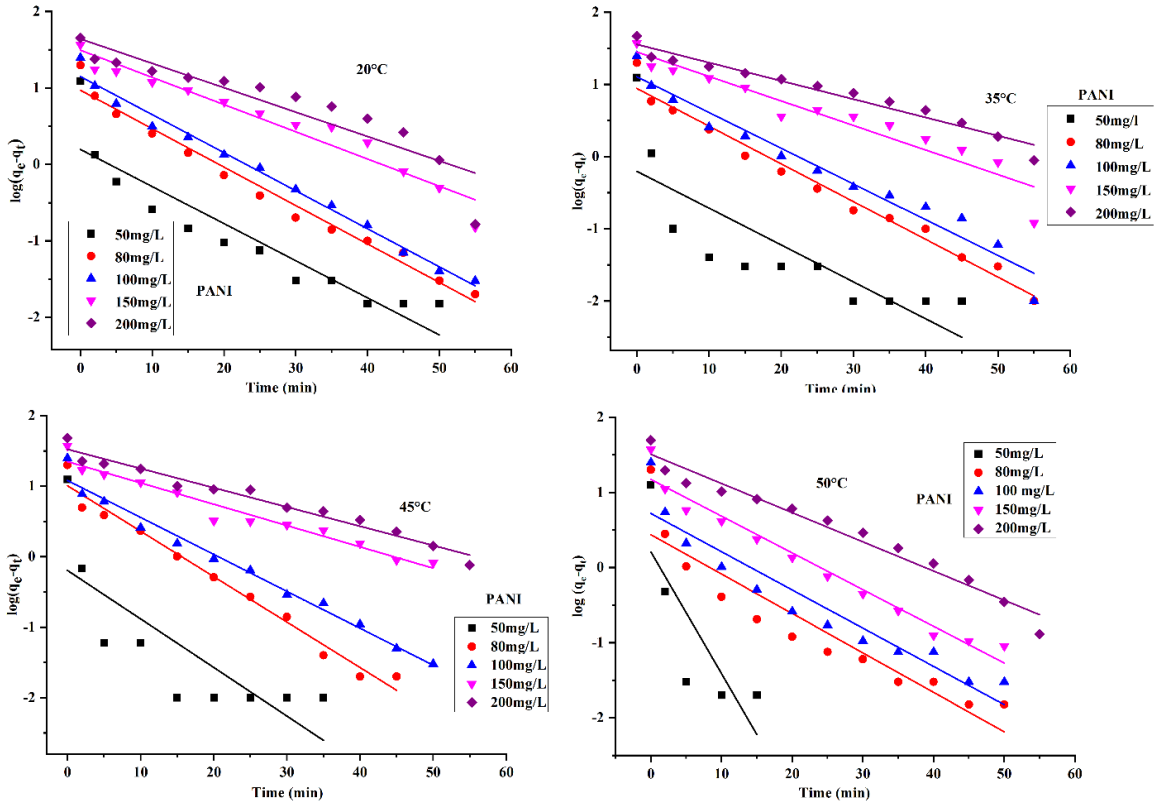

Figure 5.6 Pseudo-first order kinetic plot of AG25 dye removal on PANI at 20°C, 35°C, 45°C, and 50°C.

The straight line (plotted between *t/qt* vs. *t*) was obtained from pseudo-second order kinetic model, as shown in **Figures 5.7 and 5.9**. **Tables 5.3** and **5.5** presents the pseudo-second order kinetic parameters (q_e, k_2) calculated for AG25 dye adsorption onto PANI and PANI/MMT nanocomposite samples. The rate constant (k_2) and equilibrium adsorption capacity (q_e) values were calculated from the intercept and the slope. In the kinetic adsorption study, it was observed that the rate constant (k_2) and equilibrium adsorption capacity (q_e) values were higher for PANI/MMT nanocomposites as compared to pure PANI. These calculated k_2 values were decreased with increasing AG25 initial dye concentration for PANI/MMT and pure PANI adsorbent. As the temperature rises, the values of rate constant (k_2) and equilibrium adsorption

capacity (q_e) were increased. It shows that the higher temperature was more efficient for AG25 adsorption onto PANI and PANI/MMT samples. High correlation coefficients ($R^2 \geq 0.99$) were obtained at 35°, 45°, and 50°C, for different initial dye concentrations. It confirms that the pseudo-second order model is an appropriate model to describe AG25 dye kinetic adsorption using PANI as well as PANI/MMT.

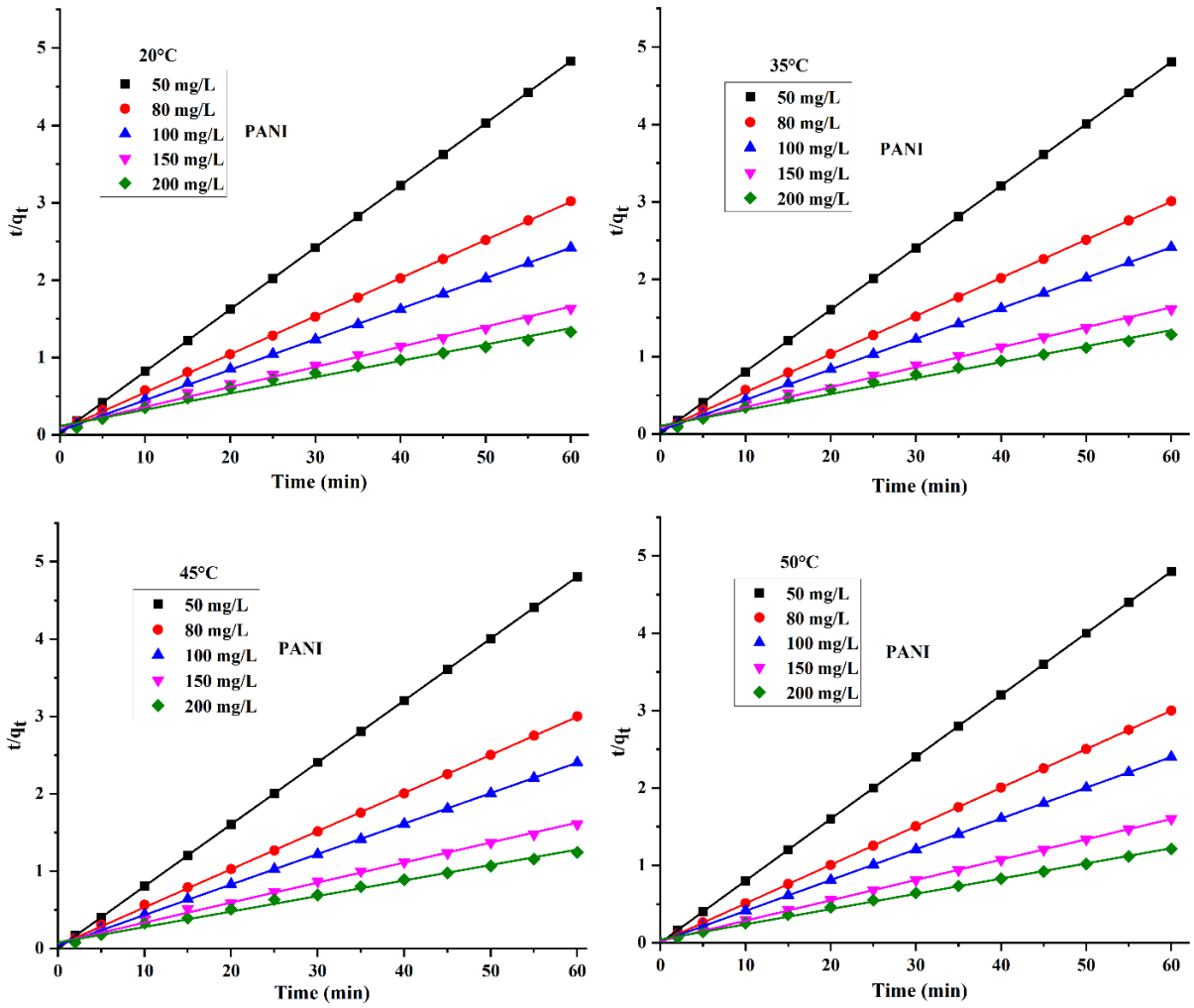

Figure 5.7 Pseudo-second order kinetic plot of AG25 dye removal on PANI at 20°C, 35°C, 45°C, and 50°C.

Table 5.2 Kinetic parameters of pseudo-first order calculated for AG25 dye removal on PANI

C_o (mg/L)	$q_{e(exp)}$ (mg/g)	$q_{e(cal)}$ (mg/g)	k_1 (min^{-1})	R^2
Temperature (T=20°C)				
50	12.425	1.572	0.112	0.8333
80	19.88	9.358	0.116	0.9791
100	24.78	14.11	0.115	0.9877
150	36.75	31.19	0.082	0.9414
200	45.12	43.75	0.073	0.8357
Temperature (T=35°C)				
50	12.48	0.629	0.118	0.6179
80	19.95	8.822	0.120	0.9778
100	24.86	12.77	0.114	0.9558
150	37.28	28.21	0.078	0.9040
200	46.70	35.95	0.058	0.9534
Temperature (T=45°C)				
50	12.48	0.641	0.159	0.5791
80	19.99	10.17	0.148	0.9773
100	24.94	12.08	0.121	0.9803
150	37.31	22.32	0.070	0.9522
200	48.26	33.36	0.063	0.9643
Temperature (T=50°C)				
50	12.5	1.622	0.374	0.5452
80	19.98	2.746	0.121	0.8572
100	24.97	5.252	0.117	0.8944
150	37.45	14.89	0.113	0.9618
200	49.49	32.11	0.089	0.9630

Table 5.3 Kinetic parameters of pseudo-second order calculated for AG25 dye removal on PANI

C_o (mg/L)	$q_{e(exp)}$ (mg/g)	$q_{e(cal)}$ (mg/g)	k_2 (g/mg min)	R^2
Temperature (T=20°C)				
50	12.425	12.46	0.417	0.9999
80	19.88	20.28	0.043	0.9995
100	24.78	25.37	0.028	0.9994
150	36.75	38.53	0.0066	0.9928
200	45.12	47.43	0.0038	0.9813
Temperature (T=35°C)				
50	12.48	12.49	1.25	1
80	19.95	20.28	0.052	0.9996
100	24.86	25.34	0.034	0.9996
150	37.28	38.77	0.0074	0.9942
200	46.70	48.56	0.0040	0.9845
Temperature (T=45°C)				
50	12.48	12.49	2.08	1
80	19.99	20.30	0.060	0.9996
100	24.94	25.40	0.039	0.9996
150	37.31	38.65	0.0087	0.9958
200	48.26	49.97	0.005	0.9913
Temperature (T=50°C)				
50	12.5	12.50	4.57	1
80	19.98	20.05	0.256	0.9999
100	24.97	25.13	0.109	0.9999
150	37.45	38.02	0.030	0.9997
200	49.49	50.89	0.009	0.9977

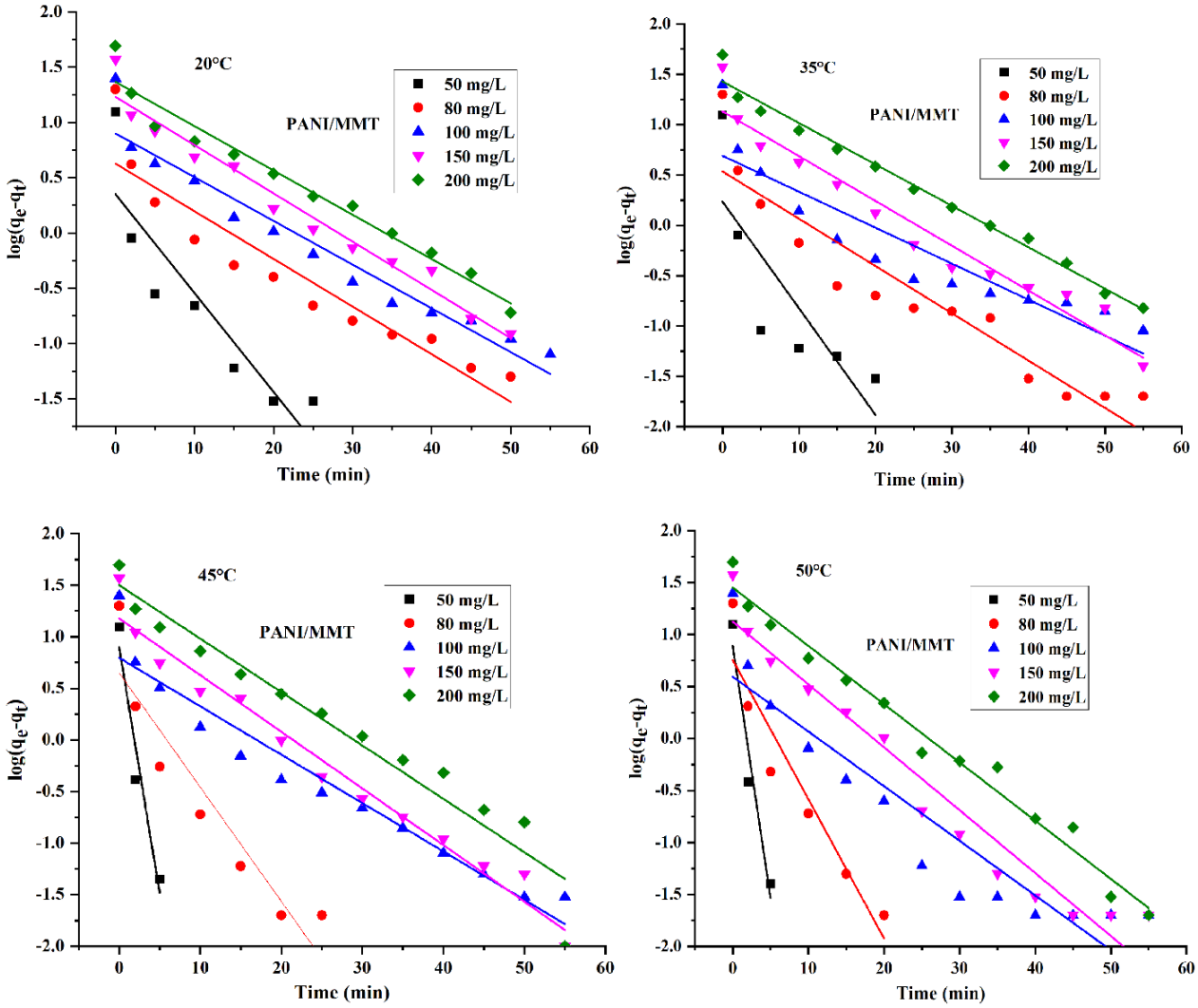

Figure 5.8 Kinetics of pseudo-first order model for AG25 dye adsorption onto PANI/MMT at 20°, 35°C, 45°C, and 50°C.

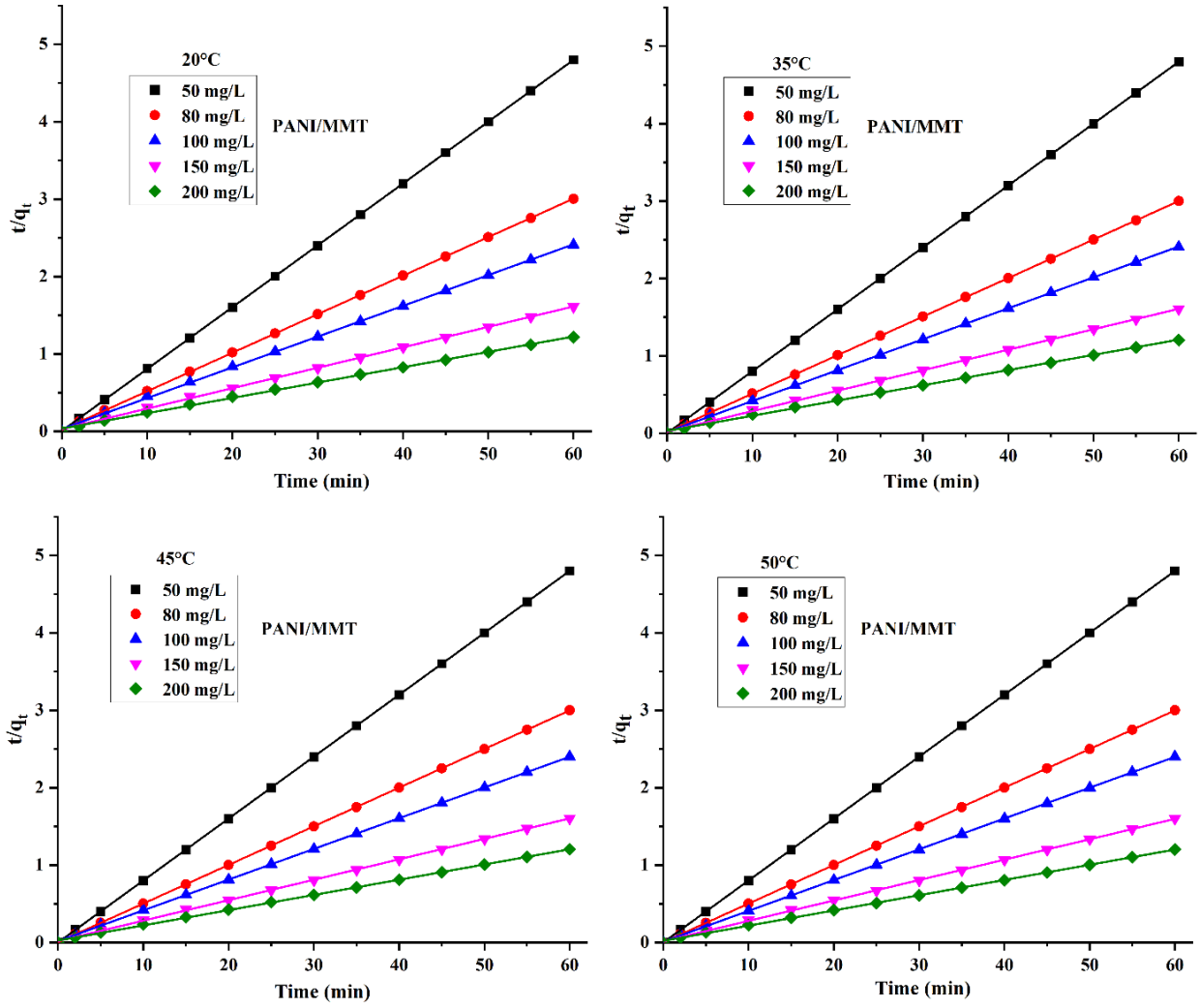

Figure 5.9 Kinetics of pseudo-second order model for AG25 dye adsorption onto PANI/MMT at 20^{o}, 35°C, 45°C, and 50°C.

Table 5.4 Kinetic parameters of pseudo-first order calculated for AG25 dye removal on PANI/MMT

C_o (mg/L)	$q_{e(exp)}$ (mg/g)	$q_{e(cal)}$ (mg/g)	k_1 (min^{-1})	R^2
Temperature (T=20°C)				
50	12.5	2.247	0.206	0.7685
80	19.97	4.244	0.099	0.8731
100	24.88	7.958	0.091	0.9362
150	37.24	17.06	0.101	0.9637
200	49.30	23.31	0.092	0.9607
Temperature (T=35°C)				
50	12.5	1.725	0.244	0.5985
80	20	3.434	0.108	0.8755
100	24.92	4.916	0.082	0.8220
150	37.31	13.59	0.103	0.9450
200	49.69	26.86	0.095	0.9836
Temperature (T=45°C)				
50	12.5	7.891	1.095	0.8887
80	20	4.474	0.255	0.8590
100	25	6.258	0.108	0.9311
150	37.36	15.09	0.127	0.9701
200	49.78	31.71	0.119	0.9340
Temperature (T=50°C)				
50	12.5	7.798	7.798	0.8876
80	20	5.711	0.309	0.8828
100	25	3.922	0.121	0.8449
150	37.47	13.36	0.139	0.9443
200	49.83	28.31	0.129	0.9788

Table 5.5 Kinetic parameters of pseudo-second order calculated for AG25 dye removal on PANI/MMT

C_o (mg/L)	$q_{e(exp)}$ (mg/g)	$q_{e(cal)}$ (mg/g)	k_2 (g/mg min)	R^2
Temperature (T=20°C)				
50	12.5	12.52	0.79	0.9999
80	19.97	20.09	0.11	0.9999
100	24.88	25.17	0.047	0.9997
150	37.24	37.90	0.022	0.9994
200	49.30	50.50	0.010	0.9985
Temperature (T=35°C)				
50	12.5	12.51	1.64	1
80	20	20.10	0.160	0.9999
100	24.92	25.05	0.085	0.9999
150	37.31	37.85	0.030	0.9997
200	49.69	50.91	0.012	0.9990
Temperature (T=45°C)				
50	12.5	12.5	5.16	1
80	20	20.04	0.517	0.9999
100	25	25.20	0.080	0.9999
150	37.36	37.87	0.035	0.9997
200	49.78	50.89	0.014	0.9994
Temperature (T=50°C)				
50	12.5	12.5	5.161	1
80	20	20.04	0.567	0.9999
100	25	25.15	0.132	0.9999
150	37.47	37.95	0.040	0.9998
200	49.83	50.86	0.017	0.9995

5.2.6 Adsorption equilibrium

An adsorption isotherm study was performed for AG25 dye with Langmuir, Freundlich, and Temkin isotherm models **[9]**. The parameters of these three models were studied at 20°, 35°, and 45°C with the initial dye concentration range of 80–200 mg/L. Almost 100% removal was attained at all values of initial dye concentrations studied. Also, significantly the lower concentration takes very less time to achieve complete dye removal. **Table 5.6** gives the isotherm equations for different models **[8, 10, 11]**.

Table 5.6 Equations of Langmuir, Freundlich and Temkin isotherm models **[8, 10, 11]**

S. No.	Isotherm Model	Equations
1.	Langmuir	$q_e = q_m K_L C_e /(1 + K_L C_e)$
2.	Freundlich	$q_e = K_F C_e^{1/n}$
3.	Temkin	$q_e = B_T ln\, K_T + B_T ln\, C_e$

Where q_e (mg/g) refer to adsorbate adsorbed at equilibrium, K_L (L/mg) denotes Langmuir isotherm constant, C_e (mg/L) refers to equilibrium AG25 concentration, q_m belongs to adsorption capacity, K_F (mg/g), and *1/n* are the Freundlich isotherm constants, and B_T (Kj/mol) and K_T (L/mg) are the Temkin isotherm constants. Out of these models, the Langmuir isotherm model best fits the experimental data, as shown in **Tables 5.7(a, b)**. A linear plot of C_e/q_t against C_e for AG25 dye adsorption by PANI and PANI//MMT nanocomposites was obtained as depicted in **Figures 5.10 (a, b)**. The highest value of correlation coefficient (R^2) for Langmuir isotherm was found in a linear plot of C_e/q_e vs. C_e **(Tables 5.7(a, b))**.

The surface area of PANI is more than that of PANI/clay nanocomposites, as evidence by the BET results shown in **Table 5.8**. However, the kinetic and equilibrium adsorption data show that

PANI/clay nanocomposites have higher adsorption than PANI. This is because the outer surface of clay platelets, which are permanently negatively charged, would also adsorb the positively charged AG25 dye molecules. This is significant because the clay platelets are nano dispersed throughout the adsorbent.

Table 5.7 Calculated parameters for AG25 dye adsorption onto (a) PANI and (b) PANI/MMT nanocomposites

(a)

Langmuir isotherm			
T **(°C)**	q_m **(mg/g)**	K_L **(L/mg)**	R^2
20	34.14	0.335	0.9993
35	36.08	0.505	0.9992
45	41.71	0.366	0.9996
Freundlich isotherm			
T (°C)	***1/n***	K_F **(mg/g)**	R^2
20	0.1735	3.35	0.9497
35	0.1887	3.45	0.9352
45	0.2346	3.43	0.9514
Temkin isotherm			
T (°C)	K_T **(L/mg)**	B_T **(Kj/mol)**	R^2
20	0.25	4.46	0.9790
35	0.22	5.10	0.8120
45	0.09	6.69	0.9794

(b)

Langmuir Isotherm			
T (^{o}C)	q_m (mg/g)	K_L (L/mg)	R^2
20	51.02	0.271	0.9820
35	50.50	0.536	0.9909
45	49.87	0.969	0.9688
Freundlich Isotherm			
T (^{o}C)	$1/n$	K_F (mg/g)	R^2
20	0.3285	3.34	0.8999
35	0.2853	3.73	0.9869
45	0.1533	4.27	0.7624
Temkin Isotherm			
T (^{o}C)	K_T (L/mg)	B_T (Kj/mol)	R^2
20	0.03	9.92	0.9002
35	0.1	8.80	0.9692
45	0.06	4.65	0.6659

Table 5.8 Specific **s**urface area of PANI and its nanocomposites

Samples	Pore diameter (nm)	Pore volume (cm^3/g)	BET (m^2/g)
PANI	17.55	0.12	26.32
PANI/MMT	15.63	0.07	18.28

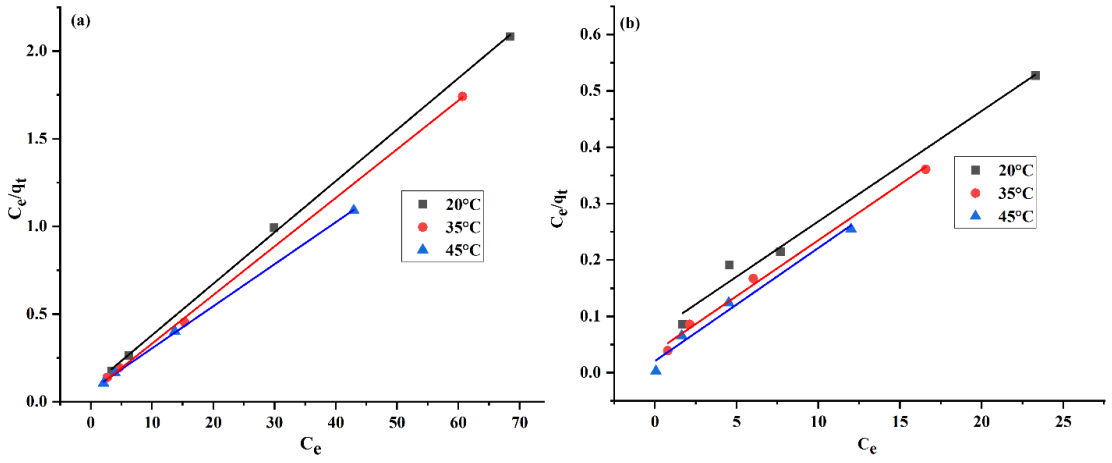

Figure 5.10 Ce/qe vs Ce Langmuir plot for (a) PANI and (b) PANI/MMT (adsorbent = 0.4 g, C_o = 80-200 mg/L)

5.3 Conclusion of the above study

PANI and PANI/MMT nanocomposites are excellent adsorbents for anionic dye (AG25) adsorption. The dye removal is mainly dependent on the initial dye concentration, temperature, and adsorbent amount. Nearly 100% removal of AG25 dye is achieved in 30 min at C_o = 50 mg/L, pH = 6, adsorbent = 0.4 g, T = 20°C. At higher temperatures, i.e., 45°C and 50°C, the PANI/MMT removed 100% dye within 10 min of contact time. The adsorption of AG25 dye is higher with PANI/MMT nanocomposite and takes less time to remove 100% as compared to the PANI sample. The best model for adsorption kinetics is the pseudo-second order model. Adsorption thermodynamic characteristics are best described by the Langmuir model. Overall, the study concludes that PANI/MMT nanocomposite is an efficient adsorbent for AG25 textile dye adsorption and is a better adsorbent than PANI. The faster adsorption would be especially important in applications wherein the adsorbents are an immobilized phase in a continuous adsorption process.

References

[1] Janaki V, Vijayaraghavan K, Oh BT, Lee KJ, Muthuchelian K, Ramasamy AK, Kannan SK (2012) Starch/polyaniline nanocomposite for enhanced removal of reactive dyes from synthetic effluent. Carbohydr Polym 90:1437–1444. doi:10.1016/j.carbpol.2012.07.012.

[2] Olad A, Azhar FF (2014) Eco-friendly biopolymer/clay/conducting polymer nanocomposite: Characterization and its application in reactive dye removal. Fiber Polym 15:1321–1329. DOI 10.1007/s12221-014-1321-6.

[3] Ansari R and Mosayebzadeh Z (2011) Application of polyaniline as an efficient and novel adsorbent for azo dyes removal from textile wastewaters. Chem Pap 65 (1):1–8. doi:10.2478/s11696-010-0083-x.

[4] Sobhanardakani S, Zandipak R (2015) Removal of anionic dyes (Direct Blue 106 and Acid Green 25) from aqueous solutions using oxidized multi-walled carbon nanotubes. Iran J Health Sci 3(3):48–57.

[5] Salem MA, Elsharkawy RG, Hablas MF (2016) Adsorption of brilliant green dye by polyaniline/ silver nanocomposite: Kinetic, equilibrium, and thermodynamic studies. Eur Polym J 75:577–590. https ://doi.org/10.1016/j.eurpo lymj.2015.12.027.

[6] Inthapanya X, Wu S, Han Z, Zeng G, Wu M, Yang C (2019) Adsorptive removal of anionic dye using calcined oyster shells: Isotherms, kinetics, and thermodynamics. Environ Sci Pollut Res 6:5944–5954. doi:10.1007/s11356-018-3980-0.

[7] Youssef AM, Ahmed AI, El-Bana UA (2012) Adsorption of cationic dye (MB) and anionic dye (AG 25) by physically and chemically activated carbons developed from rice husk. Carbon Lett 13(2):61–72.

[8] Koswojo R, Utomo RP, Ju YH, Ayucitra A, Soetaredjo FE, Sunarso J, Ismadji S (2010) Acid Green 25 removal from wastewater by organo-bentonite from pacitan. Appl Clay Sci 48:81–86. doi:10.1016/j.clay.2009.11.023.

[9] Parimalam R, Raj V, Sivakumar P (2012) Removal of acid green 25 from aqueous solution by adsorption. E-J Chem 9:1683–1698. doi:10.1155/2012/197235.

[10] Ansari R, Dezhampanah H (2013) Application of polyaniline /sawdust composite for removal of acid green 25 from aqueous solutions: Kinetics and thermodynamic studies. Eur Chem Bull 2(4):220–225. https ://doi.org/10.17628 /ecb.2013.2.220-225.

[11] Salahuddin NA, Ayad MM, Essa ME (2015) Modified chitosan for efficient dye adsorption in low acid media. J Mater Chem 5(3):54–63. https ://doi.org/10.5923/j.ijmc.20150 503.02.

CHAPTER 6

ADSORPTION OF AG25 DYE ON CA AND POLYANILINE/CARBON AEROGEL ADSORBENT

This chapter deals with the adsorption of AG25 dye using CA and PANI/CA nanocomposite as an adsorbent. The adsorption process was studied with various parameters. The isotherm and kinetic studies were also done to identify the adsorption behavior of AG25 dye onto CA and PANI/CA. The calibration curve of AG25 dye was identified and given in **Chapter 5**.

6.1 Adsorption study

Various dye solutions (20 to 250 mg/L) were prepared by diluting the Acid green 25 stock solution (1 g/L). The batch adsorption study was performed by taking the known concentration of AG25 dye. An investigation of AG25 dye removal was done using carbon aerogel and PANI/carbon aerogel nanocomposite as adsorbents. The adsorption was conducted in an incubator shaker, and the samples were removed from the shaker after a fixed time and filtered to separate adsorbent from the solution with Whatman filter paper. For all adsorption studies, 100 ml of AG25 dye aqueous solution was used, and the removal efficiency was calculated using the following Eq. (1):

$$\text{Adsorption } \% = \frac{C_o - C_e}{C_o} \times 100 \qquad (1)$$

Where Co (mg/L) represented the initial AG25 concentration and Ce (mg/L) symbolized the equilibrium concentration.

The equilibrium uptake of AG25 dye onto CA and PANI/CA samples was calculated using the following Eq. (2):

$$q_e = \frac{(C_o - C_e)}{m} \times V \qquad (2)$$

Where q_e denotes equilibrium capacity (mg/g) of CA and PANI/CA samples for AG25; m (g) symbolizes the adsorbent weight; V represents the volume of AG25 dye solution.

6.2 Results and Discussion

AG25 dye removal onto CA and PANI/CA depends on the adsorbent amount, temperature, pH, initial dye concentration, and adsorption time. All these parameters are discussed below:

6.2.1 Adsorbent dose effect on AG25 dye

To determine CA and PANI/CA dose effect on AG25 dye removal, the range of adsorbent dose of CA was varied from 0.08 to 0.25 g, and the experiments were executed in an incubator shaker with an initial 50 mg/L dye solution at 20^{o}C (pH = 6). The % removal of anionic dye increases from 92.44 % to 99.98 % with CA doses of 0.08 to 0.25 g, respectively **(Figure 6.1a).** For further experimentation, 0.1 g CA was fixed as an optimized adsorbent dose. It can be seen that a minimal amount of CA can remove 100 % of AG25 dye in a short time. In the case of PANI/CA **(Figure 6.1b)**, the range of PANI/CA dose was varied from 0.1 to 0.4 g at 30°C with 50 mg/L of AG25 solution and pH =7. The time was varied up to 50 min for both the adsorbent doses. The dye removal with PANI/CA increased from 63.54 % to 99.28 %, and thus 0.4 g dose of PANI/CA was selected as an optimized adsorbent dose for further experiments.

Thus, it can be concluded that removal efficiency/adsorption is higher for CA as compared to PANI/CA. The proper selection of adsorbent dose is needed because the adsorption strongly depends upon the adsorbent amount.

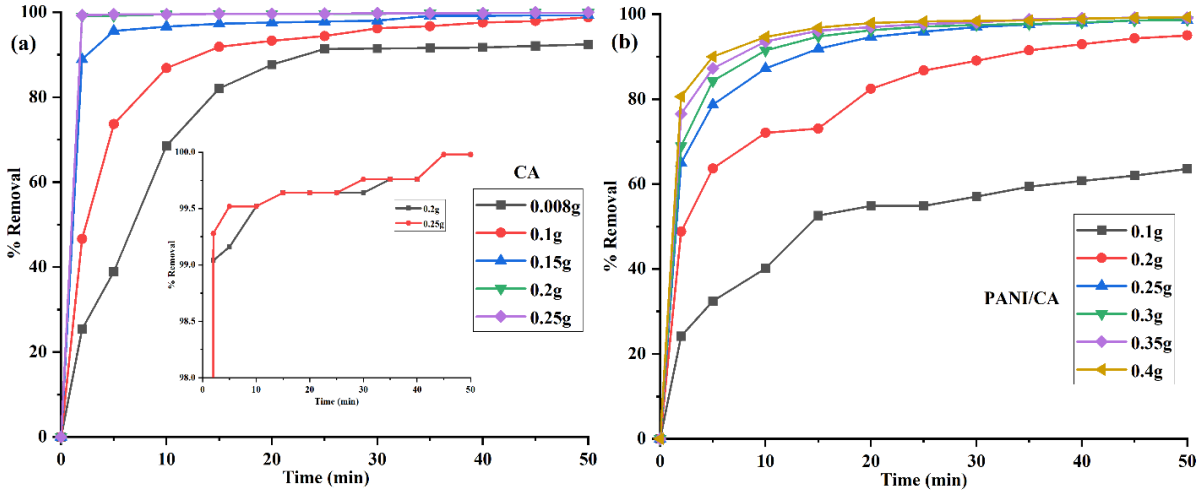

Figure 6.1 Adsorption kinetics for (a) CA (50 mg/L, pH =6, 20°C) and (b) PANI/CA nanocomposites (50 mg/L, pH = 7, 30°C).

6.2.2 pH effect on AG25 dye

pH study plays an important role in dye adsorption. Buffer solutions of NaOH and HCl were used to investigate the pH effect on AG25 dye adsorption by CA and PANI/CA. The pH range was explored from 2 to 10 for both adsorbents. pH vs. % removal is shown in **Figure 6.2a**. The pH study for CA was done with 0.1 g of optimum CA dose at 20°C (15 min) and 50 mg/L of initial AG25 solution. CA removed 100 % adsorbate in a very short period of time. The results show that CA is an effective adsorbent for AG25 dye removal over the entire pH of 2 to 10. CA adsorbed 98.66 % AG25 dye at pH 2, 99.04 % at pH 4, 100 % at pH 6, 99.28% at pH 8 and 100 % at pH 10. The percentage adsorption trend at pH 8 is different from the rest of the values. The difference between the adsorption at pH 8 and pH 6 (and pH 10) is about 0.72 %. Therefore, a neutral pH 7 was chosen as an optimized pH for the next set of experiments. For PANI/CA samples, the study was implemented with an optimum 0.4 g of PANI/CA dose at 30°C with an initial 50 mg/L solution for 30 min. PANI/CA removal efficiency was 98.92 % at pH = 2, 98.18 % at pH = 4, 98.66 % at

pH = 6, 98.8 % at pH = 8 and 97.7 % at pH = 10 as shown in **Figure 6.2b**. The high removal of dye up to pH 8 is probably due to the strong electrostatic attraction between the negatively charged AG25 dye molecules and the positively charged adsorbent surface. However, in highly alkaline conditions (pH 10), the removal rate was decreased due to the presence of OH^- ions in a large amount. Thus, the excess amount of hydroxyl ions reduced the adsorbate and adsorbent interactions [**1-4].** Since there is no major adsorption variance between pH 6 and pH 8, the study with PANI/CA was further continued at an optimized neutral pH 7.

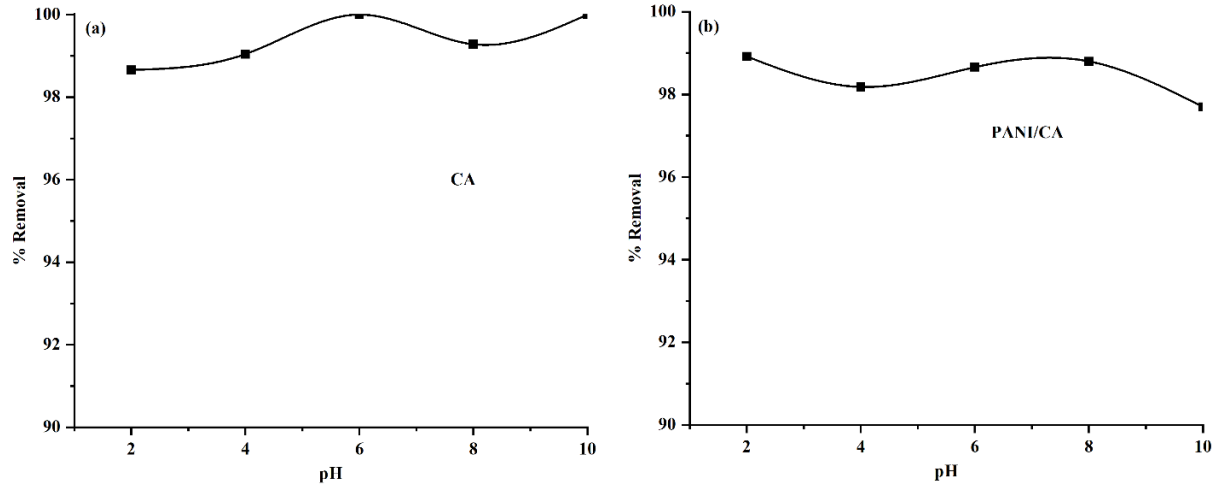

Figure 6.2 pH effect on (a) CA and (b) PANI/CA nanocomposites samples.

6.2.3 Effect of AG25 dye concentration

Figure 6.3 depicts the AG25 concentration effect on adsorption. This study was treated with 50 to 300 mg/L of AG25 solution with an optimized dose of CA (0.1 g) and PANI/CA (0.4 g) adsorbents at optimum pH 7 at 30^oC. The study with CA was performed in the time range of 0 to 30 min (optimized), as shown in **Figure 6.3a**. For 50 mg/L concentration, CA removed 100 % AG25, and in the case of 300 mg/L, the removal was 99.82 %. Removal with CA was more than 99 % at all

concentrations (50 -300 mg/L) of AG25 anionic dye. Even in just one minute, the removal was more than 98 %. The study with PANI/CA was performed in the time range of 0 to 60 min (optimized), and the results are given in **Figure 6.3b**. The extent of removal with PANI/CA ranged from 99.4 % (50 mg/L) to 52.82 % (300 mg/L). At higher concentrations, removal decreased because the adsorption sites would be saturated. Our study indicates interestingly that CA adsorbent is more effective compared to PANI/CA nanocomposite. For further temperature studies, 50 mg/L was selected as an optimized dye concentration for both adsorbents.

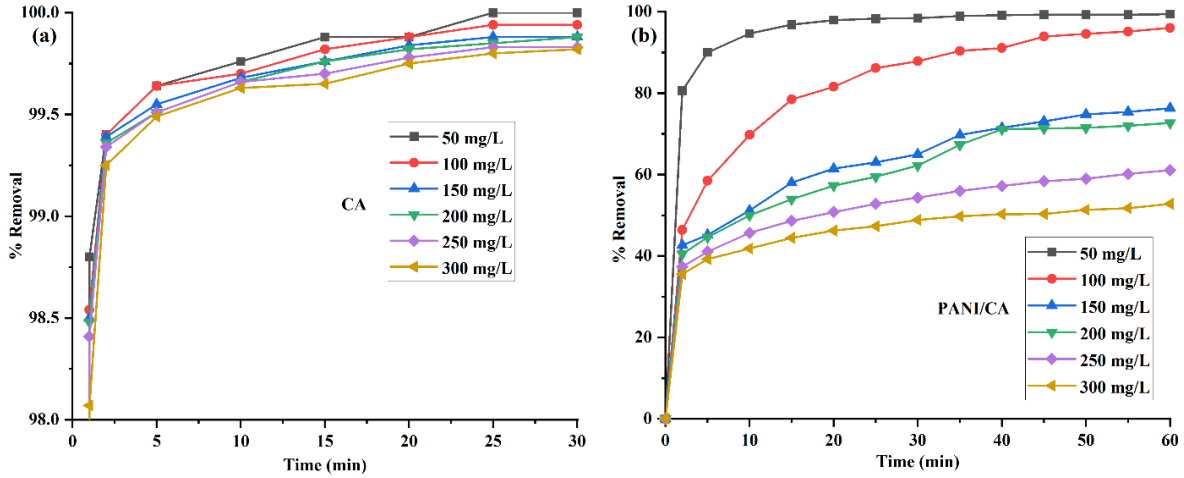

Figure 6.3 Initial AG25 concentration-effect onto (a) CA (50-300 mg/L, 0.1 g, pH = 7, 30^{o}C) and (b) PANI/CA nanocomposite samples (50-300 mg/L, 0.4 g, pH = 7, 30^{o}C).

6.2.4 Effect of Temperature

Figure 6.4 shows the effect of temperature (20^{o}C, 25^{o}C, and 30^{o}C) on adsorption by CA and PANI/CA nanocomposites. This study was done with 50 mg/L of AG25 solution, optimum pH 7, and with the optimum dose of CA (0.1 g) and PANI/CA (0.4 g). The contact time was varied from 0 to 30 min for CA adsorbent and 0 to 60 min for PANI/CA adsorbent. CA adsorbent removed more than 99 % dye at all three temperatures **(Figure 6.4a)** *i.e.* 99.76 % at 20^{o}C, 99.88 % at 25^{o}C

and 100 % at 30°C, in 30 min. In just two minutes, it removed 98.06 %, 98.92 %, 99.4 % of the dye at 20°, 25°, and 30°C temperatures, respectively. The results show that CA adsorbent performs satisfactorily at all temperatures studied. It also shows that temperature does not much effect on the adsorption process. The temperature kinetic study with PANI/CA adsorbent is shown in **Figure 6.4b**. It shows the removal of AG25 in the range of 95.98 % to 99.28 % in 60 min. The data of PANI/CA adsorbent indicate that with a rise in temperature, the removal rate of AG25 dye increases due to more available adsorption sites of PANI/CA at a higher temperature.

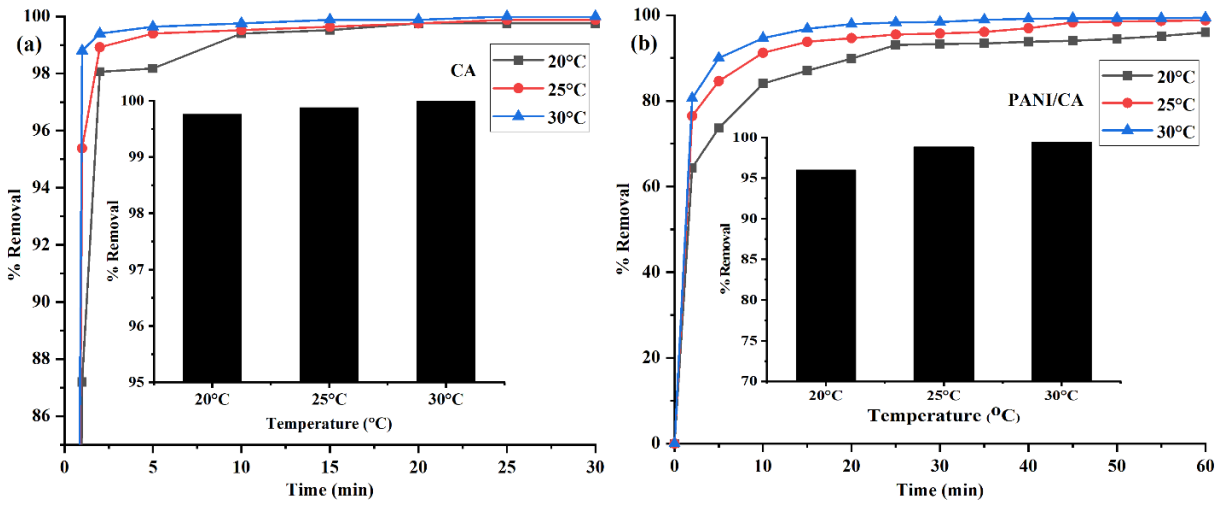

Figure 6.4 Temperature effect onto AG25 removal using CA (a) and PANI/CA (b) adsorbent.

6.2.5 Kinetic study

Dye removal kinetics are important for describing the adsorption process's effectiveness. Herein, two models were investigated for adsorption kinetics i.e. pseudo-first order and second order model. Kinetic study of AG25 adsorption on CA and PANI/CA was examined with 50-300 mg/L AG25 concentration, 0.1 g CA amount, 0.4 g PANI/CA amount, pH 7, and time-varying from 0 -

30 min for CA and 0 – 60 min for PANI/CA at 20°, 25° and 30°C. First order adsorption process is described by Eq. 3 and the second order by Eq. 4.

$$\log(q_e - q_t) = \ log\, q_e \ - \frac{k_1}{2.303} t \tag{3}$$

Where q_e presented the adsorption capacity in mg/g at time *t*; k_1 stands rate constant (min^{-1}); q_t (mg/g) refers to AG25 adsorption at equilibrium. The values k_1, q_e*(calculated)*, and correlation coefficient may be evaluated through a plot of $log(q_e\text{-}q_t)$ vs. *t* **(Figures 6.5 and 6.7)**.

A second order linear Eq. (4) is shown below:

$$\frac{t}{q_t} = \ \frac{1}{k_2\, {q_e}^2} + \frac{t}{q_e} \tag{4}$$

where k_2 (min^{-1}) stands second order rate constant. q_e *(calculated)* and correlation coefficient values are determined by t/q_t vs. *t* plot (linear fitting). Pseudo first order does not describe the data well for both CA and PANI/CA compared to the second order **(Table 6.1 and 6.3)**. **Figures 6.6 and 6.8** presents the kinetic plots of the second order model for AG25 adsorption on CA and PANI/CA, respectively. The results of second order model for CA and PANI/CA are shown in **Tables 6.2 and 6.4.** Second order model has measured the best-suited model for AG25 dye based on the highest correlation coefficient for both studies. A proper straight line was obtained for AG25 with a second-order model.

For CA, R^2 values are greater than 0.99. At 25°C, the R^2 values are equal to 1 for both 50 and 100 mg/L of dye solution. At 30°C, the R^2 values are equal to 1 for all AG25 (50 – 300 mg/L) concentrations. The results of the second order show that the q_e *(experimental)* and q_e *(calculated)* values are very close, as shown in **Table 6.2**. Furthermore, the rate constant (k_2) reduces with

higher AG25 concentration. For a kinetic study on PANI/CA **(Table 6.4)**, q_e *(experimental)* and q_e *(calculated)* data are close to each other. Kinetic analysis results reveal that the adsorption amount (q_e) values increased for both adsorbents *viz* CA and PANI/CA by increasing AG25 concentration (50 mg/L to 300 mg/L). The study shows that q_e values in CA are much higher than PANI/CA values. At a high AG25 concentration, the q_e calculated values for CA reached 299 mg/g, which is quite higher than PANI/CA adsorbent (39.9 mg/g). This indicates that CA adsorbs more dye as compared to PANI/CA adsorbent.

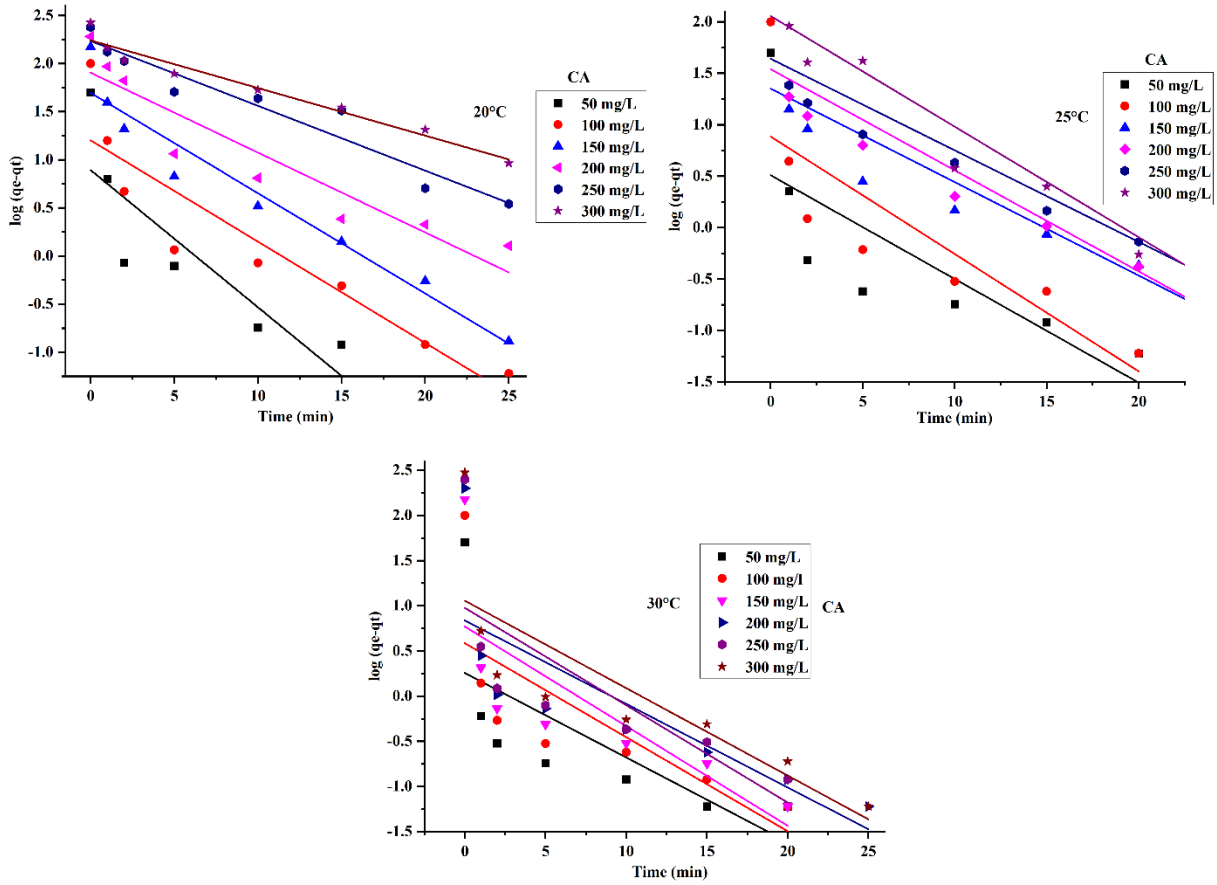

Figure 6.5 Kinetic pseudo first order plot of AG25 dye onto CA [50 -300 mg/L, pH = 7, 0.1 g, 30 min, T = 20°, 25°, 30°C).

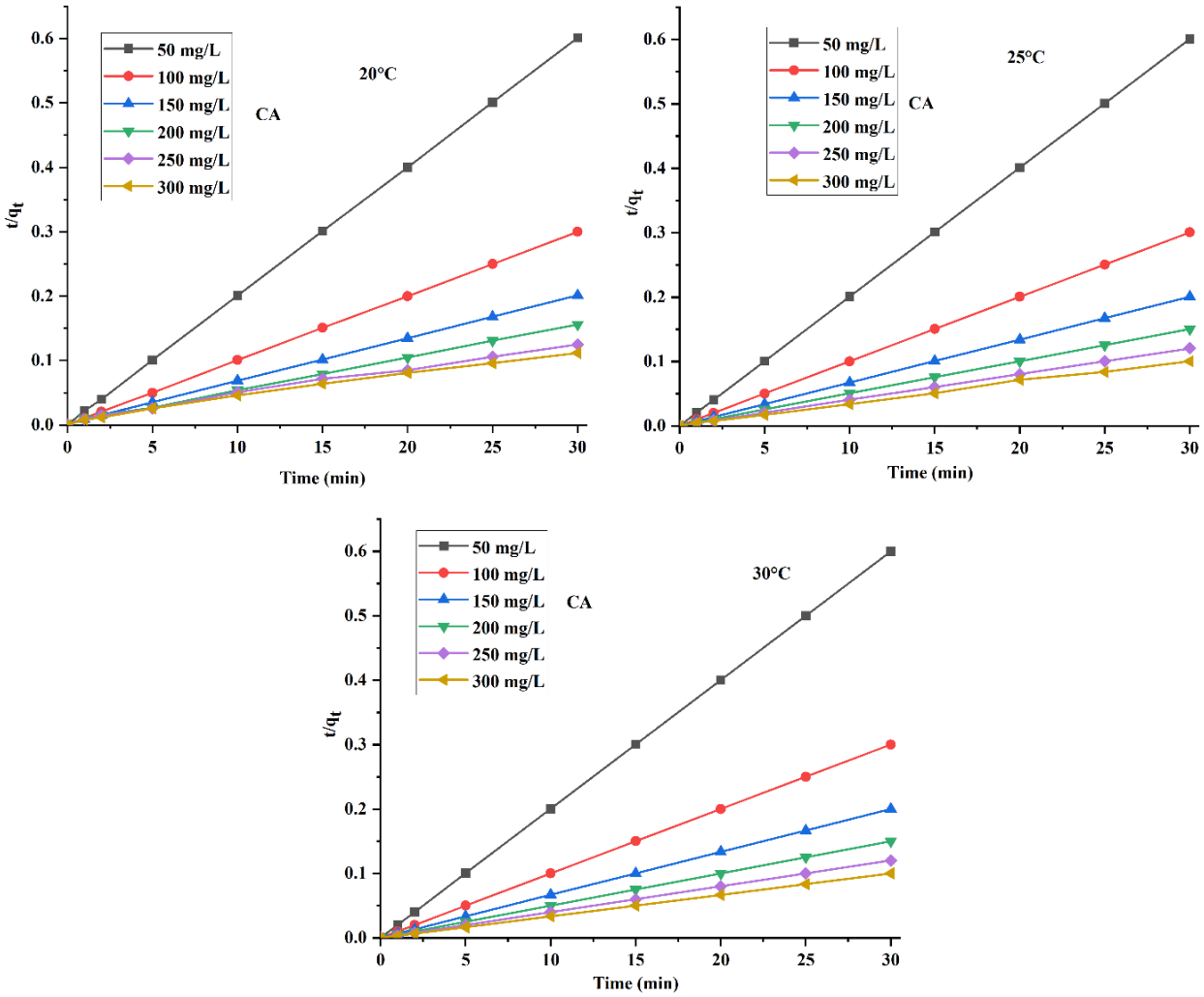

Figure 6.6 Kinetic second order plot of AG25 dye onto CA [50 -300 mg/L, pH = 7, 0.1 g, 30 min, T = 20°, 25°, 30°C).

Table 6.1 Calculated parameters for AG25 removal onto CA (First order)

C_o (mg/L)	$q_{e(exp)}$ (mg/g)	$q_{e(cal)}$ (mg/g)	K_1 (min^{-1})	R^2
		T=20°C		
50	49.9	7.83	0.328	0.656
100	99.7	16.0	0.242	0.824
150	149	49.6	0.240	0.933
200	191	80.4	0.191	0.860
250	239	172	0.155	0.927
300	267	174	0.114	0.952
		T=25°C		
50	49.9	3.23	0.232	0.525
100	99.8	7.67	0.263	0.636
150	150	22.4	0.209	0.800
200	199	34.6	0.226	0.857
250	249	43.7	0.205	0.831
300	298	114	0.247	0.918
		T=30°C		
50	50	1.81	0.215	0.401
100	99.9	3.86	0.240	0.475
150	150	5.90	0.254	0.512
200	200	6.89	0.213	0.573
250	250	9.49	0.248	0.491
300	299	11.4	0.223	0.604

Table 6.2 Calculated parameters for AG25 removal onto CA (Second order).

C_o (mg/L)	$q_{e(exp)}$ (mg/g)	$q_{e(cal)}$ (mg/g)	k_2 (g/mg min)	R^2
		T=20°C		
50	49.9	50	0.299	1.0
100	99.7	100	0.100	1.0
150	149	150	0.026	1.0
200	191	195	0.008	0.999
250	239	246	0.003	0.993
300	267	271	0.002	0.992
		T=25°C		
50	49.9	50.0	0.695	1
100	99.8	99.8	0.341	1
150	150	150	0.071	1.0
200	199	200	0.047	1.0
250	249	250	0.033	1.0
300	298	298	0.013	0.998
		T=30°C		
50	50	50	1.436	1
100	99.9	100	0.822	1
150	150	150	0.508	1
200	200	200	0.367	1
250	250	249	0.315	1
300	299	299	0.230	1

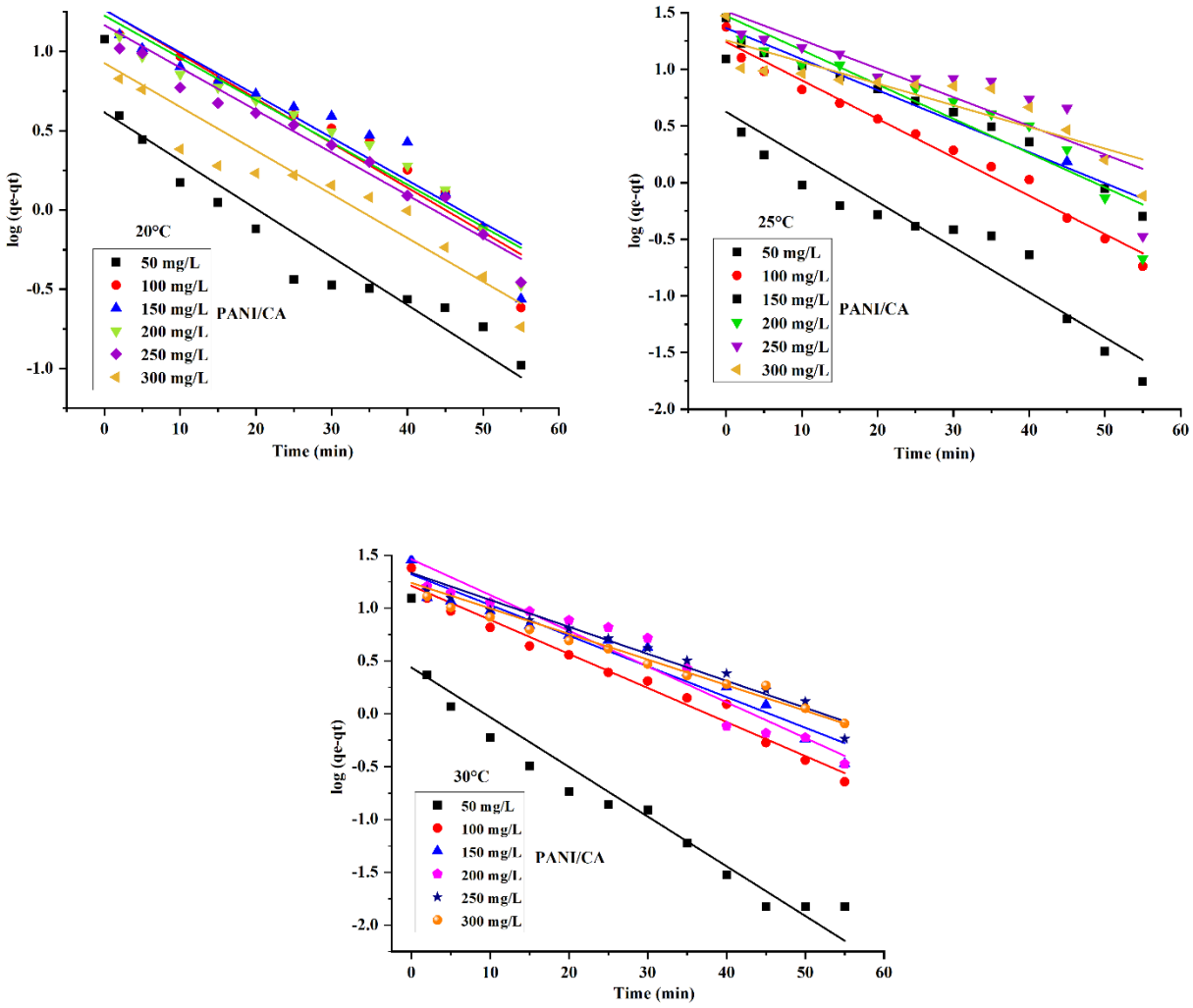

Figure 6.7 Kinetic pseudo first order plot of AG25 dye onto PANI/CA [50 -300 mg/L, pH = 7, 0.4 g, 60 min, T = 20°, 25°, 30°C).

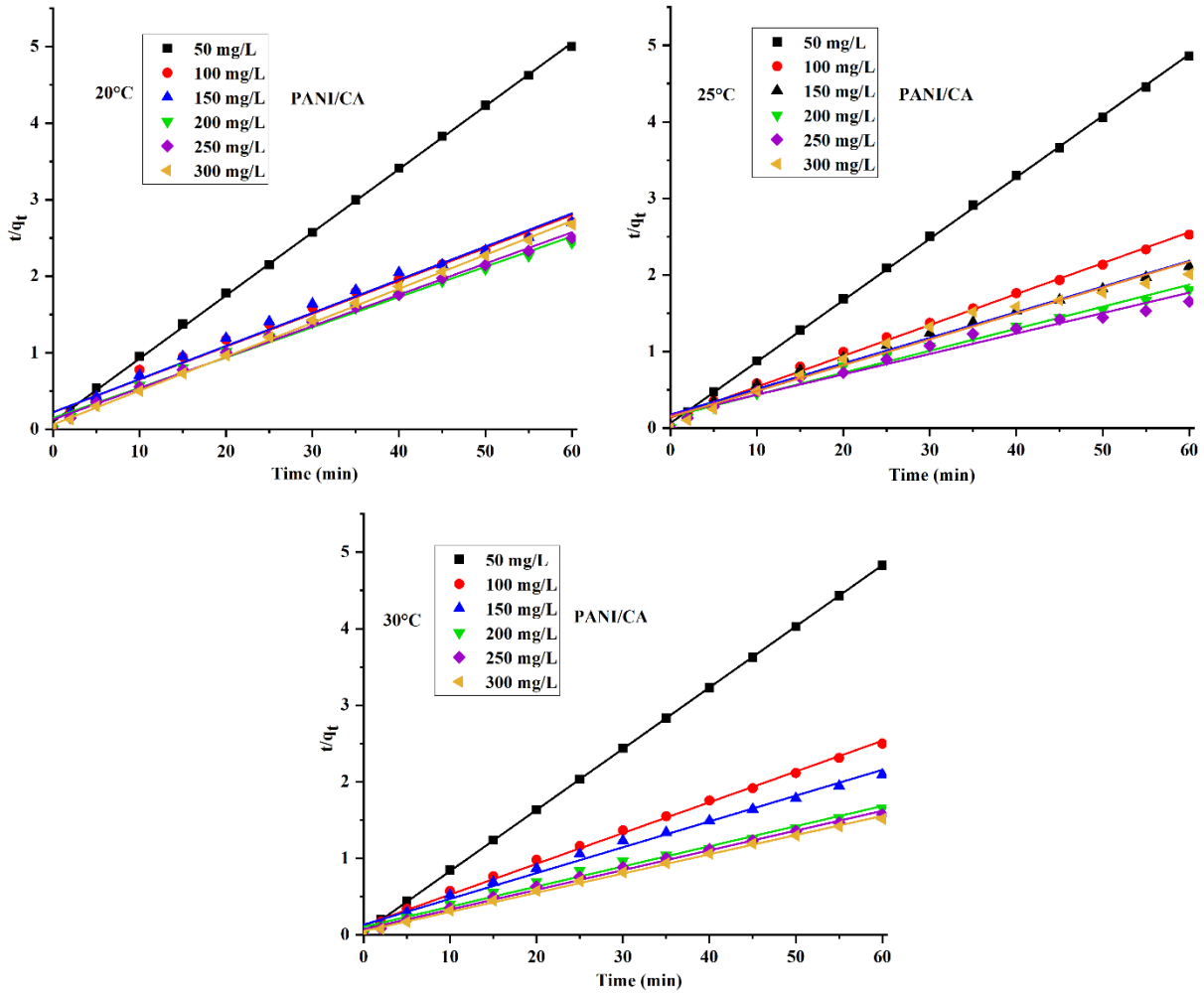

Figure 6.8 Kinetic pseudo second order plot of AG25 dye onto PANI/CA [50 -300 mg/L, pH = 7, 0.4 g, 60 min, T = 20°, 25°, 30°C).

Table 6.3 Calculated parameters for AG25 removal onto PANI/CA (First order).

C_o (mg/L)	$q_{e(exp)}$ (mg/g)	$q_{e(cal)}$ (mg/g)	K_1 (min^{-1})	R^2
		T=20°C		
50	12.0	4.13	0.070	0.889
100	22.2	18.4	0.065	0.936
150	22.2	18.3	0.062	0.912
200	24.6	16.8	0.061	0.943
250	24.0	14.7	0.062	0.956
300	22.4	8.44	0.063	0.877
		T=25°C		
50	12.4	4.22	0.092	0.901
100	23.8	14.5	0.078	0.981
150	28.4	23.2	0.063	0.973
200	33.2	29.8	0.070	0.881
250	36.3	32.6	0.059	0.789
300	29.9	18.0	0.044	0.783
		T=30°C		
50	12.4	2.75	0.107	0.897
100	24.0	16.3	0.074	0.976
150	28.6	20.9	0.067	0.948
200	36.3	29.0	0.078	0.938
250	38.2	21.5	0.059	0.945
300	39.6	17.4	0.056	0.925

Table 6.4 Calculated parameters for AG25 removal onto PANI/CA (Second order).

C_o (mg/L)	$q_{e(exp)}$ (mg/g)	$q_{e(cal)}$ (mg/g)	k_2 (g/mg min)	R^2
		T=20°C		
50	12.0	12.1	0.069	0.999
100	22.2	23.3	0.008	0.987
150	22.2	23.1	0.008	0.984
200	24.6	25.3	0.011	0.992
250	24.0	24.5	0.013	0.995
300	22.4	22.6	0.032	0.999
		T=25°C		
50	12.4	12.5	0.100	1
100	23.8	24.8	0.012	0.996
150	28.4	29.9	0.006	0.988
200	33.2	34.8	0.006	0.984
250	36.3	37.5	0.004	0.968
300	29.9	29.6	0.008	0.970
		T=30°C		
50	12.4	12.5	0.197	1
100	24.0	24.9	0.013	0.996
150	28.6	29.7	0.009	0.990
200	36.3	38.0	0.007	0.989
250	38.2	38.8	0.009	0.995
300	39.6	39.9	0.013	0.997

6.2.6 Isotherm study of AG25

The adsorption isotherm of AG25 onto CA and PANI/CA at 20°, 25°, and 30°C are presented in **Figures 6.9 and 6.10**. A detailed study was investigated to understand the adsorption mechanism

with three adsorption isotherms viz. Langmuir, Freundlich, and Temkin models **[5]**. These models can be used to describe the interaction between adsorbate AG25 and adsorbent CA and PANI/CA.

6.2.6.1 Langmuir model

Langmuir's model assumes that the surface of adsorption is homogeneous **[6]**. The equation for the Langmuir model is expressed by **[7, 8]:**

$$q_e = \frac{q_m K_L C_e}{1 + K_L C_e} \quad (5)$$

The equation is rewritten in the linear form **[8, 9]:**

$$\frac{C_e}{q_e} = \frac{C_e}{q_m} + \frac{1}{K_L q_m} \quad (6)$$

Where q_e represents AG25 adsorbed at equilibrium (mg/g)*;* q_m symbolizes the maximum adsorption capacity; C_e (mg/L) refers to the AG25 equilibrium concentration.; K_L represents Langmuir constant. With the linear curve of Ce/qe versus Ce, the q_m, as well as K_L values, were calculated. These calculated data are presented in **Tables 6.5 and 6.6.** Langmuir isotherm's important characteristics can be described by separation factor R_L **(Table 6.7),** and the equation for R_L is given below **[9, 10]**:

$$R_L = \frac{1}{1 + K_L C_o} \quad (7)$$

Where C_o (mg/g) is AG25 solution concentration, K_L symbolizes the Langmuir constant, and R_L values indicate the behavior of adsorption.

6.2.6.2 Freundlich model

Freundlich is an analytical model that applies to processes of adsorption taking place on heterogonous surfaces **[8]**. The equation for Freundlich model is expressed by **[5, 11-13]**:

$$q_e = K_F C_e^{\frac{1}{n}} \quad (8)$$

The linear form is expressed by equation **[5, 11-13]**:

$$\log q_e = \log K_F + \frac{1}{n} \log C_e \quad (9)$$

Where q_e is AG25 adsorbed at equilibrium (mg/g); C_e (mg/L) refers to AG25 equilibrium concentration, q_e (mg/g) is AG25 adsorbed at equilibrium; K_F (mg/g) and n represents Freundlich constants. K_F is related to adsorption efficiency, and *n* is related to adsorption strength. These constant's values have been determined from the plot of *log* q_e vs. *log* C_e. K_F is obtained from intercept and *1/n* from the slope. The adsorption system is unfavorable or favorable depending upon the n value. With temperature rise, the Freundlich constant increased, indicating that the phase is endothermic. The calculated data on CA and PANI/CA are shown in **Tables 6.5 and 6.6**. Freundlich model graphs are shown in **Figures 6.9b** and **6.10b.**

6.2.6.3 Temkin model

Temkin model indicates that the energy of adsorption decreases linearly as adsorbent and adsorbate (dye molecules) interact **[5]**. Temkin isotherm can be represented via linear Eq. 10 **[14-16]**:

$$q_e = \frac{RT}{b_T} \ln K_T + \left[\frac{RT}{b_T}\right] \ln C_e$$

$$q_e = B \ln K_T + B \ln C_e \quad (10)$$

Where, $B = \frac{RT}{b_T}$, b_T belongs to Temkin constant, K_T refers to the equilibrium binding constant, R (8.314 J/mol/K) stands by universal gas constant. T symbolizes the absolute temperature. B (J/mol) refers to adsorption heat. All constants were determined using the Temkin plot of q_e vs. lnC_e **(Figures 6.9c and 6.10c).**

Tables 6.5 and 6.6 show the constants attained from Langmuir, Freundlich, and Temkin equations for AG25 dye on CA and PANI/CA at different temperatures. The isotherm parameters for CA are exhibited in **Table 6.5**. The correlation coefficients (R^2) indicate that the adsorption behavior of AG25 on CA is satisfactorily described by Langmuir and Freundlich models and also shows that the surface has monolayer adsorption. The isotherm curves of AG25 on the CA adsorbent are presented in **Figure 6.9.** The Langmuir q_m *(calculated)* values increased from 251 to 518 mg/g for a temperature rise from 20^o to 30^{o}C, which shows the stronger bonding between AG25 dye and CA adsorbent and suggests that the reaction is endothermic for AG25 on CA. For CA, the K_L value is higher at 30^{o}C, which illustrates that the adsorption rate of AG25 is greater in CA at a higher temperature. Freundlich's constant K_F values increased from 107 to 390 L/g with an increase in temperature. The Freundlich constant *1/n* value lies between 0.25 and 0.69, and that implies the adsorption is favorable.

The adsorption on PANI/CA is adequately described by the Langmuir model for all temperatures with correlation coefficients of 0.998, 0.988, and 0.981, respectively. The isotherm curves for AG25 dye on PANI/CA are shown in **Figure 6.10,** and the summary of calculated parameters are given in **Table 6.6**. It can be seen that the K_L value for PANI/CA is more at 20^{o}C (lower temperature). The Langmuir parameter q_m *(calculated)* values increase from 24.4 to 38.8 mg/g

with a temperature rise. The q_m values of CA (518 mg/g) adsorbent were considerably higher than the PANI/CA (38.8 mg/g) adsorbent. Thus, CA is an efficient adsorbent for AG25 removal.

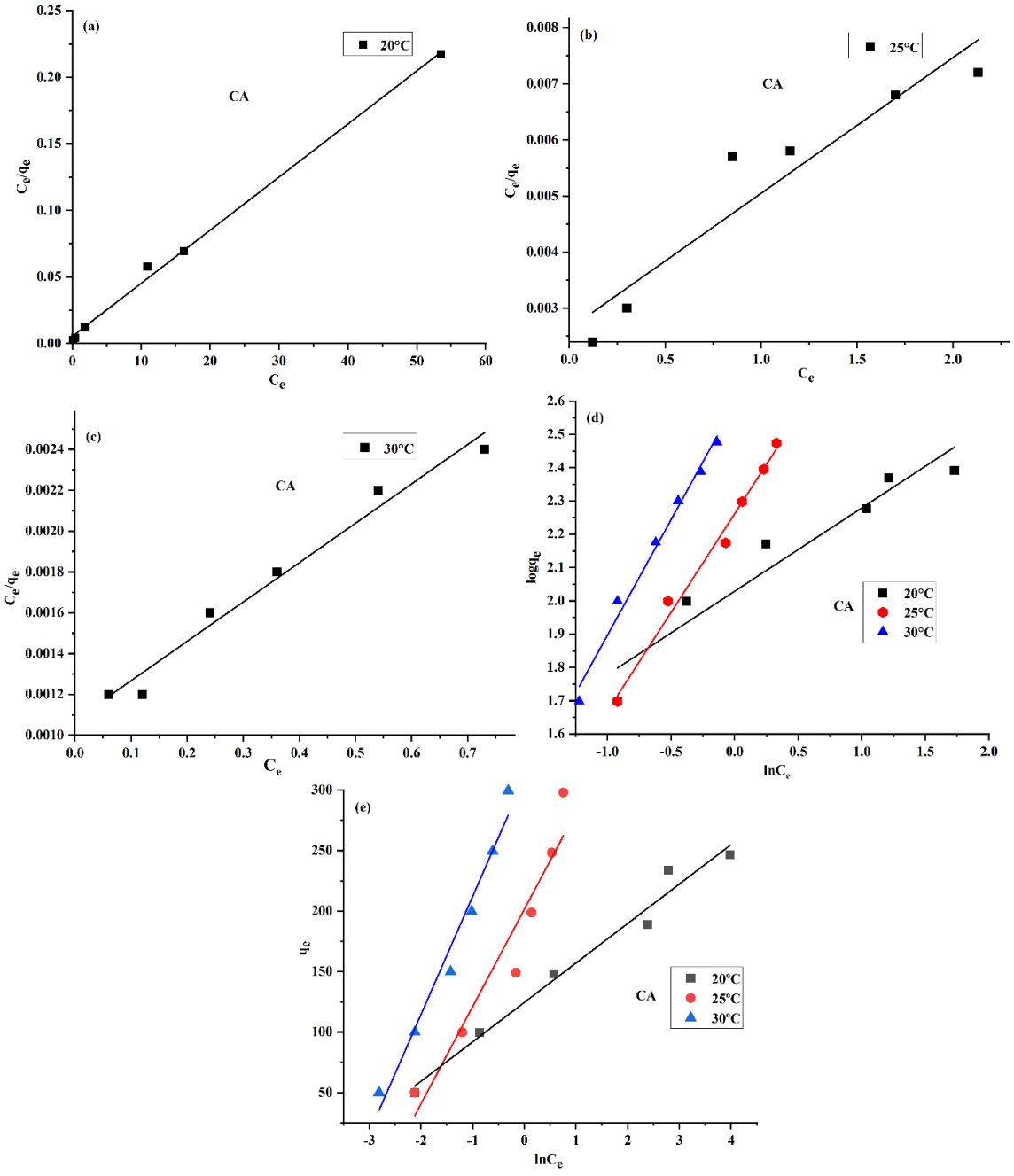

Figure 6.9 (a, b, c) Langmuir, (d) Freundlich and (e) Temkin plot of CA sample at 20°, 25° and 30°C.

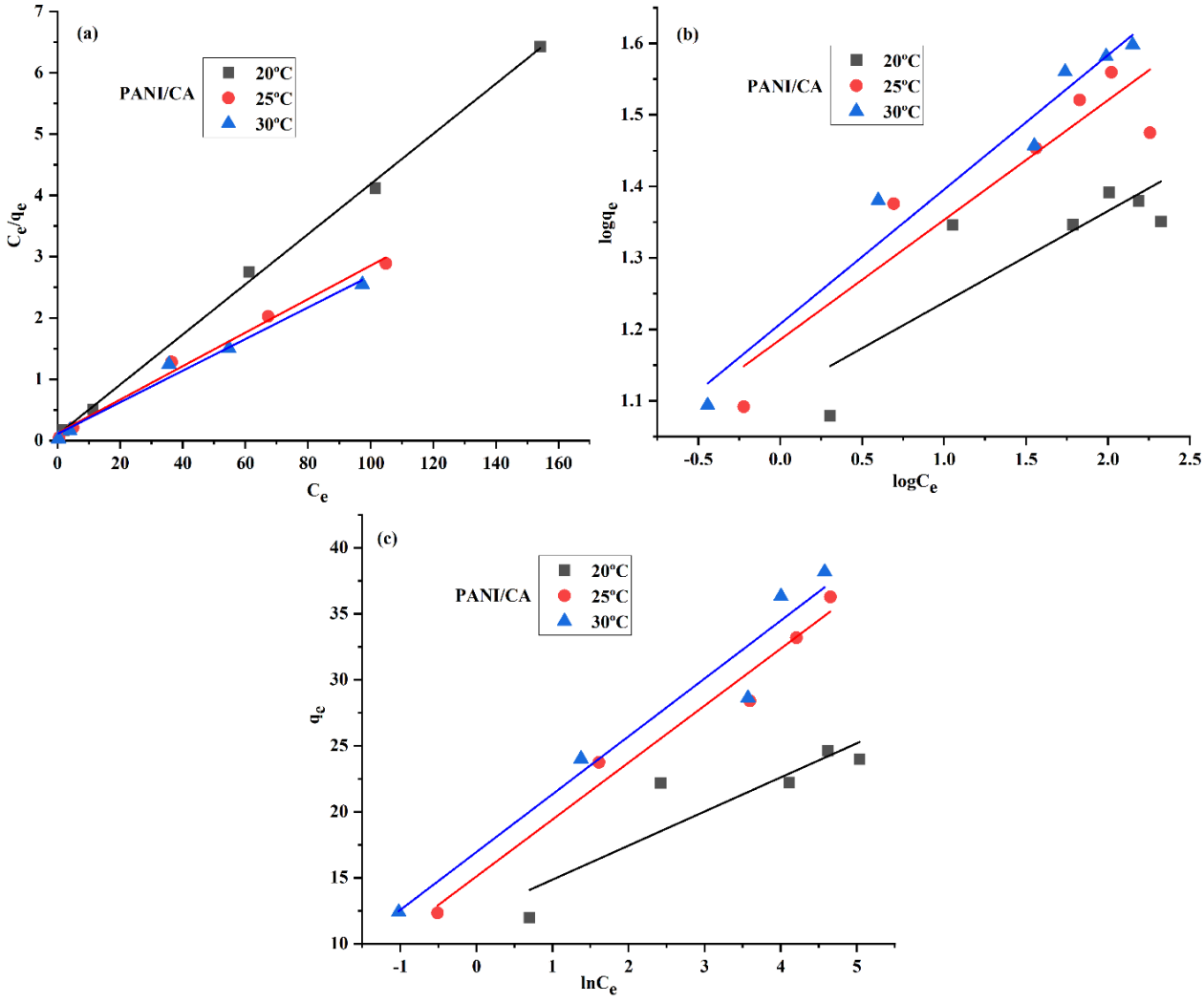

Figure 6.10 (a) Langmuir, (b) Freundlich and (c) Temkin plot of PANI/CA sample at 20°, 25° and 30°C.

Table 6.5 Isotherm study of CA

Langmuir isotherm			
T **(ºC)**	q_m **(mg/g)**	K_L **(L/mg)**	R^2
20	251	0.75	0.996
25	413	0.92	0.879
30	518	1.80	0.970
Freundlich isotherm			
T (ºC)	***1/n***	K_F **(L/g)**	R^2
20	0.25	107	0.903
25	0.59	183	0.985
30	0.69	390	0.983
Temkin isotherm			
T (ºC)	K_T	B_T	R^2
20	45.7	32.6	0.973
25	12.3	80.4	0.901
30	24.0	97.5	0.966

Table 6.6 Isotherm study of PANI/CA.

Langmuir isotherm			
T **(°C)**	q_m **(mg/g)**	K_L **(L/mg)**	R^2
20	24.4	0.42	0.998
25	36.6	0.23	0.988
30	38.8	0.24	0.981
Freundlich isotherm			
T (°C)	***1/n***	K_F **(L/g)**	R^2
20	0.15	12.4	0.716
25	0.20	14.8	0.937
30	0.19	16.1	0.940
Temkin isotherm			
T (°C)	K_T	B_T	R^2
20	116	2.58	0.749
25	33.2	4.31	0.965
30	47.9	4.38	0.933

Table 6.7 Different nature of R_L values

Process	**Unfavorable**	**Linear**	**Favorable**	**Irreversible**
R_L values	$R_L > 1$	$R_L = 1$	$0 < R_L < 1$	$R_L = 0$

6.3 Conclusion

It is concluded that the AG25 removal with CA adsorbent is very fast, it adsorbed more than 98 % dye in the initial one minute. CA removed more than 99 % dye at lower (50 mg/L) as well as higher (300 mg/L) AG25 concentrations. Surprisingly, the PANI/CA nanocomposites adsorbent is

less efficient with slower kinetics, possibly due to the blockage of CA pores with PANI. The kinetics of AG25 onto CA and PANI/CA follow the pseudo-second order model. The highest R^2 = 1 values have been obtained for CA adsorbent for all (50-300 mg/L) AG25 concentrations. The best description of the adsorption equilibrium for AG25 on CA was with two models: Langmuir and Freundlich. For PANI/CA, the data fit was best described by the Langmuir model.

References

[1] Mahmoodi N.M, Hayati B and Arami M. 2010. Textile dye removal from single and ternary systems using date stones: kinetic, isotherm, and thermodynamic studies. J Chem Eng Data. 55:4638–4649.

[2] Baseri J.R, Palanisamy P.N and Sivakumar P. 2012. Application of polyaniline nano composite for the adsorption of acid dye from aqueous solutions. E-J Chem. 9(3):1266-1275.

[3] Khairy M, Kamal R, Amin N.H, Mousa M.A. 2016. Kinetics and isotherm studies of Remazol Red adsorption onto polyaniline/ cerium oxide nanocomposites. J Bas & Environ Sci. 3:123 – 132.

[4] Gouthaman A, Azarudeen R.S, Gnanaprakasam A, Sivakumar V.M, Thirumarimurugan M. 2018. Polymeric nanocomposites for the removal of Acid red 52 dye from aqueous solutions: Synthesis, characterization, kinetic and isotherm studies. Ecotoxicol Environmen Saf. 160:42–51. https://doi.org/10.1016/j.ecoenv.2018.05.011.

[5] Li Z, Jia Z, Ni T, Li S (2017) Adsorption of methylene blue on natural cotton based flexible carbon fiber aerogels activated by novel air-limited carbonization method. J Mol Liq 242:747–756. doi: 10.1016/j.molliq.2017.07.06.

[6] Ren T, Han, Y, Zhang M, Zhang B, Gou X. 2014. Formation of carbon aerogels from glucose and as adsorbents for removal of methylene blue. J Mater Sci Res. 3:74-81. http://dx.doi.org/10.5539/jmsr.v3n2p74.

[7] Langmuir I. 1916. The constitution and fundamental properties of solids and liquids. J Am Chem. Soc. 38:2221–2295.

[8] Yu Z, Hu C, Dichiara A.B, Jiang W. and Gu J. 2020. Cellulose nanofibril/carbon nanomaterial hybrid aerogels for adsorption removal of cationic and anionic organic dyes, *Nanomaterials*, 10, 169. doi:10.3390/nano10010169.

[9] Cai X, Tan G, Deng Z, Liu J and Gui D (2019) Preparation of hierarchical porous carbon aerogels by microwave assisted sol-gel process for supercapacitors Polym 11:429. doi:10.3390/polym11030429.

[10] Ayawei N, Ebelegi A.N, Wankasi D. 2017. Modelling and interpretation of adsorption isotherms. J Chem. Volume Article ID 3039817:11 pages. https://doi.org/10.1155/2017/3039817.

[11] Weber T.W. and Chakravorti R.K. 1974. Pore and solid diffusion models for fixed-bed adsorbers. AlChE J. 20:228.

[12] Freundlich H.M.F. 1906. Over the adsorption in solution. J Phys Chem. 57:385–471.

[13] Foo K.Y, Hameed B.H. 2010. Insights into the modeling of adsorption isotherm systems. Chem Eng J. 156:2–10. doi:10.1016/j.cej.2009.09.013.

[14] Nounou M.N, Nounou H.N. 2010. Multiscale estimation of the Freundlich adsorption isotherm. Int J Environ Sci Tech. 7:509-518.

[15] Tempkin M.I, Pyzhev V. 1940. Kinetics of ammonia synthesis on promoted iron catalysts. Acta Physiochim. URSS. 12:217–222.

[16] Dada A.O, Olalekan A.P, Olatunya A.M, Dada O. 2012. Langmuir, Freundlich, Temkin and Dubinin–Radushkevich isotherms studies of equilibrium sorption of Zn^{2+} unto phosphoric acid modified rice husk. J Appl Chem. 3:38-45.

.

CHAPTER 7

ADSORPTION OF METHYLENE BLUE DYE ON POLYANILINE AND POLYANILINE/MONTMORILLONITE ADSORBENT

This chapter deals with the adsorption of Methylene blue (MB) dye using polyaniline (PANI) and polyaniline/montmorillonite clay (PANI/MMT) nanocomposites as an adsorbent. The adsorption was investigated using different parameters. Methylene blue dye adsorption behavior on polyaniline and polyaniline/montmorillonite clay nanocomposite adsorbents was investigated using isotherm and kinetic experiments.

7.1 Adsorption study

7.1.1 Preparation of the stock solution and finding the maximum wavelength of Methylene blue (MB) dye

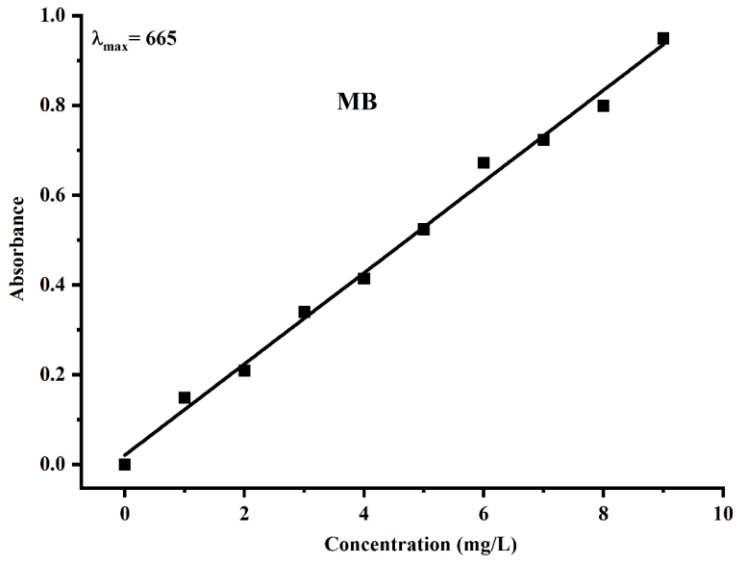

Figure 7.1 Calibration curve of Methylene blue dye

One gram of MB was diluted in one liter of distilled water to make a stock solution. The calibration curve determined the maximum wavelength of 665 nm by varying the dye concentration from 1 to 9 mg/L. The calibration curve is presented in **Figure 7.1.**

7.1.2 Batch adsorption

Methylene blue dye adsorption investigation was performed with an incubator shaker in a batch manner. Different concentrations of dye solution (20-200 mg/L) were prepared by diluting the stock solution. Different parameters were optimized, such as pH effect, effect of concentration of MB dye, adsorbent amount, time, and temperature. Removal percentage of adsorbate from the solution was measured using UV-Vis spectrophotometer by finding out the concentration of the solution. The removal efficiency of Methylene blue dye was measured by the equation.

$$\%\ \boldsymbol{Removal} = \frac{\boldsymbol{C_o - C_e}}{\boldsymbol{C_o}} \times \mathbf{100} \qquad (1)$$

Where, C_e (mg/L) = equilibrium concentration of the dye (MB), C_o (mg/L) = initial MB dye concentration.

7.2 Results and discussion

The adsorption study yielded a promising result. The pH, dye concentration, contact time, temperature and adsorbent dose have all parameters been investigated and are discussed below. Kinetic and isotherm studies were done with the MB dye solution of concentration 80 to 150 mg/L at different temperatures, i.e., 20^o, $30^{o,}$ and 40^oC.

7.2.1 Effect of adsorbent amount

Figure 7.2 shows the data for adsorbent dose effect. The adsorption efficiency of PANI and PANI/MMT for MB dye was identified with 50 mg/L of dye solution and the adsorbent amount was varied from 0.1 to 0.5 g. The entire study was conducted at 30^{o}C with 100 ml of MB dye solution at pH = 7. As shown in **Figure 7.2**, the removal of MB dye increases with an increasing dose of adsorbent from 0.1 g to 0.5 g. About 81.15 % of MB dye was removed with 0.1 g of PANI amount, which increased to 88.65 % for an adsorbent dose of 0.5 g. The reason for this is that the adsorbent has more active sites, which can interact with the MB dye. The adsorption results of PANI/MMT nanocomposites showed that the MB dye could be removed. The removal capacity of PANI/MMT as an adsorbent was very high; even at 0.1 g of adsorbent dose, the removal was 99.65 %. At a dose of 0.3 g, complete removal of the dye was achieved. Further adsorption studies were conducted using a 0.3 g of adsorbent dose.

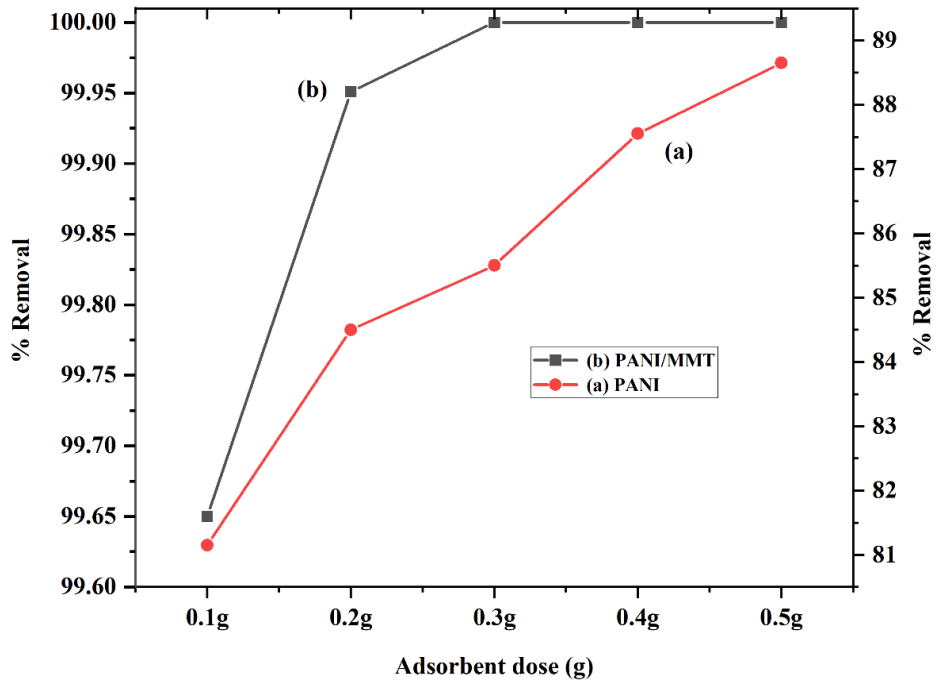

Figure 7.2 Study of the effect of PANI and PANI/MMT dose on the removal of MB dye (20 mg/L, 0-30 min, pH = 7, T = 30^{o}C)

7.2.2. Effect of pH

The most significant factor within the adsorption system is pH. The pH study for Methylene blue was conducted in the pH range of 2 to 10 (2, 4, 6, 7, 8, and 10) at 30^{o}C with a 0.3 g of adsorbent and a dye solution of 20 mg/L. The adjustment of the pH was made by the addition of 1M HCl and 1M NaOH solutions. The maximum removal of MB dye onto PANI (97.85 %) was at pH 10, and the minimum was found at pH 2 (54 %), after 30 min of contact time. Thus, the percentage adsorption of MB dye onto PANI increases as the MB dye solution pH rises. On other side, PANI/MMT nanocomposite adsorbent achieves 100 % removal at pH 7. This is illustrated in **Figure 7.3**. Therefore for further study, pH 7 was selected for PANI/MMT adsorbent, and pH 10 was selected for PANI adsorbent. The graph for the effect of pH is shown in **Figure 7.3.**

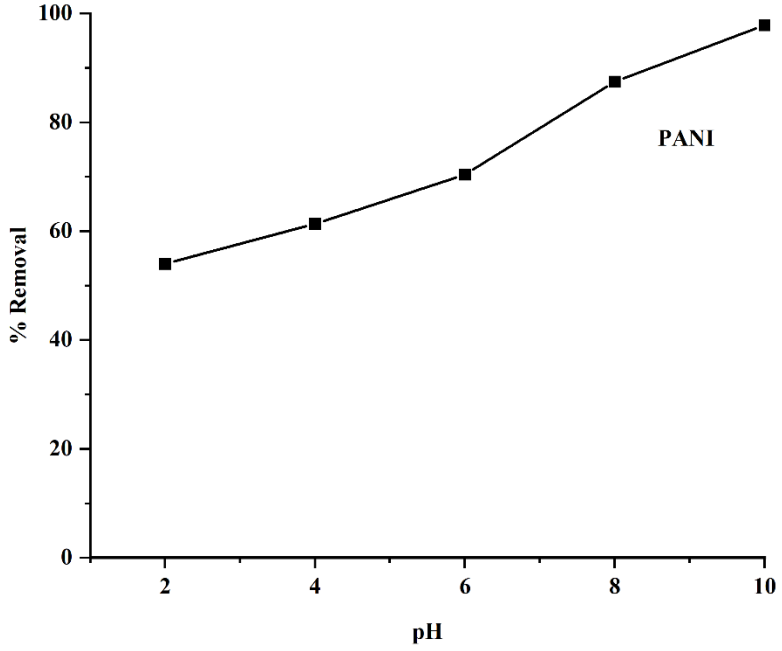

Figure 7.3 Effect of pH on adsorption by PANI (20 mg/L, 0.3 g, 30^{o}C, 0-30 min)

7.2.3 Effect of initial dye concentration and contact time

Different concentrations of MB dye solution (20-150 mg/L) were taken in a conical flask with 0.3 g of PANI and PANI/MMT adsorbents, and the adsorption study was carried out at 30^{o}C in an incubator shaker, at 180 rpm speed. The effect of different dye concentrations and contact times for Methylene blue dye adsorption by PANI and PANI/MMT is shown in **Figure 7.4**.

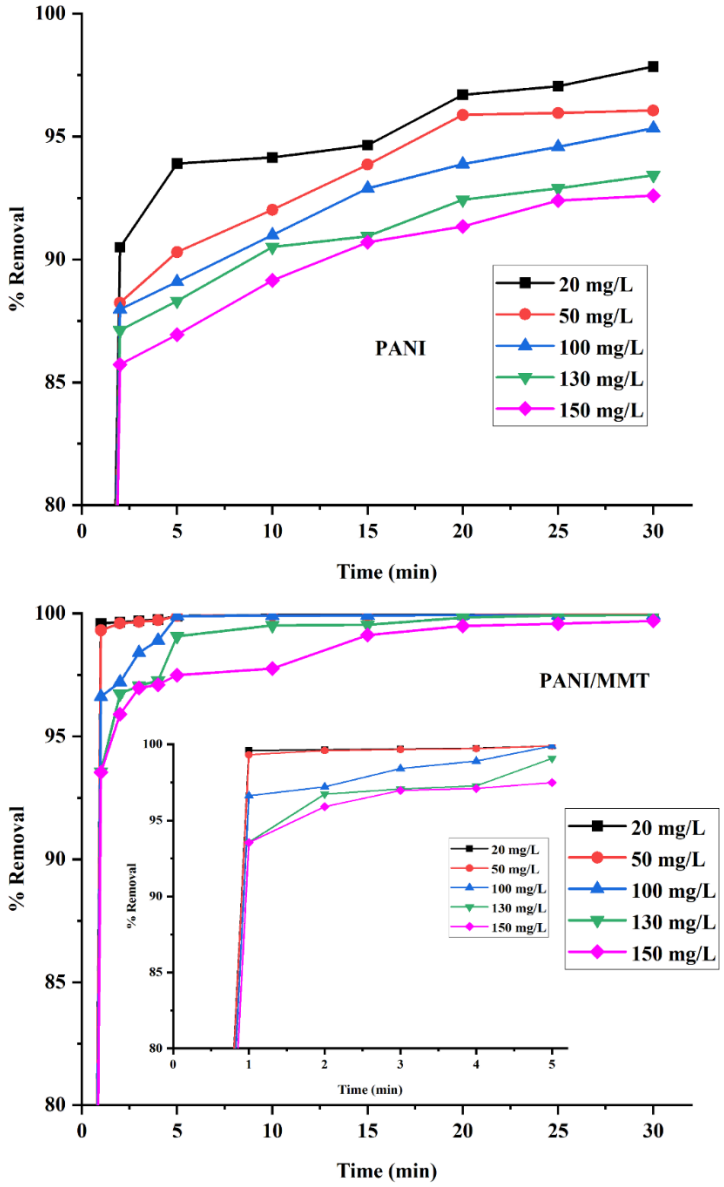

Figure 7.4 Effect of contact period and initial dye concentration on MB adsorption using PANI and PANI/MMT (20-150 mg/L, pH 7, 0-30 min, T = 30^{o}C)

PANI/MMT was efficient to effect a 99.32 % reduction of 50 mg/L of dye within a time of one minute. The MB dye uptake was found to be higher at lower dye concentrations. The higher concentration dye solutions take relatively more time (5 min) to reach more than 99 % removal. PANI results show that 97.85 % (20 mg/L) and 96.06 % (50 mg/L) of dye were removed from the solution in 30 min.

7.2.4 Effect of temperature

The temperature study effect for MB dye elimination was performed at 20^{o}C, 30^{o}C, 40^{o}C, and 50^{o}C with a 50 mg/L of dye concentration using PANI and PANI/MMT nanocomposite adsorbents. The results are represented in **Figure 7.5.**

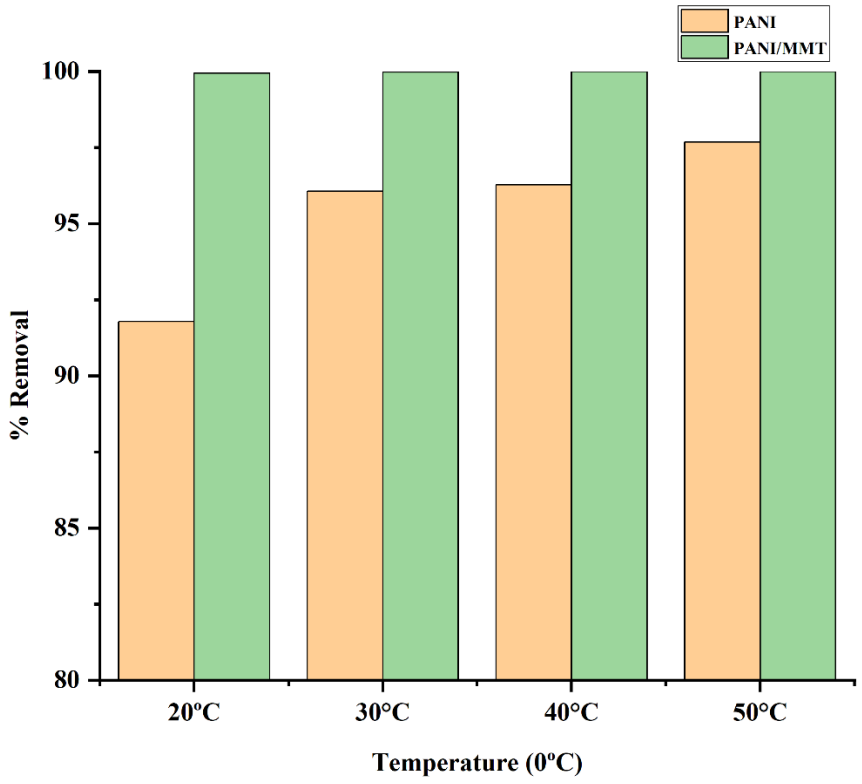

Figure 7.5 Temperature effect on MB removal using PANI and PANI/MMT (50 mg/L, 0-30 min, 0.3 g, and 20-50^{o}C)

The highest percentage removal by PANI/MMT was 99.94 % at 20^{o}C, 99.98 % at 30^{o}C, and 100 % at 40^{o}C and 50^{o}C, respectively. The percentage of adsorption by PANI/MMT was more than 99 % within 1 min for all the temperatures studied. Thus, the results show that temperature has no significant effect on MB dye adsorption by PANI/MMT. However, pure PANI removal increases from 91.78 % to 97.68 % (30 min) with a rise in solution temperature. The adsorption efficiency, therefore greatly depends upon temperature.

7.2.5 Kinetic study of Methylene blue dye

Kinetic study of Methylene blue by PANI and PANI/MMT was investigated with an adsorbent dose of 0.3 g, dye concentration of 80-150 mg/L, a contact time of 30 min, and temperature of 20-40^{o}C. For the kinetic study, the experimental data of MB dye was analyzed with two different kinetic models (pseudo 1st and 2nd order models). The adsorption mechanism was identified using these models. The results of the kinetic study are illustrated in **Tables 7.1 and 7.2** The equations for the kinetic models are given below:

The linear equations for pseudo 1st and pseudo 2nd order models are represented by equation 2 and 3 **[1-3]:**

$$\log(q_{e-}\ q_t) = log q_e\ -\ \frac{k_1}{2.303}t \qquad (2)$$

$$\frac{t}{q_t} = \frac{1}{k_2 q_{e^2}} + \frac{t}{q_e} \qquad (3)$$

where, q_e (mg/g) and q_t (mg/g) symbolize the amount of Methylene blue dye adsorbed at equilibrium and at a time (min) t, respectively. k_1 (min^{-1}) refers to rate constant of pseudo 1st order and k_2 (min^{-1}) refers to rate constant of pseudo 2nd order.

The values of 1st order rate constant k_1 and q_e were calculated from the intercept and slope of the plot log ($q_e - q_t$) versus t. The values of 2nd order rate constant k_2 and q_e were obtained by a plot of t/q_t against t. It has been observed that pseudo 2nd model gives the best adsorption fitting data. **Tables 7.1 and 7.2** lists the rate constants as well as the corresponding regression coefficients. The linearity $R^2 = 1$ and >0.99 were obtained with a pseudo 2nd order model, which gives the best curve fitting plot for both adsorbents.

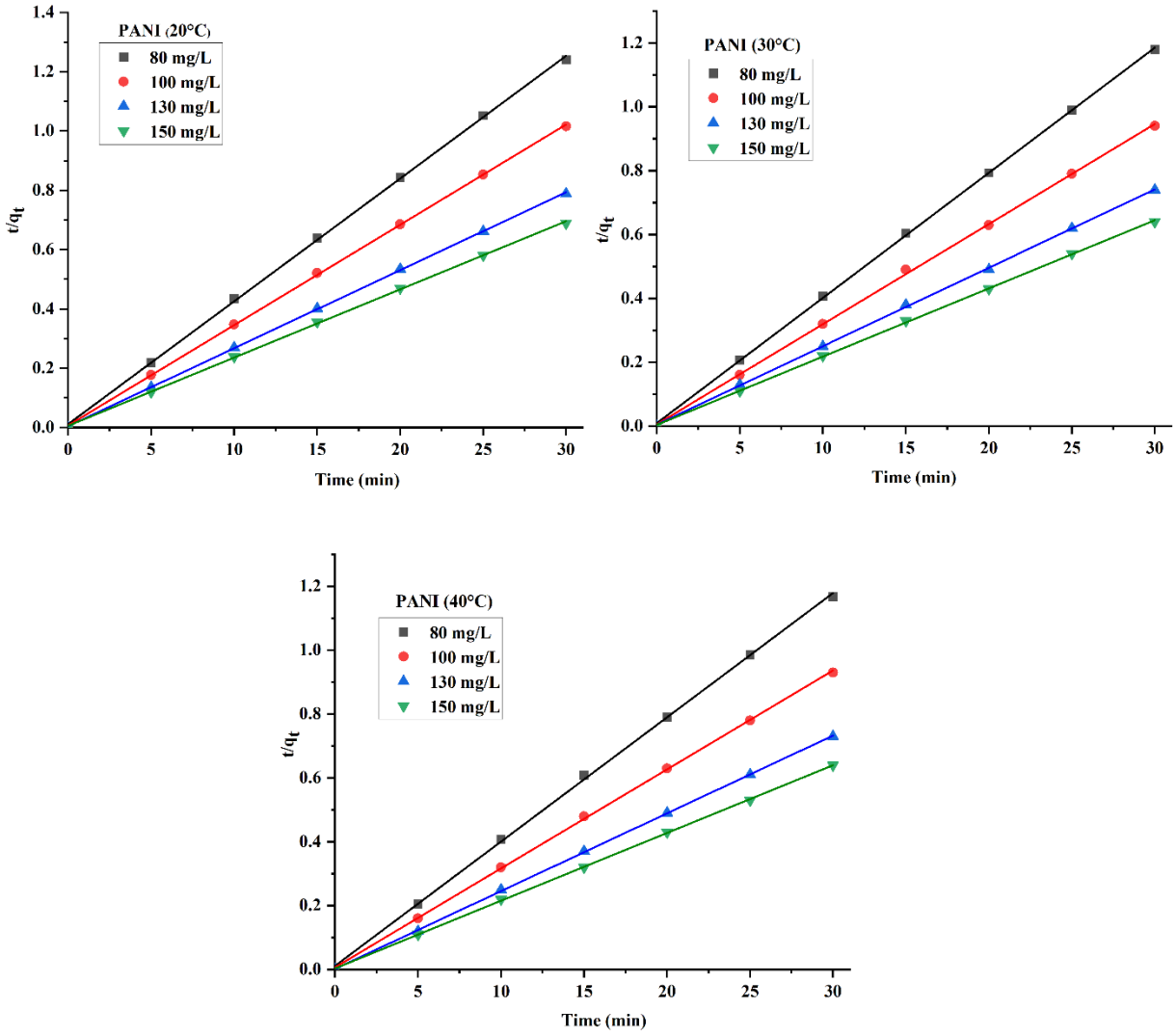

Figure 7.6 Adsorption kinetic study for methylene blue by PANI (T = 20°C, 30°C, and 40°C, pH 10, t = 30 min)

Figures 7.6 and 7.7 represent the kinetic plots of pseudo 2nd order for PANI and PANI/MMT adsorbents. The graphs were plotted between *t/qt* vs. *t* at three different temperatures (20°, 30°, 40°C). When the MB concentration is increased from 80 to 150 mg/L, the values of $q_{e,\ cal}$ (calculated) increase. Also, $q_{e,cal}$ (calculated) values are very similar to $q_{e,exp}$ (experimental) values.

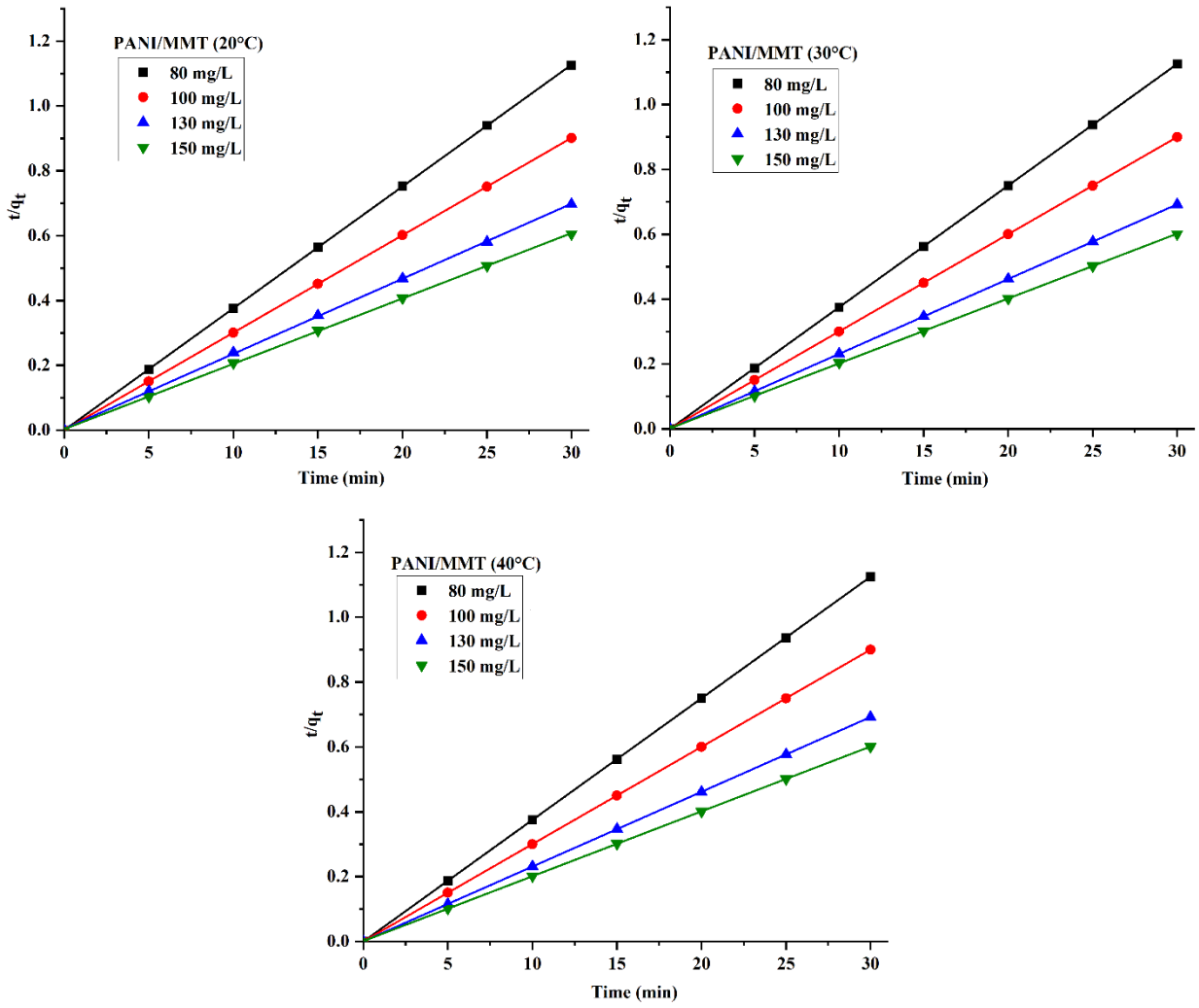

Figure 7.7: Adsorption kinetic study for methylene blue by PANI/MMT (T = 20°C, 30°C, and 40°C, pH 7, t = 30 min)

Table 7.1 Kinetic data of MB onto PANI

PANI				
Kinetic study at 20^{o}C				
C_0 **(mg/L)**	80	100	130	150
$q_{e(exp)}$ **(mg/g)**	24.24	29.52	38.01	43.49
$q_{e(cal)}$ **(mg/g)**	24.31	29.55	38.00	43.47
k_2 **(g/mg min)**	0.170	0.169	0.162	0.092
R^2	0.99967	0.9998	0.99984	0.99956
Kinetic study at 30^{o}C				
C_0 **(mg/L)**	80	100	130	150
$q_{e(exp)}$ **(mg/g)**	25.44	31.78	40.49	46.3
$q_{e(cal)}$ **(mg/g)**	25.52	31.88	40.7	46.81
k_2 **(g/mg min)**	0.168	0.183	0.140	0.116
R^2	0.99977	0.99951	0.99968	0.99969
Kinetic study at 40^{o}C				
C_0 **(mg/L)**	80	100	130	150
$q_{e(exp)}$ **(mg/g)**	25.68	31.99	40.9	46.84
$q_{e(cal)}$ **(mg/g)**	25.69	32.25	41.05	47.14
k_2 **(g/mg min)**	0.142	0.149	0.331	0.140
R^2	0.99951	0.99967	0.99985	0.9998

Table 7.2 Kinetic data of MB onto PANI/MMT

PANI/MMT				
Kinetic study at 20°C				
C_o **(mg/L)**	80	100	130	150
$q_{e(exp)}$ **(mg/g)**	26.62	33.26	43.02	49.89
$q_{e(cal)}$ **(mg/g)**	26.62	33.30	43.19	49.97
k_2 **(g/mg min)**	4.03	1.27	0.128	0.117
R^2	1	1	0.99984	0.99984
Kinetic study at 30°C				
C_o **(mg/L)**	80	100	130	150
$q_{e(exp)}$ **(mg/g)**	26.65	33.32	43.30	49.85
$q_{e(cal)}$ **(mg/g)**	26.65	34.34	43.36	49.97
k_2 **(g/mg min)**	5.02	2.57	1.156	0.228
R^2	1	1	1	0.99996
Kinetic study at 40°C				
C_o **(mg/L)**	80	100	130	150
$q_{e(exp)}$ **(mg/g)**	26.66	33.33	43.31	49.89
$q_{e(cal)}$ **(mg/g)**	26.66	34.34	43.36	50.00
k_2 **(g/mg min)**	6.69	2.57	1.26	0.310
R^2	1	1	1	0.99999

7.2.6 Isotherm study

Isotherm study was performed on 50-150 mg/L MB dye solution at 20°, 30°, and 40°C. The study was done by adding 0.3 g of PANI and PANI/MMT adsorbent into 100 ml of MB dye solution. Three well-known models: Langmuir, Freundlich, and Temkin have been investigated on MB dye

adsorption by PANI and PANI/MMT adsorbents. The calculated parameters of all three models are summarized in **Tables 7.3 and 7.4**.

In the Langmuir model, monolayer adsorption takes place on the adsorbent's surface **[4].** Langmuir isotherm equation is written as follows **[5]**:

$$\frac{C_e}{q_e} = \frac{C_e}{q_{max}} + \frac{1}{q_{max}\, k_L} \qquad (4)$$

where C_e (mg/L) is the MB dye equilibrium concentration. q_e (mg/g) is the amount of MB dye adsorbed at equilibrium. k_L belongs to Langmuir constant. q_{max} represents maximum adsorption capacity. **Figure 7.8** shows the linear plot of the Langmuir model for MB dye removal that was obtained by plotting the graph between C_e/q_e versus C_e. The parameters q_{max} and K_L are calculated from the intercept and the slope **(Tables 7.3 and 7.4).**

In the Freundlich model, multilayer adsorption takes place on the adsorbent's surface **[6].** Freundlich isotherm equation is written as follows **[5]**:

$$lnq_e = \ln K_F + \frac{1}{n} lnC_e \qquad (5)$$

Where K_F represents the Freundlich constant which indicates the adhesion of Methylene blue dye to the PANI and PANI/MMT nanocomposite adsorbents, another parameter *1/n* represents the heterogeneity factor. And, *1/n* values provide information about the adsorption system whether it is unfavorable (*1/n* > 1) or favorable (*1/n* < 1) **[7]**. As listed in **Tables 7.3 and 7.4,** K_F and *1/n* values were calculated via drawing *log* q_e vs. *log* C_e plots. R^2 values were also obtained from the linear plot.

The Temkin model focuses on adsorbent-adsorbent interactions. Temkin equation is defined as following **[7]**:

$$q_e = B_T \, lnK_T + B_T \, lnC_e \qquad \textbf{(6)}$$

$$B_T = \frac{RT}{b}$$

Where B_T stands the Temkin constant, K_T is represented as an equilibrium binding constant. *T (K)* and *R* (8.314 J/mol K) are the absolute temperatures and universal gas constant. Temkin constant refers to *b*. All the Temkin variable values are determined from the q_e vs. *ln* C_e (linear plot) plot. Tables 7.3 and 7.4 include the values of Temkin for both adsorbents.

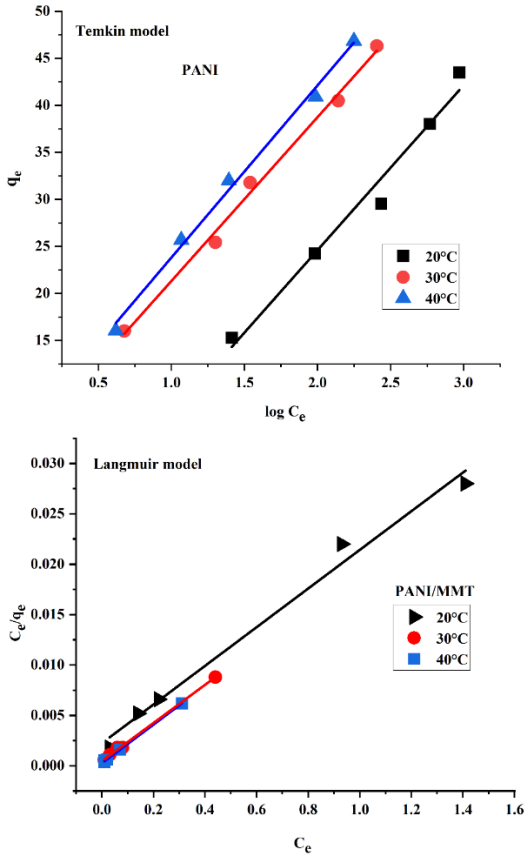

Figure 7.8 Langmuir and Temkin isotherm models of MB dye by PANI and PANI/MMT adsorbents.

According to calculated R^2 values, Langmuir model was found to be the best-fit model for MB dye adsorption by PANI/MMT nanocomposites. This implies that the dominant mechanism of dye adsorption of MB by PANI/MMT monolayer. Since the clay layers are nano-disperse, this would explain these results. However, the K_L and R^2 (0.98381-0.99852) values increase with temperature. The results of the PANI adsorbent show that the Temkin model is found to be the best-suited isotherm for MB dye adsorption and the obtained values of K_T and R^2 (0.96807 – 0.99324) increases with temperature from 20^o to 40^{o}C. **Figure 7.8** shows the best fit model of MB dye by PANI (Temkin model) and PANI/MMT (Langmuir model) adsorbent at 20^o, 30^{o,} and 40^{o}C.

Table 7.3 Isotherm data of MB dye onto PANI

PANI			
Langmuir Isotherm			
***T* (^{o}C)**	***q_m* (mg/g)**	***K_L* (L/mg)**	***R^2***
20	82.03	0.054	0.94828
30	75.93	0.140	0.98458
40	79.23	0.153	0.95981
Freundlich Isotherm			
***T* (^{o}C)**	***1/n***	***K_F* (mg/g)**	***R^2***
20	0.65209	2.21	0.98853
30	0.60257	2.87	0.96662
40	0.62148	2.96	0.94007
Temkin Isotherm			
***T* (^{o}C)**	***K_T* (L/mg)**	***B_T***	***R^2***
20	0.0181	17.53	0.96807
30	0.0125	17.41	0.99230
40	0.0135	18.29	0.99324

Table 7.4 Isotherm data of MB dye onto PANI/MMT

PANI/MMT			
Langmuir Isotherm			
***T* (°C)**	***q_m* (mg/g)**	***K_L* (L/mg)**	***R^2***
20	52.13	8.525	0.98381
30	52.85	40.25	0.99764
40	52.22	73.65	0.99852
Freundlich Isotherm			
T (°C)	***1/n***	***K_F* (mg/g)**	***R^2***
20	0.27714	5.26	0.97635
30	0.18549	5.87	0.78030
40	0.25389	6.51	0.66632
Temkin Isotherm			
T (°C)	***K_T* (L/mg)**	***B_T***	***R^2***
20	2.12	8.43	0.97811
30	7.38	9.06	0.90100
40	17.9	8.30	0.82897

7.3 Conclusion

PANI and PANI/MMT samples were synthesized and studied for their efficiency for Methylene blue adsorption. The ability of PANI and PANI/MMT adsorbents for Methylene dye removal was evaluated under different conditions, namely, effect of adsorbent, pH, time, temperature, and concentration of dye. The deduction of methylene blue was more than 99 % (pH = 7) in one min by PANI/MMT adsorbent. This rate was less for pure PANI adsorbent. PANI removed 97.85 % (pH = 10) in 30 min at 30°C. For MB dye removal by PANI, the best fit was achieved with the Temkin model, and for PANI/MMT, the best fit was obtained with the Langmuir model. The pseudo second order kinetic model accurately described the kinetics of methylene blue by PANI

and PANI/MMT. Removal uptake of PANI/MMT adsorbent was higher than PANI adsorbent. Therefore, the results proved that PANI/MMT is a better adsorbent than pure PANI. Thus, because of its outstanding removal capacity, PANI/MMT can be effectively used for textile wastewater treatment. This adsorbent is much more efficient for the deduction of Methylene blue dye and significantly takes less time for complete (>99 %) dye removal. **The dye removal by the prepared PANI/MMT adsorbent is faster by a factor of at least 20 than the earlier reported studies in the literature.** The PANI/MMT nanocomposite adsorbent eliminated almost 100 % dye in a very short time. Faster adsorption would result in the design of a high volume (scale-up) and a lower cost, continuous wastewater treatment adsorption system. The potential of PANI/MMT adsorbent is very high for wastewater treatment on a bigger scale. The adsorbent PANI/MMT and the synthesis processing technique used may be considered to be at the forefront of the development of adsorbents for wastewater treatment.

References

[1] Salem MA, Elsharkawy RG, Hablas MF (2016) Adsorption of brilliant green dye by polyaniline/silver nanocomposite: Kinetic, equilibrium, and thermodynamic studies. Eur Polym J 75:577–590.

[2] Lach J, Ociepa-Kubicka A (2017) The removal of chloramphenicol from water through adsorption on activated carbon. E3S Web of Conferences 19:02008. DOI: 10.1051/e3sconf/20171902008.

[3] Budnyak T.M, Aminzadeh S, Pylypchuk I.V, Sternik D, Tertykh V.A, Lindstrom M.E, Sevastyanova O (2018) Methylene blue dye sorption by hybrid materials from technical lignins, J Environ Chem Eng. https://doi.org/10.1016/j.jece.2018.07.041.

[4] Mouni L, Belkhiri L, Bollinger J-C, Bouzaza A, Aymen Assadi A, Tirri A, Dahmoune F, Madani K, Remini H (2018) Removal of Methylene Blue from aqueous solutions by adsorption on Kaolin: Kinetic and equilibrium studies. Appl Clay Sci153:38–45.

[5] He Y, Jiang DB, Chen J, Jiang DY, Zhang YX (2018) Synthesis of MnO_2 nanosheets on montmorillonite for oxidative degradation and adsorption of methylene blue. J Colloid Interface Sci 510:207–220. https://doi.org/10.1016/j.jcis.2017.09.066.

[6] Pawar RP, Lalhmunsiama, Gupta P, Sawant SY, Shahmoradi B, Lee S-M (2018) Porous synthetic hectorite clay-alginate composite beads for effective adsorption of methylene blue dye from aqueous solution. Int J Biol Macromol 114:1315–1324.

[7] Tanzifi M, Yaraki MT, Karami M, Karimi S, Kiadehi AD, Karimipour K, Wang S (2018) Modelling of dye adsorption from aqueous solution on polyaniline/carboxymethyl cellulose/TiO2 nanocomposites. J Colloid Interface Sci 519:154–173.

CHAPTER 8

ADSORPTION STUDY OF PANI/MMT NANOCOMPOSITES PREPARED BY VARYING MONOMER TO OXIDANT RATIO

This chapter covers the synthesis and adsorption study comparison of different monomer/oxidant ratios (1:1, 2:1, 4:1) nanocomposites. In this study, PANI/MMT nanocomposites were prepared by varying monomer/oxidant ratio, via the *in-situ* polymerization method. The effect of different monomer/oxidant ratio nanocomposites for the adsorption of AG25 dye (anionic dye) was studied. These studies have been performed to find out the best monomer/oxidant ratio nanocomposites for the removal of AG25 dye.

8.1 Synthesis of 1:1 monomer/oxidant PANI/MMT nanocomposites

The synthesis of 1:1 monomer/oxidant PANI and PANI/MMT nanocomposites has been described in **Chapter 4, Section 4.1.**

8.2 Synthesis of 2:1 monomer/oxidant PANI/MMT nanocomposites

For the synthesis of 2:1 monomer/oxidant nanocomposites, firstly the dispersion of MMT clay was done using an ultrasonicator probe. In a typical procedure to prepare nanocomposites, 1 w/v % of MMT clay was introduced into 100 mL of distilled water. Then, dispersion of clay was performed into an ultrasonicator probe for 10 min. The further reaction was carried out into a magnetic stirrer. In the next step, aniline solution was ready with dissolving 7 ml of aniline in 1M HCl (50 ml) solution, and APS solution by taking 9 g of ammonium persulfate in 50 ml of 1M HCl solution. Afterward, the prepared aniline solution was added to the dispersed MMT clay suspension under magnetic stirring at 0°C. After 20 min of constant stirring, a solution of ammonium persulfate has pored to the above suspension by magnetic stirring. The polymerization was performed for 4 h

under constant stirring and constant temperature (0°C). After 4 h, the polymerized solution was vacuum filtered and then washed using 1HCL, distilled water, and acetone to eliminate the impurities from the suspension. The drying was done at 50°C under a vacuum oven.

Pure PANI has been synthesized by the same procedure but without the addition of MMT clay.

8.3 Synthesis of 4:1 monomer/oxidant PANI/MMT nanocomposites

For the synthesis of 4:1 monomer/oxidant nanocomposites, the following steps have been followed. Aniline solution was prepared by dissolving 20 ml of aniline in 50 ml of 1M HCl solution and ammonium persulfate solution was prepared by taking 12 g of ammonium persulfate in 50 ml of 1M HCl solution. The reaction proceeded onto a magnetic stirrer. The aniline solution was added drop-wisely into the dispersed MMT clay solution and stirred continuously for 20 min at 0°C. Under constant stirring, ammonium persulfate solution was then dropped slowly into the above suspension to initiate the polymerization. The reaction continued for 4 h in an ice bath under magnetic stirring at 0°C. The nanocomposite suspension was filtered by vacuum filtration. Then, the washing was done with 1M HCl, distilled water, and acetone until the filtrate solution was colorless. The final product 4:1 monomer/oxidant nanocomposite was obtained after drying at 50°C under a vacuum oven.

Pure PANI has been synthesized by the same procedure but without the addition of MMT clay.

8.4 Adsorption Study

The adsorption study of AG25 dye was performed by using different monomer/oxidant ratios (1:1, 2:1, 4:1) PANI/MMT nanocomposites. The experimental study was done with 100 ml of known initial AG25 dye concentration, adsorbent dose, and pH into an incubator shaker at a constant

speed of 180 rpm for a contact time of 60 min. After a fixed time interval, the AG25 dye solution has been removed from the incubator shaker and then filtration was done to separate adsorbent and adsorbate from the solution. After that, the absorbance of samples was examined by a UV-Vis spectrophotometer and the concentration was evaluated by the calibration curve. The percentage of AG25 removal was calculated via the given equation:

$$\text{Adsorption \%} = \frac{C_o - C_e}{C_o} \times 100$$

Where C_e and C_o (mg/L) = Equilibrium concentration and initial concentration of AG25 dye, respectively.

8.4.1 Results and Discussion

The adsorption comparison study of AG25 dye onto 1:1, 2:1, and 4:1 monomer/oxidant ratio PANI/MMT nanocomposites were performed with 50 mg/L of AG25 dye concentration. The whole study was conducted at a temperature of 20°C for 60 min in 250 mL of conical flasks with a 0.2 g of the fixed adsorbent amount at pH 6 and agitation speed of 180 rpm. In **Figure 8.1**, the comparison of AG25 dye adsorption onto three different monomer/oxidant ratio nanocomposites is shown. In the results, it was observed that the adsorption capacity of AG25 was not much affected by the monomer/oxidant ratio. Results showed that the PANI/MMT adsorbent which was prepared with a 1:1 monomer/oxidant ratio is a little more effective for removing AG25 dye. The adsorption capacity of a 1:1 nanocomposite adsorbent was higher than other prepared adsorbents. This may be because the presence of a higher monomer/oxidant ratio covers the clay surface. Thus, the adsorption data indicated that the 1:1 nanocomposite adsorbent is slightly better compared to the 2:1 and 4:1 nanocomposite adsorbent.

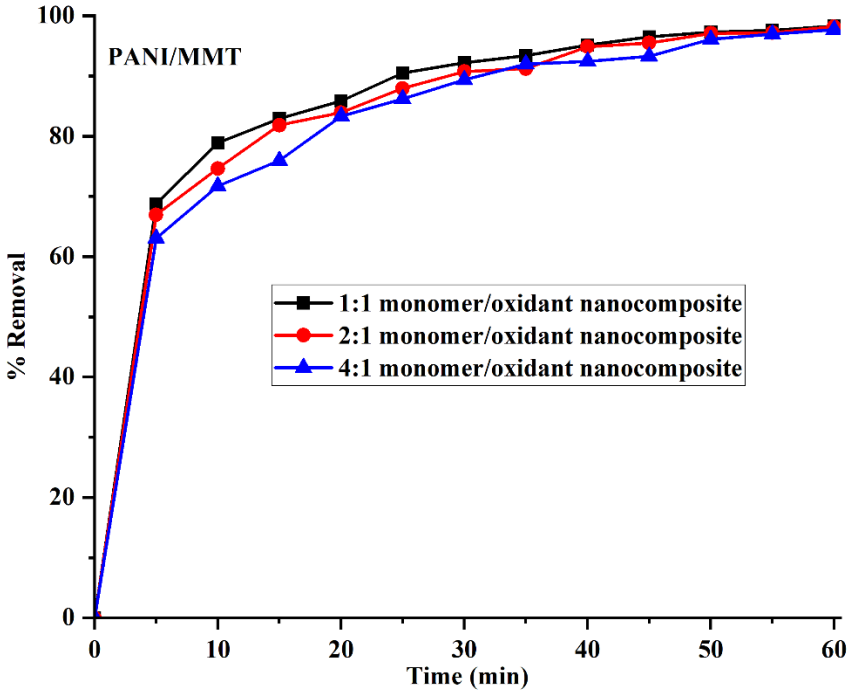

Figure 8.1 Adsorption comparison of AG25 dye onto PANI/MMT nanocomposite prepared at different monomer/oxidant ratios.

Adsorption comparison of 1:1, 2:1, and 4:1 PANI and PANI/MMT nanocomposites adsorbent for AG25 dye

Figure 8.2 shows the comparison data of different monomer/oxidant ratio PANI and PANI/MMT nanocomposite adsorbents for the treatment of AG25 dye. The results analysis illustrate that the removal of AG25 dye was higher with PANI/MMT nanocomposite adsorbents as compared to pure PANI adsorbents. It was observed that the adsorption rate of AG25 dye decreases with an increase in monomer/oxidant ratio for both PANI and PANI/MMT nanocomposite adsorbents.

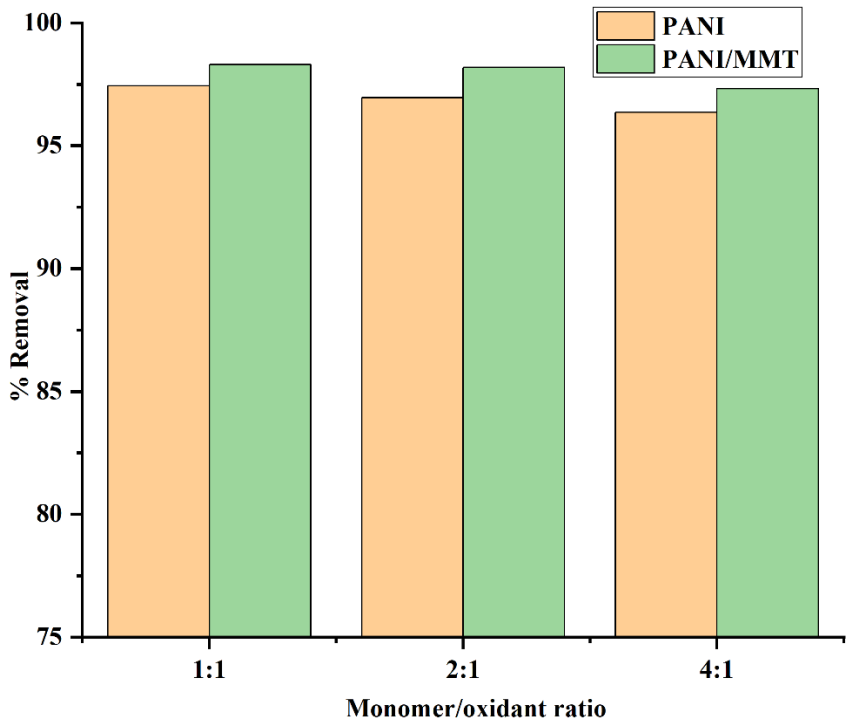

Figure 8.2 Comparison data of different monomer/oxidant ratio PANI and PANI/MMT nanocomposites.

8.5 Conclusion

From the above study, it was concluded that the 1:1, 2:1, and 4:1 (monomer/oxidant ratio) PANI/MMT nanocomposite adsorbent is better than 1:1, 2:1, and 4:1 PANI adsorbent for AG25 dye (anionic dye) adsorption. This is probably because MMT platelets, when dispersed at nano-level, possess a very large surface area, and hence PANI/MMT would use their complementary properties resulting in higher adsorption of AG25 dye.

CHAPTER 9

CONCLUSIONS AND FUTURE SCOPE

9.1 Conclusions

The present study aimed to synthesize and characterize polyaniline and its nanocomposites and their adsorption behavior. The prepared materials have been utilized for Acid green 25 and Methylene blue dye adsorption treatment. Polyaniline and its nanocomposites have been successfully synthesized at different temperatures through an *in-situ* polymerization method with ammonium persulfate (oxidizing agent) and HCl catalyst. The conclusions of the present study are given below:

9.1.1 Adsorption of Acid green 25 dye onto PANI and PANI/MMT nanocomposites

- PANI and PANI/MMT are highly efficient as an adsorbent for AG25 dye adsorption.
- Optimized adsorption conditions were found to be: adsorbent dose = 0.4 g, pH = 6 and contact time 30 min.
- As compared to PANI adsorbent, PANI/MMT nanocomposite adsorbent has a higher adsorption rate of AG25 dye and it consumes lesser contact time for 100 % removal of anionic dye.
- PANI and PANI/MMT adsorbed around 88% and 93% of AG25 dye in one min.
- Higher temperature is more favorable for 100% removal in a shorter time i.e. 10 min.
- The temperature strongly affected the adsorption rate. The percentage removal increased as the temperature increased, indicating that the adsorption nature is endothermic.
- Kinetics adsorption of AG25 onto both PANI and PANI/MMT adsorbents is best interpreted by pseudo-second order. The kinetic results found that with an increase in AG25 dye

concentration, the k_2 values were decreased. But the k_2 and q_e were found to be increased by increasing temperature.

- Langmuir model adequately describes the thermodynamics of adsorption onto PANI and PANI/MMT nanocomposite adsorbents.

9.1.2 Adsorption of Acid green 25 dye onto CA and PANI/CA nanocomposites

- Optimum conditions of CA and PANI/CA adsorption to remove AG25 dye: pH = 7, adsorbent dose = 0.1 g for CA and 0.4 g for PANI/CA, time 0-30 min for CA and 0-60 min for PANI/CA.
- CA has a greater removal efficiency than PANI/CA adsorbent.
- CA removed more than 99 % dye at lower as well as higher AG25 concentration and temperature. The adsorption was not much affected by temperature.
- The removal was found to decrease by increasing AG25 dye concentration for PANI/CA adsorbent and this behavior was observed due to the saturation of PANI/CA adsorption sites.
- The adsorption of PANI/CA adsorbents increases as the temperature rises because of the presence of more active adsorption sites at higher temperatures.
- Pseudo-second-order model well described kinetic study of AG25 onto CA and PANI/CA. The values of q_e (calculated) and q_e (experimental) are quite similar to each other.
- The best description of the adsorption equilibrium for AG25 on CA was found with two models Langmuir and Freundlich. Increasing q_m and K_F values with temperature demonstrating endothermic adsorption. For PANI/CA, the data fit was best defined by the Langmuir model and suggesting monolayer adsorption.
- The highest adsorption rate of 518 mg/g has been obtained on pure CA adsorbent.

- This is the first study on AG25 adsorption with CA and PANI/CA adsorbents. The adsorption results onto CA indicate that CA is a highly promising adsorbent for AG25 dye removal.

9.1.3 Adsorption of Methylene blue dye onto PANI and PANI/MMT nanocomposites

- Optimized conditions: adsorbent dose = 0.3 g for PANI and PANI/MMT, pH = 10 for PANI, pH = 7 for PANI/MMT, contact time = 30 min.
- PANI/MMT adsorbent shows better results for MB dye adsorption (100 %) as compared to pure PANI adsorbent.
- PANI/MMT removed more than 99 % in one min of lower MB dye concentration and higher concentration takes 5 min for > 99 % removal.
- With an increase in the temperature, the % removal onto PANI was increased, thus the temperature was strongly affecting the adsorption rate. Onto PANI/MMT, the temperature has no significant effect, it removes >99% of MB dye at all studied temperatures in a short time.
- With a rise in solution pH, the adsorption percentage of dye on PANI was increasing. For PANI/MMT adsorbent, the maximum removal was attained at neutral pH.
- The percentage removal increased as the temperature increased, indicating that the adsorption nature is endothermic.
- The pseudo-second-order model best represented the data of both PANI and PANI/MMT adsorbent, the q_e (experimental), and q_e (calculated) values were found to increase with increasing concentration and temperature.
- MB adsorption isotherm best fits the Temkin model for PANI adsorbent and the Langmuir model for PANI/MMT adsorbent, signifying monolayer adsorption.

- The adsorption capacity of PANI/MMT adsorbent is much higher than previous studies at least by a factor of 20.

9.1.4 Comparison of adsorption of Acid green 25 dye onto PANI/MMT nanocomposites prepared at different monomer/oxidant ratio

- AG25 dye adsorption has also been performed on 1:1, 2:1, and 4:1 (monomer/oxidant ratio) PANI/MMT nanocomposite adsorbents.
- The adsorption results showed that 1:1 monomer/oxidant composition adsorb more dye as compared to 2:1 and 4:1 nanocomposites.

Overall, the adsorption study results of Acid green 25 and Methylene blue dye onto PANI and its nanocomposites demonstrate that the removal of dye is dependent on various factors, i.e., the effect of adsorbent amount, pH, initial dye concentration, time, and temperature. The removal of AG25 and MB takes place efficiently at a very fast rate, PANI and its nanocomposites will be excellent adsorbents in continuous adsorption systems. In this study, the prepared adsorbents gave an excellent adsorption result, and this is because of the different processing routes that have been used to prepare nanocomposites. Overall, the present study results show that PANI/MMT and PANI/CA nanocomposite are efficient adsorbents for textile dye adsorption and are better adsorbents than the earlier reported.

9.2 Future Scope

- PANI and its nanocomposites can be used for the treatment of textile wastewater on an industrial scale, possibly in a continuous system.
- Aspects of excellent adsorption capacity and excellent conductivity, and high durability may be utilized as a smart material having new applications.

Polymer Bulletin
https://doi.org/10.1007/s00289-020-03222-3

ORIGINAL PAPER

Synthesis of polyaniline/clay nanocomposites by in situ polymerization and its application for the removal of Acid Green 25 dye from wastewater

Shivani Kalotra[1] · **Rajeev Mehta**[1]

Received: 1 October 2019 / Revised: 8 March 2020 / Accepted: 27 April 2020

Abstract

Synthesis, characterization and adsorption studies of polyaniline (PANI) and polyaniline/montmorillonite clay (PANI/MMT) nanocomposites have been carried out. In situ polymerization method was used to synthesize PANI/MMT nanocomposites using HCl as a catalyst and ammonium persulfate as an oxidizing agent. The molar ratio of monomer/oxidant was 1:1, and the polymerization was done at two different temperatures, i.e.,. 0° and 20 °C. Complete removal of Acid Green 25 (AG25) dye was achieved with PANI/MMT adsorbent. The kinetic adsorption data of AG25 dye were found to fit pseudo-second-order kinetic model. Since the removal of this dye takes place efficiently at a very fast rate, PANI/MMT nanocomposites will be excellent adsorbents in continuous adsorption systems.

Keywords Polyaniline · Montmorillonite clay · Nanocomposites · Adsorption · Acid Green 25 dye

Introduction

Contamination in water produced from several industries such as paper, textiles, cosmetics, pharmaceuticals, leather, plastics, printing and rubber industry is highly toxic and harmful to human beings [1, 2]. Textile industry in particular discharges a very large amount of dye bearing wastewater. There are three

Electronic supplementary material The online version of this article (https://doi.org/10.1007/s00289-020-03222-3) contains supplementary material, which is available to authorized users.

✉ Rajeev Mehta
rajeevmehta33@yahoo.com

Shivani Kalotra
shivani.kalotra@gmail.com

[1] Department of Chemical Engineering, Thapar Institute of Engineering and Technology, Patiala 147004, India

Published online: 09 May 2020

Chemical Engineering Communications

ISSN: (Print) (Online) Journal homepage: https://www.tandfonline.com/loi/gcec20

Carbon aerogel and polyaniline/carbon aerogel adsorbents for Acid Green 25 dye: synthesis, characterization and an adsorption study

Shivani Kalotra & Rajeev Mehta

To cite this article: Shivani Kalotra & Rajeev Mehta (2021): Carbon aerogel and polyaniline/carbon aerogel adsorbents for Acid Green 25 dye: synthesis, characterization and an adsorption study, Chemical Engineering Communications, DOI: 10.1080/00986445.2021.1919650

To link to this article: https://doi.org/10.1080/00986445.2021.1919650